Body temperature and the minor spliceosome control disease-associated and tissue-specific alternative splicing and gene expression

Inaugural-Dissertation

to obtain the academic degree
Doctor rerum naturalium (Dr. rer. nat.)

submitted to the Department of Biology, Chemistry, Pharmacy
of Freie Universität Berlin

by

Stefan Meinke

2020

Declaration

This work was carried out between July 2016 and June 2020 under the supervision of Prof. Dr. Florian Heyd at the Institute of Chemistry and Biochemistry, Freie Universität Berlin, Germany.

First reviewer:
Prof. Dr. Florian Heyd
RNA Biochemistry
Institute of Chemistry and Biochemistry
Freie Universität Berlin
Takustr. 6
14195 Berlin, Germany

Second reviewer:
Prof. Dr. Markus Wahl
Structural Biochemistry
Institute of Chemistry and Biochemistry
Freie Universität Berlin
Takustr. 6
14195 Berlin, Germany

Date of defense: 28.08.2020

Acknowledgements

First of all, I want to thank my supervisor Florian Heyd for giving me the opportunity to work in his group. Thank you for all the support, time, productive discussions, and motivation to do this thesis.

Secondly, I want to thank Markus Wahl for doing the second review.

I want to acknowledge all former and current lab members of the Wahl lab and the Chakrabarti lab for their help regarding protein biochemistry.

A very big thank you goes to all former and current lab members of the Heyd group. You created a great working atmosphere, which helped to stay motivated. I am very grateful for all your help with experiments and solving problems together. Special thanks go to Tom, Magdalena, Olga, Lennart, Marco, Alex N., and Alex K. for our occasional afterwork beers and all the funny evenings and moments together.

I want to thank Antje for all the help with RNA and plasmid preparations, and especially for a very welcomed game, which helped to clear the mind after working days.

Furthermore, I want to acknowledge Karin for all the administrative help and nice conversations.

Last but not least, I want to thank my friends and especially my family who always did everything to support me. But my biggest thanks go to Janine. You supported me during all ups and downs. Without you all this would not have been possible. Especially, because you gave (and will give) me the best presents in life - our children, who never failed to cheer me up.

Abstract

Alternative splicing (AS) is a dynamic and highly regulated process to expand the proteome diversity by allowing the generation of multiple possible messenger RNA (mRNA) isoforms from a single primary transcript. The splicing process impacts multiple biological processes, including gene expression (GE). By AS the cells can rapidly adapt to changing internal or external stimuli, such as temperature changes. In homeothermic organisms, the core body temperature oscillates in a circadian manner in a range of around 1 °C - 4 °C and these subtle temperature changes are sufficient to control AS. However, whether and how cells can sense and react to these minor changes is not fully understood.

In this thesis, we identified the Cdc2-like kinases (CLKs) 1 and 4 as the temperature sensors, which react to changes in the body temperature within a physiologically relevant range with higher activity at lower temperatures. We showed that the mRNA encoding the cold-inducible RNA binding protein (CIRBP) is CLK1/4-dependent alternatively spliced at different temperatures, resulting in a warm-induced isoform with lower stability.

Reversible phosphorylation-dependent mechanisms rely on the activity of kinases and phosphatases. In contrast to CLK1/4, we showed the anti-oncogenic protein phosphatase 2A (PP2A) to be more active at higher temperatures. RNA sequencing (RNA-Seq) analyses revealed a global impact of PP2A on AS and GE as phosphatase inhibition using okadaic acid (OA) almost completely abolished temperature sensitivity in HEK293 cells. Besides, the tumor-suppressive transcription factor p53 gets activated at higher temperatures in a PP2A-dependent manner, likely through AS of *MDM4*. In contrast, oncogenic MYC is more active at lower temperatures, which is consistent with negative regulation of phosphatase activity. These data point to a novel, body temperature-dependent mechanism which activates p53 tumor-suppressive function and provides a molecular mechanism for the use of PP2A inhibitors or hyperthermia in cancer therapies.

AS can result in the production of a premature translation termination codon (PTC) and, thereby, control GE by nonsense-mediated mRNA decay (NMD). We found for multiple RNA binding proteins (RBPs) that temperature-dependent alternatively spliced isoforms are often targeted by the NMD pathway leading to body temperature-responsive, rhythmic GE levels. As an example, we showed that the temperature-dependent and NMD-inducing inclusion of *SRSF10* exon 3 results in reduced GE levels in a rhythmic manner and suggests that the production of the

NMD-targeted isoform is under control of an autoregulatory feedback loop.

In SRSF10, splicing of the NMD-inducing, exon 3-containing isoform is under direct competition of a minor and a major splice site in *SRSF10* exon 2. Finally, we revealed that SRSF10 autoregulates its expression by activating the inclusion of exon 3. Interestingly, usage of the minor splice site in exon 2, which leads to the production of a coding mRNA, is reduced through the presence of a downstream major splice site leading to AS of the NMD-inducing isoform. We found that *SRSF10* transcript levels correlate with the minor spliceosome component RNA binding region (RNP1, RRM) containing 3 (RNPC3) in a tissue- and developmental stage-specific manner. Our data suggest that *SRSF10* expression levels control the expression of all other serine/arginine-rich (SR) proteins via cross-regulation. Therefore, the minor spliceosome also controls major intron splicing, which globally affects AS and GE.

In summary, this work expands our knowledge of how cells sense and adapt to changes in the body temperature. We showed that the activity of CLK1/4 and PP2A is differently affected by fluctuations in the body temperature, resulting in distinctive AS patterns and expression changes of target genes. We revealed that the temperature-dependent AS-NMD pathway leads to cycling GE and identified the minor spliceosome as a regulator of *SRSF10* GE levels, which impacts the expression levels of all SR proteins, thereby globally affecting major intron splicing.

Zusammenfassung

Alternatives Spleißen (AS) ist ein dynamischer und stark regulierter Prozess, der es ermöglicht die Proteinvielfalt durch die Bildung mehrerer potenzieller mRNA Isoformen von einem primären Transkript zu erhöhen. Spleißen beeinflusst zahlreiche zelluläre Prozesse, einschließlich Genexpression (GE). Durch AS können sich Zellen schnell an wechselnde interne oder externe Stimuli anpassen, wie z.B. an Änderungen der Temperatur. In homoiothermen Organismen oszilliert die Körpertemperatur zirkadian um 1 °C - 4 °C und diese kleinen Temperaturänderungen sind ausreichend, um AS zu beeinflussen. Ob und wie Zellen diese feinen Änderungen wahrnehmen und darauf reagieren ist nicht vollständig bekannt.

In dieser Arbeit haben wir die *Cdc2-like* Kinasen (CLKs) 1 und 4 als Temperatursensoren identifiziert, die auf Körpertemperaturänderungen im physiologischen Bereich reagieren, mit höherer Aktivität bei niedrigeren Temperaturen. Wir zeigten, dass die mRNA, die das Kälte-induzierte RNA-bindende Protein (CIRBP) kodiert, CLK1/4-abhängig bei unterschiedlichen Temperaturen alternativ gespleißt wird, was zu einer Wärme-induzierten Isoform mit geringerer Stabilität führt.

Reversible phosphorylierungsabhängige Mechanismen hängen von der Aktivität von Kinasen und Phosphatasen ab. Im Gegensatz zur CLK1/4 zeigten wir, dass die anti-onkogene Proteinphosphatase 2A (PP2A) bei höheren Temperaturen aktiver ist. RNA-Sequenzierungsanalysen zeigten einen globalen Einfluss der PP2A auf AS und GE, da Inhibition der Phosphatase durch Okadasäure nahezu vollständig die Temperaturempfindlichkeit in HEK293 Zellen aufhob. Außerdem wird der Tumor-supprimierende Transkriptionsfaktor p53 bei höheren Temperaturen PP2A-abhängig aktiviert, sehr wahrscheinlich durch AS von *MDM4*. Im Gegensatz dazu ist der onkogene Faktor MYC bei geringeren Temperaturen aktiver, was mit einer negativen Regulation der Phosphataseaktivität konsistent ist. Diese Daten weisen auf einen neuen, körpertemperaturabhängigen Mechanismus hin, der die Tumor-inhibierende Funktion von p53 aktiviert und einen molekularen Mechanismus für die Nutzung von PP2A Inhibitoren oder Hyperthermie bei Krebstherapien liefert.

AS kann zur Bildung eines vorzeitigen Stopcodons (PTC) führen und dadurch die GE durch *nonsense-mediated mRNA decay* (NMD) regulieren. Wir fanden heraus, dass durch temperaturabhängiges AS entstandene Isoformen zahlreicher RNA-bindender Proteine (RBPs) oft durch den NMD Prozess abgebaut werden, was zu körpertemperaturabhängigen, rhythmischen GE Level führt. Beispielsweise zeigten wir, dass die temperaturabhängige und NMD-induzierende

Inklusion von *SRSF10* Exon 3 rhythmisch zu reduzierten GE Levels führt, was vermuten lässt, dass die Produktion der NMD-induzierenden Isoform durch eine autoregulierende Feedbackschleife kontrolliert wird.

In *SRSF10* ist das Spleißen der NMD-induzierenden, Exon 3-enthaltenden Isoform durch die direkte Konkurrenz einer *minor* und einer *major* Spleißstelle in *SRSF10* Exon 2 reguliert. Wir zeigten, dass SRSF10 die eigene Expression durch die Aktivierung der *SRSF10* Exon 3 Inklusion autoreguliert. Interessanterweise ist die Nutzung der *minor* Spleißstelle in Exon 2, die zur Produktion der kodierenden mRNA führt, durch die Präsenz einer *downstream major* Spleißstelle, dessen AS zur NMD-induzierenden Isoform führt, reduziert. Wir fanden heraus, dass die Menge der *SRSF10* Transkripte mit der der *minor* Spleißosom-Komponente *RNPC3* Gewebs- und Entwicklungsstadium-spezifisch korreliert. Unsere Daten deuten somit darauf hin, dass das *SRSF10* Expressionlevel die Expression aller anderen SR Proteine kontrolliert. Somit kontrolliert das *minor* Spleißosom auch *major* Intron spleißen, was wiederum global AS und GE beeinflusst.

Zusammenfassend erweitert diese Arbeit unser Wissen darüber, wie Zellen Änderungen in der Körpertemperatur wahrnehmen und an diese adaptieren. Wir zeigten, dass die Aktivität der CLK1/4 und PP2A gegensätzlich von Schwankungen der Körpertemperatur beeinflusst wird, was zu unterschiedlichen AS Mustern und Änderungen der Expression von Zielgenen führt. Wir präsentierten, dass der temperaturabhängige AS-NMD Prozess zur zyklischen GE führt und identifizierten das *minor* Spleißosom als Regulator der *SRSF10* GE Levels, was die Expression aller SR Proteine beeinflusst und sich global auf *major* Intron-Spleißen auswirkt.

Contents

1 Introduction

1.1 Pre-mRNA splicing

Genetic information is encoded in the deoxyribonucleic acid (DNA), transcribed into ribonucleic acid (RNA), and translated into protein to perform a biological function. To allow translation, precursor messenger RNA (pre-mRNA) needs to be processed in mature RNA. In eukaryotes, RNA processing occurs mostly co-transcriptionally (Baurén and Wieslander, 1994) and in 3 major steps: addition of a 7-methylguanosine residue (m7G) to the 5' end (5' capping), polyadenylation of the 3' end (poly(A) tail) and pre-mRNA splicing. The 5' capping and the poly(A) tail are important processing events for mRNA stability, nuclear export, and subsequent translation initiation. With the third process, pre-mRNA splicing, non-coding sequences (introns) are excised and coding regions (exons) are ligated together. Intronic sequences and boundaries to neighboring exons are defined by conserved sequences at the 5' splice site, the 3' splice site, and the branch point (BP) adenosine followed by a polypyrimidine tract. The removal of introns and the ligation of exons is achieved by two consecutive S_N2-type transesterification reactions. First, the 2' hydroxyl group of the BP adenosine attacks the phosphate group of the 5' splice site (Figure 1.1), generating a 2'-5'-phosphodiester bond. Second, the free 3' hydroxyl group of the upstream exon attacks the phosphate group of the 3' splice site, leading to the ligation of the 5' and 3' exons, and the release of the intron in a lariat structure (Figure 1.1).

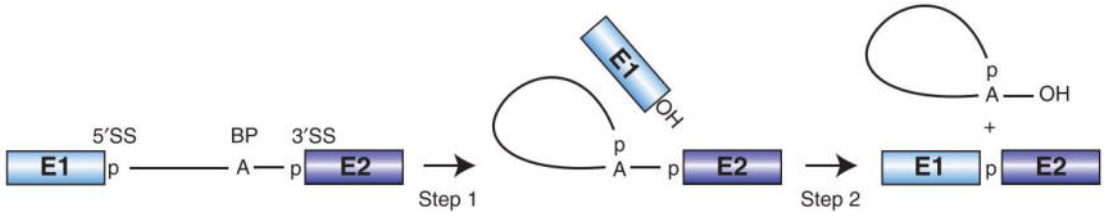

Figure 1.1: Splicing is carried out by two transesterification reactions.
Schematic of the splicing mechanism. The boxes and solid lines represent exons (E1, E2) and the intron, respectively. The branch point (BP) adenosine (A) and the phosphate groups (p) of the 5' and 3' splice site (SS) are also shown. (Figure taken from (Will and Lührmann, 2011)).

This nuclear pre-mRNA splicing process is catalyzed by a multi-megadalton ribonucleoprotein complex, called the spliceosome. In most eukaryotes two distinct

types of spliceosomes coexist: the U2-dependent (major) spliceosome, which generally catalyzes splicing of introns with the characteristic GT-AG splice sites. It is assembled from the U1, U2, U5, and U4/U6 small nuclear ribonucleoprotein particles (snRNP) and multiple non-snRNPs splicing factors. The U12-dependent (minor) spliceosome is composed of the minor-specific U11, U12, U4atac, U6atac, and the shared U5 snRNP. It catalyzes splicing of less than 1 % of introns, which mostly contain non-consensus AT-AC splice sites, distinct BP and polypyrimidine tract sequences (Jackson, 1991; Patel and Steitz, 2003; Turunen et al., 2013). Despite its low abundance, the minor spliceosome is essential for ontogenesis, as deficiencies in its activity or minor intron splicing are lethal or result in developmental defects and disorders (Doggett et al., 2018; Verma et al., 2018). In addition, minor splice site sequences, including the genes harboring these minor introns, are evolutionary highly conserved (Basu et al., 2008; Younis et al., 2013).

The spliceosome is assembled in a highly dynamic and stepwise manner (Wahl et al., 2009)(Figure 1.2). The initial phase of major spliceosome assembly involves intron definition by recognition of characteristic consensus sequences (Green, 1986). This includes the recruitment of the U1 snRNP to the 5' splice site, binding of splicing factor 1 (SF1) to the BP, and interaction of the U2 auxiliary factor (U2AF) with the polypyrimidine tract and the 3' splice site, which results in the formation of the E complex (Figure 1.2). In the following step, SF1 is replaced by the U2 snRNP generating the pre-spliceosomal A complex. Subsequently, the pre-assembled U4/U6.U5 tri-snRNP is recruited, forming the catalytically inactive B complex. After conformational and compositional rearrangements this complex gets activated (B^{act} complex). During activation, U1 and U4 are released, yielding in the catalytically active spliceosome (B* complex), which catalyzes the first transesterification reaction, generating the C complex. Further conformational rearrangements occur prior to the second splicing reaction. Afterward, the spliceosome dissociates, releasing the mRNA and snRNPs for further rounds of splicing, and the intron lariat is degraded (Wahl et al., 2009; Will and Lührmann, 2011). The assembly of the minor spliceosome is very similar to that of the major spliceosome. The main difference is the formation of a U11/U12 di-snRNP, which binds the minor intron as a unit (Turunen et al., 2013).

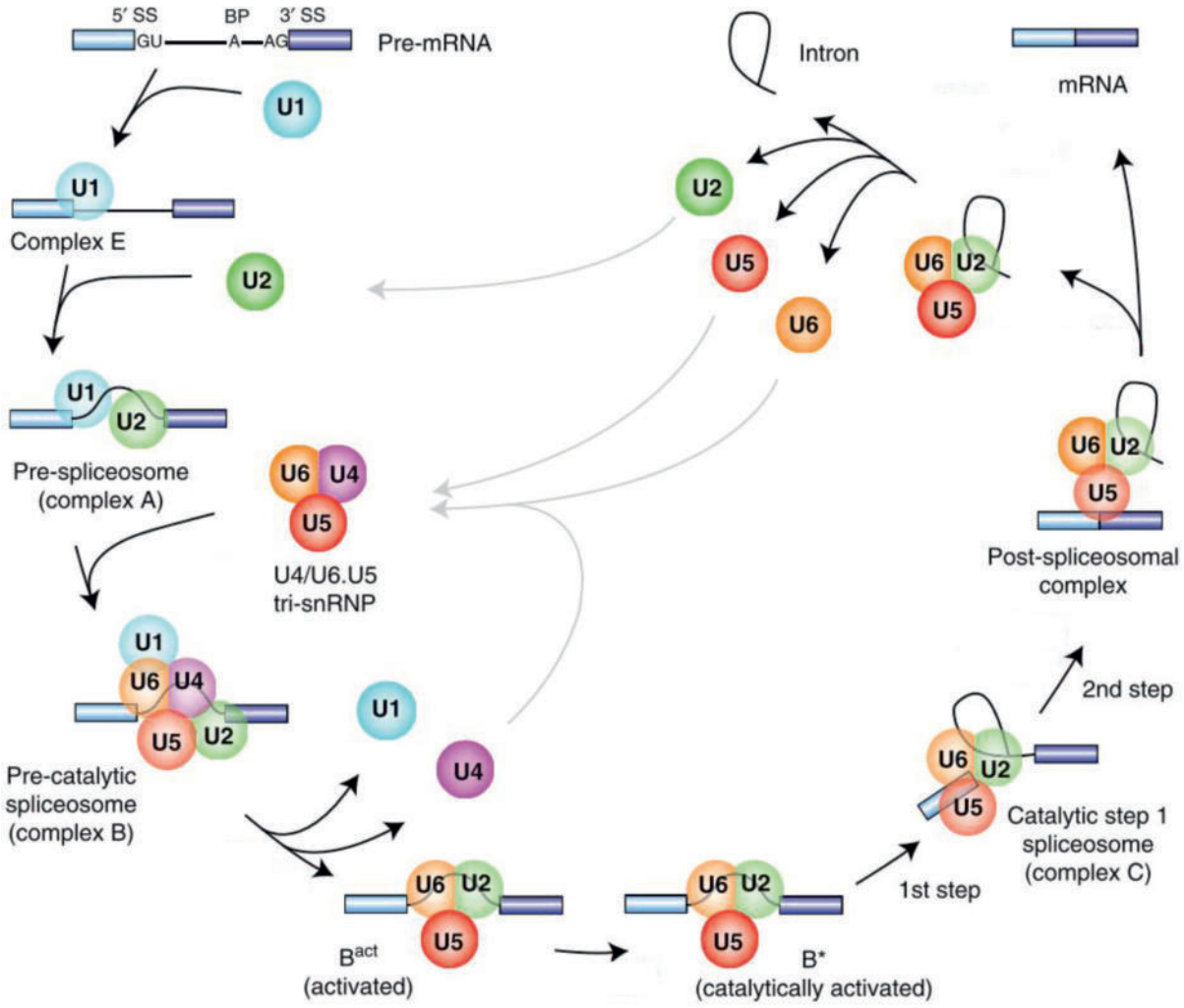

Figure 1.2: Dynamic assembly of the major spliceosome.
Simplified model of the splicing reaction catalyzed by the major spliceosome. The first fully assembled spliceosome is represented by the pre-B complex. After the splicing reaction the mRNA and snRNP components are released. Exons are illustrated as boxes, the intron as a line, circles indicate snRNP components. (Figure adapted from (Will and Lührmann, 2011)).

1.2 Alternative splicing

In humans around 95 % of multi-exon genes undergo AS, leading to a distinct mRNA isoform originating from a single pre-mRNA transcript. For instance, AS of the gene homolog of human Down syndrome cell adhesion molecule (DSCAM) in *Drosophila melanogaster* can generate more than 38,000 isoforms (Schmucker et al., 2000). Thereby, the proteome, generated from a limited number of genes, can be expanded (Barbosa-Morais et al., 2012; Matlin et al., 2005; Merkin et al., 2012; Nilsen and Graveley,

2010; Pan et al., 2008; Wang et al., 2008). There are different modes of AS: differential inclusion or exclusion of an alternative cassette exon (CE), mutually exclusive splicing of only one of two or more adjacent alternative exons, usage of an alternative 5' or 3' splice site, retention of an intron, or usage of alternative promoter or poly(A) sites (Figure 1.3). All forms result in the production of different mRNA isoforms based on a single pre-mRNA transcript. On RNA level, AS can impact mRNA stability, translational efficiency, and cellular localization (Mockenhaupt and Makeyev, 2015). Additionally, AS can affect GE by creating aberrant transcripts targeting them to mRNA surveillance pathways, i.e. NMD, non-stop decay, or no-go decay (Garneau et al., 2007). For instance, AS can result in the formation of a PTC, leading to mRNA degradation through the NMD pathway (McGlincy and Smith, 2008). Proteins derived from alternatively spliced mRNAs can differ in their amino acid sequence and, therefore, can exhibit differences in structure, enzymatic activity, molecular interactions, cellular localization, and protein stability (Liu et al., 2017).

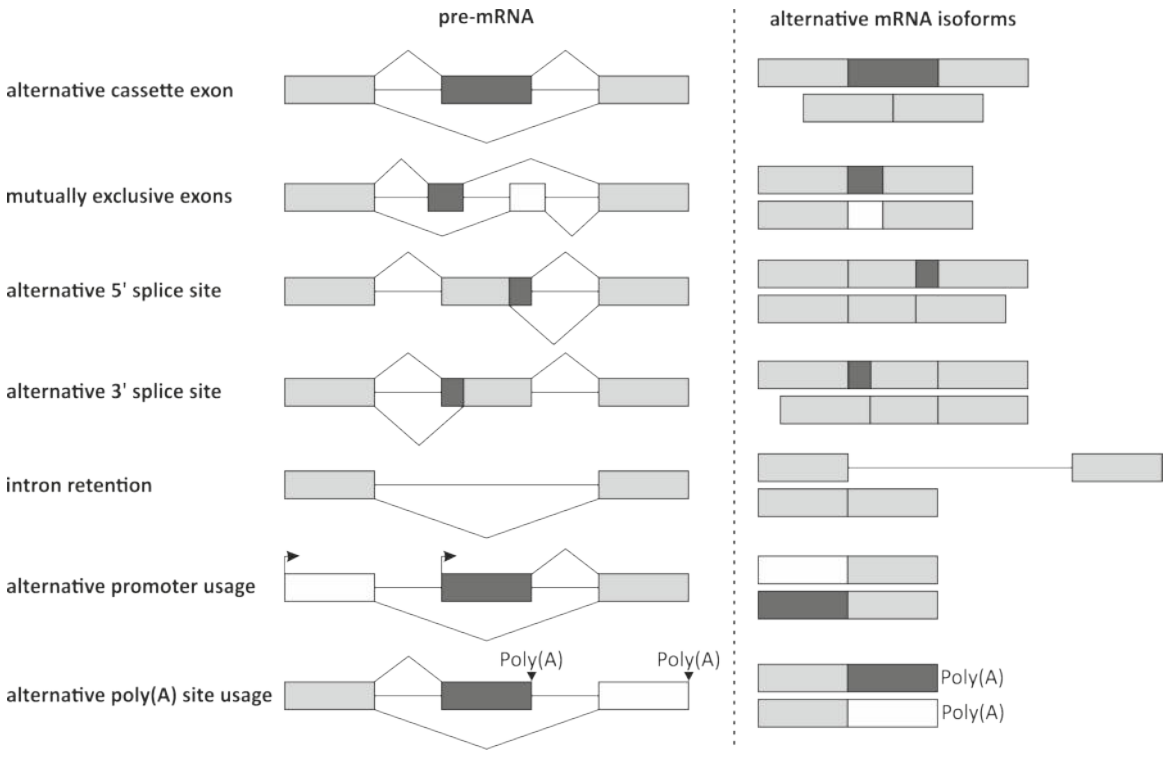

Figure 1.3: Types of alternative pre-mRNA splicing.
Pre-mRNA (left) can be differentially spliced resulting in various mRNA transcript isoforms (right). Constitutive exons are shown in light grey boxes, alternative exons or sequences in dark grey or white boxes, respectively, and introns are illustrated as lines.

1.3 Splicing regulation

AS is a dynamic process tightly regulated by *cis*- and *trans*-acting splicing regulatory elements, which influence the usage of a splice site dependent on the position in the pre-mRNA and type of regulation. *Cis*-regulatory elements are present both within exons or introns and either promote or inhibit exon recognition, i.e exonic splicing enhancer (ESE), exonic splicing silencer (ESS), intronic splicing enhancer (ISE) and intronic splicing silencer (ISS) (Black, 2003). Two well-studied families of splicing regulators are the SR proteins and heterogeneous nuclear ribonucleoproteins (hnRNPs). SR proteins generally activate exon inclusion by both direct binding to specific exonic regions and by recruiting the U1 snRNP and U2AF via protein-protein interactions to the 5' splice site and 3' splice site, respectively (Fu and Ares, 2014; Long and Caceres, 2009)(Figure 1.4). In contrast, hnRNPs are generally viewed as negative splicing regulators, e.g. hnRNP A/B antagonizes the function of SR proteins and hnRNP I (also known as the polypyrimidine tract-binding protein (PTB)) prevents onward spliceosome assembly through interference with the recognition of the 3' splice site by the U2 snRNP (Mayeda and Krainer, 1992; Mayeda et al., 1994; Sharma et al., 2008) (Figure 1.4).

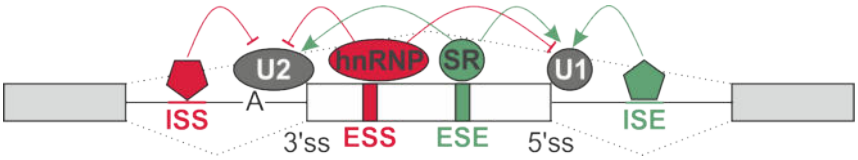

Figure 1.4: Regulation of AS by SR proteins and hnRNPs.
SR proteins and hnRNPs are well-studied RBPs, which are known to generally promote or inhibit splicing, respectively, by binding to *cis*-regulatory elements. ISS – intronic splicing silencer, ESS – exonic splicing silencer, ESE – exonic splicing enhancer, ISE – intronic splicing silencer, 3'ss – 3' splice site, 5'ss – 5' splice site.

For many RBPs cross-regulatory mechanisms are described, where they influence the binding and function of each other cooperatively or competitively (Bradley et al., 2015; Kumar and Lopez, 2005; Rossbach et al., 2009). One example is the competition of hnRNP C with U2AF65 at cryptic splice sites, as hnRNP C prevents the inclusion of suppressed Alu element-containing exons, which otherwise would disrupt transcript integrity (Zarnack et al., 2013).

The regulation of AS also depends on the relative position of RBP binding sites to the regulated exon and the sequence context (Taliaferro et al., 2016; Ule et al., 2006). For instance, binding of neuro-oncological ventral antigen (NOVA) to an upstream intron inhibits alternative exon inclusion, while binding in an intronic region downstream of the exon enhances its selection (Licatalosi et al., 2008). Additionally, SR proteins contain ultraconserved elements in alternative exons, controlling the presence of a PTC (Lareau et al., 2007). Thus, SR proteins regulate their own expression levels through NMD, which is understood as a key mechanism for homeostatic expression (Ni et al., 2007; Sureau et al., 2001). However, while many RBPs, including SR proteins, use autoregulation to maintain stable mRNA abundance (Müller-McNicoll et al., 2019), their expression levels and regulation of alternative splice isoforms differ in a cell type-, tissue-, and developmental stage-specific manner (Furlanis and Scheiffele, 2018; Wang et al., 2008; Warzecha et al., 2009; Weyn-Vanhentenryck et al., 2018).

Furthermore, post-translational modifications, especially reversible phosphorylation, of spliceosomal components or SR proteins affect the splicing result. The phosphorylation status is fundamental for the assembly and catalytic activation of the spliceosomal components PRP28 or PRP31 (Mathew et al., 2008; Schneider et al., 2010). SR protein phosphorylation has been shown to control the activity, the interaction with other proteins, and the sub-cellular and sub-nuclear localization of SR proteins in nuclear speckles (Lin et al., 2005; Shepard and Hertel, 2009; Zhou and Fu, 2013). One interesting target is SRSF10, as it was shown to be a splicing activator in its phosphorylated state but becomes a splicing repressor upon dephosphorylation (Feng et al., 2008; Shin et al., 2004). An additional layer of splicing regulation is achieved by the coupling of splicing and transcription, as the speed of transcription elongation affects differential splice site selection and accessibility for RBPs (Bentley, 2014; de la Mata et al., 2003; Kornblihtt, 2015). Moreover, RNA secondary structures influence splicing, for instance by preventing splice site recognition by the spliceosome, the binding of RBPs to the maturing transcript, or altering the accessibility of *cis*-regulatory elements, as it was described for the fibronectin EDA exon (McManus and Graveley, 2011; Yang et al., 2011). AS can rapidly adapt to various stimuli. In a human T cell line, Martinez et al. identified 178 alternatively spliced exons upon T cell activation (Martinez et al., 2012). For instance, tumor necrosis factor receptor-associated factor 3

(TRAF3) and the coat protein complex II (COPII) assembly protein SEC16 have been shown to be alternatively spliced upon T cell activation, activating the non-canonical NFκB pathway or increasing COPII transport efficiency, respectively (Michel et al., 2014; Wilhelmi et al., 2016). Besides, external temperature changes of 1 °C are sufficient for *U2AF26* AS alterations *in vivo* (Preußner et al., 2017).

In conclusion, pre-mRNA splicing is tightly regulated by a plethora of factors and mechanisms, and dysregulation of the splicing network can cause numerous diseases, such as cancer or neurological defects (Scotti and Swanson, 2016; Singh and Cooper, 2012).

1.4 The role of SR proteins in mRNA maturation

SR proteins represent a group of RBPs which is characterized by the presence of an N-terminal RNA recognition motif (RRM) and an arginine (R) and serine (S)-rich (RS) C-terminal domain (Manley and Krainer, 2010). While the RRM binds to the target RNA, the RS domain is associated with protein-protein interactions (Graveley, 2000). Substrate specificity and binding affinity is set by the number and orientation of the RRMs within an SR protein as well as by the combination with other domains (Cléry et al., 2008). SR proteins undergo post-translational modifications, which impact on their functionality. Besides lysine acetylation (Edmond et al., 2011) or arginine methylation (Sinha et al., 2010), phosphorylation of serine residues within the RS domain is the most important modification. Phosphorylation is collaboratively carried out by serine/arginine protein kinases (SRPKs) and CLKs and mediates nucleocytoplasmic shuttling of SR proteins (Aubol et al., 2016; Cáceres et al., 1998). It is described that phosphorylation of the RS domain modulates RNA binding specificity and promotes protein-protein interactions in the early stages of spliceosome assembly (Howard and Sanford, 2015; Xiao and Manley, 1997). Besides their role in splicing regulation, SR proteins also function in post-splicing mRNA processing events, i.e. mRNA nuclear export, NMD, and translation (Huang and Steitz, 2005). Karni et al. showed that SRSF1 regulates AS of *MKNK2*, which is involved in translation regulation. SRSF1 stimulates splicing of the oncogenic Mnk2b isoform, which promotes mitogen-activated protein kinase (MAPK)-independent eukaryotic

translation initiation factor 4E (eIF4E) phosphorylation, and thereby enhancing cap-dependent translation (Karni et al., 2007).

However, the RBP SRSF10 is an exceptional SR protein as it was generally found to be a splicing repressor (Cowper et al., 2001). Shin and colleagues found that the splicing inhibitory function of SRSF10 gets activated upon heat-induced dephosphorylation or during mitosis (Shin et al., 2004; Shin and Manley, 2002), but SRSF10 becomes a splicing activator in its phosphorylated state (Feng et al., 2008). For instance, SRSF10 promotes alternative exon inclusion in *BCL-2-associated transcription factor 1 (BCLAF1)* during tumorigenesis (Zhou et al., 2014a), while CE inclusion in *LIPIN1* during adipogenesis is repressed by SRSF10 (Li et al., 2014). SRSF10-responsive AS events are associated with cell survival under stress conditions, as it was shown, for instance, for splicing of genes encoding CASPASE 1, BRCA1-associated protein 1, or MDM4 in chicken DT40 cells (Zhou et al., 2014b). Besides, SRSF10 is associated with DNA damage-induced splicing changes of other transcripts and, thus, regulates mediators of apoptosis, cell cycle, and DNA repair (Shkreta et al., 2016). Additionally, SRSF10 is involved in myoblast differentiation by regulating *LRRFIP1* splicing in cardiac and skeletal muscles (Wei et al., 2015), plays a role in *Xenopus* neuronal differentiation (Liu et al., 2005), and was shown to have an oncogenic effect in cervical cancer by regulating splicing of the membrane-bound interleukin-1 receptor accessory protein (mIL1RAP)(Liu et al., 2018).

1.5 Alternative splicing and cancer

Since AS impacts a plethora of cellular processes, it is not surprising that many diseases are a result of splicing defects. For instance, in Taybi-Linder syndrome (TALS) patients, mutations in the minor spliceosome-associated snRNP U4atac lead to decreased splicing efficiency of U12-type introns (Edery et al., 2011; He et al., 2011). Alterations or dysregulation of AS seem to affect all hallmarks of tumor biology, such as cell metabolism, apoptosis signaling, angiogenesis, immune escape, invasion, and metastasis (Hanahan and Weinberg, 2011; Oltean and Bates, 2014)(see also Figure 1.5). Indeed, mutations in *cis*- and *trans*-regulatory elements, core spliceosomal factors, or 5' and 3' splice sites contribute to missplicing. This contributes to the development of various cancers, as it has been shown, for instance, in hematolymphoid neoplasias and

acute myeloid leukemia (Singh and Cooper, 2012). The impact of splicing in cancer development is highlighted by numerous examples. First, cancer cells preferentially express splicing isoforms with proliferation-promoting functions. One example is an alternative splice variant of epidermal growth factor receptor (EGFR) lacking exon 4, which is functionally constitutively active and thus promotes proliferation (Wang et al., 2011). A second example is the tumor growth suppressor p53, which, among other splice isoforms, can be spliced to lack the first 40 amino acids. However, this splice variant still binds to DNA and competes with wild type (WT) p53, affecting its growth-suppressive function. The important role of p53 in maintaining cell homeostasis and preventing cellular transformation is further highlighted by the finding that in more than 50 % of all cancers p53 is inactivated (Hollstein et al., 1991; Levine et al., 1991; Surget et al., 2013). Moreover, some splicing-regulating proteins, such as SRSF1, have been linked to multiple characteristics of cancer development and progression. SRSF1 has been shown to regulate AS of the gene encoding the Ron tyrosine receptor kinase, proteins of the B cell lymphoma 2 (BCL-2) family, and MAPK-interacting kinase 2 (Mnk2), and thus enhancing cell mobility and invasion, cell survival, and proliferation, respectively (Ghigna et al., 2005; Karni et al., 2007; Moore et al., 2010).

Since splicing functions on all levels of tumorigenesis, cancer therapeutics that intervene with splicing have become promising. For instance, the gene encoding Mnk2 (*MKNK2*) is alternatively spliced generating two isoforms: Mnk2a, which acts tumor-suppressive, and the oncogenic form Mnk2b. By specifically targeting *MKNK2* using synthetically modified antisense oligonucleotides (ASOs), which induce a splicing switch towards the Mnk2a isoform, the oncogenic properties of glioblastoma cells were inhibited and cells were sensitized to chemotherapy *in vivo* (Mogilevsky et al., 2018). Furthermore, the application of splicing inhibitory antitumor drugs, such as spliceostatin A or pladienolide B, which target the splicing factor SF3b, showed promising effects in preventing cancer cell proliferation (Kaida et al., 2007; Kotake et al., 2007).

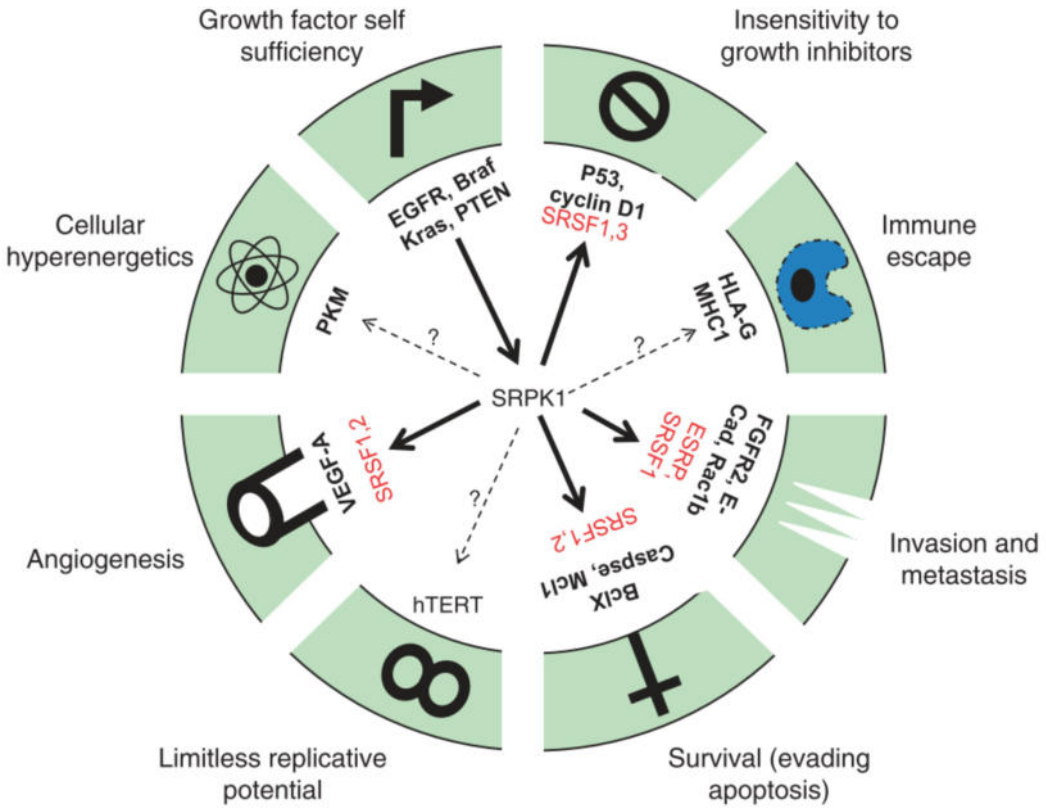

Figure 1.5: Alternative splicing events regulate different hallmarks of cancer.
The proto-oncogene SRSF1 is involved in several tumorigenic pathways and regulation of splice factors themselves is promoted by cancer hallmarks (Figure taken from (Oltean and Bates, 2014)).

1.6 Protein phosphatase 2A (PP2A) and its role in oncogenesis

Cellular signaling processes are regulated by reversible phosphorylation of proteins and thus are controlled by protein kinases and phosphatases. The presence or absence of a phosphate group either positively or negatively affects the activity of the post-translationally modified proteins. Therefore, protein phosphorylation plays a fundamental role in cellular processes, such as proliferation, survival, apoptosis, metabolism, and immunity (Graves and Krebs, 1999; Manning et al., 2002). The protein phosphatases 1 and 2A (PP1/2A) belong to the phosphoprotein phosphatase family and account for over 90 % of the cell's phosphatase activity (Pippa and Odero, 2020). PP2A forms numerous heterotrimeric holoenzymes, which contributes to its broad substrate specificity. In humans, the catalytic (C) and scaffold (A) subunits are each encoded by two different genes with each two isoforms: *PPP2CA* and *PPP2CB* for the C

subunit, *PPP2R1A* and *PPP2R1B* for the A subunit. The third variable component is the regulatory subunit (B), which determines substrate specificity, subcellular localization, and fine-tuning of phosphatase activity (Slupe et al., 2011; Virshup and Shenolikar, 2009). It is encoded by 15 genes, giving rise to more than 23 isoforms which belong to four different families: B (B55/PR55), B' (B56/PR61), B" (PR48/PR72/PR130), B"' (PR93/PR110)/striatin, each containing 2 to 5 isoforms and additional splice variants (Figure 1.6).

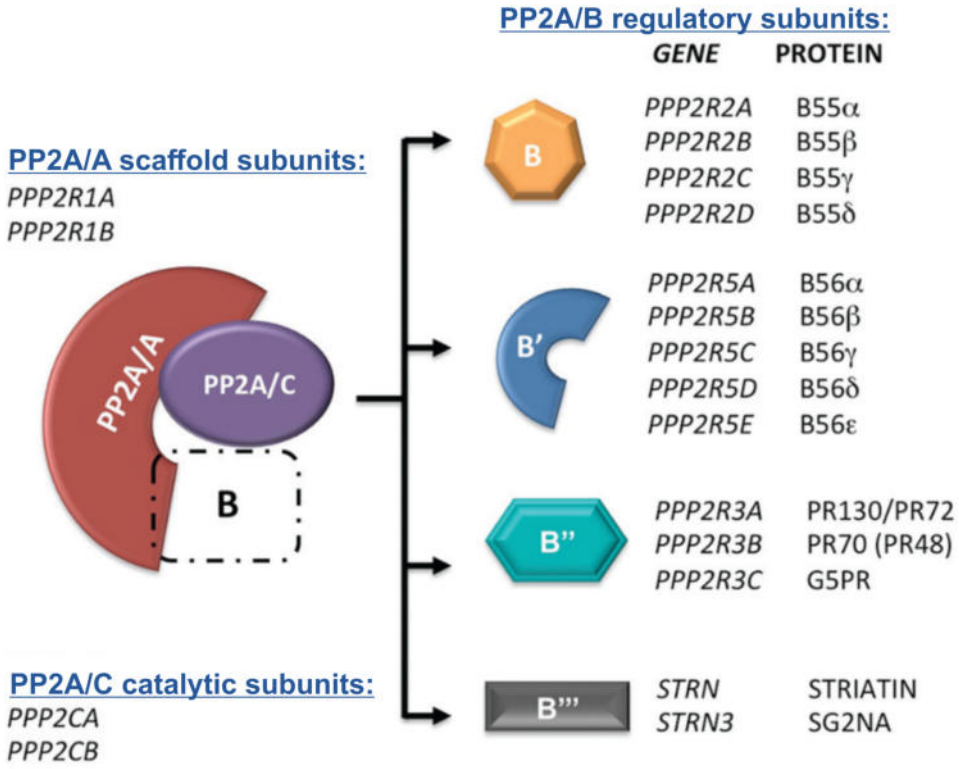

Figure 1.6: Heterotrimeric PP2A holoenzymes are composed of a scaffold (A), catalytic (C), and a regulatory (B) subunit.(Figure taken from (Kurimchak and Graña, 2012)).

Unlike kinases, PP1/2A have not been shown to recognize defined consensus motifs within their substrates. Mostly both the catalytic and the regulatory subunits target the peptide sequence. The regulatory subunits were shown to be expressed in a tissue-specific and time-dependent manner (McCright et al., 1996; Strack et al., 1998), which contributes to its substrate specificity. PP2A activity and localization can be regulated by differential phosphorylation and methylation, affecting the formation and composition of the phosphatase complex (Bononi et al., 2011; Sangodkar et al., 2016). For instance, the expression level of the catalytic subunit PP2AC is regulated on

the translational level to maintain constant protein levels (Baharians and Schönthal, 1998). While phosphorylation of Y307 inhibits the interaction of PP2AC with the PP2A PR55/PR61 subunit, leading to phosphatase inhibition, methylation at L309 promotes PP2A activity by increasing the binding affinity of the A/C subunit towards regulatory B subunits (Seshacharyulu et al., 2013). Besides the different subunits, several other proteins have been described to interact with and affect the activity of PP2A. Type 2A-interacting protein (TIP) negatively regulates PP2A activity and thereby impacts the Ataxia telangiectasia mutated (ATM)/Ataxia telangiectasia and Rad3 related (ATR)-regulated DNA damage and repair signaling pathway (McConnell et al., 2007). Other PP2AC inhibitory proteins are inhibitor-2 of PP2A (I2PP2A) and cancerous inhibitor of PP2A (CIP2A), promoting cell transformation by depleting PP2AC catalytic activity (Junttila et al., 2007; Neviani et al., 2005).

A subset of the regulatory B subunits is described to direct PP2A to oncogenes, controlling cancer progression by dephosphorylation (Eichhorn et al., 2009). For instance, B56α directs PP2A to c-MYC resulting in its inactivation by dephosphorylation of S62 (Arnold and Sears, 2006). Additionally, B56δ-PP2A-directed dephosphorylation of the protein tyrosine phosphatase cell division cycle 25 (CDC25) deactivates its phosphatase activity, preventing CDC25-mediated cell cycle progression (Margolis et al., 2006). The tumor-suppressor protein p53, which mainly acts as a transcription factor, regulates apoptosis and cell cycle progression in response to cellular stresses dependent on its phosphorylation state (Shouse et al., 2008). In *Drosophila melanogaster*, hyperphosphorylation of the cell death-regulating protein BCL-2, due to knockdown of either of the A, C, or B56 subunits, initiated p53-mediated apoptosis (Li et al., 2002). These are just some examples of PP2A acting as a tumor suppressor protein, regulating key signaling pathways involved in cell growth and survival.

1.7 Objectives

AS is affected by various internal or external stimuli and must be tightly regulated to ensure mRNA integrity and to prevent splicing-associated developmental defects or diseases. Based on the findings that temperature-regulated *U2AF26* AS is mediated via SR protein phosphorylation and blocked upon CLK inhibition (Preußner et al., 2017), we assumed kinases and/or phosphatases to be responsible for temperature-driven AS changes. Therefore, we wanted to address the question of whether and how CLKs or PP1/2A act as temperature sensors and what are the functional consequences. Especially, how does temperature influence disease-associated target GE and AS events?

The body temperature of homeothermic organisms changes 1 °C - 4 °C in a time of the day-dependent manner (Refinetti and Menaker, 1992). Since AS is affected by subtle temperature changes and can generate transcripts harboring PTCs, targeting them to NMD, we wanted to know whether temperature also influences AS coupled to NMD to generate temperature-controlled rhythms in GE.

The minor spliceosome contributes to less than 1 % of splicing events, yet its function is essential for cell survival (Turunen et al., 2013). SRSF10 is the only SR protein harboring a minor intron and represents a special SR protein, as it was shown to switch from a general splicing repressor to a splicing activator via (temperature-dependent) phosphorylation (Cowper et al., 2001; Shin et al., 2004). In this study we aimed to answer the question: How does the minor spliceosome contribute to global GE and splicing regulation?

To address these questions, we used classical biochemical methods in combination with RNA-Seq analyses. We used cell culture-based approaches using different inhibitors (e.g. kinase, phosphatase, or translation inhibitors) and analyzed splicing and GE patterns to investigate underlying biological functions. Application of the CRISPR/Cas9 technology or mutational analyses using minigenes enabled us to gain detailed insights into splicing regulation. RNA-Seq analyses revealed the global effects of temperature or inhibitor treatments on a transcriptome-wide scale.

2 Results

2.1 CLK1/4 and PP1/2A globally control temperature-dependent alternative splicing and gene expression

This subchapter refers to:

*Haltenhof, T., Kotte, A., De Bortoli, F., Schiefer, S., **Meinke, S.**, Emmerichs, A.-K., Petermann, K.K., Timmermann, B., Imhof, P., Franz, A., Loll, B., Wahl, M.C., Preussner, M., Heyd, F. A conserved kinase-based body temperature sensor globally controls alternative splicing and gene expression. Mol Cell. 2020. 78(1):57-69.*

My contribution:
SM generated *CIRBP*-edited cells using CRISPR/Cas9 and characterized temperature- and TG003-dependent *CIRBP* AS and GE.

***Meinke, S.**, Haltenhof, T., Kowar, A., Karni, R., Preussner, M., Heyd, F. Elevated body temperature activates tumor-suppressive phosphatase activity. (in preparation)*

My contribution:
SM cloned and expressed the PP2AC protein, established and performed the *in vitro* phosphatase assays with help from TH and AK. SM performed splicing-sensitive RT-PCR, RT-qPCR analyses, and designed and cloned the minigene mutants. Bioinformatics analyses were performed by MP. SM contributed to designing the study, planning experiments, analyzing the data, and writing the manuscript.

Body temperature cycles were shown to regulate rhythmic and time of the day-dependent AS of numerous exons (Preußner et al., 2017; Preußner and Heyd, 2018). However, the molecular temperature sensors responsive to changes of 1 °C in the physiologically relevant temperature range of 35 °C (mild hypothermia) to 39 °C (fever) remained unknown. SR proteins are fundamental regulators of AS and changes of the phosphorylation state of their RS domain result in differential splicing of target exons. The activity of SR proteins is determined by their phosphorylation state, with higher

phosphorylation levels at a lower temperature or vice versa (Xiao and Manley, 1998; Yeakley et al., 1999). In a former publication it was shown that temperature-dependent SR protein phosphorylation, and consequently their activity, is regulated by CLKs (Preußner et al., 2017). Thus, CLK-mediated SR protein phosphorylation results in temperature-dependent changes in AS.

Subsequently, we wanted to investigate the role of CLKs as potential thermo-sensors. We found CLK1/4 kinase activity to be strongly temperature-dependent within a physiologically relevant temperature range with higher activity at lower temperatures (Figure 2.1, top; performed by Tom Haltenhof). This is consistent with SR protein phosphorylation levels *in vivo* (Preußner et al., 2017). Having determined temperature-dependent CLK1/4 activity *in vitro*, we next wanted to investigate the impact of temperature-driven SR protein phosphorylation on AS and GE *in vivo*. Therefore, we performed RNA-Seq analyses of HEK293 cells, which were pre-entrained at 39 °C for 12 hours (h), treated with the CLK1/4 inhibitor TG003 (Muraki et al., 2004) or dimethyl sulfoxide (DMSO) as a solvent control, and further incubated for 6 h at 35 °C or 39 °C, respectively. We identified around 1700 CE which were alternatively spliced in the DMSO control conditions at 35 °C or 39 °C (Figure 2.1, middle; performed by Marco Preussner). Remarkably, inhibition of CLK1/4 using TG003 resulted in strong impairment of temperature-responsive exon inclusion (Figure 2.1, middle). This argues for the cold-induced CLK activity – and thus SR protein phosphorylation - as one main driver of temperature-dependent AS. Beside their role in AS, SR proteins control other (pre-)mRNA processing events as well, for instance, nuclear export, translation, and degradation (Long and Caceres, 2009). Thus, we next analyzed our RNA-seq dataset for temperature-responsive GE. We found 1064 temperature-sensitive genes in the DMSO control, of which around 50 % completely lost the temperature response after TG003 treatment (data not shown, see publication 1). Together, temperature-driven and CLK-mediated phosphorylation of SR proteins globally controls AS and GE, with wide implications in circadian, tissue-specific, and disease-associated settings.

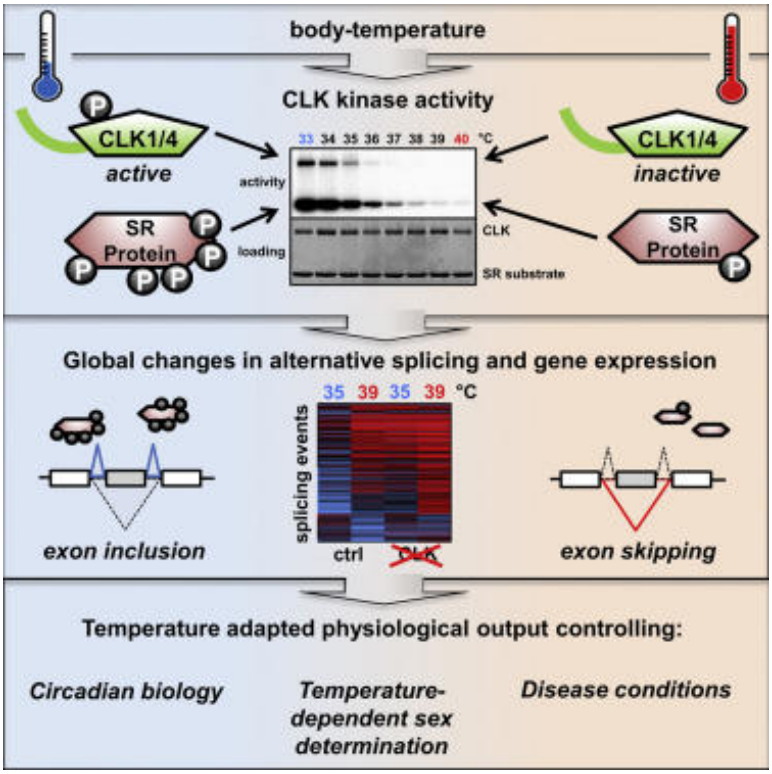

Figure 2.1: CLK1/4 activity globally controls temperature-dependent GE and AS. Body temperature-dependent activity of CLK1/4 results in increased phosphorylation of SR proteins at lower temperatures, while higher temperatures lead to kinase inactivation. Differential SR protein phosphorylation in a physiologically relevant temperature range in turn globally affects AS and GE levels of numerous genes. This has a potential impact on several biological mechanisms, for instance circadian biology, temperature-dependent sex determination, or in disease conditions (Graphical abstract taken from (Haltenhof et al., 2020)).

One especially interesting target, which is temperature- and TG003-responsive, both on AS and on transcript levels, is *CIRBP*. While the *CIRBP* GE levels were upregulated in cold conditions (Figure 2.2 A, 35 °C DMSO), this temperature-response was completely inhibited upon TG003 treatment (Figure 2.2 A, 35 °C TG003). AS analysis of *CIRBP* revealed an alternative 3' end which was promoted at 39 °C in the DMSO control but became temperature-insensitive in CLK1/4-inhibited conditions (Figure 2.2 B). In this warm-induced isoform, an alternative 3' splice site is used, resulting in the inclusion of the alternative last exon 7b (which is coupled to exon 8 inclusion), instead of the canonical last exon 7a (Figure 2.2 B). CLK1/4 inhibition abolished the temperature-sensitivity of this AS event and promoted exon 7b inclusion. We found the sequence downstream of the canonical polyadenylation site to be highly evolutionarily conserved, including the 3' splice site of the alternative 7b exon (Figure 2.2 B, bottom).

Accordingly, we observed heat-induced exon 7b inclusion at higher temperatures resulting in decreased GE levels in primary mouse hepatocytes (Figure 2.2 C and D). We investigated *CIRBP* AS and GE in primary hepatocytes of young mice kept at room temperature (RT) or exposed to lower ambient temperature, resulting in decreased body temperature (Preußner et al., 2017). We found reduced exon 7b inclusion at lower temperatures *in vivo* (Figure 2.2 E, left), which was consistent with enhanced total *CIRBP* transcript levels (Figure 2.2 E, right). This confirms temperature-dependent AS and GE regulation *in vivo*. Next, we generated cell lines lacking *CIRBP* exons 7b and 8 using CRISPR/Cas9 in HEK293 cells (Figure 2.2 F and G). This resulted in increased *CIRBP* mRNA levels and a decreased temperature response in these modified cells (Figure 2.2 H). The remaining temperature sensitivity could be mediated by further mechanisms that affect temperature-dependent *CIRBP* expression.

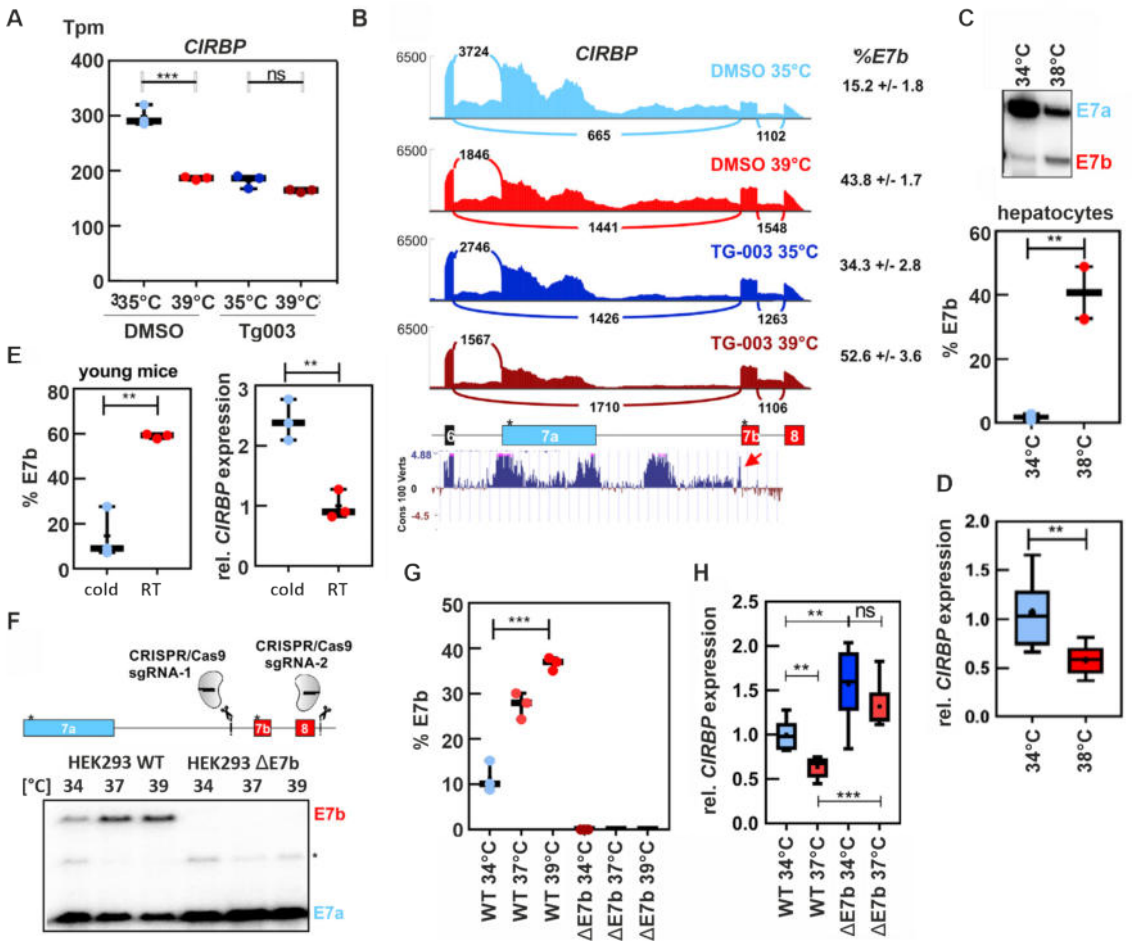

Figure 2.2: Body temperature-regulated CLK1/4 activity controls *CIRBP* AS and GE levels *in vivo*.
(A) *CIRBP* temperature-dependent GE is abolished upon TG003 treatment. Plotted are the Whippet-derived transcripts per million (tpm) values (Sterne-Weiler et al., 2018).
(B) Temperature-dependent AS of the *CIRBP* 3'end. Top: Sashimi Plots showing the read distributions for the different conditions. Right: Percentages of exon 7b (E7b) inclusion (n = 3, mean ± SD). Below: Exon/Intron structure of *CIRBP* pre-mRNA. Exons are depicted as boxes, introns by lines. Asterisks indicate stop codons. Bottom: Basewise comparison among 100 vertebrates by PhyloP from the UCSC genome browser is shown. The red arrow indicates the conserved 3' splice site of E7b.
(C, D) *CIRBP* AS (C) and relative GE levels (D) in mouse primary hepatocytes. AS was investigated by radioactive RT-PCR (C). A representative gel is shown on top and the quantification of E7b inclusion is shown on the bottom (box-whisker-plot with lines representing median and cross representing mean expression levels, n > 2). GE was analyzed by qRT-PCR (normalized to *GAPDH*) (D, box-whisker-plot with lines representing median and cross representing mean expression levels, n = 8).
(E) *CIRBP* AS (left) and GE (right) in the liver of young mice (12-13 days) kept at RT or 18 °C for 2 h (cold) (box-whisker-plot with lines representing median and cross representing mean expression levels, n = 3).
(F, G) CRISPR/Cas9-mediated deletion of *CIRBP* exons 7b and 8 in HEK293 cells. Position of guide RNAs (top) and exemplary gel (bottom) of a splice-sensitive radioactive RT-PCR of *CIRBP* at the indicated temperatures (F) and quantification (G).

(H) Relative *CIRBP* GE in cells lacking the temperature-dependent E7b. Transcript levels were investigated after 12 h incubation at the indicated temperatures by RT-qPCR and plotted in a box-whisker-plot with lines representing median and cross representing mean expression levels (relative to *GAPDH*, $n > 5$). Unpaired t-test derived p-value $^{**}p < 0.01$, $^{***}p < 0.001$. For further information see Publication 1.

After having shown that CLK1/4 act as highly responsive thermo-sensors, which mediate temperature-dependent SR protein phosphorylation and AS (Haltenhof et al., 2020), it is still an open question to which extend phosphatases contribute to SR protein phosphorylation and AS in the physiologically relevant temperature range. To investigate whether phosphatase activity is directly responsive to temperature changes, we expressed a His_{10}-tagged human PP2A catalytic subunit (PP2AC) in High Five insect cells. Purified protein was used in *in vitro* phosphatase assays with dephosphorylation of phosphorylated RS peptide as a read-out. We observed an almost linear increase in PP2AC-mediated dephosphorylation with increasing temperature in the range from 30 °C to 43 °C (Figure 2.3 A and B, $R^2 = 0.9888$, $p < 0.0001$). In the physiologically relevant temperature range between 35 °C and 39 °C there is a 1.4-fold increase in phosphatase activity. This argues for a potential impact of body temperature changes on cellular processes, which are regulated by reversible protein phosphorylation. In contrast to the temperature-mediated on/off-effect on CLK1/4 activity, phosphatase activity changed gradually (Figure 2.3 C). Together with the high abundance of phosphatases in cells (> 50-fold higher than CLK1; (Wang et al., 2015)), this points to an involvement of phosphatases in regulating temperature-dependent phosphorylation levels *in vivo*.

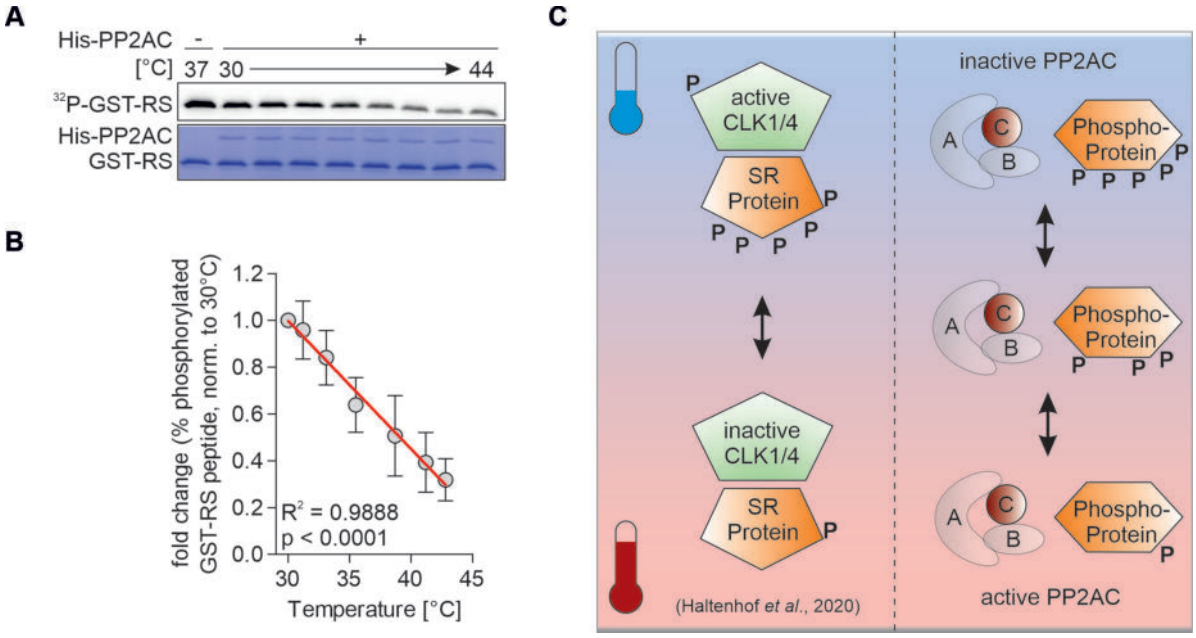

Figure 2.3: Body temperature-regulated SR protein phosphorylation is controlled by PP2A activity.
(A, B) *In vitro* phosphatase assay using purified His_{10}-tagged PP2AC and purified, phosphorylated GST-tagged RS peptide. After SDS-PAGE equal loading was confirmed by Coomassie staining (A, bottom), phosphorylation was detected using autoradiography (A, top) and quantified relative to the highest phosphorylation at 30 °C (n = 5, mean ± SD). The first lane in (A) shows the phosphorylation of the GST-RS substrate at 37 °C in the absence of PP2AC as a control.
(C) Schematic of body temperature-regulated CLK1/4 and PP2A activity. Cold-induced CLK1/4 kinase activity results in autophosphorylation and phosphorylation of SR substrates. In contrast, PP2A activity linearly increases with increasing temperatures leading to substrate dephosphorylation. For further information see Publication 2.

To investigate the potential role of PP2A in temperature-responsive cellular functions, we analyzed AS upon PP2A inhibition using the phosphatase inhibitor OA (Cohen, 1991). HEK293 cells were pre-entrained at 33 °C for 12 h to reduce phosphatase activity and then shifted to 39 °C (or kept at 33 °C) for 2 h in the presence or absence of OA. RNA-Seq analyses using Whippet (Sterne-Weiler et al., 2018) identified 2134 AS events with a change in percentage spliced in (ΔPSI) > 15 % in DMSO 33 °C versus (vs.) 39 °C, of which 1132 events were temperature-controlled CE (Figure 2.4 A). Body temperature-dependent AS was almost completely abolished under phosphatase-inhibited conditions, only 27 CE remained temperature-dependent after PP1/2A activity inhibition. This strongly argues for the involvement of phosphatase activity in temperature-controlled AS. The 39 °C OA-treated samples essentially matched the splicing pattern of the 33 °C DMSO samples, which is consistent with

cold-inhibited PP1/2A activity *in vitro* (compare Figure 2.3 and Figure 2.4 A). We confirmed these global observations using RT-PCR for 4 out of 4 tested target genes (Figure 2.4 B).

In order to compare the impact of body temperature-dependent phosphatase activity with CLK1/4 activity on AS we compared our RNA-Seq data set from the OA treatment to the data obtained from CLK1/4 inhibition using TG003 (Figure 2.4 C, see also (Haltenhof et al., 2020)). A comparison of the temperature-dependent AS events in the DMSO treated cells showed a significant overlap of regulated CE (Figure 2.4 C, top), indicating that there is a comparable effect of temperature on AS despite different temperature profiles. Furthermore, phosphatase inhibition resulted in a cold-like pattern, whereas TG003 treatment shifted the splicing pattern towards heat (Figure 2.4 C). This is consistent with temperature antagonistically controlling CLK1/4 kinase and PP1/2A phosphatase activity. Additionally, in cells treated with OA temperature-regulated AS was almost completely abolished, while in CLK1/4 inhibited conditions some temperature-sensitivity remained. This argues for a potential involvement of additional temperature-responsive kinases, for instance CLK2 and CLK3, which are not inhibited by TG003. In contrast, the inhibited temperature-dependent AS by OA indicates that potentially all phosphatases involved in this regulation are OA-sensitive. Together, these data demonstrate that most of the body temperature-dependent AS events react to PP1/2A inhibition by OA, which argues for PP1/2A to be essential regulators of body temperature-responsive AS.

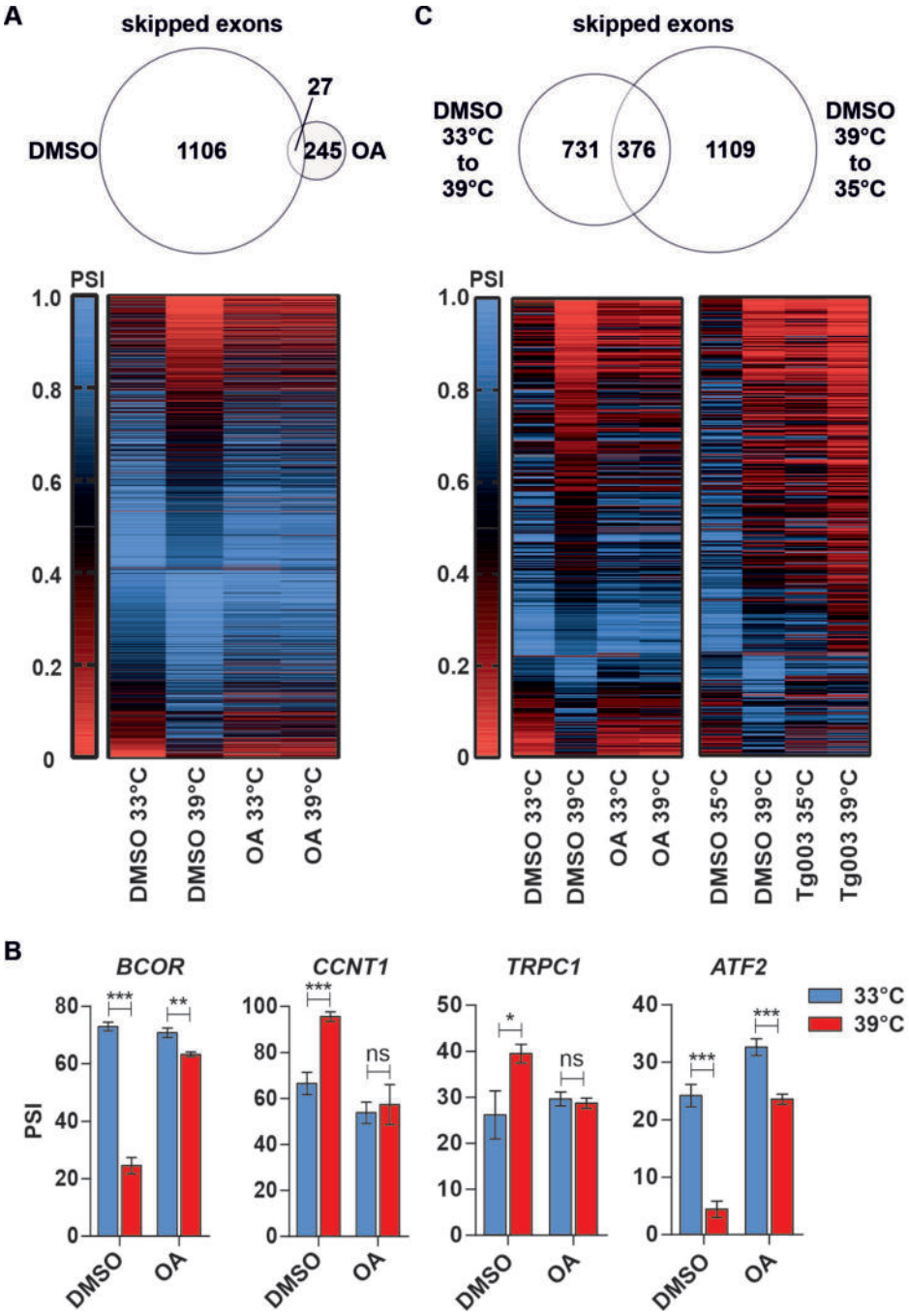

Figure 2.4: Phosphatase inhibition prevents temperature-responsive AS.
(A) Temperature-regulated significantly altered (ΔPSI > 15 % and probability > 0.9) skipped exon events are shown. A Venn diagram illustrates significantly altered CE splicing events in DMSO and OA (top). A heat-map represents mean PSI values of all significantly altered splicing events in DMSO.
(B) Quantifications of splicing-sensitive radioactive RT-PCRs for the validation of temperature- and OA-sensitive *BCOR*, *CCNT1*, *TRPC1* and *ATF2* AS (n = 3, mean ± SD).
(C) Heat-map as in (A) comparing temperature-dependent skipped exon events between PP1/2A-inhibited samples and CLK1/4-inhibited samples (Haltenhof et al., 2020). On top, a Venn diagram showing significantly altered CE events in DMSO-treated control cells shifted from 33 °C to 39 °C or shifted from 39 °C to 35 °C. Student's unpaired t-test-derived p values *p < 0.05, **p < 0.01, ***p < 0.001, ns – not significant. For further information see Publication 2.

For comparison, we next wanted to investigate whether temperature-sensitive GE is also regulated by phosphatases. Indeed, consistent with our splicing data, in OA-treated cells temperature-induced GE changes were almost completely abolished (Figure 2.5 A). In contrast, CLK1/4 inhibition only reduced temperature-sensitivity (Figure 2.5 A). Next, we aimed to investigate the dynamics of temperature-controlled AS and GE. Therefore, HEK293 cells were incubated at 33 °C, 35 °C, 37 °C or 39 °C for 2 (T2) or 12 h (T12) and analyzed by RNA-Seq. High-confidence CE events showed AS changes with a similar amplitude after 2 and 12 h (Figure 2.5 B). In contrast, GE changes were more pronounced after 12 h, showing that temperature-mediated AS changes precede altered GE levels (Figure 2.5 C). These data suggest that body temperature-induced alterations in splicing rewire a transcription factor network to then regulate changes in transcription. Based on this, we investigated which transcription factors are affected by temperature. Transcription factor enrichment analyses (Kuleshov et al., 2016) using linear temperature-dependent genes (Figures 2.5 D and E) revealed that distinct sets of transcription factors control either heat- or cold-induced GE specifically after 12 h (Figure 2.5 F). Interestingly, we found tumor-suppressive transcription factors, such as p53 and SMAD4 (Miyaki et al., 1999; Wang et al., 2018), controlling heat-induced genes; and oncogenes, like MYC and MAX (Cascón and Robledo, 2012; Walz et al., 2014), controlling cold-induced GE. More than 30 % of p53-bound transcripts were specifically upregulated at 39 °C, while more than 20 % of MYC-bound transcripts were upregulated at 33 °C (Figure 2.5 G). In accordance, we found temperature- and OA-dependent GE in 323 cancer-associated genes (Figure 2.5 H; (Futreal et al., 2004)). Also, most of these genes were warm-induced, including many tumor-suppressor genes, indicating a directional effect of temperature on cancer-associated GE programs. These data provide a possible molecular explanation for the use of PP2A inhibitors (O'Connor et al., 2018) and hyperthermia (Ohnishi, 2005) in tumor therapies.

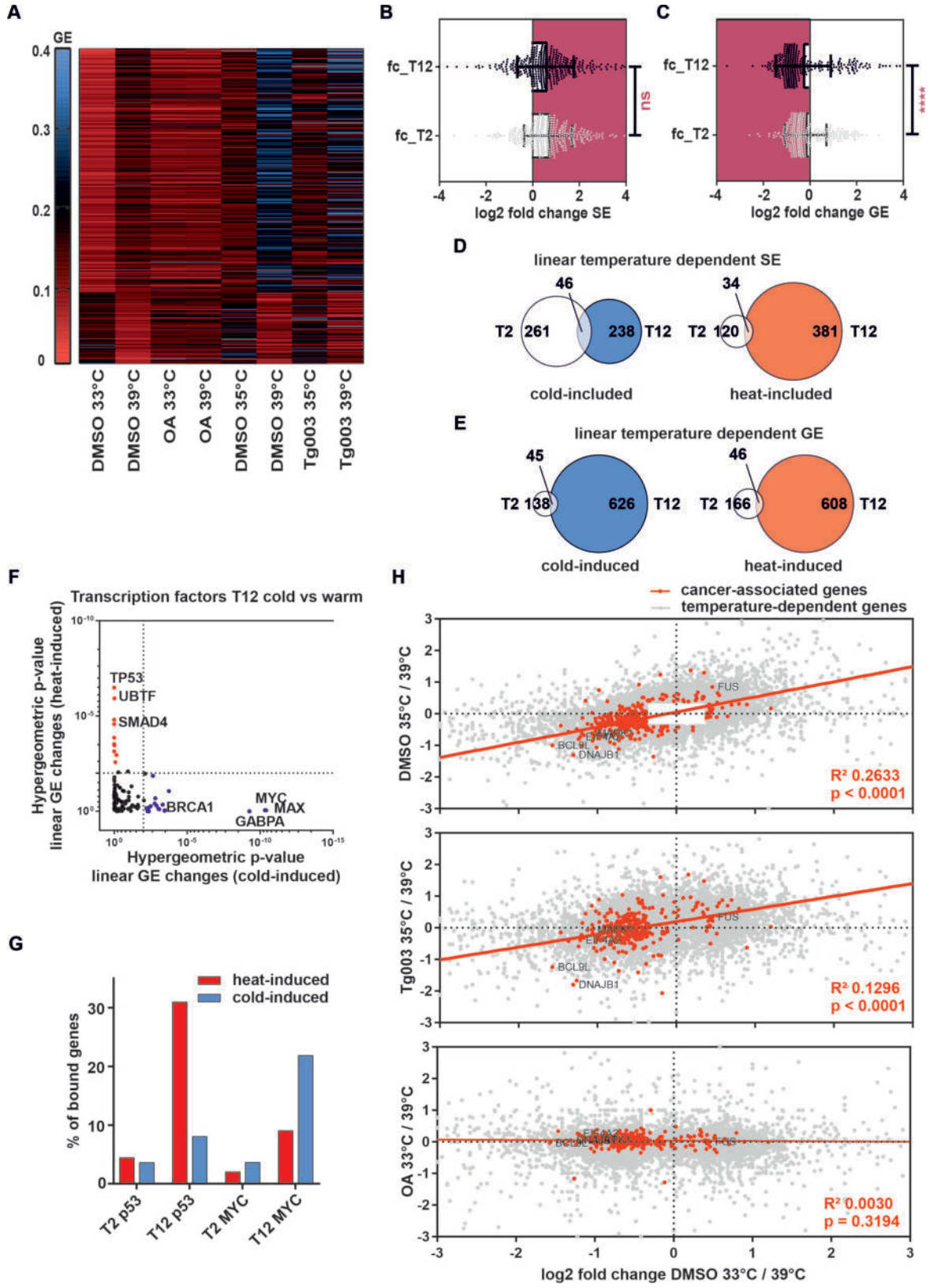

Figure 2.5: Body temperature-regulated expression of cancer-associated genes depends on phosphatase activity.
(A) Heat-map as in Figure 2.4 C showing that in PP1/2A inhibited cells temperature-sensitive GE is almost completely inhibited, whereas some temperature-responsive GE remains after CLK1/4 inhibition using TG003.

(B, C) Analysis of temperature-dependent AS and GE dynamics. (B) For each splicing event the log2 fold change PSI[33 °C] / PSI[39 °C] was calculated for 2 h (fc_T2) and 12 h (fc_T12)(n = 241). Cold-induced exons are indicated in purple. (C) For each gene the log2 fold change GE[33 °C] / [39 °C] was calculated and plotted as in (B). Heat-induced genes after 2 and 12 h are indicated in purple (n = 241).
(D, E) Venn Diagrams comparing linear temperature-dependent skipped exons (SE, D) or GE (E) between 2 and 12 h.
(F) Transcription factor enrichment analysis (Kuleshov et al., 2016) of linear temperature-dependent genes showing heat- and cold-induced GE controlled by distinct sets of transcription factors after 12 h.
(G) Fraction of p53 (left) or MYC (right) bound genes with temperature-dependent GE after 2 or 12 h. Genes with a fold-change (33/39 °C) larger than 1.5 are categorized as heat-induced or cold-induced.
(H) Linear regression fit comparing GE changes in DMSO 33 °C vs. 39 °C to DMSO 35 °C vs. 39 °C (top), TG003 35 °C vs. 39 °C (middle), or OA 33 °C vs. 39 °C (bottom). Plotted are all genes which are temperature-dependent either in DMSO 33 °C vs. 39 °C or in DMSO 35 °C vs. 39 °C (fold-change > 1.3; n = 9217). Highlighted in red are all cancer-associated genes (n = 323; based on (Futreal et al., 2004)). For cancer associated-genes the goodness of fit is indicated by R^2 and p-values. The 5 cancer-associated genes *BCL9L*, *DNAJB1*, *EIF4A2*, *MAPK1*, and *FUS* are highlighted. Student's t test-derived p-values, ****p < 0.0001, ns – not significant. For further information see Publication 2.

To find a potential connection of temperature-dependent AS after 2 h and altered p53 target GE after 12 h we screened for fast altered splicing events in cancer-associated genes. We identified 66 alternatively spliced genes, which are temperature-dependent and mostly react to phosphatase inhibition but not to TG003 treatment (Figure 2.6 A). One interesting AS event is the differential inclusion of exon 6 of the p53 regulator MDM4 (Figure 2.6 B). The *MDM4* exon 6 skipping isoform has been described to be targeted by the NMD pathway, resulting in reduced MDM4 protein levels (Bezzi et al., 2013). Heat-induced exon 6 skipping activates p53, correlating with increased p53 target genes. *MDM4* AS is also antagonistically affected by OA and TG003 (Figure 2.6 B), which could be mediated by altered SRSF3 activity due to differential phosphorylation levels (Dewaele et al., 2016). We propose a mechanistic model for the temperature-controlled expression of *P53* and deliver a potential explanation for the requirement of *P53* WT expression for successful thermotherapy.

However, we would like to point out that other heat-induced splicing isoforms were also described as oncogenic. One particularly interesting heat-induced, oncogenic splicing event is AS of the *MKNK2* gene. Usage of an alternative 3' splice site in its last exon 14 (E14) results in two different isoforms: the tumor-suppressive isoform

Mnk2a containing a binding site for MAP kinases, and the oncogenic Mnk2b isoform lacking the MAPK-binding site. Our RNA-Seq analysis clearly shows that *MKNK2* AS is strongly temperature-dependent with an increase in oncogenic Mnk2b at higher temperatures (Figure 2.6 C). Using radioactive RT-PCR we confirmed *MKNK2* AS to be temperature-depended and controlled by PP1/2A but not CLK1/4 (Figure 2.6 D). To identify the *cis*-regulatory element responsible for temperature-controlled *MKNK2* AS we used mutational analysis of an *MKNK2* minigene harboring the sequence ranging from E13 to E14 (Figure 2.6 E, left). First, we deleted the majority of E14a (1,800 nucleotides) via mutational PCR. The resulting minigene was still responsive to temperature changes, with a significant induction of oncogenic Mnk2b splicing at 39 °C (Figure 2.6 E, right). However, by further deleting nucleotides in E14a we identified a 148 nucleotide sequence, whose absence completely abolished heat-induced splicing changes (Figure 2.6 E).

With these data we showed that temperature-dependent phosphatase activity globally controls AS and GE levels and identified a potential molecular mechanism for PP1/2A-based cancer therapy and thermotherapy for p53 WT tumors. Additionally, identification of the *cis*-regulatory element responsible for temperature-regulated oncogenic *MKNK2* AS enables new possibilities for therapeutics in Mnk2b-driven cancers.

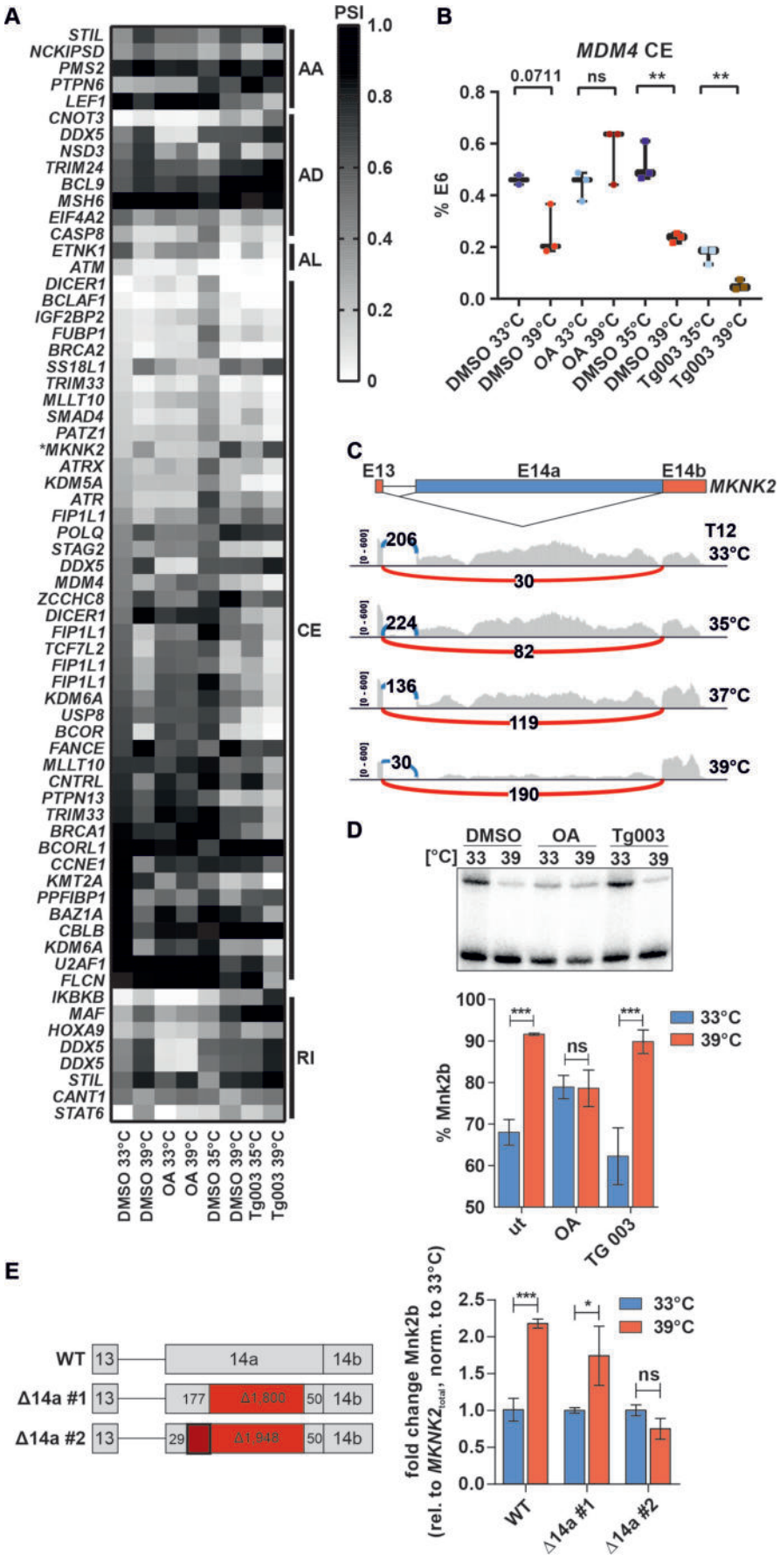

Figure 2.6: PP1/2A control AS of cancer-associated genes in a temperature-dependent manner.

(A) Heat-map of all cancer-associated, temperature-dependent AS events. Gene names are shown on the left, the splicing type is indicated on the right. AA - alternative acceptor site, AD - alternative donor site, AL - alternative last exon, CE - cassette exon, RI - retained intron. * The complicated AS event at the 3'end of *MKNK2* (see Figure (C)) escaped our Whippet analysis, PSI values are based on manual quantification of Sashimi blots.
(B) AS of *MDM4* exon 6 is strongly temperature- and OA-dependent, but less affected by CLK1/4 inhibition. PSI values are derived from Whippet (Sterne-Weiler et al., 2018).
(C) Sashimi plots showing temperature-dependent AS of *MKNK2* Exon 14 (E14). Warm temperatures favor the usage of an alternative 3' splice site in E14 leading to the production of the oncogenic Mnk2b isoform.
(D) Radioactive RT-PCR showing that temperature-dependent *MKNK2* splicing is OA- but not TG003-sensitive. Top: representative gel, bottom: quantification.
(E) Left: Schematic of mutated minigenes to identify the *cis*-regulatory element responsible for temperature-controlled *MKNK2* AS. Regions marked in red were deleted by PCR. Dark red box indicates a region of 148 nucleotides, which is crucial for temperature-mediated *MKNK2* AS. Right: qPCR analysis of Mnk2b (relative to total *MKNK2*, normalized to 33 °C)(n = 3, mean ± SD). Statistical significance was determined by unpaired t-tests. *$p < 0.05$, **$p < 0.01$, ***$p < 0.001$, ns – not significant. For further information see Publication 2.

2.2 AS-NMD shapes the temperature-dependent transcriptome

This subchapter refers to:

*Neumann, A., **Meinke, S.**, Goldammer, G., Strauch, M., Schubert, D., Timmermann, B., Heyd, F., Preussner, M. (2020) Alternative splicing coupled nonsense-mediated decay shapes the temperature-dependent transcriptome. (submitted)*

My contribution:
SM performed *CIRBP* and *SRSF10* RT-PCR and RT-qPCR analyses, generated the *SRSF2*-edited cell line using CRISPR/Cas9, and characterized temperature-dependent AS and GE. SM helped with writing the manuscript.

Subtle body temperature changes regulate AS of numerous exons and in our studies, we identified CLK1/4 and PP1/2A as central mediators to control splicing by temperature-dependent phosphorylation of SR proteins in the physiologically relevant temperature range. SR proteins autoregulate their expression levels by the inclusion of an NMD-inducing exon (Sureau et al., 2001; Ni et al., 2007). Besides SR proteins, hnRNPs and other RBPs can be subjected to AS-NMD (Lykke-Andersen and Jensen, 2015) and, therefore, AS-NMD can globally alter GE. In this study, we wanted to investigate to which extend AS-NMD is regulated by temperature changes and how this mechanism globally shapes body temperature-dependent GE.

To address these questions, we used primary mouse hepatocytes as a model system to first identify NMD-inducing splice isoforms. Therefore, the cells were incubated at 34 °C or 38 °C and treated with cycloheximide (CHX) or DMSO as solvent control. As NMD is a co-translational process, we used CHX as a translation inhibitor, which in turn also blocks the NMD pathway (Hurt et al., 2013). Among others, our RNA-Seq approach identified over 60 RBPs with temperature-regulated NMD exons (RNA-Seq analyses were performed by Alexander Neumann).

Two particularly interesting targets, which were already mentioned before, were *CIRBP* and *SRSF10*. In line with CLK-regulated CIRBP activity and reduced *CIRBP* GE levels upon exon 7b inclusion (see chapter 2.1, (Haltenhof et al., 2020)), we now

show that the production of the exon 7b-containing isoform was promoted at a higher temperature (Figures 2.7 A and B, left). CHX stabilized the exon 7b splice variant (Figure 2.7 A, left), resulting in a particularly high abundance at 38 °C, which correlated with reduced GE levels at higher temperatures (Figure 2.7 A and B, left). In contrast, we found cold-induced inclusion of the regulatory *SRSF10* exon 3 (see also chapter 2.3 for further information on this *SRSF10* splicing event), which was more pronounced after CHX treatment, correlating with reduced *SRSF10* mRNA abundance (Figure 2.7 A and B, right). To investigate whether body temperature cycles could result in oscillating splicing of NMD exons, leading to rhythms in GE, we incubated HEK293 cells for 72 h under 12 h square-wave temperature cycles at 34 °C or 38 °C, respectively, and analyzed the productive *SRSF2* and *SRSF10* GE levels (Figure 2.7 C and D). AS of *SRSF2* and *SRSF10* responded to the temperature rhythms, resulting in oscillating GE levels in a 24 h rhythm (Figure 2.7 D). *SRSF2* showed decreased expression during the warm phase, while *SRSF10* GE levels were upregulated. This is consistent with the data from mouse hepatocytes pointing to a cell type-independent and evolutionarily conserved mechanism for temperature-mediated SR protein regulation (Figure 2.7 D). This conservation is further in agreement with previously described findings, that not only in SR protein-coding genes but for all RBPs, NMD-inducing exons harbor highly conserved sequences (Lareau et al., 2007; Thomas et al., 2020). Already after 4 to 8 h of incubation at one temperature the expression levels changed, which indicates that AS of the NMD-targeted isoform is under control of an autoregulatory feedback loop (Figure 2.7 D). Next, we generated CRISPR/Cas9-edited HEK293 cells lacking the temperature-dependent exon 3 of either *SRSF2* (SRSF2ΔE3) or *SRSF10* (SRSF10ΔE3). In both cell lines, removing the temperature-sensitive exon resulted in a loss of rhythmic GE when the cells were incubated under square-wave temperature rhythms (Figure 2.7 D). These data show that GE levels of some RBPs are regulated by a temperature-sensitive AS event, which leads to an NMD-inducing isoform. In *CIRBP* and *SRSF10* NMD exon inclusion anticorrelates with GE levels, which could globally affect essential functions in splicing and GE.

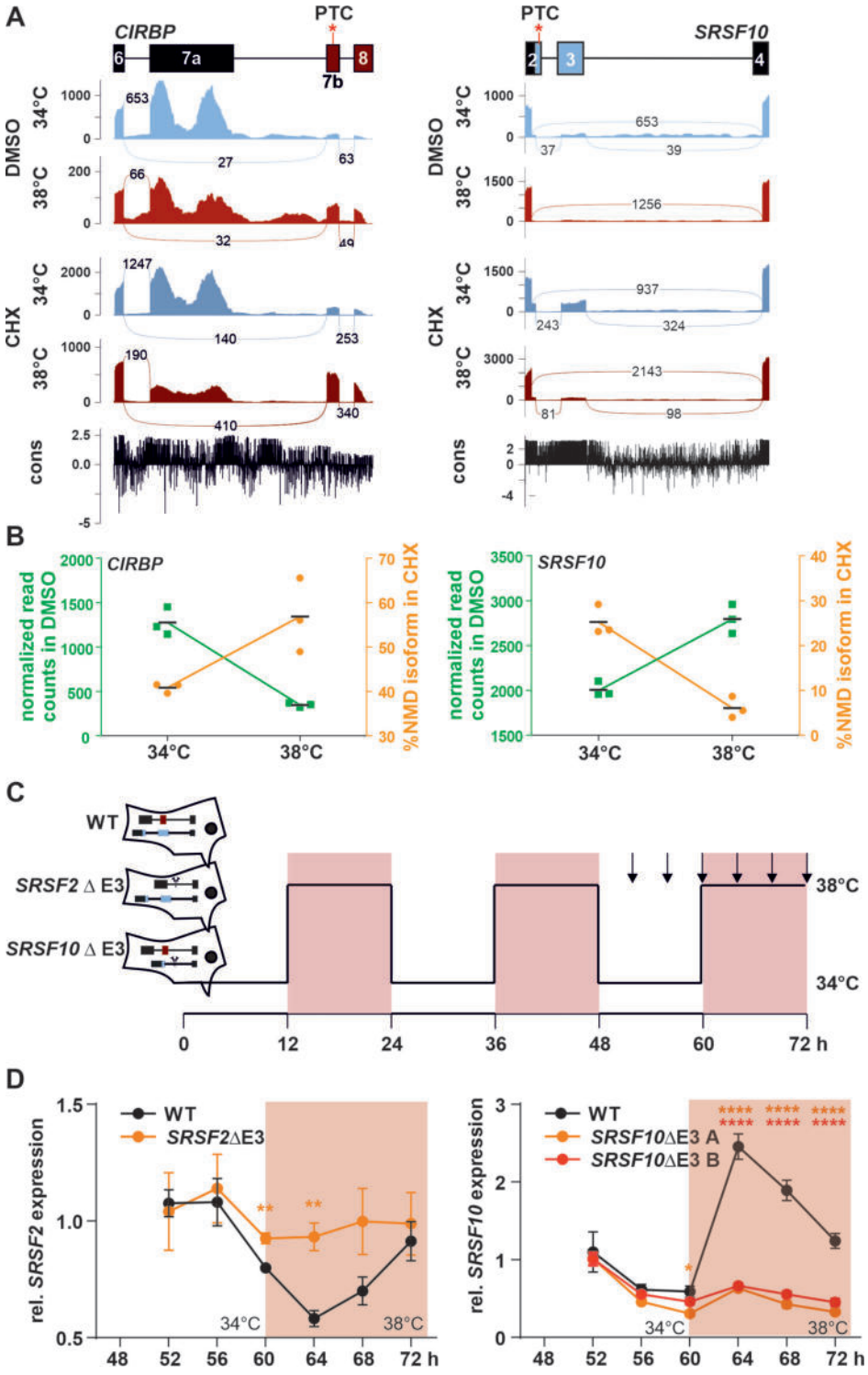

Figure 2.7: Temperature-dependent AS-NMD controls GE levels of RBPs.
(A, B) Temperature-sensitive AS-NMD events for *CIRBP* (left) and *SRSF10* (right). (A) On top, the exon/intron structure is shown, in the middle Sashimi plots show the distribution of raw sequencing reads, and below the sequence conservation across placental species is indicated. (B) Normalized read counts and percentage of the NMD isoform in CHX at 34 °C and 38 °C are plotted.
(C) To analyze rhythmic GE in WT and CRISPR/Cas9-edited HEK293 cells, the cells were temperature-entrained over 3 days (12 h at 34 °C and 38 °C, respectively). Arrows indicate the time points at which cells were harvested.

(D) *SRSF2* and *SRSF10* GE levels in WT HEK293 cells and cells lacking the NMD exon 3 either in *SRSF2* or *SRSF10*, respectively, were analyzed by RT-qPCR (relative to *GAPDH*). Expression is normalized to the time point 52 h. For *SRSF10* two independently generated cell clones were analyzed ((B) n = 3, (C) n = 4, mean ± SEM). Statistical significance was determined using unpaired t-test, p-values *$p < 0.05$, **$p < 0.01$, ****$p < 0.0001$. For further information see Publication 3.

2.3 SRSF10 and the minor spliceosome control tissue-specific and dynamic SR protein expression

This subchapter refers to:

***Meinke, S.**, Goldammer, G., Weber, A.I., Tarabykin, V., Neumann, A., Preussner, M., Heyd, F. Srsf10 and the minor spliceosome control tissue-specific and dynamic SR protein expression. Elife. 2020 Apr 27;9. Doi: 10.7554/eLife.56075*

My contribution:
SM performed wet lab experiments with GG and with help from MP. SM contributed to planning experiments, analyzing the data, and writing the manuscript.

As mentioned above, SR proteins play a crucial role in AS regulation. SR proteins contain ultraconserved elements in alternative exons that control the presence of PTCs, allowing them to regulate their abundance by NMD (Lareau et al., 2007). So far, autoregulation has been described for several SR proteins (Lejeune et al., 2001; Sureau et al., 2001), but not for SRSF10.

In *SRSF10* the conserved region harbors two competing 5' splice sites in exon 2 (E2). While usage of the upstream (up) minor splice site is coupled to E4 inclusion and production of a protein-coding mRNA, the use of the downstream (dn) major splice site leads to E3 inclusion, the presence of a PTC, and the employment of an alternative polyadenylation site in E3 (Figure 2.8 A). The dn-E3 variant is not a canonical NMD target, as the stop codon in E2 is less than 50 nucleotides upstream of the E2/3 junction (Nagy and Maquat, 1998) and thus could encode for a hypothetical short protein (SRSF10-s, see below). In an experimental approach we combined an *SRSF10* minigene, containing mouse exons 2 to 4 (Figure 2.8 B, top), and siRNA-mediated knockdown of endogenous human *SRSF10* in HeLa cells. This revealed strong autoregulation of SRSF10 (Figure 2.8 B, bottom). AS of *SRSF10* results in three possible protein isoforms: SRSF10-fl (inclusion of exon 7a), SRSF10-2 (inclusion of exon 7b, see Figure 2.8 A), and the hypothetical short protein variant SRSF10-s. Rescue experiments using

GFP-tagged SRSF10 mouse variants (not targeted by human-specific siRNA) showed that SRSF10-fl and SRSF10-2 rescued the dn-E3 splicing defect upon knockdown, whereas overexpression of the SRSF10-s isoform did not affect *SRSF10* AS (Figure 2.8 C). These findings confirmed SRSF10-fl and SRSF10-2 as activators of *SRSF10* E3 inclusion. However, the SRSF10-s variant was hardly detectable, suggesting high protein instability and no biological function. Using systematic mutational analyses of the minigene we identified the *cis*-regulatory element required for SRSF10 autoregulation (Figure 2.8 D). We used the sequence of *GMFB* exon 4 to 5, as *GMFB* intron 4 is also a minor intron. Replacing nucleotides 17 to 60 by the *GMFB* exon 4 sequence was sufficient to abolish SRSF10-mediated AS (Figure 2.8 E, ESE). We identified a GA-rich element as an *SRSF10*-dependent ESE. These data revealed a conserved element in *SRSF10* exon 3, which is necessary for an autoregulatory feedback loop that controls *SRSF10* expression levels.

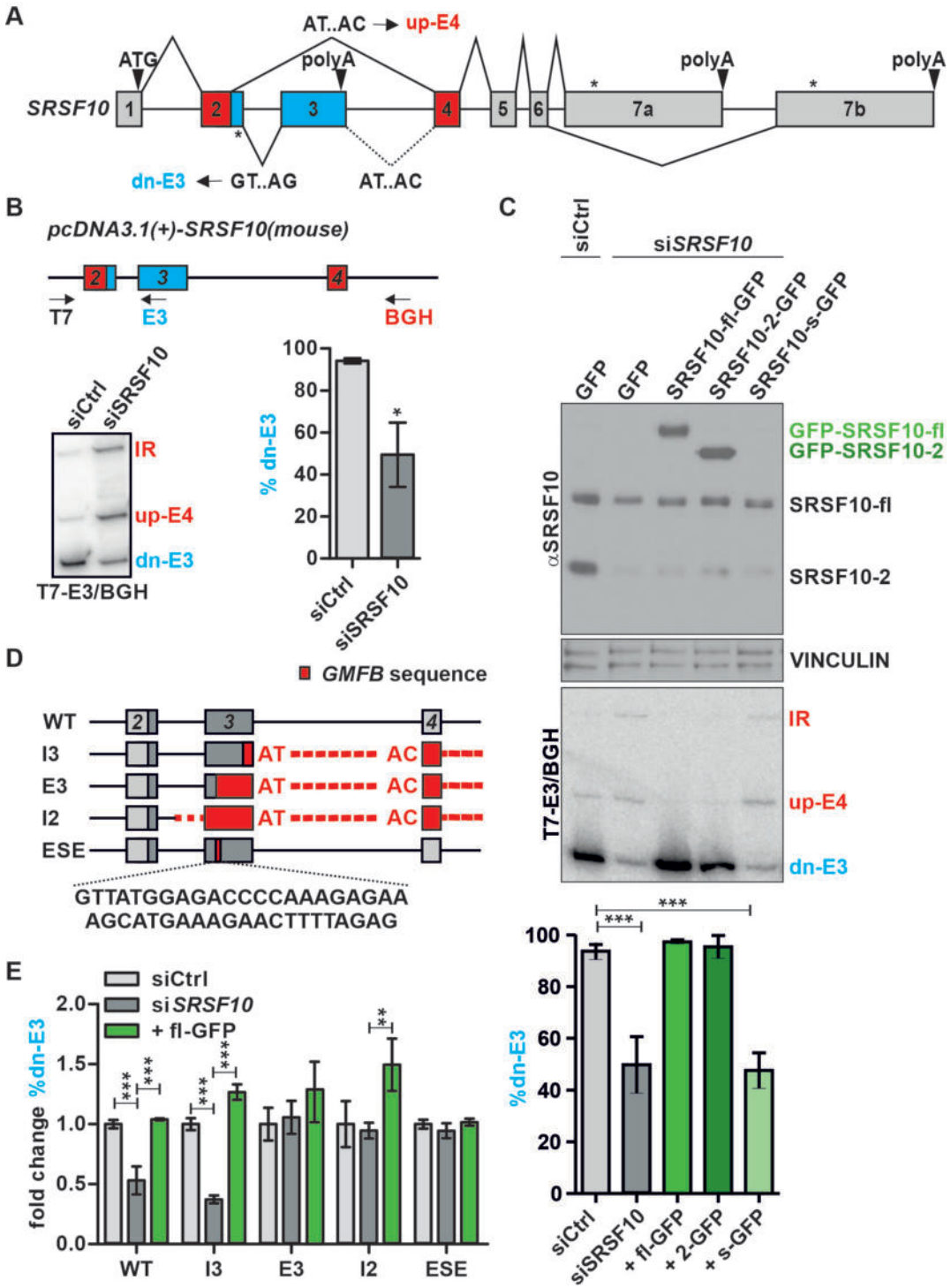

Figure 2.8: SRSF10 autoregulates its splicing through a conserved enhancer in exon 3.
(A) Schematic of the exon/intron structure of *SRSF10*. Usage of the downstream (dn) major splice site in *SRSF10* exon 2 (GT..AG) leads to exon 3 inclusion and a non-protein coding isoform, while usage of the upstream minor splice site (AT..AC) results in exon 4 inclusion. A minor 5' splice site in exon 3 is present but not used in the endogenous context (dotted lines). * indicate stop codons.
(B) *SRSF10* minigene splicing upon siRNA-mediated knockdown of endogenous *SRSF10* in HeLa cells. Top: exon/intron structure of the *SRSF10* minigene reporter containing mouse exons 2 to 4 (and complete intervening introns) with indicated primer binding sites (arrows). Bottom: exemplary gel and quantification of the dn-E3 isoform splicing after knockdown of endogenous *SRSF10* (n = 5, mean ± SD).

(C) Knockdown and rescue of SRSF10. Top: Western Blot of SRSF10 after siRNA-mediated knockdown and transfection with overexpression vectors for the different GFP-tagged SRSF10 isoforms. VINCULIN was used as a loading control. Middle: Exemplary gel of *SRSF10* minigene splicing upon knockdown and rescue. Bottom: Quantification of the dn-E3 isoform ($n \geq 3$, mean ± SD).
(D) Exon/intron structure of the *SRSF10* minigenes used for mutational analysis. Below the sequence of the identified ESE is shown.
(E) Quantification of *SRSF10* minigene splicing upon knockdown and rescue. Splicing of mutants is shown relative to the WT from Figure (B) and for each mutant relative to the Ctrl siRNA ($n = 5$, mean ± SD). Student's t test-derived p values *$p < 0.05$, **$p < 0.01$, ***$p < 0.001$. See Publication 4 for further information.

SRSF10 E2 contains two competing 5' splice sites which are specifically recognized either by the minor or the major spliceosome. To investigate the importance of this splice site competition for SRSF10 autoregulation, we generated minigenes with either major or minor splice sites and analyzed AS of these constructs (Figure 2.9 A). We found that in control conditions (siCtrl) minigenes harboring either only major or only minor splice sites showed a strong increase in exon 4 usage, while exon 3 was hardly included (Figure 2.9 B). Since both mutated minigenes remained responsive to SRSF10 knockdown and overexpression, SRSF10 can regulate AS through both the major and the minor spliceosome. In the presence of directly competing 5' splice sites in exon 2, the downstream splice site, leading to exon 3 inclusion and a non-productive mRNA isoform, was no longer used. This suggests that, *in vivo*, *SRSF10* AS, resulting in a protein-coding isoform, is negatively controlled through the presence of a competing (and favored) downstream major splice site in exon 2. Next, we performed siRNA-mediated knockdown of the fundamental U11/U12 component *RNPC3* to reduce minor spliceosome abundance and thereby its activity (Figure 2.9 C). Indeed, expression of the protein-coding *SRSF10* up-E4 isoform was significantly decreased, while the levels of the non-coding dn-E3 variant remained unaffected (Figure 2.9 C). Together, these data link the abundance of the minor spliceosome, and thus its activity, to *SRSF10* GE by regulating productive vs. non-productive AS.

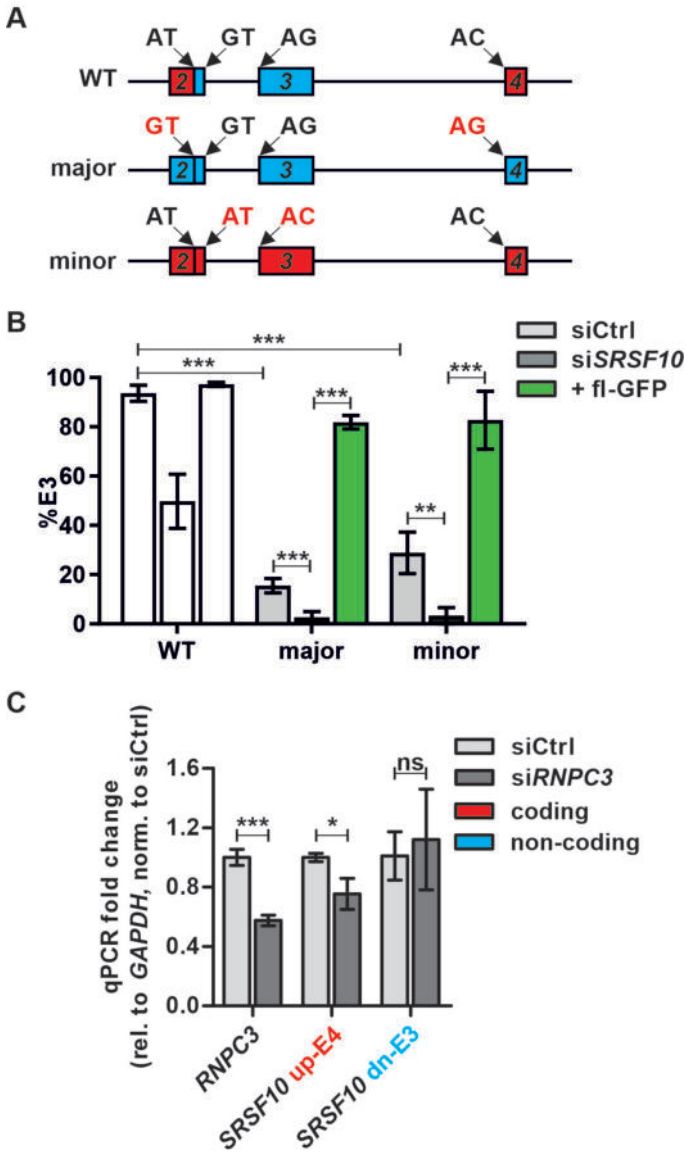

Figure 2.9: The minor spliceosome controls *SRSF10* expression.
(A) Schematic of the exon/intron structure of WT and mutated *SRSF10* minigenes harboring either only major (GT..AG, blue) or minor (AT..AC, red) splice sites.
(B) Quantification of AS-sensitive PCRs of the minigenes from (A) (relative to WT from Figure 2.8, n = 4, mean ± SD).
(C) qPCR confirmed knockdown of *RNPC3* (left) and *SRSF10* expression levels (right) (n = 4, mean ± SD). Student's t-test-derived p values *p < 0.05, **p < 0.01, ***p < 0.001. See Publication 4 for further information.

To further investigate this regulatory mechanism *in vivo*, we analyzed RNA sequencing data from 25 different mouse tissues and compared *SRSF10* and *RNPC3* GE levels, respectively. Calculated tpm values using Whippet (Sterne-Weiler et al., 2018) revealed tissue-specific GE for both *SRSF10* and *RNPC3* (Figure 2.10 A). Linear regression analysis showed an almost perfect correlation of *SRSF10* and *RNPC3* GE across the 25 tissues

in mouse ($R^2 = 0.85$, $p < 0.0001$, Figure 2.10 B). In contrast, the levels of the housekeeping gene *GAPDH*, which contains no minor intron, did not correlate with *RNPC3* (Figure 2.10 C). Similarly, *SRSF10* and *RNPC3* GE levels significantly correlated across 31 human tissues ($R^2 = 0.33$, $p = 0.0007$) and during neuronal development of mouse embryonic stem cells (ESCs) as an additional model system ($R^2 = 0.33$, $p = 0.0006$, Figure 2.10 D and E). These results, together with our minigene and knockdown data, indicate that minor spliceosome activity regulates *SRSF10* GE levels in a tissue-specific manner and during development.

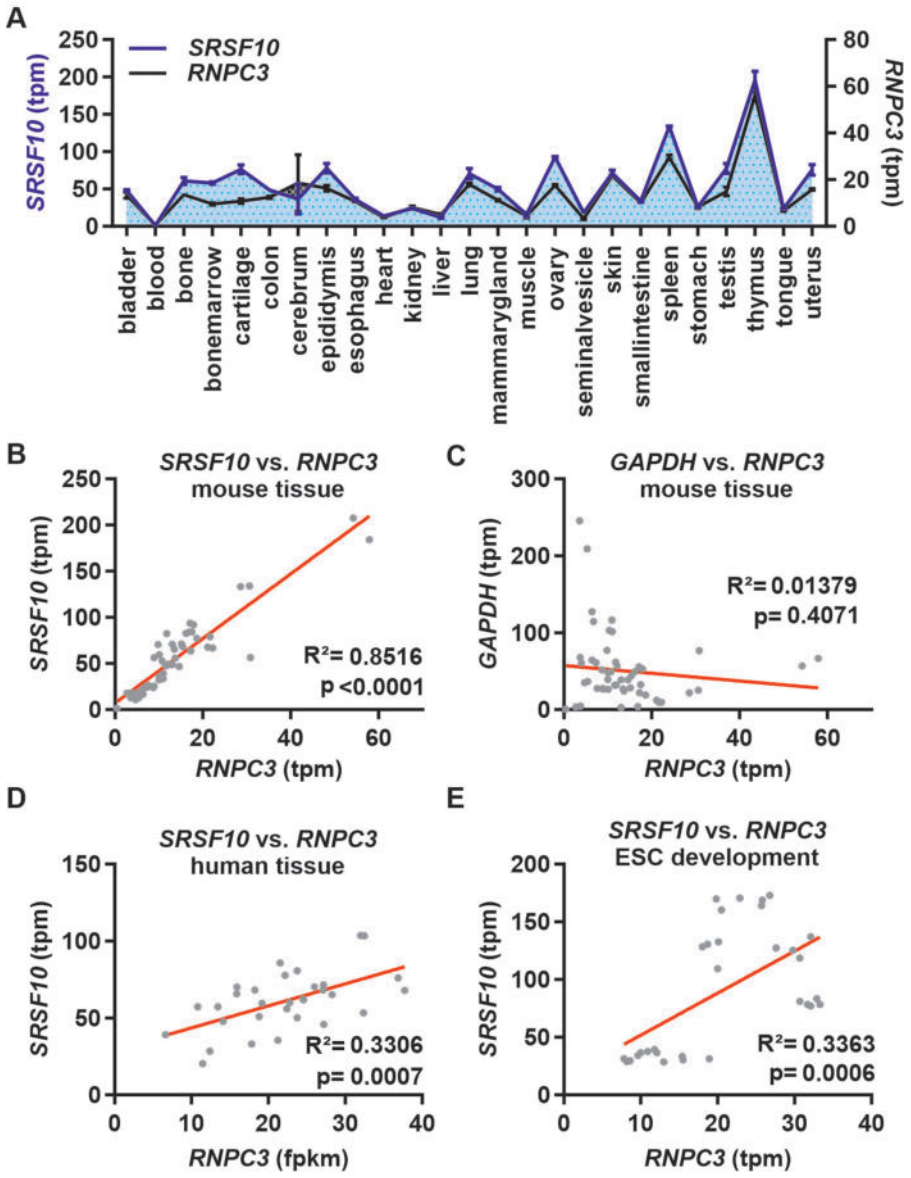

Figure 2.10: Minor spliceosome and *SRSF10* expression correlate in a tissue-specific manner.
(A) Relative GE levels (tpm values) of *SRSF10* and *RNPC3* across 25 mouse tissues.
(B, C) Linear regression analyses for comparison of *SRSF10* (B) and *GAPDH* (C) tpm values with *RNPC3* in 25 different mouse tissues.
(D) Linear regression fit of *SRSF10* and *RNPC3* vs. expression (fragments per kilobase of exon model per million reads mapped (fpkm)) across 31 human tissues (Uhlén et al., 2015).
(E) Correlation analysis of calculated tpm values for *SRSF10* vs. *RNPC3* in differentiating mouse ES cells (Hubbard et al., 2012). See Publication 4 for further information.

Having shown that the minor spliceosome controls *SRSF10* expression levels, we now investigated whether minor spliceosome activity also affects GE levels of other SR proteins in a tissue- and developmental stage-specific manner. Interestingly, we found that expression of all SR proteins correlated with the minor spliceosome, represented

by *RNPC3*, in the 25 analyzed mouse tissues ($R^2 > 0.42$, $p < 0.0001$, Figure 2.11 A). In addition, we found a significant correlation of all SR proteins with *RNPC3* during neuronal differentiation of mouse ES cells (see Publication 4). To experimentally confirm these results *in vivo*, we isolated RNA from mouse cerebral cortices from embryonic days (E) 12.5 and 15.5. qPCR analysis showed significantly increased *RNPC3* GE levels during the transition from E 12.5 to E 15.5 (Figure 2.11 B) and the same is true for *SRSF10* (Figure 2.11 C). In line with that, GE levels of other tested SR proteins were upregulated as well (Figure 2.11 C). These results are consistent with our model that higher minor spliceosome activity, indicated by higher *RNPC3* abundance, results in preferential usage of the *SRSF10* up-E4 minor splice site, leading to increased protein-coding *SRSF10* mRNA levels. Concerted upregulation of other SR proteins indicates a co-regulation of SR proteins, even though SRSF10 is the only SR protein harboring a minor splice site. We hypothesize that *SRSF10* levels could directly influence the levels of other SR proteins, as SR proteins are known to cross-regulate each other (Bradley et al., 2015). To test this, we made use of our CRISPR/Cas9-edited cell line lacking the non-productive *SRSF10* exon 3 and observed increased *SRSF10* expression (Figure 2.11 D for protein expression, Figure 2.11 E for mRNA levels). Interestingly, the less active SRSF10-2 isoform, resulting from differential last exon splicing, showed a higher protein level compared to SRSF10-fl (Figure 2.11 D), indicating that this isoform could be used to partially compensate for the loss of autoregulation via exon 3. Furthermore, the upregulation of *SRSF10* GE levels in the CRISPR/Cas9-edited cell line was sufficient for the increase of mRNA levels of all other SR proteins (Figure 2.11 E). Based on these results, we conclude that minor spliceosome activity directly controls *SRSF10* GE levels, which in turn is sufficient to change the expression levels of all other SR proteins in a tissue- and differentiation stage-specific manner (Figure 2.11 F). These data suggest a mechanism through which the minor spliceosome controls major intron splicing by differentially controlling SR protein levels.

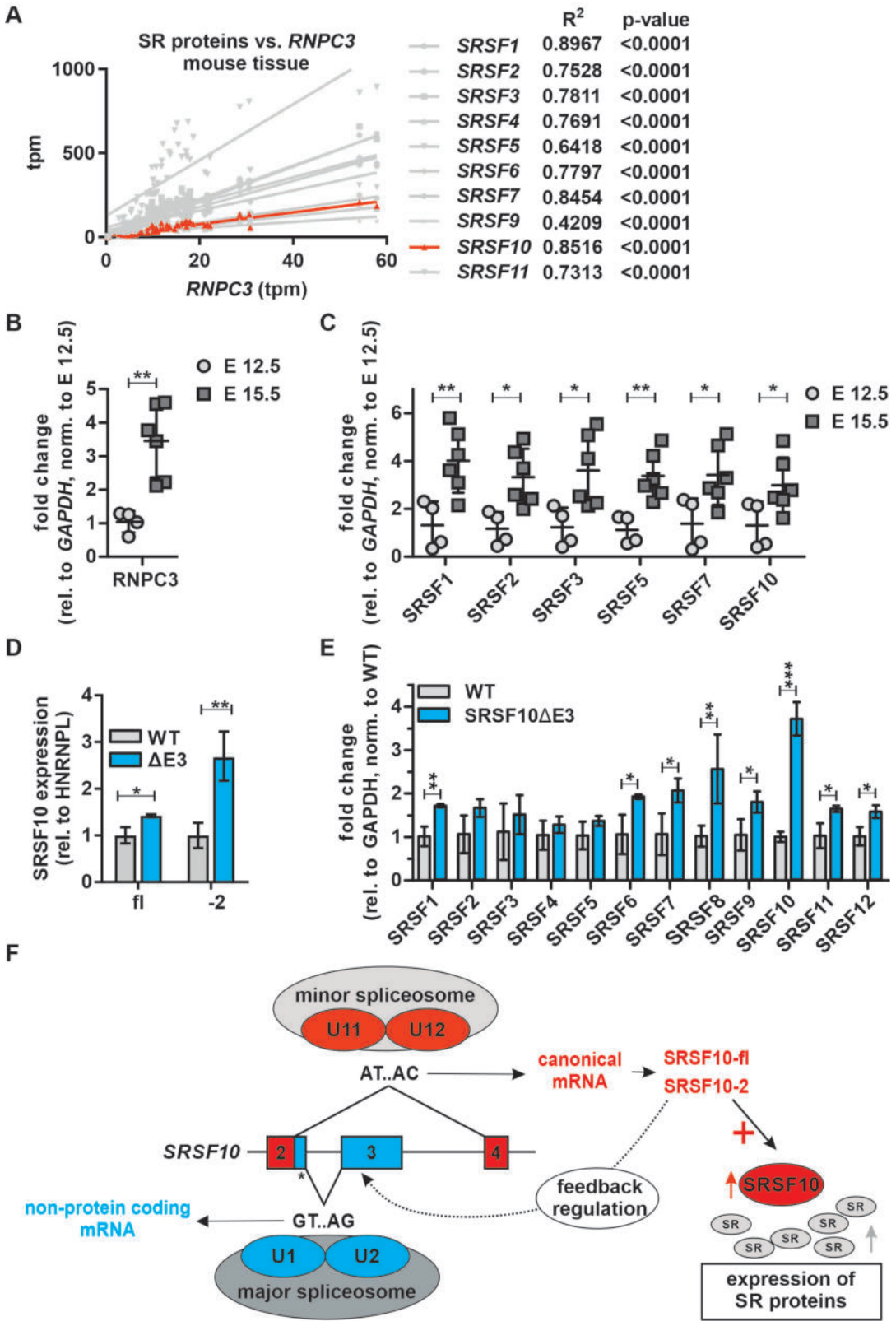

Figure 2.11: SRSF10 and the minor spliceosome control tissue-specific SR protein expression.
(A) Linear regression analysis of calculated tpm values for SR proteins against *RNPC3* in 25 different mouse tissues. *SRSF12* was omitted due to generally low expression levels.
(B) qPCR of *RNPC3* in mouse cortex samples of E 12.5 and E 15.5 (relative to *GAPDH*, normalized to E 12.5, n ≥ 4, mean ± SD).

(C) GE levels of SR proteins in the mouse cortex of E 12.5 and E 15.5. For *SRSF10* only the up-E4 isoform was analyzed (relative to *GAPDH*, normalized to E 12.5, $n \geq 4$, mean ± SD).
(D) Quantification of Western Blots of SRSF10-fl and SRSF10-2 in CRISPR/Cas9-edited HEK293 cells lacking the autoregulatory exon 3 (ΔE3, relative to HNRNP L, $n = 3$, mean ± SD).
(E) Relative SR protein expression in WT or SRSF10ΔE3 HEK293 cells. For *SRSF10* only the functional up-E4 isoform was analyzed (relative to *GAPDH*, normalized to WT, $n = 3$, mean ± SD).
(F) Model for minor spliceosome-mediated control of SR proteins. Statistical significance was determined by an unpaired t-test, $^{*}p < 0.05$, $^{**}p < 0.01$, $^{***}p < 0.001$. For further information see Publication 4.

3 Discussion

3.1 CLK1/4 and PP1/2A globally control temperature-dependent AS and GE

The body temperature of homeothermic organisms is tightly controlled to be stable in a narrow range. However, body temperature oscillates in a circadian manner within 1 °C – 4 °C (Buhr et al., 2010; Refinetti and Menaker, 1992). But a molecular sensor capable of sensing these minor changes and translating them into biological processes remained enigmatic. Especially, whether and how these subtle changes in the core body temperature have an impact on AS and GE remained elusive.

In this work we show that both kinase and phosphatase activity is extremely sensitive to small temperature changes in the physiologically relevant range. We identified the evolutionarily conserved, thermo-sensory mechanism of CLK1/4 on the molecular level with higher activity at lower temperatures, leading to cold-induced SR protein phosphorylation. In addition, we found PP2A to be more active at higher temperatures and, strikingly, both kinase and phosphatase activity globally control body temperature-dependent AS and GE in the physiologically relevant temperature range. Interestingly, the tumor-suppressive transcription factor p53 and its bound targets were heat-induced, while targets of oncogenic MYC were more likely to be induced at lower temperatures. Consistently, we identified over 300 cancer-associated genes to be temperature- and PP1/2A-dependent on the GE level. Besides, 66 cancer-associated genes were alternatively spliced in a temperature-dependent manner and reacted to phosphatase inhibition.

SR proteins function on several aspects of RNA metabolism, ranging from transcription to mRNA processing, export, and translation (Long and Caceres, 2009). It has been shown that the phosphorylation status of SR proteins controls their sub-cellular and intra-nuclear localization, as well as their interaction with spliceosomal proteins (Xiao and Manley, 1998) or one another (Yeakley et al., 1999), which in turn affects the splicing outcome. Preussner *et al.* showed that temperature-dependent phosphorylation of SRSF2 and SRSF7 affects *U2AF26* AS, while the binding to its target RNAs is not affected (Preußner et al., 2017). Our data of cold-induced CLK1/4 phosphorylation

of SR proteins and heat-induced PP1/2A phosphatase activity (Figure 2.1 and Figure 2.3) are consistent with SRSF10 being dephosphorylated by PP1 upon heat shock and becoming a splicing repressor, while it is a splicing activator when phosphorylated (at colder temperature)(Feng et al., 2008; Shi and Manley, 2007).

We revealed that body temperature cycles control the AS-NMD-mediated autoregulation of SR proteins (Figure 2.7). When an SR protein is inactive based on its phosphorylation level, its mRNA and protein level will increase. Switching the SR protein to its activated state by altered phosphorylation due to temperature-dependent CLK activity will induce NMD exon inclusion within its pre-mRNA, leading to NMD-targeted degradation. SR proteins could also induce NMD exon inclusion in other RBPs and thereby regulate their abundance and activity, which influences the temperature-dependent transcriptome (Neumann et al., unpublished).

Temperature-regulated AS-NMD is not restricted to SR proteins, but we also found temperature-controlled NMD-inducing splicing events enriched for RBPs in general. CIRBP is an RBP, that is involved in multiple cellular processes, such as transcription, RNA stability, export, and translation (Morf et al., 2012; Xia et al., 2012; Yang and Carrier, 2001). The expression of *CIRBP* is not only induced after exposure to colder temperatures, but is also regulated by hypoxia, UV radiation, heat stress, and oxidative stress (Zhong and Huang, 2017). Furthermore, it has been shown that body temperature-controlled *CIRBP* expression is required for circadian GE (Morf et al., 2012). In 2016, Gotic *et al.* presented that temperature regulates *CIRBP* transcript levels by altered splicing efficiency (Gotic et al., 2016). We now connect temperature-driven CLK1/4 activity controlling *CIRBP* AS with temperature-controlled GE (Figure 2.2). In TG003-treated cells, cold-induced expression of *CIRBP* is completely abolished (Figure 2.2 A). We revealed a highly conserved 3' end in the *CIRBP* mRNA, whose inclusion is strongly promoted at higher temperatures but almost temperature-independent under CLK1/4-inhibited condition (Figure 2.2 B). AS of *CIRBP* exon 7b anticorrelates with *CIRBP* GE levels in primary hepatocytes and young mice, confirming the regulation *in vivo* (Figure 2.2 C, E). However, after deletion of the temperature-responsive *CIRBP* exon 7b some temperature-sensitivity remained. This indicates that additional mechanisms or kinases/phosphatases control this splicing event or splicing efficiency in general, either

independently or as a part of a greater regulatory network (Figure 2.2 F-H).

CIRBP plays an important role in inflammation, hypothermia, and cancer (Lujan et al., 2018; Qiang et al., 2013). Interestingly, CIRBP is a regulator of the p53 pathway upon DNA damage (Lee et al., 2015). At higher temperatures CLK1/4-dependent *CIRBP* AS results in heat-induced reduction of *CIRBP* expression levels and p53 gets activated. This is consistent with knockdown of *CIRBP* activating p53-mediated cell death and its overexpression suppressing apoptosis through downregulation of p53 (Lee et al., 2015). In accordance with that, tumor-promoting transcription factors, such as MYC and MAX, are cold-induced (as CIRBP), contributing to cell proliferation by apoptosis inhibition. Additionally, CIRBP was found to be upregulated in multiple solid cancers, such as colon, prostate, liver, and pancreas carcinomas, further suggesting a tumor-promoting function (Zhong and Huang, 2017). In an approach using mouse xenograft models, i.e. melanoma and breast cancer, it was shown that downregulation of CIRBP decreased proliferation, invasion, and migration, resulting in reduced tumor growth upon cellular stress (Chang et al., 2016). Furthermore, in prostate cancer knockdown of CIRBP enhanced the therapeutic response to chemotherapy (Zeng et al., 2009). Therefore, chemotherapy in combination with thermotherapy, which leads to the heat-induced reduction of CIRBP mediated by temperature-dependent CLK1/4 and PP1/2A activity, could represent a novel therapeutic approach for prostate cancer. However, it should be noted that CIRBP expression was also shown to be significantly decreased in most human endometrial carcinomas (Hamid et al., 2003). Due to its many functions in cellular processes, the role of CIRBP in cell transformation and cancer progression might be cell type-specific and needs to be further investigated.

Besides cold-induced CLK1/4 activity we identified PP2A to be directly temperature-regulated with an increased activity at higher temperatures, further promoting heat-induced SR protein dephosphorylation (Figure 2.3). In comparison to the almost on/off switch in CLK1/4 activity, PP2AC activity gradually increased with temperature, resulting in dephosphorylation of a pre-phosphorylated RS peptide in an *in vitro* phosphatase assay. Inhibition of PP1/2A using OA globally abolished temperature-responsive AS, whereas some temperature-sensitivity remained after TG003 treatment (Figure 2.4). This indicates that phosphatase activity is an essential

mediator of global temperature-sensitive AS. However, as the OA concentration used in this study inhibits both PP1 and PP2A (Cohen, 1991) it is still an open question whether both phosphatases act in a concerted manner, or separately. For instance, PP1 was shown to interact with various RBPs, including SR proteins (Novoyatleva et al., 2008) and is required for heat shock-induced dephosphorylation of SRSF10 (Shi et al., 2011). To address this question, additional inhibitors that are more specific to PP2A, for instance calyculin A, microcystin, or fostriecin (Honkanen and Golden, 2002), or knockdown of either PP1 or PP2A could be used to better discriminate between PP1- and PP2A-regulated events. Additionally, the *in vitro* phosphatase assays so far were performed using purified PP2AC. Further studies are needed to investigate whether PP1 activity is temperature-dependent as well. Besides, as mentioned above, the entire PP2A holoenzyme consists of three different subunits and in our *in vitro* phosphatase assays we only showed temperature-sensitivity for the PP2AC subunit. Therefore, to better understand temperature-dependent phosphatase activity, and thus AS and GE regulation, one should perform phosphatase assays using the PP2AC in addition to the scaffold and regulatory subunits. Indeed, after adding both PP2AC and the purified scaffolding subunit PP2R1A to an *in vitro* phosphatase reaction in a 1:1 molar ratio, the RS peptide dephosphorylation remained temperature-dependent, but the kinetics of the reaction was slower (data not shown). Furthermore, the diverse regulatory subunits are differentially spliced and expressed in a tissue-specific manner, which makes it even more challenging to completely unravel the molecular mechanism of temperature-mediated PP2A regulation. SR proteins or RS peptides are specific substrates for phosphorylation via CLK1/4 or SRPKs. In contrast, PP1/2A dephosphorylate a plethora of substrates, predominantly defined by the regulatory subunits (Janssens and Goris, 2001; Shi, 2009). The usage of additional substrates may result in differential temperature-sensitive substrate dephosphorylation. Additionally, the efficiency of B subunit binding is controlled by the accessibility and post-translational modifications of the carboxyl-terminus of the C subunit (Longin et al., 2007). The leucine carboxyl methyltransferase 1 (LCMT-1) and phosphatase methylesterase 1 (PME-1) are responsible for methylation and demethylation, respectively, of the C subunit, regulating PP2A function (Stanevich et al., 2011). In LCMT-1 knockdown experiments cells responded with apoptosis induction (Lee and Pallas, 2007), high-

lighting the role of functional PP2A in cell death signaling. An interesting question that remains is whether such post-translational modifications, besides CLK-mediated phosphorylation, are temperature-dependent as well. Upstream regulators of kinases or phosphatases could be temperature-dependent, resulting in differential CLK1/4 or PP2A activity or interactions with their substrates. CLK1/4-mediated, body temperature-dependent SR protein phosphorylation globally causes differential AS and GE of multiple target genes. An interesting question that remains is whether other RBPs, such as hnRNPs, are also phosphorylated (or in general post-translationally modified) and whether other kinases' activities also change in a temperature-dependent manner with a fundamental impact on temperature-mediated target gene splicing and GE. For instance, we also found the calcium/calmodulin-dependent protein kinase type IIβ (CamKIIb) to respond to subtle temperature changes. Just as the CLK1/4, CamKIIb shows higher activity at colder temperatures (unpublished). Furthermore, it would be very interesting to explore the detailed molecular mechanism responsible for temperature-dependent phosphatase activity, as it was done for CLK1/4.

PP2A is considered a tumor suppressor and is aberrantly expressed or functionally inactivated in various cancers, for instance in breast, skin, cervix, ovary, lung, and colon cancer (Sangodkar et al., 2016). Mutations or expression changes affecting the scaffold or regulatory subunits lead to inefficient assembly of the holoenzyme, which, among others, results in phosphorylation-dependent constant activation of proliferation-promoting signaling pathways, such as Akt ((Kuo et al., 2008); reviewed by (Seshacharyulu et al., 2013)). PP2A was shown to interact with p53 (Shouse et al., 2008), c-MYC (Arnold and Sears, 2006), and CDC25 (Margolis et al., 2006), which further makes it an interesting target for cancer therapies. Our data propose higher MYC activity at 33 °C and PP2A-mediated destabilization of MYC at higher temperatures. This is consistent with higher MYC activity in its phosphorylated state, promoting cell growth in cancer cells with insufficient PP2A activity (Arnold and Sears, 2006).

The involvement of PP2A in diverse signaling pathways and its regulation in cancer cells is still puzzling. Intervention with PP2A or interacting substrates has wide implications for the discovery or development of drugs targeting PP2A activity. For instance, the above-mentioned interaction of PME-1/LCMT-1 with PP2A, leading to

(de-)methylation and, therefore, changing PP2A holoenzyme composition, substrate specificity, and function introduces a possible mechanism for tumor therapy by promoting cancer cell death. Besides, cancer cells express endogenous PP2A inhibitors like CIP2A, which can serve as therapeutic targets for cancer treatment (Soofiyani et al., 2017). Yet, strategies to interfere with endogenous PP2A inhibitors to promote its activity might have systemic effects and are not specific to the oncogenic driver (Leonard et al., 2020). Therefore, therapies which selectively target PP2A holoenzyme composition, and thereby increasing specific substrate targeting, would have the potential as a therapeutic strategy. This was shown for small molecule activators of PP2A, i.e. DT-061 or iHAP, which selectively stabilize B56α-PP2A or B56ε-PP2A, respectively (Leonard et al., 2020; Morita et al., 2020). To further investigate the impact of PP2A subunits on tumor initiation or progression, genetically-engineered mouse models can be used to examine the effect of altered PP2A complexes or activity on oncogenic signaling and therapy outcomes (Reynhout and Janssens, 2019). Interestingly, cancer-associated mutations in the PP2A Aα scaffolding subunit increased cancer formation by 50 to 60 % in the lungs of mice treated with benzopyrene, which is dependent on p53 activity (Ruediger et al., 2011). These data highlight the fundamental role of PP2A and p53 in tumor progression and contribute to our suggested molecular mechanism, i.e. temperature-controlled activation of p53 via *MDMD4* AS. However, the direct connection of *MDM4* AS resulting in p53 activation still has to be shown, for instance by using splice-site blocking morpholinos or CRISPR/Cas9-mediated genome editing to modulate *MDM4* splicing. As p53 is mutated in over 50 % of cancers (Perri et al., 2016) it would be very interesting to compare cells with WT or mutated/inactivated p53 with respect to the temperature-responsiveness. According to our model, cells harboring mutated p53 should be less sensitive to heat-induced apoptosis induction, which could be tested, for instance, by activated caspase 8 staining via flow cytometry.

Already in the 19th century Dr. William Coley described the positive effect of a stimulated immune reaction, which resulted in fever, on tumor repression (Hoption Cann et al., 2002). Since then, hyperthermia, also in combination with radiation, showed positive outcomes in cancer therapy, for instance in tumor cells harboring WT p53

(Ohnishi, 2005). It is assumed that a mild increase in temperature leads, among others, to an improved adaptive immune response based on the generation of heat shock factors, the activation of antigen-presenting cells, stimulation of lymphocyte trafficking, and the release of chemoattractants for leukocytes (Skitzki et al., 2009). However, detailed molecular mechanisms, revealing the functionality of hyperthermia are still poorly understood. Our findings of heat-induced p53 activity due to altered *MDM4* splicing, therefore, add another possible explanation for the use of hyperthermia in tumor therapies.

However, due to its association in numerous signaling pathways, some examples also showed tumor-promoting functions of PP2A. For instance, the AMP-activated protein kinase (AMPK), which plays a role in energy balance under stress conditions, is inhibited by PP2A-mediated dephosphorylation upon heat-shock. This increases heat shock protein 70 (*HSP70*) expression and is thought to be beneficial for cell survival (Wang et al., 2010). Additionally, heat shock transcription factor 2 (HSF2) competes with the catalytic subunit of PP2A for the same binding in PR65 (A subunit), thus inhibiting PP2A under heat stress (Hong and Sarge, 1999). Besides, the B55α-PP2A isoform was shown to be fundamental for pancreatic cancer progression by controlling increased AKT, ERK, and Wnt signaling (Hein et al., 2016).

Based on our observation on the cold-induced expression of oncogenes, such as MYC, one could hypothesize that organisms (humans/animals) with a decreased body temperature are more likely to develop tumors. However, cancer-associated genes include both pro- and anti-tumorigenic genes and some oncogenic genes showed heat-induced expression (Figure 2.5 H). One example is the increased expression and splicing of oncogenic Mnk2b at 39 °C (Figure 2.6 A, C, D), which also was shown to be upregulated in breast, lung, and colon cancer (Maimon et al., 2014). The tumor microenvironment is slightly warmer than the surrounding tissue due to a higher metabolic rate and the immune-inflammatory milieu. This would favor heat-induced expression and AS of oncogenic genes as part of the immune evasion mechanism of cancerous cells. For instance, while the tumor-suppressive Mnk2a isoform activates the p38-MAPK stress pathway, resulting in cell death, the heat-induced Mnk2b isoform

is not an activator of p38-MAPK, making this isoform pro-oncogenic (Maimon et al., 2014). The identified sequence, which is responsible for heat-induced Mnk2b splicing, harbors, among others, a consensus binding motif for SRSF1. Elevated GE levels of *SRSF1* increased Mnk2b levels (Karni et al., 2007) and both Mnk2b and SRSF1 are upregulated in breast cancer cells (Maimon et al., 2014). This is consistent with a reduced binding of SRSF1 to *MKNK2* by deletion of the binding sequence and reduced Mnk2b levels by abolishing the temperature response.

Besides its association with cancer, PP2A function has also been linked to neurodegenerative diseases such as Alzheimer's disease (Sontag and Sontag, 2014). Generally, the Tau protein is involved in regulating microtubule dynamics. However, aberrantly hyperphosphorylated Tau forms neurofibrillary tangles, which is thought to play an important role in the development of Alzheimer's disease. The Bα subunit-containing isoform of PP2A is the primary Tau-binding phosphatase (Sontag et al., 1996) and PP2A activity accounts for around 71 % of total Tau phosphatase activity in the human brain (Liu et al., 2005). Changes in PP2A catalytic activity, subunit expression, or post-translational modifications were observed in brain samples of Alzheimer's patients (Gong et al., 1995; Sangodkar et al., 2016; Sontag et al., 2004). The body temperature of people decreases with aging (Fox et al., 1973; Wongsurawat et al., 1990), while the risk of getting diagnosed with Alzheimer's disease increases (Ganguli and Rodriguez, 2011; Hebert et al., 1995). Our findings of cold-induced kinase activity together with cold-inhibited PP2A activity are consistent with decreased body temperature in the elderly population and the higher risk of getting Alzheimer's disease as a consequence of Tau hyperphosphorylation. As mentioned above, besides CLK 1/4, we also found the kinase CamKIIb to be more active at lower temperatures (unpublished). CamKIIb, together with CamKIIα, are largely restricted to the brain, and, among many others, CamKII was shown to phosphorylate Tau at several serine and threonine residues (Martin et al., 2013). We, therefore, suggest a molecular basis for the connection of decreased body temperature and the incidence of Alzheimer's disease and provide insights for new potential therapeutic approaches.

In summary, we identified a network of kinases, phosphatases, SR proteins, and alternatively spliced genes, which is highly regulated in a temperature-dependent

manner, sensitive enough to respond to changes of 1 °C - 2 °C, and likely to be mutually dependent.

3.2 SRSF10 and the minor spliceosome control tissue-specific and dynamic SR protein expression

SRSF10 GE is controlled by an autoregulated minor intron resulting in a negative feedback loop. Usage of a minor splice site in exon 2 results in the formation of a productive *SRSF10* isoform (up-E4), but is repressed by direct competition of a downstream major splice site leading to an unstable isoform (dn-E3), which is targeted by the NMD pathway. We show that *SRSF10* expression levels tightly correlate with minor spliceosome abundance across different tissues and differentiation states. Surprisingly, this holds true for other SR proteins as well, and abolishing SRSF10 autoregulation induces the expression of all SR proteins.

In minigene experiments, the control of *SRSF10* GE levels through the minor spliceosome seems to be dominant over the autoregulatory feedback loop, suggesting that minor spliceosome activity sets the expression level of *SRSF10*, which is maintained by autoregulation (Figure 2.8 and 2.9). We used *RNPC3* expression levels as a read-out for minor spliceosome abundance and activity, and siRNA-mediated *RNPC3* knockdown to inhibit minor spliceosomal functionality. Since the *RNPC3* knockdown was not efficient and showed only a mild effect on *SRSF10* AS, another approach to directly modulate minor intron splicing would be the use of U11- or U12-targeting morpholinos to prevent binding to its target pre-mRNAs. The identified mechanism of SRSF10 regulating the expression of all other SR proteins suggests an extensive crosstalk between SR proteins and highlights the impact of the minor spliceosome on major intron splicing. The formation of NMD-inducing isoforms via AS is understood as a mechanism to control homeostatic GE levels (Ni et al., 2007). However, cross-regulation is known for many RBPs (Kumar and Lopez, 2005; Rossbach et al., 2009). Therefore, we suggest a model by which SRSF10 controls the GE levels of other SR proteins, and potentially other RBPs, by repressing the formation of NMD-targeted isoforms either by directly binding to the respective mRNAs, or indirectly through interactions with the respective RBP. Furthermore, altered SR protein activity, for instance via post-translational modifications, could change SR protein abundance. Reduced SR protein activity would result in reduced autoregulatory NMD exon inclusion and thus lead to a higher mRNA abundance (Ni et al., 2007). For *SRSF10*, cold-induced inclusion of its regulatory exon 3

resulted in decreased mRNA levels of functional SRSF10 (Figure 2.7 A, B). In addition, rhythmic temperature changes resulted in oscillating *SRSF10* GE levels (Figure 2.7 C, D), which seems to be contrary to the previously mentioned homeostatic control of expression levels in SR proteins and needs to be further investigated. SR protein activity depends, among others, on the phosphorylation state and could be controlled by a direct or indirect effect of SRSF10 on regulating kinases and phosphatases. However, the detailed mechanisms need to be investigated. The presented data show that the minor spliceosome controls the expression level of *SRSF10* and thus the expression of all other SR proteins. Due to the involvement of SR proteins in various biological processes, minor spliceosome activity will not only affect the splicing of most major introns but might indirectly also impact other aspects of mRNA metabolism. This is of special relevance for diseases caused by minor spliceosome deficiencies (Jutzi et al., 2018; Verma et al., 2018) as inefficient major intron splicing due to dysregulated SR proteins (Cologne et al., 2019) may contribute to the observed phenotypes.

4 References

Arnold, H. K. and Sears, R. C. (2006). Protein phosphatase 2a regulatory subunit b56alpha associates with c-myc and negatively regulates c-myc accumulation. *Molecular and cellular biology*, 26:2832–2844.

Aubol, B. E., Wu, G., Keshwani, M. M., Movassat, M., Fattet, L., Hertel, K. J., Fu, X.-D., and Adams, J. A. (2016). Release of sr proteins from clk1 by srpk1: A symbiotic kinase system for phosphorylation control of pre-mrna splicing. *Molecular cell*, 63:218–228.

Baharians, Z. and Schönthal, A. H. (1998). Autoregulation of protein phosphatase type 2a expression. *The Journal of biological chemistry*, 273:19019–19024.

Barbosa-Morais, N. L., Irimia, M., Pan, Q., Xiong, H. Y., Gueroussov, S., Lee, L. J., Slobodeniuc, V., Kutter, C., Watt, S., Colak, R., Kim, T., Misquitta-Ali, C. M., Wilson, M. D., Kim, P. M., Odom, D. T., Frey, B. J., and Blencowe, B. J. (2012). The evolutionary landscape of alternative splicing in vertebrate species. *Science (New York, N.Y.)*, 338:1587–1593.

Basu, M. K., Makalowski, W., Rogozin, I. B., and Koonin, E. V. (2008). U12 intron positions are more strongly conserved between animals and plants than u2 intron positions. *Biology direct*, 3:19.

Baurén, G. and Wieslander, L. (1994). Splicing of balbiani ring 1 gene pre-mrna occurs simultaneously with transcription. *Cell*, 76:183–192.

Bentley, D. L. (2014). Coupling mrna processing with transcription in time and space. *Nature reviews. Genetics*, 15:163–175.

Bezzi, M., Teo, S. X., Muller, J., Mok, W. C., Sahu, S. K., Vardy, L. A., Bonday, Z. Q., and Guccione, E. (2013). Regulation of constitutive and alternative splicing by prmt5 reveals a role for mdm4 pre-mrna in sensing defects in the spliceosomal machinery. *Genes & development*, 27:1903–1916.

Black, D. L. (2003). Mechanisms of alternative pre-messenger rna splicing. *Annual review of biochemistry*, 72:291–336.

Bononi, A., Agnoletto, C., De Marchi, E., Marchi, S., Patergnani, S., Bonora, M., Giorgi, C., Missiroli, S., Poletti, F., Rimessi, A., and Pinton, P. (2011). Protein kinases and phosphatases in the control of cell fate. *Enzyme research*, 2011:329098.

Bradley, T., Cook, M. E., and Blanchette, M. (2015). Sr proteins control a complex network of rna-processing events. *RNA (New York, N.Y.)*, 21:75–92.

Buhr, E. D., Yoo, S.-H., and Takahashi, J. S. (2010). Temperature as a universal resetting cue for mammalian circadian oscillators. *Science (New York, N.Y.)*, 330:379–385.

Cascón, A. and Robledo, M. (2012). Max and myc: a heritable breakup. *Cancer research*, 72:3119–3124.

Cáceres, J. F., Screaton, G. R., and Krainer, A. R. (1998). A specific subset of sr proteins shuttles continuously between the nucleus and the cytoplasm. *Genes & development*, 12:55–66.

Chang, E. T., Parekh, P. R., Yang, Q., Nguyen, D. M., and Carrier, F. (2016). Heterogenous ribonucleoprotein a18 (hnrnp a18) promotes tumor growth by increasing protein translation of selected transcripts in cancer cells. *Oncotarget*, 7:10578–10593.

Cléry, A., Blatter, M., and Allain, F. H.-T. (2008). Rna recognition motifs: boring? not quite. *Current opinion in structural biology*, 18:290–298.

Cohen, P. (1991). Classification of protein-serine/threonine phosphatases: identification and quantitation in cell extracts. *Methods in enzymology*, 201:389–398.

Cologne, A., Benoit-Pilven, C., Besson, A., Putoux, A., Campan-Fournier, A., Bober, M. B., De Die-Smulders, C. E. M., Paulussen, A. D. C., Pinson, L., Toutain, A., Roifman, C. M., Leutenegger, A.-L., Mazoyer, S., Edery, P., and Lacroix, V. (2019). New insights into minor splicing-a transcriptomic analysis of cells derived from tals patients. *RNA (New York, N.Y.)*, 25:1130–1149.

Cowper, A. E., Cáceres, J. F., Mayeda, A., and Screaton, G. R. (2001). Serine-arginine (sr) protein-like factors that antagonize authentic sr proteins and regulate alternative splicing. *The Journal of biological chemistry*, 276:48908–48914.

de la Mata, M., Alonso, C. R., Kadener, S., Fededa, J. P., Blaustein, M., Pelisch, F., Cramer, P., Bentley, D., and Kornblihtt, A. R. (2003). A slow rna polymerase ii affects alternative splicing in vivo. *Molecular cell*, 12:525–532.

Dewaele, M., Tabaglio, T., Willekens, K., Bezzi, M., Teo, S. X., Low, D. H. P., Koh, C. M., Rambow, F., Fiers, M., Rogiers, A., Radaelli, E., Al-Haddawi, M., Tan, S. Y., Hermans, E., Amant, F., Yan, H., Lakshmanan, M., Koumar, R. C., Lim, S. T., Derheimer, F. A., Campbell, R. M., Bonday, Z., Tergaonkar, V., Shackleton, M., Blattner, C., Marine, J.-C., and Guccione, E. (2016). Antisense oligonucleotide-mediated mdm4 exon 6 skipping impairs tumor growth. *The Journal of clinical investigation*, 126:68–84.

Doggett, K., Williams, B. B., Markmiller, S., Geng, F.-S., Coates, J., Mieruszynski, S., Ernst, M., Thomas, T., and Heath, J. K. (2018). Early developmental arrest and impaired gastrointestinal homeostasis in u12-dependent splicing-defective , javax.xml.bind.jaxbelement@37d16309, -deficient mice. *RNA (New York, N.Y.)*, 24:1856–1870.

Edery, P., Marcaillou, C., Sahbatou, M., Labalme, A., Chastang, J., Touraine, R., Tubacher, E., Senni, F., Bober, M. B., Nampoothiri, S., Jouk, P.-S., Steichen, E., Berland, S., Toutain, A.,

Wise, C. A., Sanlaville, D., Rousseau, F., Clerget-Darpoux, F., and Leutenegger, A.-L. (2011). Association of tals developmental disorder with defect in minor splicing component u4atac snrna. *Science (New York, N.Y.)*, 332:240–243.

Edmond, V., Moysan, E., Khochbin, S., Matthias, P., Brambilla, C., Brambilla, E., Gazzeri, S., and Eymin, B. (2011). Acetylation and phosphorylation of srsf2 control cell fate decision in response to cisplatin. *The EMBO journal*, 30:510–523.

Eichhorn, P. J. A., Creyghton, M. P., and Bernards, R. (2009). Protein phosphatase 2a regulatory subunits and cancer. *Biochimica et biophysica acta*, 1795:1–15.

Feng, Y., Chen, M., and Manley, J. L. (2008). Phosphorylation switches the general splicing repressor srp38 to a sequence-specific activator. *Nature structural & molecular biology*, 15:1040–1048.

Fox, R. H., Woodward, P. M., Exton-Smith, A. N., Green, M. F., Donnison, D. V., and Wicks, M. H. (1973). Body temperatures in the elderly: a national study of physiological, social, and environmental conditions. *British medical journal*, 1:200–206.

Fu, X.-D. and Ares, M. (2014). Context-dependent control of alternative splicing by rna-binding proteins. *Nature reviews. Genetics*, 15:689–701.

Furlanis, E. and Scheiffele, P. (2018). Regulation of neuronal differentiation, function, and plasticity by alternative splicing. *Annual review of cell and developmental biology*, 34:451–469.

Futreal, P. A., Coin, L., Marshall, M., Down, T., Hubbard, T., Wooster, R., Rahman, N., and Stratton, M. R. (2004). A census of human cancer genes. *Nature reviews. Cancer*, 4:177–183.

Ganguli, M. and Rodriguez, E. (2011). Age, alzheimer's disease, and the big picture. *International psychogeriatrics*, 23:1531–1534.

Garneau, N. L., Wilusz, J., and Wilusz, C. J. (2007). The highways and byways of mrna decay. *Nature reviews. Molecular cell biology*, 8:113–126.

Ghigna, C., Giordano, S., Shen, H., Benvenuto, F., Castiglioni, F., Comoglio, P. M., Green, M. R., Riva, S., and Biamonti, G. (2005). Cell motility is controlled by sf2/asf through alternative splicing of the ron protooncogene. *Molecular cell*, 20:881–890.

Gong, C. X., Shaikh, S., Wang, J. Z., Zaidi, T., Grundke-Iqbal, I., and Iqbal, K. (1995). Phosphatase activity toward abnormally phosphorylated tau: decrease in alzheimer disease brain. *Journal of neurochemistry*, 65:732–738.

Gotic, I., Omidi, S., Fleury-Olela, F., Molina, N., Naef, F., and Schibler, U. (2016). Temperature regulates splicing efficiency of the cold-inducible rna-binding protein gene cirbp. *Genes & development*, 30:2005–2017.

Graveley, B. R. (2000). Sorting out the complexity of sr protein functions. *RNA (New York, N.Y.)*,

6:1197–1211.

Graves, J. D. and Krebs, E. G. (1999). Protein phosphorylation and signal transduction. *Pharmacology & therapeutics*, 82:111–121.

Green, M. R. (1986). Pre-mrna splicing. *Annual review of genetics*, 20:671–708.

Haltenhof, T., Kotte, A., De Bortoli, F., Schiefer, S., Meinke, S., Emmerichs, A.-K., Petermann, K. K., Timmermann, B., Imhof, P., Franz, A., Loll, B., Wahl, M. C., Preußner, M., and Heyd, F. (2020). A conserved kinase-based body-temperature sensor globally controls alternative splicing and gene expression. *Molecular cell*, 78:57–69.e4.

Hamid, A. A., Mandai, M., Fujita, J., Nanbu, K., Kariya, M., Kusakari, T., Fukuhara, K., and Fujii, S. (2003). Expression of cold-inducible rna-binding protein in the normal endometrium, endometrial hyperplasia, and endometrial carcinoma. *International journal of gynecological pathology : official journal of the International Society of Gynecological Pathologists*, 22:240–247.

Hanahan, D. and Weinberg, R. A. (2011). Hallmarks of cancer: the next generation. *Cell*, 144:646–674.

He, H., Liyanarachchi, S., Akagi, K., Nagy, R., Li, J., Dietrich, R. C., Li, W., Sebastian, N., Wen, B., Xin, B., Singh, J., Yan, P., Alder, H., Haan, E., Wieczorek, D., Albrecht, B., Puffenberger, E., Wang, H., Westman, J. A., Padgett, R. A., Symer, D. E., and de la Chapelle, A. (2011). Mutations in u4atac snrna, a component of the minor spliceosome, in the developmental disorder mopd i. *Science (New York, N.Y.)*, 332:238–240.

Hebert, L. E., Scherr, P. A., Beckett, L. A., Albert, M. S., Pilgrim, D. M., Chown, M. J., Funkenstein, H. H., and Evans, D. A. (1995). Age-specific incidence of alzheimer's disease in a community population. *JAMA*, 273:1354–1359.

Hein, A. L., Seshacharyulu, P., Rachagani, S., Sheinin, Y. M., Ouellette, M. M., Ponnusamy, M. P., Mumby, M. C., Batra, S. K., and Yan, Y. (2016). Pr55αsubunit of protein phosphatase 2a supports the tumorigenic and metastatic potential of pancreatic cancer cells by sustaining hyperactive oncogenic signaling. *Cancer research*, 76:2243–2253.

Hollstein, M., Sidransky, D., Vogelstein, B., and Harris, C. C. (1991). p53 mutations in human cancers. *Science (New York, N.Y.)*, 253:49–53.

Hong, Y. and Sarge, K. D. (1999). Regulation of protein phosphatase 2a activity by heat shock transcription factor 2. *The Journal of biological chemistry*, 274:12967–12970.

Honkanen, R. E. and Golden, T. (2002). Regulators of serine/threonine protein phosphatases at the dawn of a clinical era? *Current medicinal chemistry*, 9:2055–2075.

Hoption Cann, S. A., van Netten, J. P., and van Netten, C. (2002). Dr william coley and tumour regression: a place in history or in the future. *Medical Hypotheses*, 79(2):672–80.

Howard, J. M. and Sanford, J. R. (2015). The rnaissance family: Sr proteins as multifaceted regulators of gene expression. *Wiley interdisciplinary reviews. RNA*, 6:93–110.

Huang, Y. and Steitz, J. A. (2005). Srprises along a messenger's journey. *Molecular cell*, 17:613–615.

Hubbard, K. S., Gut, I. M., Lyman, M. E., Tuznik, K. M., Mesngon, M. T., and McNutt, P. M. (2012). High yield derivation of enriched glutamatergic neurons from suspension-cultured mouse escs for neurotoxicology research. *BMC neuroscience*, 13:127.

Hurt, J. A., Robertson, A. D., and Burge, C. B. (2013). Global analyses of upf1 binding and function reveal expanded scope of nonsense-mediated mrna decay. *Genome research*, 23:1636–1650.

Jackson, I. J. (1991). A reappraisal of non-consensus mrna splice sites. *Nucleic acids research*, 19:3795–3798.

Janssens, V. and Goris, J. (2001). Protein phosphatase 2a: a highly regulated family of serine/threonine phosphatases implicated in cell growth and signalling. *The Biochemical journal*, 353:417–439.

Junttila, M. R., Puustinen, P., Niemelä, M., Ahola, R., Arnold, H., Böttzauw, T., Ala-aho, R., Nielsen, C., Ivaska, J., Taya, Y., Lu, S.-L., Lin, S., Chan, E. K. L., Wang, X.-J., Grènman, R., Kast, J., Kallunki, T., Sears, R., Kähäri, V.-M., and Westermarck, J. (2007). Cip2a inhibits pp2a in human malignancies. *Cell*, 130:51–62.

Jutzi, D., Akinyi, M. V., Mechtersheimer, J., Frilander, M. J., and Ruepp, M.-D. (2018). The emerging role of minor intron splicing in neurological disorders. *Cell stress*, 2:40–54.

Kaida, D., Motoyoshi, H., Tashiro, E., Nojima, T., Hagiwara, M., Ishigami, K., Watanabe, H., Kitahara, T., Yoshida, T., Nakajima, H., Tani, T., Horinouchi, S., and Yoshida, M. (2007). Spliceostatin a targets sf3b and inhibits both splicing and nuclear retention of pre-mrna. *Nature chemical biology*, 3:576–583.

Karni, R., de Stanchina, E., Lowe, S. W., Sinha, R., Mu, D., and Krainer, A. R. (2007). The gene encoding the splicing factor sf2/asf is a proto-oncogene. *Nature structural & molecular biology*, 14:185–193.

Kornblihtt, A. R. (2015). Transcriptional control of alternative splicing along time: ideas change, experiments remain. *RNA (New York, N.Y.)*, 21:670–672.

Kotake, Y., Sagane, K., Owa, T., Mimori-Kiyosue, Y., Shimizu, H., Uesugi, M., Ishihama, Y., Iwata, M., and Mizui, Y. (2007). Splicing factor sf3b as a target of the antitumor natural product pladienolide. *Nature chemical biology*, 3:570–575.

Kuleshov, M. V., Jones, M. R., Rouillard, A. D., Fernandez, N. F., Duan, Q., Wang, Z., Koplev, S.,

Jenkins, S. L., Jagodnik, K. M., Lachmann, A., McDermott, M. G., Monteiro, C. D., Gundersen, G. W., and Ma'ayan, A. (2016). Enrichr: a comprehensive gene set enrichment analysis web server 2016 update. *Nucleic acids research*, 44:W90–W97.

Kumar, S. and Lopez, A. J. (2005). Negative feedback regulation among sr splicing factors encoded by rbp1 and rbp1-like in drosophila. *The EMBO journal*, 24:2646–2655.

Kuo, Y.-C., Huang, K.-Y., Yang, C.-H., Yang, Y.-S., Lee, W.-Y., and Chiang, C.-W. (2008). Regulation of phosphorylation of thr-308 of akt, cell proliferation, and survival by the b55alpha regulatory subunit targeting of the protein phosphatase 2a holoenzyme to akt. *The Journal of biological chemistry*, 283:1882–1892.

Kurimchak, A. and Graña, X. (2012). Pp2a counterbalances phosphorylation of prb and mitotic proteins by multiple cdks: Potential implications for pp2a disruption in cancer. *Genes & cancer*, 3:739–748.

Lareau, L. F., Inada, M., Green, R. E., Wengrod, J. C., and Brenner, S. E. (2007). Unproductive splicing of sr genes associated with highly conserved and ultraconserved dna elements. *Nature*, 446:926–929.

Lee, H. N., Ahn, S.-M., and Jang, H. H. (2015). Cold-inducible rna-binding protein, cirp, inhibits dna damage-induced apoptosis by regulating p53. *Biochemical and biophysical research communications*, 464:916–921.

Lee, J. A. and Pallas, D. C. (2007). Leucine carboxyl methyltransferase-1 is necessary for normal progression through mitosis in mammalian cells. *The Journal of biological chemistry*, 282:30974–30984.

Lejeune, F., Cavaloc, Y., and Stevenin, J. (2001). Alternative splicing of intron 3 of the serine/arginine-rich protein 9g8 gene. identification of flanking exonic splicing enhancers and involvement of 9g8 as a trans-acting factor. *The Journal of biological chemistry*, 276:7850–7858.

Leonard, D., Huang, W., Izadmehr, S., O'Connor, C. M., Wiredja, D. D., Wang, Z., Zaware, N., Chen, Y., Schlatzer, D. M., Kiselar, J., Vasireddi, N., Schüchner, S., Perl, A. L., Galsky, M. D., Xu, W., Brautigan, D. L., Ogris, E., Taylor, D. J., and Narla, G. (2020). Selective pp2a enhancement through biased heterotrimer stabilization. *Cell*.

Levine, A. J., Momand, J., and Finlay, C. A. (1991). The p53 tumour suppressor gene. *Nature*, 351:453–456.

Li, H., Cheng, Y., Wu, W., Liu, Y., Wei, N., Feng, X., Xie, Z., and Feng, Y. (2014). Srsf10 regulates alternative splicing and is required for adipocyte differentiation. *Molecular and cellular biology*, 34:2198–2207.

Li, X., Scuderi, A., Letsou, A., and Virshup, D. M. (2002). B56-associated protein phosphatase

2a is required for survival and protects from apoptosis in drosophila melanogaster. *Molecular and cellular biology*, 22:3674–3684.

Licatalosi, D. D., Mele, A., Fak, J. J., Ule, J., Kayikci, M., Chi, S. W., Clark, T. A., Schweitzer, A. C., Blume, J. E., Wang, X., Darnell, J. C., and Darnell, R. B. (2008). Hits-clip yields genome-wide insights into brain alternative rna processing. *Nature*, 456:464–469.

Lin, S., Xiao, R., Sun, P., Xu, X., and Fu, X.-D. (2005). Dephosphorylation-dependent sorting of sr splicing factors during mrnp maturation. *Molecular cell*, 20:413–425.

Liu, F., Dai, M., Xu, Q., Zhu, X., Zhou, Y., Jiang, S., Wang, Y., Ai, Z., Ma, L., Zhang, Y., Hu, L., Yang, Q., Li, J., Zhao, S., Zhang, Z., and Teng, Y. (2018). Srsf10-mediated il1rap alternative splicing regulates cervical cancer oncogenesis via mil1rap-nf-textkappa b-cd47 axis. *Oncogene*, 37:2394–2409.

Liu, F., Grundke-Iqbal, I., Iqbal, K., and Gong, C.-X. (2005). Contributions of protein phosphatases pp1, pp2a, pp2b and pp5 to the regulation of tau phosphorylation. *The European journal of neuroscience*, 22:1942–1950.

Liu, Y., Gonzàlez-Porta, M., Santos, S., Brazma, A., Marioni, J. C., Aebersold, R., Venkitaraman, A. R., and Wickramasinghe, V. O. (2017). Impact of alternative splicing on the human proteome. *Cell reports*, 20:1229–1241.

Long, J. C. and Caceres, J. F. (2009). The sr protein family of splicing factors: master regulators of gene expression. *The Biochemical journal*, 417:15–27.

Longin, S., Zwaenepoel, K., Louis, J. V., Dilworth, S., Goris, J., and Janssens, V. (2007). Selection of protein phosphatase 2a regulatory subunits is mediated by the c terminus of the catalytic subunit. *The Journal of biological chemistry*, 282:26971–26980.

Lujan, D. A., Ochoa, J. L., and Hartley, R. S. (2018). Cold-inducible rna binding protein in cancer and inflammation. *Wiley interdisciplinary reviews. RNA*, 9.

Lykke-Andersen, S. and Jensen, T. H. (2015). Nonsense-mediated mrna decay: an intricate machinery that shapes transcriptomes. *Nature reviews. Molecular cell biology*, 16:665–677.

Maimon, A., Mogilevsky, M., Shilo, A., Golan-Gerstl, R., Obiedat, A., Ben-Hur, V., Lebenthal-Loinger, I., Stein, I., Reich, R., Beenstock, J., Zehorai, E., Andersen, C. L., Thorsen, K., Ørntoft, T. F., Davis, R. J., Davidson, B., Mu, D., and Karni, R. (2014). Mnk2 alternative splicing modulates the p38-mapk pathway and impacts ras-induced transformation. *Cell reports*, 7:501–513.

Manley, J. L. and Krainer, A. R. (2010). A rational nomenclature for serine/arginine-rich protein splicing factors (sr proteins). *Genes & development*, 24:1073–1074.

Manning, G., Whyte, D. B., Martinez, R., Hunter, T., and Sudarsanam, S. (2002). The protein

kinase complement of the human genome. *Science (New York, N.Y.)*, 298:1912–1934.

Margolis, S. S., Perry, J. A., Forester, C. M., Nutt, L. K., Guo, Y., Jardim, M. J., Thomenius, M. J., Freel, C. D., Darbandi, R., Ahn, J.-H., Arroyo, J. D., Wang, X.-F., Shenolikar, S., Nairn, A. C., Dunphy, W. G., Hahn, W. C., Virshup, D. M., and Kornbluth, S. (2006). Role for the pp2a/b56delta phosphatase in regulating 14-3-3 release from cdc25 to control mitosis. *Cell*, 127:759–773.

Martin, L., Latypova, X., Wilson, C. M., Magnaudeix, A., Perrin, M.-L., Yardin, C., and Terro, F. (2013). Tau protein kinases: involvement in alzheimer's disease. *Ageing research reviews*, 12:289–309.

Martinez, N. M., Pan, Q., Cole, B. S., Yarosh, C. A., Babcock, G. A., Heyd, F., Zhu, W., Ajith, S., Blencowe, B. J., and Lynch, K. W. (2012). Alternative splicing networks regulated by signaling in human t cells. *RNA (New York, N.Y.)*, 18:1029–1040.

Mathew, R., Hartmuth, K., Möhlmann, S., Urlaub, H., Ficner, R., and Lührmann, R. (2008). Phosphorylation of human prp28 by srpk2 is required for integration of the u4/u6-u5 tri-snrnp into the spliceosome. *Nature structural & molecular biology*, 15:435–443.

Matlin, A. J., Clark, F., and Smith, C. W. J. (2005). Understanding alternative splicing: towards a cellular code. *Nature reviews. Molecular cell biology*, 6:386–398.

Mayeda, A. and Krainer, A. R. (1992). Regulation of alternative pre-mrna splicing by hnrnp a1 and splicing factor sf2. *Cell*, 68:365–375.

Mayeda, A., Munroe, S. H., Cáceres, J. F., and Krainer, A. R. (1994). Function of conserved domains of hnrnp a1 and other hnrnp a/b proteins. *The EMBO journal*, 13:5483–5495.

McConnell, J. L., Gomez, R. J., McCorvey, L. R. A., Law, B. K., and Wadzinski, B. E. (2007). Identification of a pp2a-interacting protein that functions as a negative regulator of phosphatase activity in the atm/atr signaling pathway. *Oncogene*, 26:6021–6030.

McCright, B., Rivers, A. M., Audlin, S., and Virshup, D. M. (1996). The b56 family of protein phosphatase 2a (pp2a) regulatory subunits encodes differentiation-induced phosphoproteins that target pp2a to both nucleus and cytoplasm. *The Journal of biological chemistry*, 271:22081–22089.

McGlincy, N. J. and Smith, C. W. J. (2008). Alternative splicing resulting in nonsense-mediated mrna decay: what is the meaning of nonsense? *Trends in biochemical sciences*, 33:385–393.

McManus, C. J. and Graveley, B. R. (2011). Rna structure and the mechanisms of alternative splicing. *Current opinion in genetics & development*, 21:373–379.

Merkin, J., Russell, C., Chen, P., and Burge, C. B. (2012). Evolutionary dynamics of gene and isoform regulation in mammalian tissues. *Science (New York, N.Y.)*, 338:1593–1599.

Michel, M., Wilhelmi, I., Schultz, A.-S., Preussner, M., and Heyd, F. (2014). Activation-induced tumor necrosis factor receptor-associated factor 3 (traf3) alternative splicing controls the noncanonical nuclear factor κb pathway and chemokine expression in human t cells. *The Journal of biological chemistry*, 289:13651–13660.

Miyaki, M., Iijima, T., Konishi, M., Sakai, K., Ishii, A., Yasuno, M., Hishima, T., Koike, M., Shitara, N., Iwama, T., Utsunomiya, J., Kuroki, T., and Mori, T. (1999). Higher frequency of smad4 gene mutation in human colorectal cancer with distant metastasis. *Oncogene*, 18:3098–3103.

Müller-McNicoll, M., Rossbach, O., Hui, J., and Medenbach, J. (2019). Auto-regulatory feedback by rna-binding proteins. *Journal of molecular cell biology*, 11:930–939.

Mockenhaupt, S. and Makeyev, E. V. (2015). Non-coding functions of alternative pre-mrna splicing in development. *Seminars in cell & developmental biology*, 47-48:32–39.

Mogilevsky, M., Shimshon, O., Kumar, S., Mogilevsky, A., Keshet, E., Yavin, E., Heyd, F., and Karni, R. (2018). Modulation of mknk2 alternative splicing by splice-switching oligonucleotides as a novel approach for glioblastoma treatment. *Nucleic acids research*, 46:11396–11404.

Moore, M. J., Wang, Q., Kennedy, C. J., and Silver, P. A. (2010). An alternative splicing network links cell-cycle control to apoptosis. *Cell*, 142:625–636.

Morf, J., Rey, G., Schneider, K., Stratmann, M., Fujita, J., Naef, F., and Schibler, U. (2012). Cold-inducible rna-binding protein modulates circadian gene expression posttranscriptionally. *Science (New York, N.Y.)*, 338:379–383.

Morita, K., He, S., Nowak, R. P., Wang, J., Zimmerman, M. W., Fu, C., Durbin, A. D., Martel, M. W., Prutsch, N., Gray, N. S., Fischer, E. S., and Look, A. T. (2020). Allosteric activators of protein phosphatase 2a display broad antitumor activity mediated by dephosphorylation of mybl2. *Cell*.

Muraki, M., Ohkawara, B., Hosoya, T., Onogi, H., Koizumi, J., Koizumi, T., Sumi, K., Yomoda, J.-i., Murray, M. V., Kimura, H., Furuichi, K., Shibuya, H., Krainer, A. R., Suzuki, M., and Hagiwara, M. (2004). Manipulation of alternative splicing by a newly developed inhibitor of clks. *The Journal of biological chemistry*, 279:24246–24254.

Nagy, E. and Maquat, L. E. (1998). A rule for termination-codon position within intron-containing genes: when nonsense affects rna abundance. *Trends in biochemical sciences*, 23:198–199.

Neviani, P., Santhanam, R., Trotta, R., Notari, M., Blaser, B. W., Liu, S., Mao, H., Chang, J. S., Galietta, A., Uttam, A., Roy, D. C., Valtieri, M., Bruner-Klisovic, R., Caligiuri, M. A., Bloomfield, C. D., Marcucci, G., and Perrotti, D. (2005). The tumor suppressor pp2a is

functionally inactivated in blast crisis cml through the inhibitory activity of the bcr/abl-regulated set protein. *Cancer cell*, 8:355–368.

Ni, J. Z., Grate, L., Donohue, J. P., Preston, C., Nobida, N., O'Brien, G., Shiue, L., Clark, T. A., Blume, J. E., and Ares, M. (2007). Ultraconserved elements are associated with homeostatic control of splicing regulators by alternative splicing and nonsense-mediated decay. *Genes & development*, 21:708–718.

Nilsen, T. W. and Graveley, B. R. (2010). Expansion of the eukaryotic proteome by alternative splicing. *Nature*, 463:457–463.

Novoyatleva, T., Heinrich, B., Tang, Y., Benderska, N., Butchbach, M. E. R., Lorson, C. L., Lorson, M. A., Ben-Dov, C., Fehlbaum, P., Bracco, L., Burghes, A. H. M., Bollen, M., and Stamm, S. (2008). Protein phosphatase 1 binds to the rna recognition motif of several splicing factors and regulates alternative pre-mrna processing. *Human molecular genetics*, 17:52–70.

O'Connor, C. M., Perl, A., Leonard, D., Sangodkar, J., and Narla, G. (2018). Therapeutic targeting of pp2a. *The international journal of biochemistry & cell biology*, 96:182–193.

Ohnishi, T. (2005). The role of the p53 molecule in cancer therapies with radiation and/or hyperthermia. *Journal of cancer research and therapeutics*, 1:147–150.

Oltean, S. and Bates, D. O. (2014). Hallmarks of alternative splicing in cancer. *Oncogene*, 33:5311–5318.

Pan, Q., Shai, O., Lee, L. J., Frey, B. J., and Blencowe, B. J. (2008). Deep surveying of alternative splicing complexity in the human transcriptome by high-throughput sequencing. *Nature genetics*, 40:1413–1415.

Patel, A. A. and Steitz, J. A. (2003). Splicing double: insights from the second spliceosome. *Nature reviews. Molecular cell biology*, 4:960–970.

Perri, F., Pisconti, S., and Della Vittoria Scarpati, G. (2016). P53 mutations and cancer: a tight linkage. *Annals of translational medicine*, 4:522.

Pippa, R. and Odero, M. D. (2020). The role of myc and pp2a in the initiation and progression of myeloid leukemias. *Cells*, 9.

Preußner, M., Goldammer, G., Neumann, A., Haltenhof, T., Rautenstrauch, P., Müller-McNicoll, M., and Heyd, F. (2017). Body temperature cycles control rhythmic alternative splicing in mammals. *Molecular cell*, 67:433–446.e4.

Preußner, M. and Heyd, F. (2018). Temperature-controlled rhythmic gene expression in endothermic mammals: All diurnal rhythms are equal, but some are circadian. *BioEssays : news and reviews in molecular, cellular and developmental biology*, 40:e1700216.

Qiang, X., Yang, W.-L., Wu, R., Zhou, M., Jacob, A., Dong, W., Kuncewitch, M., Ji, Y., Yang, H.,

Wang, H., Fujita, J., Nicastro, J., Coppa, G. F., Tracey, K. J., and Wang, P. (2013). Cold-inducible rna-binding protein (cirp) triggers inflammatory responses in hemorrhagic shock and sepsis. *Nature medicine*, 19:1489–1495.

Refinetti, R. and Menaker, M. (1992). The circadian rhythm of body temperature. *Physiology & behavior*, 51:613–637.

Reynhout, S. and Janssens, V. (2019). Physiologic functions of pp2a: Lessons from genetically modified mice. *Biochimica et biophysica acta. Molecular cell research*, 1866:31–50.

Rossbach, O., Hung, L.-H., Schreiner, S., Grishina, I., Heiner, M., Hui, J., and Bindereif, A. (2009). Auto- and cross-regulation of the hnrnp l proteins by alternative splicing. *Molecular and cellular biology*, 29:1442–1451.

Ruediger, R., Ruiz, J., and Walter, G. (2011). Human cancer-associated mutations in the aαsubunit of protein phosphatase 2a increase lung cancer incidence in aαknock-in and knockout mice. *Molecular and cellular biology*, 31:3832–3844.

Sangodkar, J., Farrington, C. C., McClinch, K., Galsky, M. D., Kastrinsky, D. B., and Narla, G. (2016). All roads lead to pp2a: exploiting the therapeutic potential of this phosphatase. *The FEBS journal*, 283:1004–1024.

Schmucker, D., Clemens, J. C., Shu, H., Worby, C. A., Xiao, J., Muda, M., Dixon, J. E., and Zipursky, S. L. (2000). Drosophila dscam is an axon guidance receptor exhibiting extraordinary molecular diversity. *Cell*, 101:671–684.

Schneider, M., Hsiao, H.-H., Will, C. L., Giet, R., Urlaub, H., and Lührmann, R. (2010). Human prp4 kinase is required for stable tri-snrnp association during spliceosomal b complex formation. *Nature structural & molecular biology*, 17:216–221.

Scotti, M. M. and Swanson, M. S. (2016). Rna mis-splicing in disease. *Nature reviews. Genetics*, 17:19–32.

Seshacharyulu, P., Pandey, P., Datta, K., and Batra, S. K. (2013). Phosphatase: Pp2a structural importance, regulation and its aberrant expression in cancer. *Cancer letters*, 335:9–18.

Sharma, S., Kohlstaedt, L. A., Damianov, A., Rio, D. C., and Black, D. L. (2008). Polypyrimidine tract binding protein controls the transition from exon definition to an intron defined spliceosome. *Nature structural & molecular biology*, 15:183–191.

Shepard, P. J. and Hertel, K. J. (2009). The sr protein family. *Genome biology*, 10:242.

Shi, Y. (2009). Serine/threonine phosphatases: mechanism through structure. *Cell*, 139:468–484.

Shi, Y. and Manley, J. L. (2007). A complex signaling pathway regulates srp38 phosphorylation and pre-mrna splicing in response to heat shock. *Molecular cell*, 28:79–90.

Shi, Y., Nishida, K., Campigli Di Giammartino, D., and Manley, J. L. (2011). Heat shock-induced

srsf10 dephosphorylation displays thermotolerance mediated by hsp27. *Molecular and cellular biology*, 31:458–465.

Shin, C., Feng, Y., and Manley, J. L. (2004). Dephosphorylated srp38 acts as a splicing repressor in response to heat shock. *Nature*, 427:553–558.

Shin, C. and Manley, J. L. (2002). The sr protein srp38 represses splicing in m phase cells. *Cell*, 111:407–417.

Shkreta, L., Toutant, J., Durand, M., Manley, J. L., and Chabot, B. (2016). Srsf10 connects dna damage to the alternative splicing of transcripts encoding apoptosis, cell-cycle control, and dna repair factors. *Cell reports*, 17:1990–2003.

Shouse, G. P., Cai, X., and Liu, X. (2008). Serine 15 phosphorylation of p53 directs its interaction with b56gamma and the tumor suppressor activity of b56gamma-specific protein phosphatase 2a. *Molecular and cellular biology*, 28:448–456.

Singh, R. K. and Cooper, T. A. (2012). Pre-mrna splicing in disease and therapeutics. *Trends in molecular medicine*, 18:472–482.

Sinha, R., Allemand, E., Zhang, Z., Karni, R., Myers, M. P., and Krainer, A. R. (2010). Arginine methylation controls the subcellular localization and functions of the oncoprotein splicing factor sf2/asf. *Molecular and cellular biology*, 30:2762–2774.

Skitzki, J. J., Repasky, E. A., and Evans, S. S. (2009). Hyperthermia as an immunotherapy strategy for cancer. *Current opinion in investigational drugs (London, England : 2000)*, 10:550–558.

Slupe, A. M., Merrill, R. A., and Strack, S. (2011). Determinants for substrate specificity of protein phosphatase 2a. *Enzyme research*, 2011:398751.

Sontag, E., Luangpirom, A., Hladik, C., Mudrak, I., Ogris, E., Speciale, S., and White, C. L. (2004). Altered expression levels of the protein phosphatase 2a abalphac enzyme are associated with alzheimer disease pathology. *Journal of neuropathology and experimental neurology*, 63:287–301.

Sontag, E., Nunbhakdi-Craig, V., Lee, G., Bloom, G. S., and Mumby, M. C. (1996). Regulation of the phosphorylation state and microtubule-binding activity of tau by protein phosphatase 2a. *Neuron*, 17:1201–1207.

Sontag, J.-M. and Sontag, E. (2014). Protein phosphatase 2a dysfunction in alzheimer's disease. *Frontiers in molecular neuroscience*, 7:16.

Soofiyani, S. R., Hejazi, M. S., and Baradaran, B. (2017). The role of cip2a in cancer: A review and update. *Biomedicine & pharmacotherapy = Biomedecine & pharmacotherapie*, 96:626–633.

Stanevich, V., Jiang, L., Satyshur, K. A., Li, Y., Jeffrey, P. D., Li, Z., Menden, P., Semmelhack, M. F., and Xing, Y. (2011). The structural basis for tight control of pp2a methylation and function by lcmt-1. *Molecular cell*, 41:331–342.

Sterne-Weiler, T., Weatheritt, R. J., Best, A. J., Ha, K. C. H., and Blencowe, B. J. (2018). Efficient and accurate quantitative profiling of alternative splicing patterns of any complexity on a laptop. *Molecular cell*, 72:187–200.e6.

Strack, S., Zaucha, J. A., Ebner, F. F., Colbran, R. J., and Wadzinski, B. E. (1998). Brain protein phosphatase 2a: developmental regulation and distinct cellular and subcellular localization by b subunits. *The Journal of comparative neurology*, 392:515–527.

Sureau, A., Gattoni, R., Dooghe, Y., Stévenin, J., and Soret, J. (2001). Sc35 autoregulates its expression by promoting splicing events that destabilize its mrnas. *The EMBO journal*, 20:1785–1796.

Surget, S., Khoury, M. P., and Bourdon, J.-C. (2013). Uncovering the role of p53 splice variants in human malignancy: a clinical perspective. *OncoTargets and therapy*, 7:57–68.

Taliaferro, J. M., Vidaki, M., Oliveira, R., Olson, S., Zhan, L., Saxena, T., Wang, E. T., Graveley, B. R., Gertler, F. B., Swanson, M. S., and Burge, C. B. (2016). Distal alternative last exons localize mrnas to neural projections. *Molecular cell*, 61:821–833.

Thomas, J. D., Polaski, J. T., Feng, Q., De Neef, E. J., Hoppe, E. R., McSharry, M. V., Pangallo, J., Gabel, A. M., Belleville, A. E., Watson, J., Nkinsi, N. T., Berger, A. H., and Bradley, R. K. (2020). Rna isoform screens uncover the essentiality and tumor-suppressor activity of ultraconserved poison exons. *Nature genetics*, 52:84–94.

Turunen, J. J., Niemelä, E. H., Verma, B., and Frilander, M. J. (2013). The significant other: splicing by the minor spliceosome. *Wiley interdisciplinary reviews. RNA*, 4:61–76.

Uhlén, M., Fagerberg, L., Hallström, B. M., Lindskog, C., Oksvold, P., Mardinoglu, A., Sivertsson, s., Kampf, C., Sjöstedt, E., Asplund, A., Olsson, I., Edlund, K., Lundberg, E., Navani, S., Szigyarto, C. A.-K., Odeberg, J., Djureinovic, D., Takanen, J. O., Hober, S., Alm, T., Edqvist, P.-H., Berling, H., Tegel, H., Mulder, J., Rockberg, J., Nilsson, P., Schwenk, J. M., Hamsten, M., von Feilitzen, K., Forsberg, M., Persson, L., Johansson, F., Zwahlen, M., von Heijne, G., Nielsen, J., and Pontén, F. (2015). Proteomics. tissue-based map of the human proteome. *Science (New York, N.Y.)*, 347:1260419.

Ule, J., Stefani, G., Mele, A., Ruggiu, M., Wang, X., Taneri, B., Gaasterland, T., Blencowe, B. J., and Darnell, R. B. (2006). An rna map predicting nova-dependent splicing regulation. *Nature*, 444:580–586.

Verma, B., Akinyi, M. V., Norppa, A. J., and Frilander, M. J. (2018). Minor spliceosome and disease. *Seminars in cell & developmental biology*, 79:103–112.

Virshup, D. M. and Shenolikar, S. (2009). From promiscuity to precision: protein phosphatases get a makeover. *Molecular cell*, 33:537–545.

Wahl, M. C., Will, C. L., and Lührmann, R. (2009). The spliceosome: design principles of a dynamic rnp machine. *Cell*, 136:701–718.

Walz, S., Lorenzin, F., Morton, J., Wiese, K. E., von Eyss, B., Herold, S., Rycak, L., Dumay-Odelot, H., Karim, S., Bartkuhn, M., Roels, F., Wüstefeld, T., Fischer, M., Teichmann, M., Zender, L., Wei, C.-L., Sansom, O., Wolf, E., and Eilers, M. (2014). Activation and repression by oncogenic myc shape tumour-specific gene expression profiles. *Nature*, 511:483–487.

Wang, E. T., Sandberg, R., Luo, S., Khrebtukova, I., Zhang, L., Mayr, C., Kingsmore, S. F., Schroth, G. P., and Burge, C. B. (2008). Alternative isoform regulation in human tissue transcriptomes. *Nature*, 456:470–476.

Wang, H., Zhou, M., Shi, B., Zhang, Q., Jiang, H., Sun, Y., Liu, J., Zhou, K., Yao, M., Gu, J., Yang, S., Mao, Y., and Li, Z. (2011). Identification of an exon 4-deletion variant of epidermal growth factor receptor with increased metastasis-promoting capacity. *Neoplasia (New York, N.Y.)*, 13:461–471.

Wang, L.-H., Wu, C.-F., Rajasekaran, N., and Shin, Y. K. (2018). Loss of tumor suppressor gene function in human cancer: An overview. *Cellular physiology and biochemistry : international journal of experimental cellular physiology, biochemistry, and pharmacology*, 51:2647–2693.

Wang, M., Herrmann, C. J., Simonovic, M., Szklarczyk, D., and von Mering, C. (2015). Version 4.0 of paxdb: Protein abundance data, integrated across model organisms, tissues, and cell-lines. *Proteomics*, 15:3163–3168.

Wang, T., Yu, Q., Chen, J., Deng, B., Qian, L., and Le, Y. (2010). Pp2a mediated ampk inhibition promotes hsp70 expression in heat shock response. *PloS one*, 5.

Warzecha, C. C., Sato, T. K., Nabet, B., Hogenesch, J. B., and Carstens, R. P. (2009). Esrp1 and esrp2 are epithelial cell-type-specific regulators of fgfr2 splicing. *Molecular cell*, 33:591–601.

Wei, N., Cheng, Y., Wang, Z., Liu, Y., Luo, C., Liu, L., Chen, L., Xie, Z., Lu, Y., and Feng, Y. (2015). Srsf10 plays a role in myoblast differentiation and glucose production via regulation of alternative splicing. *Cell reports*, 13:1647–1657.

Weyn-Vanhentenryck, S. M., Feng, H., Ustianenko, D., Duffié, R., Yan, Q., Jacko, M., Martinez, J. C., Goodwin, M., Zhang, X., Hengst, U., Lomvardas, S., Swanson, M. S., and Zhang, C. (2018). Precise temporal regulation of alternative splicing during neural development. *Nature communications*, 9:2189.

Wilhelmi, I., Kanski, R., Neumann, A., Herdt, O., Hoff, F., Jacob, R., Preußner, M., and Heyd, F. (2016). Sec16 alternative splicing dynamically controls copii transport efficiency. *Nature communications*, 7:12347.

Will, C. L. and Lührmann, R. (2011). Spliceosome structure and function. *Cold Spring Harbor*

perspectives in biology, 3.

Wongsurawat, N., Davis, B. B., and Morley, J. E. (1990). Thermoregulatory failure in the elderly. st. louis university geriatric grand rounds. *Journal of the American Geriatrics Society*, 38:899–906.

Xia, Z., Zheng, X., Zheng, H., Liu, X., Yang, Z., and Wang, X. (2012). Cold-inducible rna-binding protein (cirp) regulates target mrna stabilization in the mouse testis. *FEBS letters*, 586:3299–3308.

Xiao, S. H. and Manley, J. L. (1997). Phosphorylation of the asf/sf2 rs domain affects both protein-protein and protein-rna interactions and is necessary for splicing. *Genes & development*, 11:334–344.

Xiao, S. H. and Manley, J. L. (1998). Phosphorylation-dephosphorylation differentially affects activities of splicing factor asf/sf2. *The EMBO journal*, 17:6359–6367.

Yang, C. and Carrier, F. (2001). The uv-inducible rna-binding protein a18 (a18 hnrnp) plays a protective role in the genotoxic stress response. *The Journal of biological chemistry*, 276:47277–47284.

Yang, Y., Zhan, L., Zhang, W., Sun, F., Wang, W., Tian, N., Bi, J., Wang, H., Shi, D., Jiang, Y., Zhang, Y., and Jin, Y. (2011). Rna secondary structure in mutually exclusive splicing. *Nature structural & molecular biology*, 18:159–168.

Yeakley, J. M., Tronchère, H., Olesen, J., Dyck, J. A., Wang, H. Y., and Fu, X. D. (1999). Phosphorylation regulates in vivo interaction and molecular targeting of serine/arginine-rich pre-mrna splicing factors. *The Journal of cell biology*, 145:447–455.

Younis, I., Dittmar, K., Wang, W., Foley, S. W., Berg, M. G., Hu, K. Y., Wei, Z., Wan, L., and Dreyfuss, G. (2013). Minor introns are embedded molecular switches regulated by highly unstable u6atac snrna. *eLife*, 2:e00780. Original DateCompleted: 20130805, Original DateCompleted: 20140206.

Zarnack, K., König, J., Tajnik, M., Martincorena, I., Eustermann, S., Stévant, I., Reyes, A., Anders, S., Luscombe, N. M., and Ule, J. (2013). Direct competition between hnrnp c and u2af65 protects the transcriptome from the exonization of alu elements. *Cell*, 152:453–466.

Zeng, Y., Kulkarni, P., Inoue, T., and Getzenberg, R. H. (2009). Down-regulating cold shock protein genes impairs cancer cell survival and enhances chemosensitivity. *Journal of cellular biochemistry*, 107:179–188.

Zhong, P. and Huang, H. (2017). Recent progress in the research of cold-inducible rna-binding protein. *Future science OA*, 3:FSO246.

Zhou, X., Li, X., Cheng, Y., Wu, W., Xie, Z., Xi, Q., Han, J., Wu, G., Fang, J., and Feng, Y. (2014a).

Bclaf1 and its splicing regulator srsf10 regulate the tumorigenic potential of colon cancer cells. *Nature communications*, 5:4581.

Zhou, X., Wu, W., Li, H., Cheng, Y., Wei, N., Zong, J., Feng, X., Xie, Z., Chen, D., Manley, J. L., Wang, H., and Feng, Y. (2014b). Transcriptome analysis of alternative splicing events regulated by srsf10 reveals position-dependent splicing modulation. *Nucleic acids research*, 42:4019–4030.

Zhou, Z. and Fu, X.-D. (2013). Regulation of splicing by sr proteins and sr protein-specific kinases. *Chromosoma*, 122:191–207.

5 Publications

5.1 Publication 1

Haltenhof, T., Kotte, A., De Bortoli, F., Schiefer, S., ***Meinke, S.****, Emmerichs, A.-K., Petermann, K.K., Timmermann, B., Imhof, P., Franz, A., Loll, B., Wahl, M.C., Preußner, M., Heyd. F. A conserved kinase-based body temperature sensor globally controls alternative splicing and gene expression. Mol Cell. 2020. 78(1):57-69.*

https://doi.org/10.1016/j.molcel.2020.01.028

5.2 Publication 2

***Meinke, S.**, Haltenhof, T., Kowar, A., Karni, R., Preußner, M., Heyd, F. Elevated body temperature activates tumor-suppressive phosphatase activity. (in preparation)*

Elevated body temperature activates tumor-suppressive phosphatase activity

Stefan Meinke[1], Tom Haltenhof[1$], Alexander Kowar[1], Rotem Karni[2], Marco Preußner[1], Florian Heyd[1*].

[1] Freie Universität Berlin, Institute of Chemistry and Biochemistry, Laboratory of RNA Biochemistry, Takustrasse 6, 14195 Berlin, Germany

[2] Department of Biochemistry and Molecular Biology, Institute for Medical Research Israel-Canada, Hebrew University-Hadassah Medical School, Jerusalem, 9112001, Israel.

[$] present address: Omiqa Corporation, c/o Freie Universität Berlin, Altensteinstrasse 40, 14195 Berlin, Germany

* corresponding author: florian.heyd@fu-berlin.de

Phone: +49 30 83862938 15

FAX: +49 30 838-4-62938

Abstract

Uncontrolled activation of cellular phosphorylation cascades is a hallmark of many diseases, most notably cancer and tauopathies. While the development of kinase inhibitors has been a central focus of drug development, the activation of tumor-suppressive phosphatases has remained a largely elusive goal. Here we show that the highly abundant anti-oncogenic phosphatase PP2A has higher activity at elevated body temperature. Remarkably, higher body temperature activates TP53 in a phosphatase-dependent manner, likely through alternative splicing of *MDM4*. Furthermore, MYC is more active at lower body temperature, consistent with a negative regulation through higher PP2A activity. Our data thus uncover a simple and endogenous mechanism to activate a central tumor suppressor and provide a molecular framework for the indication of tumor-thermotherapy. In addition, our model is consistent with and provides a molecular basis for the connection of decreased body temperature and the incidence of Alzheimer's and may pave the way for new therapeutic approaches.

Introduction

Over 90% of the cell's phosphatase activity is mediated by the serine/threonine protein phosphatases 1 and 2A[1] (PP1/2A). Transient protein phosphorylation is fundamental in cellular processes, such as cell survival, apoptosis, cell cycle progression, metabolism, and immunity[2]. PP2A is generally considered as a tumor suppressor protein and is aberrantly expressed or functionally altered in different types of cancers, including breast, skin, and colon cancer[3]. It forms heterotrimeric holoenzymes comprising a catalytic (C), a scaffold (A), and a regulatory (B) subunit. The A/C dimer forms the core enzyme, while the B subunits contribute to full PP2A activity, define substrate specificity, and subcellular localization[4]. PP2A interacts with the tumor-suppressive transcription factor TP53, contributing to its anti-tumorigenic properties[5]. Indeed, PP2A inhibitor overexpression, mutation-mediated inactivation of PP2A, or loss of phosphatase activation support cancer cell transformation[3]. Due to its tumor-suppressive function, PP2A represents a promising target for cancer therapies[6-8]. One systemic approach for tumor therapy is hyperthermia, which has been used in combination with radiotherapy or chemotherapy, improving therapeutic success[9]. Thermotherapy is thought to sensitize cancer cells to radiation or chemotherapeutic agents and to trigger the adaptive immune response against tumor cells[10]. However, an understanding of the molecular mechanism underlying thermotherapy is still missing and this gap of knowledge limits the broader use of hyperthermia in therapeutic applications.

In homeothermic organisms, the core body temperature is kept in a narrow temperature range. However, in mammals it shows circadian oscillations by 1°C – 4°C[11]. Molecular mechanisms reacting to these subtle temperature changes with impact on cellular functions remain elusive. Recently, we found that these subtle changes in body temperature are sufficient to control alternative splicing (AS)[12]. We identified the Cdc2-like kinases 1 and 4 (CLK1/4) as thermo-sensors, measuring these subtle temperature differences and translating them into global changes in AS and gene expression (GE). This is mediated via temperature-dependent serine/arginine-rich (SR) protein phosphorylation in the physiologically relevant temperature range[13]. SR proteins are generally known as splicing-activating RNA binding proteins (RBPs) and their activity is controlled by reversible phosphorylation. PP1/2A are essential regulators of the splicing reaction, as their inhibition was shown to inhibit splicing catalysis[14]. For instance, PP1 interacts with SR proteins and is required for heat-shock induced dephosphorylation of SRSF10[15].

We identified the molecular mechanism of CLK1/4 in response to subtle changes in the body temperature, but it is still unknown whether phosphatase activity is also temperature-dependent, or to which extend dephosphorylation (of SR proteins) impacts AS and GE during body temperature changes. In this work, we show that the catalytic subunit of the tumor-

suppressive PP2A is directly responsive to subtle temperature changes, with gradually increasing activity at higher temperatures. We furthermore show that inhibition of PP1/2A using okadaic acid (OA^{16}) globally abolish body temperature-dependent AS events and GE changes. Interestingly, the tumor-suppressive transcription factor TP53 is activated at higher temperatures in a PP2A-dependent manner, likely via *MDM4* AS. In contrast, oncogenic MYC-driven genes are cold-induced, consistent with negative regulation of PP2A activity. Based on these data, we suggest a novel, body temperature-dependent mechanism which activates TP53 tumor-suppressive function and provides molecular insights for the use of PP2A inhibitors or hyperthermia in cancer therapies.

Results

Body temperature-regulated SR protein phosphorylation is controlled by PP2A activity. Alternative splicing (AS) is regulated by small changes in body temperature through altered phosphorylation of SR proteins[12,17]. Recently, we identified CLK1/4 as highly responsive thermo-sensors that mediate body temperature-dependent SR protein phosphorylation and control AS[13]. *In vivo* the phosphorylation state of a protein is dynamically determined by balanced activities of site-specific kinases and rather unspecific phosphatases[18]. Experiments using the SR protein SRSF10 suggested a pivotal role of PP1 in controlling heat shock-mediated dephosphorylation[15], but it remains enigmatic to which extend phosphatases contribute to temperature-dependent differences in SR protein phosphorylation and pre-mRNA processing in the physiological temperature range. To address whether phosphatase activity is also directly temperature-responsive, we expressed and purified human His_{10}-tagged PP2A catalytic subunit (PP2AC) from High Five insect cells (Figure S1A and S1B). Purified PP2AC protein was used in *in vitro* phosphatase assays using dephosphorylation of a phosphorylated RS-repeat as read-out. Strikingly, we find stronger PP2AC-mediated dephosphorylation at higher temperatures with an almost linear increase in activity in the temperature range from 30°C to 43°C (R^2=0.9888; Figure 1A and 1B). In the physiologically relevant temperature range between 35°C and 39°C there is a 1.43-fold increase in phosphatase activity, highlighting the potential impact of body temperature changes on all cellular processes that depend on protein phosphorylation. PP2AC-mediated dephosphorylation of the SR peptide is not affected by differences in the pH between pH 6.5 and 8.5 (Figure S1C) suggesting a direct effect of temperature. While the linear change in phosphatase activity is clearly different from the almost on-off effect of temperature on CLK1/4 activity, the high abundance of phosphatases (>50-fold higher than CLK1[19]) strongly argues for an involvement in controlling temperature-dependent phosphorylation levels *in vivo*. As the activity of CLKs and potentially other kinases and phosphatases are regulated in opposite directions, we suggest that body temperature changes shift the balance between kinase and phosphatase signaling towards higher phosphorylation at lower temperature, which will impact on virtually all aspects on cellular homeostasis.

PP2A inhibition prevents temperature-controlled AS

To investigate a potential thermometer-like function of protein phosphatases, we investigated temperature-dependent AS after inhibition of both PP1 and PP2A by okadaic acid (OA, [16]). HEK293 cells were pre-incubated at 33°C for 12 hours to minimize PP1/2A activity and then shifted to 39°C (or maintained at 33°C as a control) for 2 hours in the presence or absence of OA (Figure S2A). We then used RNA-Seq and determined AS patterns using Whippet[20]; a principal component analysis reveals clear clustering of the biological replicates (Figure S2B).

In total, we identified 2134 AS events, of which the majority are alternative cassette exons (CE, 53.1%) or retained introns (RI, 16.7%, Figure S2C). We identified 1132 temperature-controlled CE and 356 RI events with a change in percentage spliced in (ΔPSI) > 15% in DMSO 33°C versus 39°C (Figure 2A and S2D). Remarkably, of these only 27 CE and 8 RI events remained temperature-dependent after inhibition of phosphatase activity (Figure 2A and S2D). These data show that temperature-sensitive AS is almost completely abolished after addition of OA (Figure 2A and S2D, see also clustering of OA 33°C and 39°C in S2B), thus strongly connecting phosphatase activity with temperature-controlled AS. Consistent with cold-reduced phosphatase activity *in vitro* (Figure 1), the 39°C OA samples essentially match the splicing pattern of the 33°C DMSO samples (Figure 2A and S2D). Using splicing sensitive RT-PCRs, we confirm these global observations for 4 out of 4 tested target genes (Figure 2B and S2E).

To compare the impact of temperature-dependent phosphatase and CLK1/4 kinase activity on AS patterns, we compared OA treatment to inhibition of CLK1/4 activity using TG003 (Figure 2C, S3A and S3B,[13]). Comparing temperature-dependent splicing events in DMSO reveals a highly significant overlap of regulated CE (hypergeometric p-value = 1.68e-404) and RI (hypergeometric p-value = 1.35e-96) events (Figure 2C and S3B), indicating that despite the different temperature schemes there is a comparable effect of temperature on AS. Globally, while OA treatment resembles cold-like splicing, CLK1/4 inhibition clearly induces a heat-like splicing pattern (Figure 2C and S3B), which is consistent with temperature antagonistically regulating CLK1/4 kinase and PP1/2A phosphatase activity. Additionally, while inhibition of CLK1/4 activity by TG003 quantitatively reduced temperature-dependent AS, some temperature-sensitivity remained (Figure 2C and especially S3B; see also [13]), potentially controlled through other CLKs (CLKs 2 and 3 are not inhibited by TG003) or other kinases/phosphatases. In contrast, temperature-regulated splicing is quantitatively abolished in OA treated cells (Figure 2C and S3B), indicating that all phosphatases involved in this process are OA-sensitive. Together, these data demonstrate that almost all body temperature-regulated AS events react to the inhibition of PP1/2A, showing that PP1/2A are essential mediators of temperature-sensitive AS.

Body temperature-controlled expression of cancer-associated genes is highly phosphatase-dependent

Next, we investigated whether temperature-controlled GE levels are also regulated by phosphatases. Consistent with our splicing data, temperature-induced changes in GE levels are abolished upon OA but only reduced upon TG003 treatment (Figure S4A). To analyze the dynamics of temperature-induced changes in AS and GE, we investigated HEK293 cells incubated at 33°C, 35°C, 37°C or 39°C for 2 (T2) or 12 hours (T12) by RNA-Seq (Figure 3A).

Previously described high-confidence CE events (Figure 2C) show AS changes with an almost identical amplitude after 2 and 12 hours (Figure 3B and S4B). In contrast, changes in GE are much more pronounced after 12 hours (Figure 3C and S4C). Consistently, we find, in an unbiased approach looking for linear temperature-dependent skipped exons or genes, more significant changes for GE after 12 hours (compare Figures S4D and S4E). These data clearly show that body temperature-induced alterations in AS precede changes in GE and would be consistent with a model where splicing changes induce rewiring of a transcription factor network to then control changes in transcription. To investigate which transcription factors are affected by temperature, we performed a transcription factor enrichment analysis [21] using linear temperature-dependent genes (Figure S4E). This analysis revealed that a distinct set of transcription factors controls heat- and cold-induced GE specifically after 12 hours (Figures 3D and S5A). The transcription factors TP53, UBTF and SMAD4 clearly control the expression of heat-induced genes, while MYC and MAX control cold-induced GE. Consistently, we find over 30% of TP53-bound transcripts specifically upregulated in heat, while MYC-bound transcripts (>20%) are upregulated in cold (Figure 3E and S5B). Increased MYC activity in cold is consistent with higher PP2A activity at higher temperature, as PP2A has been shown to mediate destabilization of MYC[1]. The transcription factors MYC and MAX are also enriched in cold-induced genes in mouse MEFs and RAW cells (Figure S5C) indicating an evolutionary conserved signaling pathway. In contrast, heat-induced activity of TP53 appears cell-type and/or species-specific, as it is not observed in mouse MEFs and RAW cells (Figure S5C). Interestingly, *TP53* and *SMAD4* are typical tumor-suppressor genes [22,23], while *MYC* and *MAX* are described as oncogenes [24], suggesting that colder temperature supports a more oncogenic environment, whereas warmer temperature leads to a tumor suppressive milieu. In line with this finding, we detect temperature- and OA-dependent GE in 323 (of 723) cancer-associated genes[25] (Figure S6). Most of these genes are favourable expressed at warm temperatures (including many tumor-suppressor genes) indicating a directional effect of temperature on cancer-associated GE programs (Figure S6). Together, these data demonstrate a strong effect of temperature on cancer-associated GE and reveal a possible molecular explanation for the use of PP2A inhibitors [26] and hyperthermia [27] in cancer treatment.

Body temperature-regulated AS of cancer-associated genes is controlled by PP1/2A

To find a potential connection of temperature-dependent AS after 2 hours and altered TP53 target GE after 12 hours we screened for altered splicing events in cancer-associated genes. We identified 66 temperature – and mostly OA but not TG003 – dependent splicing events that were significantly altered after 2 hours at different temperatures (Figure 4A and S7A, examples in S7B). This includes temperature-dependent AS of exon 6 of the TP53 regulator MDM4, which is more pronounced after 2 than after 12 hours (Figure 4B). By decreasing the amounts

of MDM4 protein, this exon was described to control TP53 stability/activity [28]. TP53 is activated by exon 6 skipping [29] and exon 6 skipping is increased at warmer temperature, correlating with increased expression of *TP53* and TP53 target genes. *MDM4* AS is antagonistically effected by TG003 and OA treatment (Figure 4C), which could be mediated via antagonistic effects on SRSF3 phosphorylation [29]. We therefore present a mechanistic basis for body temperature-controlled expression of *TP53*. These data could also provide a molecular framework for cancer thermotherapy, which, if it goes through body temperature controlled *MDM4* splicing, requires wt *TP53* to be effective.

However, we would like to point out that other heat-induced splicing isoforms, where also described as oncogenic. One particularly interesting gene is *MKNK2* as usage of an alternative 3' splice site in its last exon 14 (E14) results in two different isoforms: the tumor-suppressive isoform Mnk2a containing a binding site for MAP kinases, and the oncogenic Mnk2b isoform lacking the MAPK-binding site. Our RNA-Seq analysis clearly show, that *MKNK2* AS is strongly temperature-dependent with an increase in oncogenic *MKNK2* splicing at higher temperatures (Figure S7B and S8A). This body temperature-regulated splicing event is independent of CLK1/4 activity, but strongly based on phosphatase activity, as OA treatment completely abolished temperature-sensitivity (Figure S7B). We confirmed temperature-sensitive and PP2A-dependent, oncogenic *MKNK2* AS using splice-sensitive RT-PCR (Figure S8B and S8C). In order to identify the cis-regulatory element responsible for temperature-controlled *MKNK2* AS we used mutational analysis of the *MKNK2* minigene harboring the sequence ranging from E13 to E14 (Figure S8D, top). First, we deleted the majority of E14a (1,800 nucleotides) via mutational PCR. The resulting minigene was still responsive to temperature changes, with a significant induction of oncogenic Mnk2b splicing at 39 °C (Figure S8D, bottom). However, by further deletions in E14a we identified a 148 nucleotides sequence, which deletion completely abolished heat-induced splicing changes (Figure S8D). Next, we made use of 4 different RBP prediction tools, to identify *trans*-regulatory elements which bind in this 148 nucleotides sequence and control temperature-dependent oncogenic *MKNK2* AS (Figure S8E). This identified, amongst others, SRSF1, SRSF2, hnRNPH1 and hnRNPK as potential regulatory RBPs binding to this specific region in *MKNK2* E14a (Figure S8E). To confirm these results, we performed an siRNA screen and transfected HEK293 cells with a pool of 4 siRNAs against the respective RBP and analyzed *MKNK2* AS by RT-PCR (Figure S8F). This screen clearly confirmed SRSF1, SRSF2, hnRNPH1 and hnRNPK as regulators of *MKNK2* AS, as knockdown of the hnRNPs shifted *MKNK2* splicing towards the oncogenic Mnk2b isoform, whereas knockdown of the SR proteins leads to an increase in the tumor-suppressive Mnk2a isoform (Figure 4F). This is in line with previously published data on SRSF1 being an oncogene and leading to oncogenic *MKNK2* splicing [30,31].

Discussion

Body temperature-regulated SR protein phosphorylation is controlled by PP2A activity.

In this study, we showed that the PP2A phosphatase responds to small body temperature changes with increased activity at higher temperatures. Globally, temperature-dependent GE and AS changes are abolished upon phosphatase inhibition using OA. This indicates, that PP1/2A activity is essential for global temperature-sensitive AS. Besides the recently described cold-induced activity of CLK1/4 [13], which leads to temperature-dependent AS by differential SR protein phosphorylation, we now show temperature-sensitive PP2A activity further promoting heat-induced SR protein dephosphorylation. However, since OA both inhibits both PP1 and PP2A [16], further studies are necessary to determine whether both phosphatases act in a concerted manner, or separately. The entire PP2A holoenzyme is composed of three subunits. The regulatory subunits are differentially spliced and expressed in a tissue-specific and time-dependent manner[32,33], which could additionally affect temperature-dependent PP2A activity, resulting in differential target gene AS and expression.

While SR proteins are specific substrates for CLKs or SRPKs, PP1/2A dephosphorylates a plethora of diverse substrates, predominantly defined by the regulatory subunits [34]. Furthermore, B subunit binding to the PP2A core dimer is controlled by the accessibility and post-translational modifications of the C-terminus of the C subunit [35]. The leucine carboxyl methyltransferase 1 (LCMT-1) and phosphatase methylesterase 1 (PME-1) are responsible for methylation and demethylation, respectively, of the C subunit, regulating PP2A function [36]. An interesting question is whether other post-translational modifications, besides phosphorylation, are temperature-dependent as well. Therefore, temperature-sensitive upstream regulators of kinases and phosphatases could influence their activity or interactions with their substrates, resulting in altered phosphorylation patterns and AS outcome. The same holds true for post-translational modifications of other RBPs, such as hnRNPs, with a potential impact on temperature-dependent target gene splicing and expression.

PP2A is generally considered as a tumor suppressor. *In vitro* experiments using the phosphatase inhibitor OA showed that suppression of PP2A causes oncogenic transformation of multiple human cell lines [37], and mice lacking the B56δ subunit spontaneously developed tumors [38]. PP2A interacts with TP53 [5], c-MYC [39], and CDC25 [40], making it a promising target for cancer therapies. Our data propose an oncogenic effect of colder temperature, as MYC activity is increased at 33°C, when PP2A is inactive. This is consistent with higher MYC activity in its phosphorylated state promoting cell growth in cancer cells with insufficient PP2A activity [39]. In contrast, TP53 gets activated by *MDM4* exon 6 skipping [29], which we found to be upregulated in heat. This correlated with heat-induced expression of TP53 target genes. We found *MDM4* exon 6 skipping antagonistically effected by TG003 and OA treatment, indicating

that this splicing event is controlled by antagonistic effects on SRSF3 phosphorylation [29]. However, the direct effect of temperature-sensitive *MDM4* AS on TP53 activation still has to be shown, for instance by using splice-site blocking morpholinos or CRISPR/Cas9-mediated genome editing to modulate *MDM4* splicing. As *TP53* is mutated in over 50 % of cancers [41] it would be very interesting to compare cells with WT or mutated/inactivated *TP53* with respect to the temperature-responsiveness. Heat-induced eradication of tumors (hyperthermia) has been used in combination with radiation or chemotherapy, with positive results in cancer therapy against tumor cells with wt *TP53* [27]. One explanation for heat-induced tumor repression is an improvement of the adaptive immune response due to the generation of heat shock factors, the activation of antigen-presenting cells, stimulation of lymphocyte trafficking, and the release of chemoattractants for leukocytes [10]. However, a detailed molecular function of hyperthermia is still poorly understood. Our model provides a molecular mechanism to activate a central tumor suppressor and adds a potential explanation for the use of tumor-thermotherapy in cancers harboring wt *TP53*.

Furthermore, PP2A has been described to be the primary Tau-binding phosphatase and, therefore, plays a fundamental role in the development of the Alzheimer's disease [42]. Hyperphosphorylation of Tau results in the formation of neurofibrillary tangles and PP2A activity accounts for around 71 % of total Tau phosphatase activity in the human brain [43]. Consequently, alterations in PP2A catalytic activity, subunit expression, or post-translational modifications were found in brain samples of Alzheimer's patients [44-46]. Additionally, the risk of getting diagnosed with Alzheimer's disease increases by aging [47], while the body temperature decreases [48]. Our findings of cold-induced kinase activity [13] together with cold-inhibited PP2A activity are consistent with decreased body temperature in the elderly population and the higher risk of getting Alzheimer's disease as a consequence of Tau hyperphosphorylation.

In summary, we show that tumor-suppressive PP2A activity gets activated at elevated temperatures and provide a molecular mechanism for the use of hyperthermia in tumor therapies.

Author Contributions

SM cloned and expressed the PP2AC protein and performed the *in vitro* phosphatase assays with help from TH and AK. SM performed experiments. RK helped in experimental design. MP performed the bioinformatics analysis. SM, MP, and FH designed the study, planned experiments, analyzed the data and wrote the manuscript. MP and FH conceived and supervised the work.

Acknowledgements

The authors would like to thank Markus Wahl and Andreas Franz for insect cell culture help and protein purification supplies. Furthermore, we would like to thank Vincent Maciej for his support regarding the size exclusion chromatography. We thank the HPC Service of ZEDAT, Freie Universität Berlin, for computing time. This work was funded by the DFG grant HE5398/4-2 to FH, with additional funding provided by the DFG grant 278001972 – TRR186.

Material and Methods

Tissue cell culture:

HEK293 cells were cultured in DMEM medium (Biowest) supplemented with 10% FBS (Biochrom) and 1% penicillin/streptomycin (Biowest) at the indicated temperatures and 5% CO_2. Early passage aliquots were thawed periodically, and cell morphology is routinely assessed. Cells were tested for mycoplasma contamination monthly using a PCR-based assay. For phosphatase-dependent AS and GE analyses, confluent HEK293 cells were incubated at 33°C for 12 hours, treated with 1 µM OA (or DMSO as solvent control) for 30 min, and then shifted to 39°C or kept at 33°C for 2 hours before RNA extraction.

For the siRNA screen, HEK293 cells were transfected with 20 pmol of a pool of 4 individual siRNAs against the respective target gene using ROTI®Fect (Carl Roth) according to the manufacturer's instructions. 48 hours post-transfection, cells were harvested for RNA extraction.

Cloning, protein production and purification

hPPP2CA was amplified from HEK293-derived cDNA and cloned into a modified pFL vector using EcoRI and SalI, directing the production of a fusion protein with an N-terminal, cleavable His_{10}-tag. The resulting plasmid was validated by sequencing, transformed into Escherichia coli DH10 MultiBacY cells and integrated into the baculovirus genome via Tn7 transposition.

A Blue-white screening was used to select for positive recombinants and the bacmid DNA was isolated and transfected into adhesive Sf9 insect cells (Invitrogen) in 6-well plates using Xtreme gene 9 DNA transfection reagent (Roche Applied Science). Transfection efficiency was monitored by eYFP fluorescence. The initial V0 virus was harvested 60 hours post-transfection and used for infection of High Five insect cells (Invitrogen) to produce the second, high titer virus generation V1. The V1 virus was used to infect 400 ml High Five cells for large scale protein production. The infected cells were harvested when the eYFP signal reached a plateau and before the cell viability decreased below 90%.

The High Five cell pellet was resuspended in His-Binding Buffer (50 mM Tris-Cl, pH 7.5, 5 mM imidazole, 100 mM NaCl, 0.1 mM EDTA, supplemented with protease inhibitors (cOmplete Tablets, Roche)) followed by lysis via sonication using a Sonoplus Ultrasonic Homogenizer HD 3100 (Bandelin). The lysate was cleared by centrifugation followed by affinity chromatography purification using His-Select Nickel Affinity Gel (Sigma) beads. After washing using His-Wash Buffer (50 mM Tris-Cl, pH 7.5, 20 mM imidazole, 300 mM NaCl, 0.1 mM EDTA) His_{10}-PP2AC was eluted with His-Elution Buffer (50 mM Tris-Cl, ph 7.5, 50 300 mM imidazole, 50 mM NaCl, 0.1 mM EDTA). The eluted protein was further purified by size exclusion on a Superdex 75 10/300 GL column (GE Healthcare) in elution Buffer. Peak fractions were analyzed by SDS-PAGE. Target protein-containing fractions were pooled, concentrated and shock-frozen in liquid nitrogen.

hSRPK1 open reading frame (ORF) was cloned from HEK293-derived cDNA into a modified pET vector with an N-terminal His_6-tag, using BamHI and XbaI. The resulting plasmid was validated by sequencing. For protein expression, the construct was transformed into *E. coli* strain BL21(DE3)pLysS and expression was induced with 0.2 mM IPTG at 18°C overnight. Cells were lysed by sonication and after centrifugation the supernatant was subjected to a His-pull down. His_6-tagged hSRPK-bound beads were resuspended in 100 µl polynukleotid kinase buffer (70 mM Tris-HCl, pH7.5, 10 mM $MgCl_2$, 5 mM DTT).

For minigene cloning, human genomic DNA was used as a template to amplify *MKNK2* exons 13 to 14 and introduce HindIII and EcoRI restriction sites via PCR. The product was restriction digested using HindIII and EcoRI (Thermo Scientific) and ligated into the pcDNA3.1(+) vector. For mutational analysis *MKNK2* exon 14a sequences were deleted via 2-step PCR and cloned into pcDNA3.1(+) vector using HindIII and EcoRI restriction sites. Minigenes (0.8 µg) were transfected into HEK293 cells using ROTI®Fect (Carl Roth) according to the manufacturer's instructions. RNAs were treated with DNAse I prior to the RT reaction.

All primer sequences are available upon request.

Phosphatase Assay

For *in vitro* phosphatase assays, first, to generate the phosphorylated substrate, the 100 µl beads with bound SRPK1 were incubated with purified GST-RS substrate [13] and 0.05 µl [γ-^{32}P]ATP at 37°C for 30 min. The mixture was centrifuged and the supernatant, containing the phosphorylated GST-RS substrate, was collected. For the phosphatase reaction, 2 µl of the GST-RS substrate were incubated with purified His_{10}-hPP2AC (final concentration of 100 nM) and phosphatase buffer (25 mM Tris, pH8, 150 mM NaCl, 2 mM DTT, 50 µM $MnCl_2$, 1 mM EDTA) in a total Volume of 15 µl at the indicated temperatures for 5 min. The reactions were stopped by adding 6x SDS-loading dye. The samples were heated to 95°C for 5 min and analyzed on a 12% SDS-PAGE. Equal loading was confirmed by Coomassie staining before the gels were dried on a filter paper and exposed to phosphoscreen for 2 hours. Phosphorylation signals were detected by a Phosphoimager and analyzed using ImageQuantTL software.

RNA isolation, RT-PCR and RT-qPCR

RNA extraction and RT-PCRs were performed as previously described [12]. Briefly, total RNA was isolated using RNATri (Bio&Sell) followed by DNAse I digestion. 1 µg of RNA was used for a gene-specific RT reaction. A low-cycle PCR using a ^{32}P-labeled forward primer was performed and products were separated by denaturing PAGE and quantified using a Phosphoimager and ImageQuantTL software. For qPCR analyses, up to 4 gene-specific primers were combined in one RT reaction and qPCRs were performed using Absolute QPCR SYBR Green Mix (Thermo Fisher) in a 96-well format on a Stratagene Mx3000P instrument. The reactions were performed in duplicates, and mean values were normalized to the expression of the housekeeping gene *GAPDH* (ΔCT) and Δ(ΔCT)s were calculated for different conditions.

RNA-Seq analysis and bioinformatics

To identify phosphatase-dependent and temperature-regulated AS in human cells, confluent HEK293 cells were incubated at 33°C for 12 hours. Cells were then treated with OA (or DMSO as solvent control) and after further 30 minutes at 33°C, samples were incubated for 2 hours at either 39°C or 33°C. RNA was extracted using RNATri (Bio&Sell) followed by DNaseI digestion. Sequencing libraries were analyzed on a HiSeq4000 instrument yielding ~50 million paired-end 150-bp reads per replicate and condition. To investigate the linear response to temperature, confluent HEK293 cells were incubated at 33, 35, 37, or 39°C for 2 or 12 hours and RNA was extracted as described above. Sequencing libraries yielded 30-50 million paired-

end 100-bp reads per replicate and condition. Reads were aligned to the hg38 genome and splicing patterns as well as transcripts per million (tpm) values were determined using Whippet version 0.11 [20]. Events with a minimum PSI difference of 0.15 and a probability above 0.9 between the two temperatures in DMSO control were further investigated. For gene expression, genes were considered temperature-dependent in DMSO when first tpm values are > 5 in all samples and the mean fold-change is >1.3 between DMSO 35°C and DMSO 39°C. Downstream analyses and comparisons with RNA sequencing data after inhibition of CLK1/4 activity [13] were performed using Python2 (numpy, [49]), Matplotlib (data visualization, [50]) or GraphPad Prism 7.05. PCA blot was produced using Standard scaler and PCA in Python2.

Linear temperature dependent genes or exons were defined as follows: For skipped exons we discriminated between cold-included (ΔPSI[33°C-39°C] > 0.15; ΔPSI[33°C-35°C] > 0.03; ΔPSI[35°C-37°C] > 0.03; ΔPSI[37°C-39°C] > 0.03) or heat-included exons (ΔPSI[33°C-39°C] < -0.15; ΔPSI[33°C-35°C] < -0.03; ΔPSI[35°C-37°C] < -0.03; ΔPSI[37°C-39°C] < -0.03). For gene expression we discriminated between cold-induced (fold change GE[33°C]/GE[39°C] > 1.3; GE[33°C]/GE[35°C] > 1.1; GE[35°C]/GE[37°C] > 1.1; GE[37°C]/GE[39°C] > 1.1) and heat-induced (fold change GE[33°C]/GE[39°C] < 0.77; GE[33°C]/GE[35°C] < 0.91; GE[35°C]/GE[37°C] < 0.91; GE[37°C]/GE[39°C] < 0.91).
Cancer-associated genes are based on Census [25]. Transcription factor enrichment p-values were calculated using the X2K web platform [51]. To determine MYC and TP53-bound promotors we used Chip data provided by CHEA2016 and ENCODE (1649 expressed genes for MYC and 249 for TP53). Blotted is the percentage of this genes with a fold-change >1.5 upon temperature change.

Figures

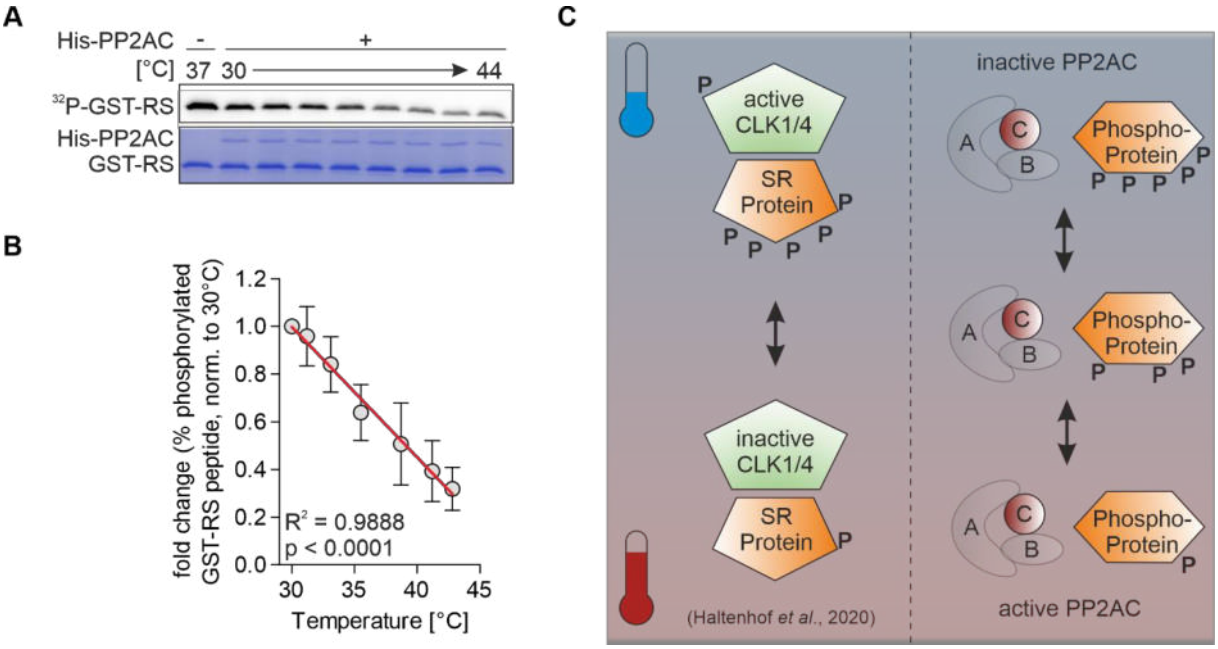

Figure 1

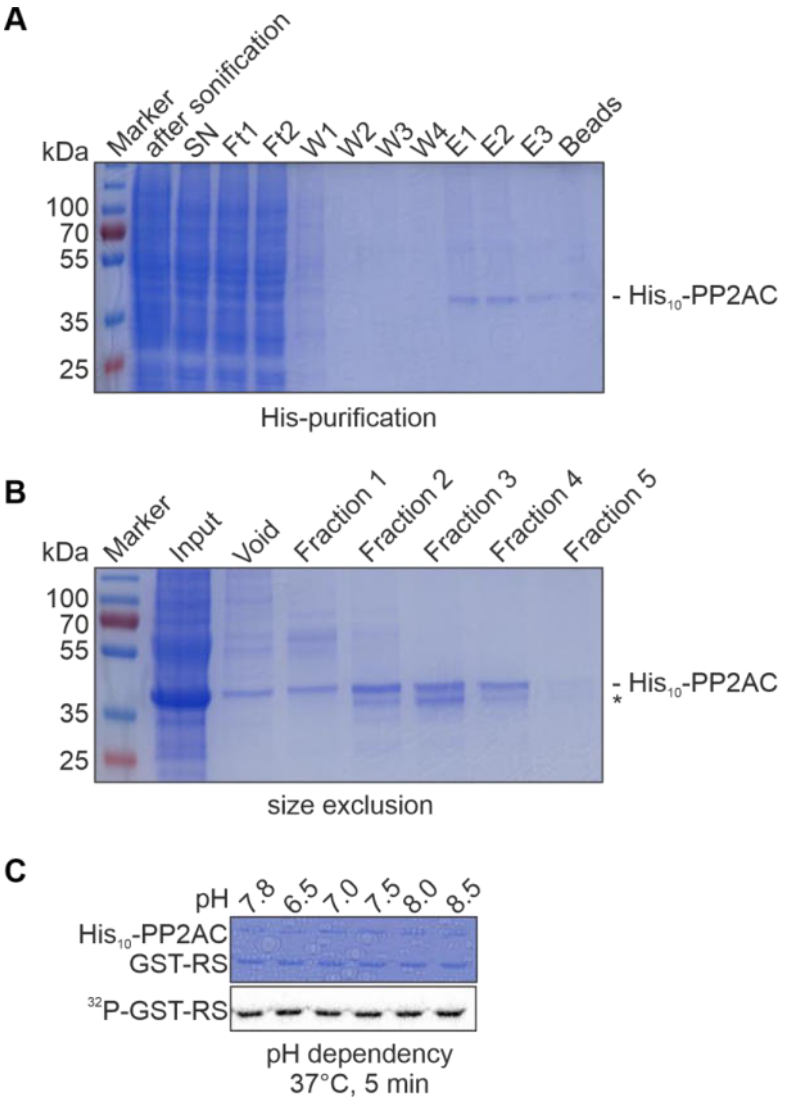
A
Marker
after sonification
SN
Ft1
Ft2
W1
W2
W3
W4
E1
E2
E3
Beads
kDa
100
70
55
35
25
- His10-PP2AC
His-purification
B
Marker
Input
Void
Fraction 1
Fraction 2
Fraction 3
Fraction 4
Fraction 5
kDa
100
70
55
35
25
- His10-PP2AC
*
size exclusion
C
pH 7.8 6.5 7.0 7.5 8.0 8.5
His10-PP2AC
GST-RS
32P-GST-RS
pH dependency
37°C, 5 min

Figure S1

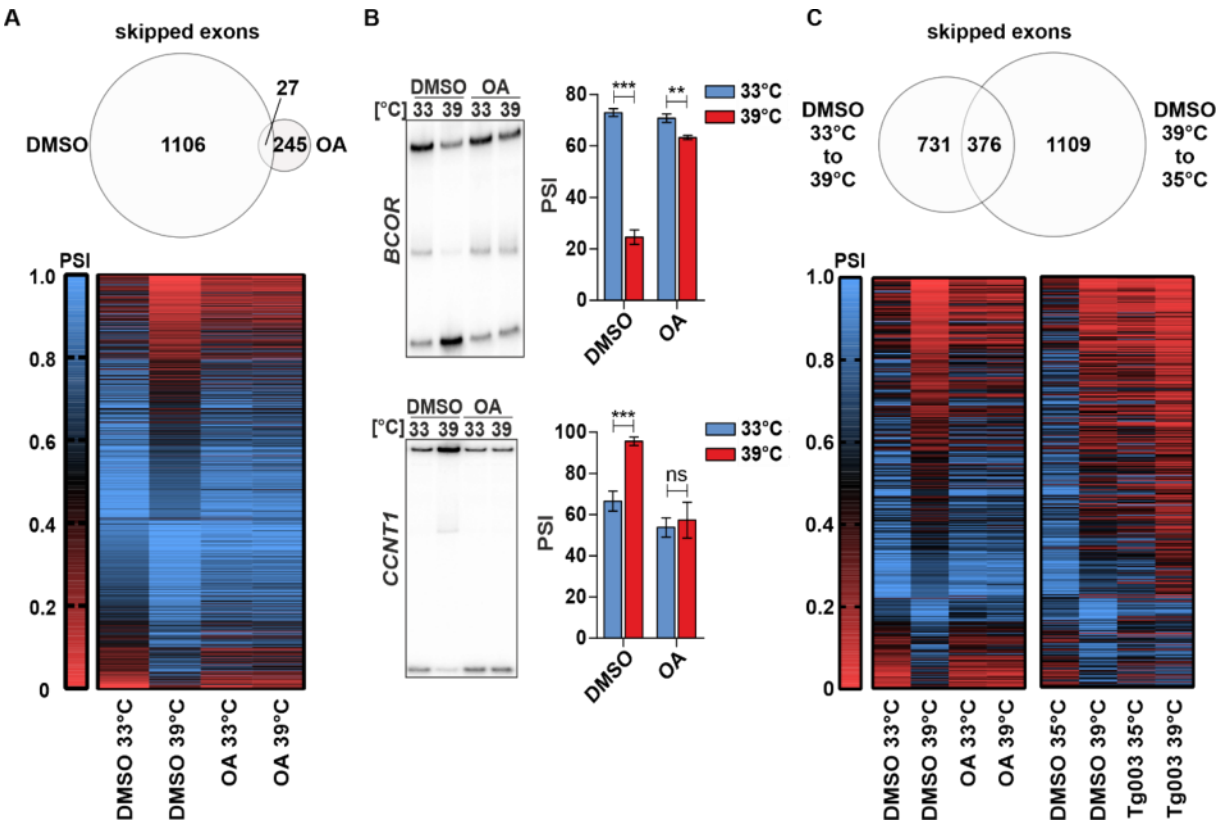
A
skipped exons
DMSO
1106
27
245
OA
PSI
1.0
0.8
0.6
0.4
0.2
0
DMSO 33°C
DMSO 39°C
OA 33°C
OA 39°C
B
DMSO OA
[°C] 33 39 33 39
BCOR
PSI
80
60
40
20
0
***
**
33°C
39°C
DMSO
OA
CCNT1
100
ns
C
skipped exons
DMSO 33°C to 39°C
731
376
1109
DMSO 39°C to 35°C
DMSO 35°C
Tg003 35°C
Tg003 39°C

Figure 2

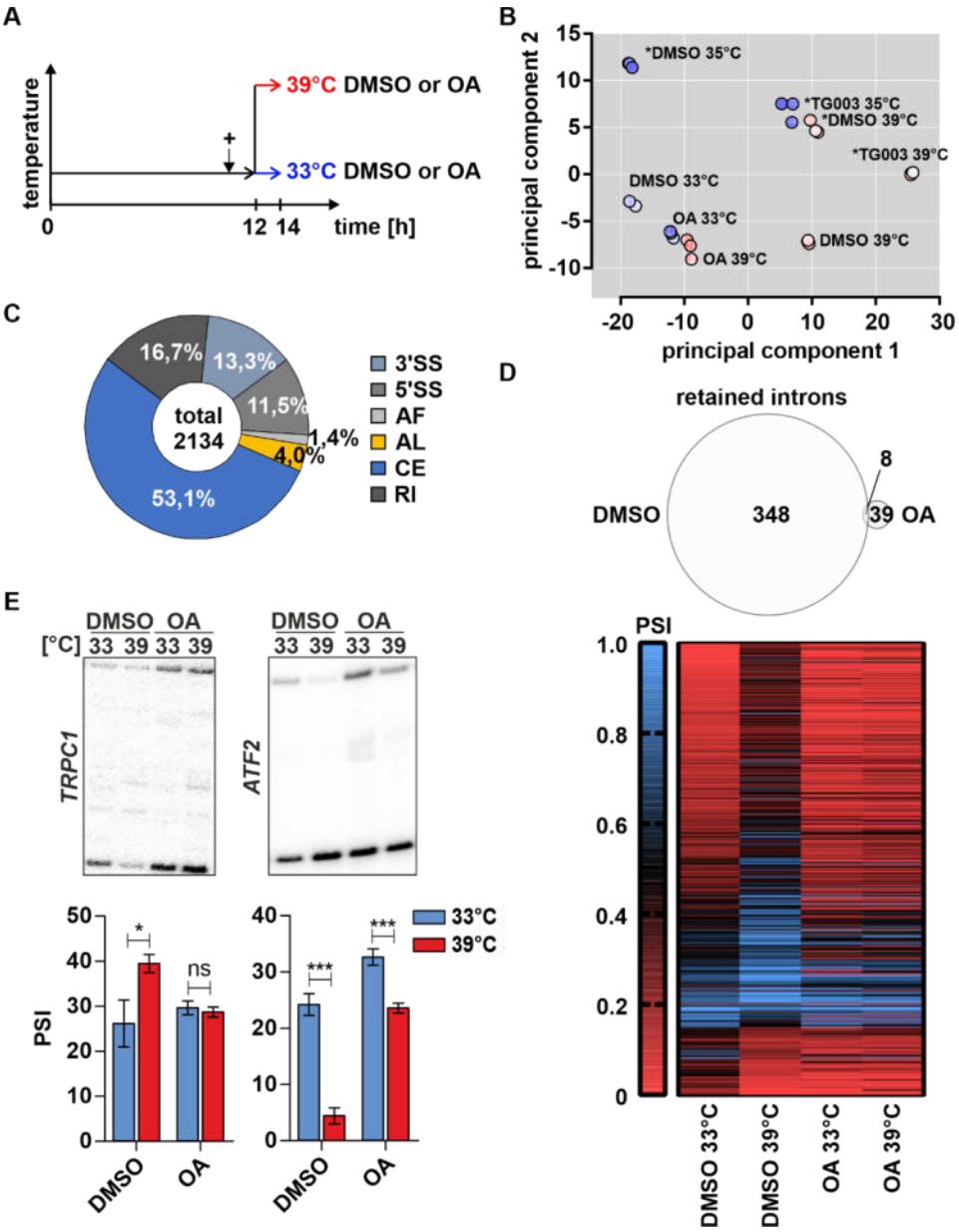
A
temperature
39°C DMSO or OA
33°C DMSO or OA
0
12 14
time [h]
B
principal component 2
principal component 1
*DMSO 35°C
*TG003 35°C
*DMSO 39°C
*TG003 39°C
DMSO 33°C
OA 33°C
DMSO 39°C
OA 39°C
C
total 2134
16,7%
13,3%
11,5%
1,4%
4,0%
53,1%
3'SS
5'SS
AF
AL
CE
RI
D
retained introns
DMSO
348
8
39 OA
PSI
DMSO 33°C
DMSO 39°C
OA 33°C
OA 39°C
E
DMSO OA
[°C] 33 39 33 39
TRPC1
ATF2
PSI
33°C
39°C
ns
DMSO
OA

Figure S2

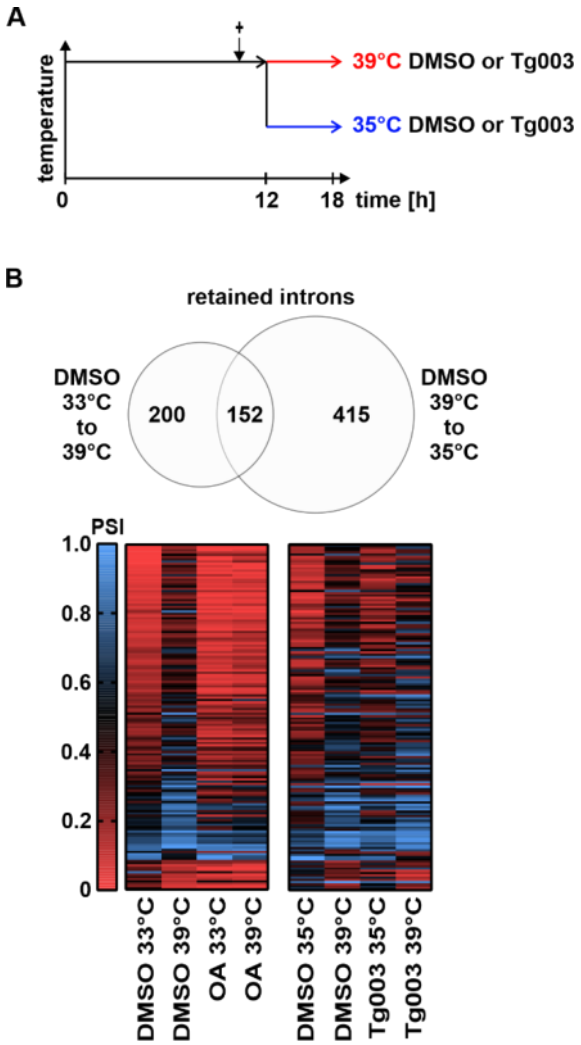
A
temperature
39°C DMSO or Tg003
35°C DMSO or Tg003
0
12
18 time [h]
B
retained introns
DMSO 33°C to 39°C
200
152
415
DMSO 39°C to 35°C
PSI
1.0
0.8
0.6
0.4
0.2
0
DMSO 33°C
DMSO 39°C
OA 33°C
OA 39°C
DMSO 35°C
DMSO 39°C
Tg003 35°C
Tg003 39°C

Figure S3

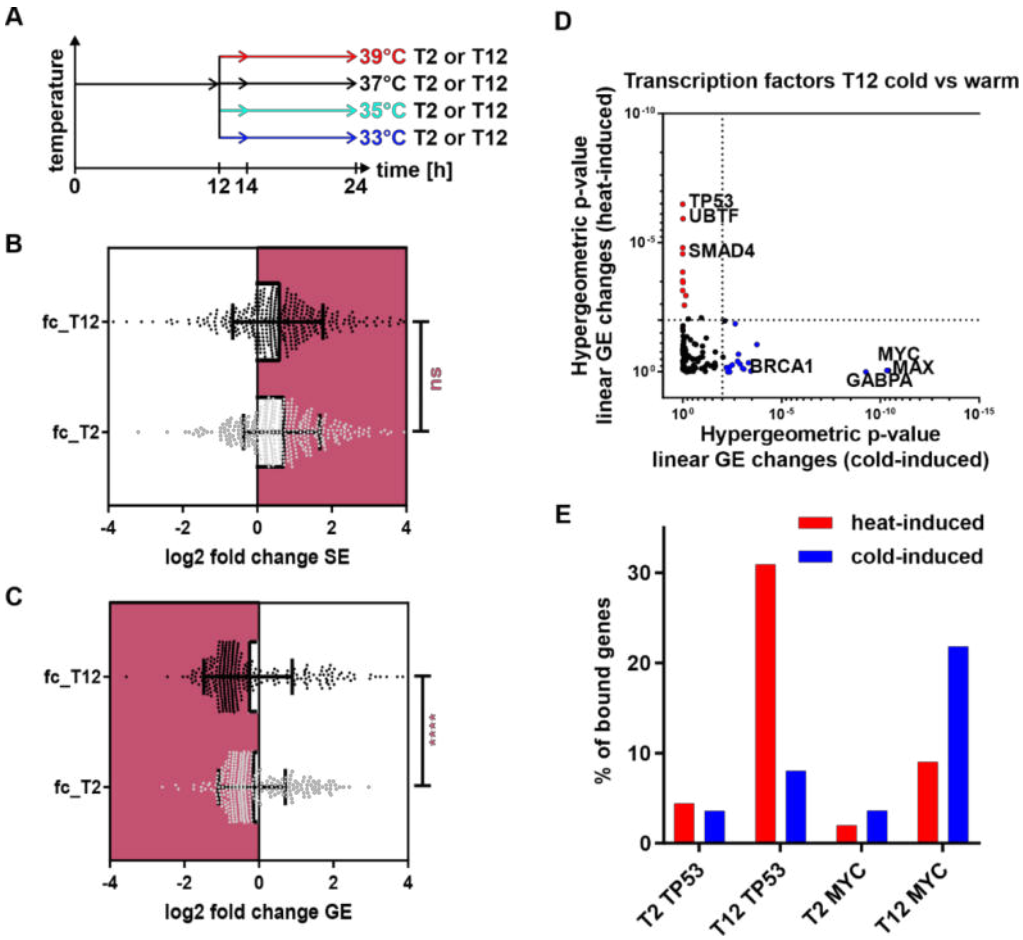
A
temperature
39°C T2 or T12
37°C T2 or T12
35°C T2 or T12
33°C T2 or T12
time [h]
0
12 14
24
B
fc_T12
fc_T2
ns
-4
-2
0
2
4
log2 fold change SE
C
fc_T12
fc_T2
****
-4
-2
0
2
4
log2 fold change GE
D
Transcription factors T12 cold vs warm
Hypergeometric p-value
linear GE changes (heat-induced)
TP53
UBTF
SMAD4
BRCA1
MYC
MAX
GABPA
Hypergeometric p-value
linear GE changes (cold-induced)
E
heat-induced
cold-induced
% of bound genes
30
20
10
0
T2 TP53
T12 TP53
T2 MYC
T12 MYC

Figure 3

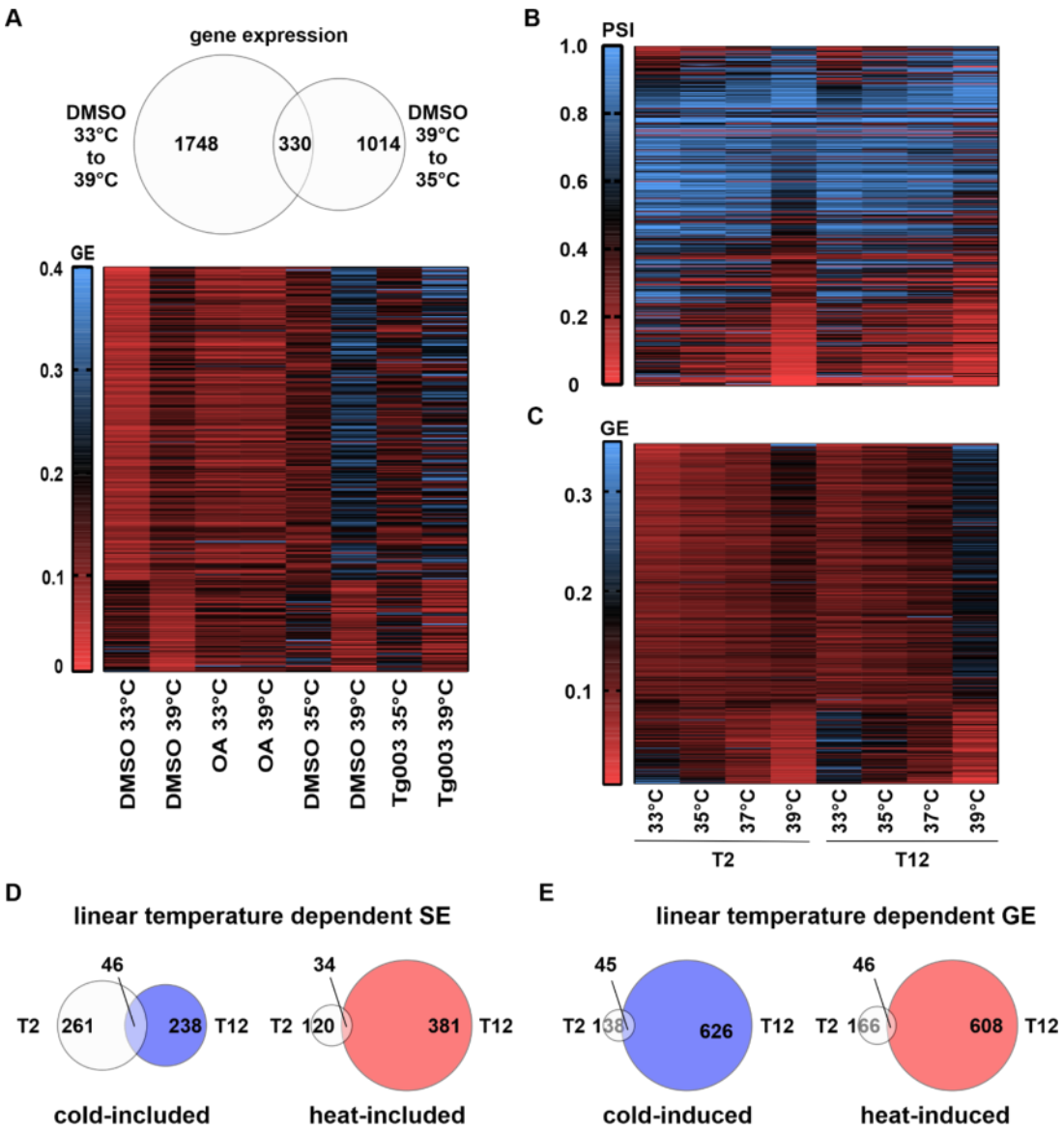
A
gene expression
DMSO 33°C to 39°C
1748
330
1014
DMSO 39°C to 35°C
GE
0.4
0.3
0.2
0.1
0
DMSO 33°C
DMSO 39°C
OA 33°C
OA 39°C
DMSO 35°C
DMSO 39°C
Tg003 35°C
Tg003 39°C
B
PSI
1.0
0.8
0.6
0.4
0.2
0
C
GE
0.3
0.2
0.1
33°C
35°C
37°C
39°C
33°C
35°C
37°C
39°C
T2
T12
D
linear temperature dependent SE
46
T2
261
238
T12
cold-included
34
T2
120
381
T12
heat-included
E
linear temperature dependent GE
45
T2
138
626
T12
cold-induced
46
T2
166
608
T12
heat-induced

Figure S4

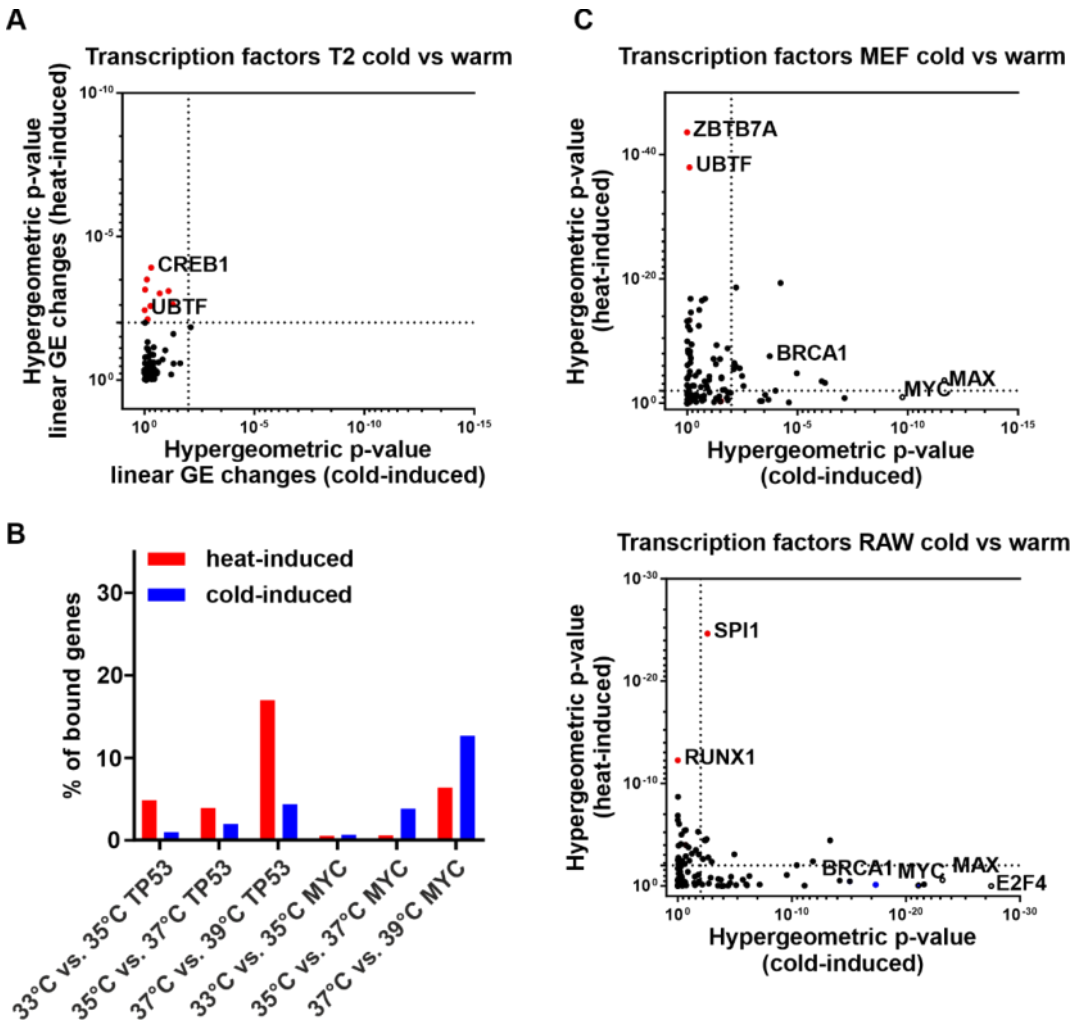
A
Transcription factors T2 cold vs warm
Hypergeometric p-value linear GE changes (heat-induced)
Hypergeometric p-value linear GE changes (cold-induced)
CREB1
UBTF
C
Transcription factors MEF cold vs warm
Hypergeometric p-value (heat-induced)
Hypergeometric p-value (cold-induced)
ZBTB7A
UBTF
BRCA1
MYC
MAX
B
heat-induced
cold-induced
% of bound genes
33°C vs. 35°C TP53
35°C vs. 37°C TP53
37°C vs. 39°C TP53
33°C vs. 35°C MYC
35°C vs. 37°C MYC
37°C vs. 39°C MYC
Transcription factors RAW cold vs warm
Hypergeometric p-value (heat-induced)
Hypergeometric p-value (cold-induced)
SPI1
RUNX1
BRCA1
MYC
MAX
E2F4

Figure S5

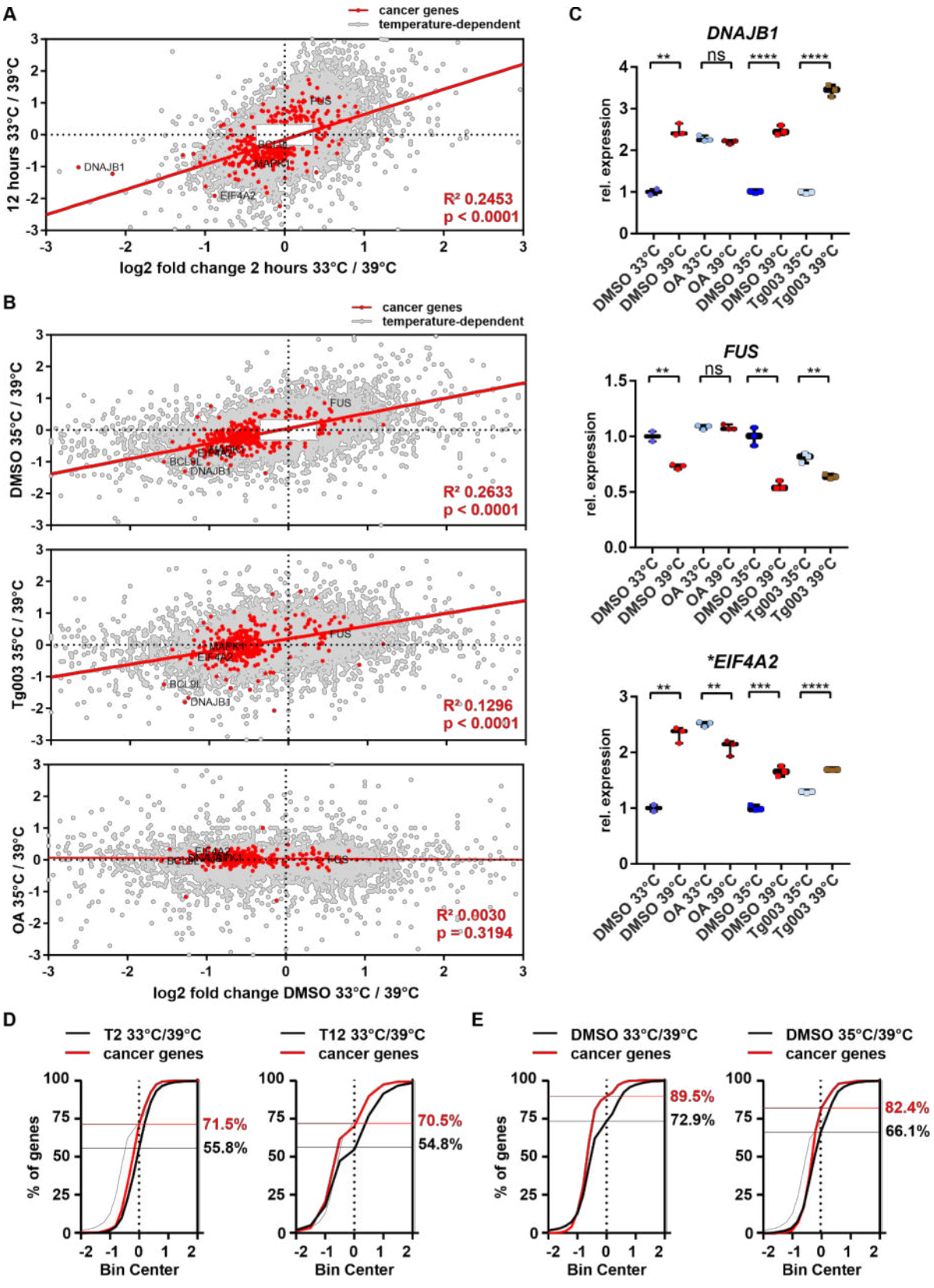
A
cancer genes
temperature-dependent
12 hours 33°C / 39°C
log2 fold change 2 hours 33°C / 39°C
DNAJB1
FUS
EIF4A2
R² 0.2453
p < 0.0001
B
DMSO 35°C / 39°C
Tg003 35°C / 39°C
OA 35°C / 39°C
log2 fold change DMSO 33°C / 39°C
BCL9L
R² 0.2633
p < 0.0001
R² 0.1296
p < 0.0001
R² 0.0030
p = 0.3194
C
DNAJB1
FUS
*EIF4A2
rel. expression
ns
DMSO 33°C
DMSO 39°C
OA 33°C
OA 39°C
DMSO 35°C
DMSO 39°C
Tg003 35°C
Tg003 39°C
D
T2 33°C/39°C
T12 33°C/39°C
cancer genes
% of genes
Bin Center
71.5%
55.8%
70.5%
54.8%
E
DMSO 33°C/39°C
DMSO 35°C/39°C
89.5%
72.9%
82.4%
66.1%

Figure S6

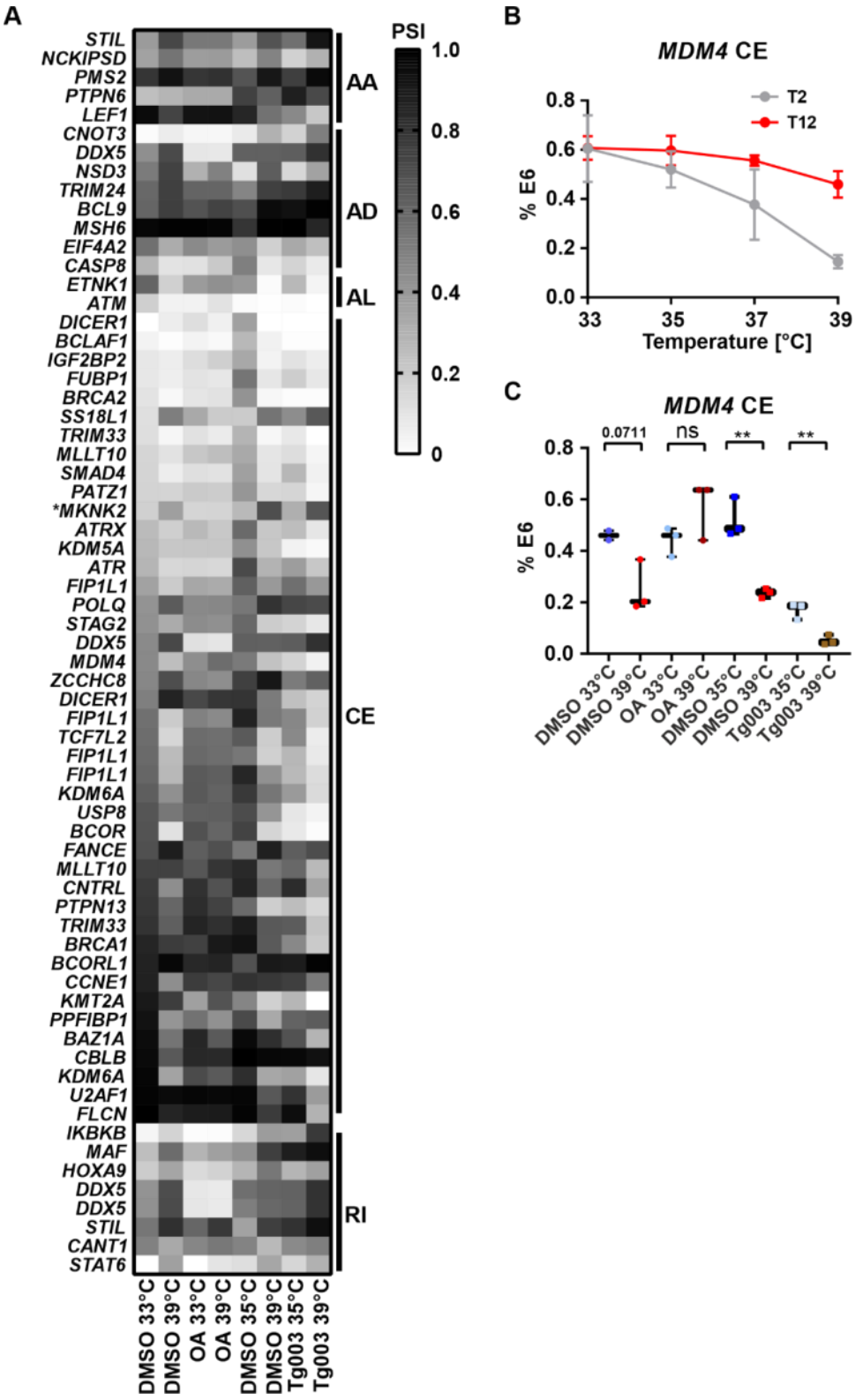
A
PSI
1.0
0.8
0.6
0.4
0.2
0
AA
AD
AL
CE
RI
STIL
NCKIPSD
PMS2
PTPN6
LEF1
CNOT3
DDX5
NSD3
TRIM24
BCL9
MSH6
EIF4A2
CASP8
ETNK1
ATM
DICER1
BCLAF1
IGF2BP2
FUBP1
BRCA2
SS18L1
TRIM33
MLLT10
SMAD4
PATZ1
*MKNK2
ATRX
KDM5A
ATR
FIP1L1
POLQ
STAG2
DDX5
MDM4
ZCCHC8
DICER1
FIP1L1
TCF7L2
FIP1L1
FIP1L1
KDM6A
USP8
BCOR
FANCE
MLLT10
CNTRL
PTPN13
TRIM33
BRCA1
BCORL1
CCNE1
KMT2A
PPFIBP1
BAZ1A
CBLB
KDM6A
U2AF1
FLCN
IKBKB
MAF
HOXA9
DDX5
DDX5
STIL
CANT1
STAT6
DMSO 33°C
DMSO 39°C
OA 33°C
OA 39°C
DMSO 35°C
DMSO 39°C
Tg003 35°C
Tg003 39°C
B
MDM4 CE
T2
T12
% E6
0.8
0.6
0.4
0.2
0.0
33
35
37
39
Temperature [°C]
C
MDM4 CE
0.0711
ns
**
**
% E6
0.8
0.6
0.4
0.2
0.0
DMSO 33°C
DMSO 39°C
OA 33°C
OA 39°C
DMSO 35°C
DMSO 39°C
Tg003 35°C
Tg003 39°C

Figure 4

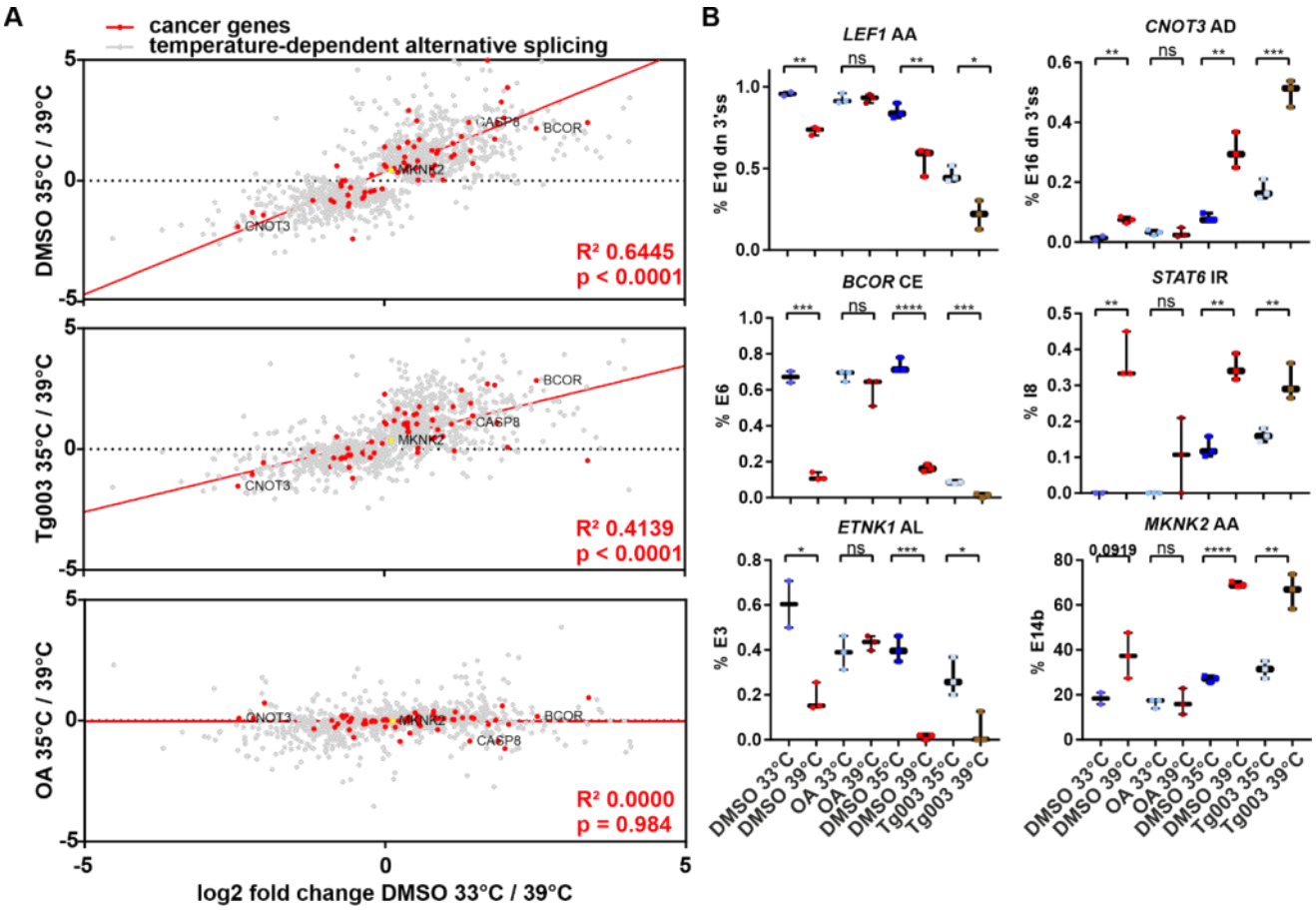
A
cancer genes
temperature-dependent alternative splicing
DMSO 35°C / 39°C
Tg003 35°C / 39°C
OA 35°C / 39°C
log2 fold change DMSO 33°C / 39°C
CASP8
BCOR
MKNK2
CNOT3
R² 0.6445
p < 0.0001
R² 0.4139
p < 0.0001
R² 0.0000
p = 0.984
B
LEF1 AA
CNOT3 AD
BCOR CE
STAT6 IR
ETNK1 AL
MKNK2 AA
% E10 dn 3'ss
% E16 dn 3'ss
% E6
% I8
% E3
% E14b
ns
0.0919
DMSO 33°C
DMSO 39°C
OA 33°C
OA 39°C
DMSO 35°C
DMSO 39°C
Tg003 35°C
Tg003 39°C

Figure S7

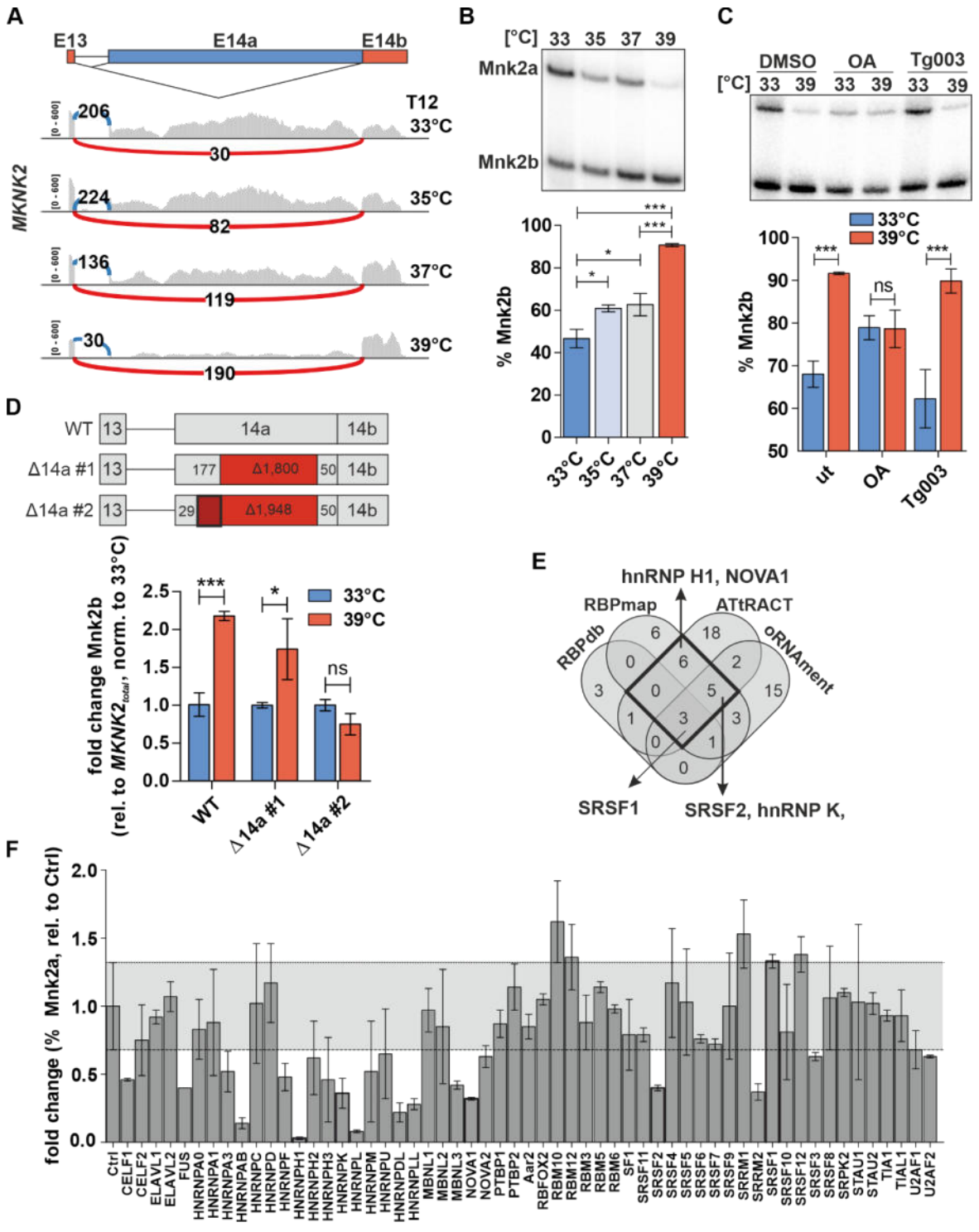
A
E13
E14a
E14b
MKNK2
T12
206
30
33°C
224
82
35°C
136
119
37°C
30
190
39°C
B
[°C] 33 35 37 39
Mnk2a
Mnk2b
% Mnk2b
33°C
35°C
37°C
39°C
C
DMSO
OA
Tg003
[°C] 33 39 33 39 33 39
33°C
39°C
% Mnk2b
ns
ut
OA
Tg003
D
WT 13 14a 14b
Δ14a #1 13 177 Δ1,800 50 14b
Δ14a #2 13 29 Δ1,948 50 14b
fold change Mnk2b
(rel. to MKNK2total, norm. to 33°C)
33°C
39°C
ns
WT
Δ14a #1
Δ14a #2
E
hnRNP H1, NOVA1
RBPmap
ATtRACT
RBPdb
oRNAment
SRSF1
SRSF2, hnRNP K,
F
fold change (% Mnk2a, rel. to Ctrl)
Ctrl
CELF1
CELF2
ELAVL1
ELAVL2
FUS
HNRNPA0
HNRNPA1
HNRNPA3
HNRNPAB
HNRNPC
HNRNPD
HNRNPF
HNRNPH1
HNRNPH2
HNRNPH3
HNRNPK
HNRNPL
HNRNPM
HNRNPU
HNRNPDL
HNRNPLL
MBNL1
MBNL2
MBNL3
NOVA1
NOVA2
PTBP1
PTBP2
Aar2
RBFOX2
RBM10
RBM12
RBM3
RBM5
RBM6
SF1
SRSF11
SRSF2
SRSF4
SRSF5
SRSF6
SRSF7
SRSF9
SRRM1
SRRM2
SRSF1
SRSF10
SRSF12
SRSF3
SRSF8
SRPK2
STAU1
STAU2
TIA1
TIAL1
U2AF1
U2AF2

Figure S8

Figure Legends

Figure 1. Body temperature-regulated SR protein phosphorylation is controlled by PP2A activity.

A, *In vitro* phosphatase assay with His_{10}-tagged hPP2AC purified from High Five insect cells. Purified GST-tagged RS-repeat peptide was phosphorylated using His_6-tagged SRPK1 and [γ-^{32}P]ATP at the indicated temperatures in an *in-vitro* kinase reaction[13]. After SDS-PAGE phosphorylation was detected using autoradiography (top) and equal loading was confirmed by Coomassie staining (bottom). The first lane in (A) shows the phosphorylation of the GST-RS substrate at 37°C in the absence of PP2AC as a control.

B, Quantification of dephosphorylation experiments as in (C), relative to highest phosphorylation at 30 °C (n = 5, mean ± SD).

C, Schematic of temperature-regulated CLK1/4 and PP2AC activity. Cold-induced CLK1/4 activity leads to higher autophosphorylation and higher phosphorylation levels of SR substrates (Haltenhof et al., 2020). In contrast, the PP2AC activity is increased at higher temperatures leading to dephosphorylation of the SR substrate.

Figure S1. Body temperature-regulated SR protein phosphorylation is controlled by PP2A activity.

A, SDS-PAGE and Coomassie staining of the purification of His_{10}-hPP2AC with HIS-Select Nickel Affinity beads. SN – supernatant, Ft – flow through, W – wash fraction, E – elution fraction

B, SDS-PAGE after size exclusion purification of His_{10}-hPP2AC. Asterisk indicate degradation products.

C, *In vitro* phosphatase assay as in (C) showing PP2AC activity is independent of the pH. The reaction was incubated at 37 °C for 5 min.

Figure 2. PP1/2A inhibition prevents temperature-controlled AS and GE.

A, AS was investigated using Whippet, temperature-controlled significantly altered (ΔPSI > 15% and Probability > 0.9) skipped exon events are presented. On top a Venn Diagram shows a comparison of significantly altered events in DMSO and OA, below a heat map illustrates mean PSI values of all significantly altered splicing events in DMSO.

B, AS of *BCOR* and *CCNT1* was validated using radioactive RT-PCR. Representative gels are shown on top, below the quantification (n = 3, mean ± SD).

C, Heat map as in Figure 2A showing that temperature-regulated skipped exon events are almost completely inhibited by OA treatment, while some temperature-sensitive AS remains upon suppression of CLK activity by TG003.

Figure S2. PP1/2A inhibition prevents temperature-controlled AS and GE.

A, Temperature profile for RNA sequencing. Confluent HEK293 cells were pre-incubated at 33 °C, treated with the phosphatase inhibitor OA, or DMSO as solvent control, and incubated at 33 or 39 °C, for 2 h. RNA was isolated and analysed by RNA sequencing in biological triplicates (n = 3, for DMSO 33 °C n = 2).

B, Principal component analysis of the investigated samples.

C, Summary of splicing events found in the RNA sequencing analysis. 3'SS/5'SS – usage of an alternative 3' or 5' splice site, respectively, AF – alternative first exon, AL – alternative last exon, CE – cassette exon, RI – retained intron.

D, AS was investigated using Whippet, temperature-controlled significantly altered (ΔPSI > 15% and Probability > 0.9) retained intron events are shown. On top a Venn Diagram shows a comparison of significantly altered events in DMSO and OA, below a heat map illustrates mean PSI values of all significantly altered splicing events in DMSO.

E, Confirmation of AS of *TRPC1* and *ATF2* by radioactive RT-PCR (top: representative gels, bottom: quantifications) (n = 3, mean ± SD).

Figure S3. PP1/2A inhibition prevents temperature-controlled AS and GE.

A, Temperature profile for RNA sequencing. Confluent HEK293 cells were pre-incubated at 39 °C, treated with the CLK inhibitor TG003, or DMSO as solvent control, and incubated at 35 or 39 °C, for 6 h (Haltenhof *et al.*, 2020). RNA was isolated and analysed by RNA sequencing in biological triplicates.

B, Heat map as in Figure 2A showing that temperature-regulated retained intron events are almost completely inhibited by OA treatment, while some temperature-sensitive AS remains upon suppression of CLK activity by TG003.

Figure 3. Body temperature-controlled expression of cancer-associated genes is highly phosphatase-dependent

A, HEK293 were shifted from 37 °C to 33, 35, 37, or 39 °C for 2 or 12 hours (T2, T12) and investigated by RNA sequencing.

B, For each splicing event in S4B the log2 fold change PSI[33°C]/PSI[39°C] was calculated for 2 hours (fc_T2) and 12 hours (fc_T12). Data are presented as scatter dot plot; bars indicate mean +/- SD. An unpaired t-test of comparing genes with cold-induced exons after 2 and 12 hours (indicated in purple) reveals no statistical significant differences (ns, $p > 0.05$).

C, For each gene in S4C the log2 fold change GE[33°C]/GE[39°C] was calculated and plotted as in D. An unpaired t-test of genes with heat-induced genes after 2 and 12 hours (indicated in purple) reveals much stronger changes after 12 hours (****, $p < 0.0001$).

D, Transcription factor enrichment analysis [21] using linear temperature-dependent genes from Figures S4D and S4E reveals that distinct sets of transcription factors control heat- and cold-induced gene expression after 12 h. For each transcription factor, the hypergeometric p-value for cold-induced genes (x-axis) is plotted against the p-value for heat-induced genes (y-axis).

E, Fraction of TP53 (left) or MYC (right) bound genes with temperature-dependent GE after 2 or 12 hours. Genes with a fold-change (33°C/39°C) larger than 1.5 are categorized as heat-induced or cold-induced.

Figure S4. Body temperature-controlled expression of cancer-associated genes is highly phosphatase-dependent

A, Heat map as in Figure 2A showing that temperature-regulated GE is almost completely inhibited by OA treatment, while some temperature-sensitive GE remains upon suppression of CLK activity by TG003.

B, C, Investigation of dynamics in temperature-dependent AS and GE. High confidence splicing events from the overlaps in Figures 2A (skipped exons) or S4A (gene expression) are plotted in heat maps in response to temperature gradients.

D, E, Venn Diagrams comparing linear temperature-dependent skipped exons (D) or GE (E) between 2 and 12 hours.

Figure S5. Body temperature-controlled expression of cancer-associated genes is highly phosphatase-dependent

A, Transcription factor enrichment analysis [21] as in Fig. 3D using linear temperature-dependent genes from Figures S4D and S4E reveals that a distinct set of transcription factors controls heat-induced gene expression after 2 h. For each transcription factor, the hypergeometric p-value for cold-induced genes (x-axis) is plotted against the p-value for heat-induced genes (y-axis).

B, Fraction of TP53 (left) or MYC (right) bound genes with temperature-dependent GE. Genes with a fold-change (33°C/35°C, 35°C/37°C, or 37°C/39°C) larger than 1.5 are categorized as heat-induced or cold-induced.

C, D Transcription factor enrichment analysis [21] as in Fig. 3D in MEF or Raw cells, respectively, reveals that distinct sets of transcription factors control heat- or cold-induced gene expression. For each transcription factor, the hypergeometric p-value for cold-induced genes (x-axis) is plotted against the p-value for heat-induced genes (y-axis).

Figure S6. Body temperature-controlled expression of cancer-associated genes is highly phosphatase-dependent

A, Linear regression fit comparing genes expression changes after 2 h at 33 °C vs 39 °C to 12 h at 33 °C vs 39 °C. Highlighted in red are all cancer-associated genes (n = 323; based on [25].) For cancer-associated genes the goodness of fit is indicated by R^2 and p-values. Additionally, 5 cancer-associated genes *BCL9L*, *DNAJB1*, *EIF4A2*, *MAPK1* and *FUS* are highlighted.

B, Linear regression fit comparing genes expression changes in DMSO 33 °C vs 39 °C to DMSO 35 °C vs 39 °C (top), TG003 35 °C vs 39 °C (middle), or OA 33 °C vs 39 °C (top). Plotted are all genes which are temperature-dependent either in DMSO 33 °C vs 39 °C or in DMSO 35 °C vs 39 °C (fold-change > 1.3; n = 9217). Highlighted in red are all cancer-associated genes (n = 323; based on [25].) For cancer associated-genes the goodness of fit is indicated by R^2 and p-values. Additionally, 5 cancer associated-genes *BCL9L*, *DNAJB1*, *EIF4A2*, *MAPK1* and *FUS* are highlighted.

C, Examples for temperature-dependent, OA but not TG003-sensitive, expression of cancer-associated gens. Expression levels were determined using Whippet-derived tpm values and is shown relative to DMSO 33 °C (left half) or DMSO 35 °C (right half). Statistical significance was determined by unpaired t-tests.

D, Heat-induced expression of cancer-associated genes. Histogram of frequency distribution for all temperature-dependent genes (black) and cancer-associated temperature-dependent genes (red) for T2 33 °C vs 39 °C (left) and T12 33 °C vs 39 °C (right). Genes were categorized into bins based on their log2 fold change gene expression. On the right the percentage of heat-induced genes is indicated.

E, Heat-induced expression of cancer-associated genes. Histogram of frequency distribution for all temperature-dependent genes (black) and cancer-associated temperature-dependent genes (red) for DMSO 33 °C vs 39 °C (left) and DMSO 35 °C vs 39 °C (right). Genes were categorized into bins based on their log2 fold change gene expression. On the right the percentage of heat-induced genes is indicated.

Figure 4. Body temperature-regulated AS of cancer-associated genes is controlled by PP1/2A

A, Heat map of all temperature-dependent AS events. Gene names are shown on the left; the splicing type is indicated on the right. AA – alternative acceptor site, AD – alternative donor site, AL – alternative last exon, CE – cassette exon, RI – retained intron. * The complicated AS event at the 3'end of *MKNK2* (see Figure S8A) escaped our Whippet analysis, PSI are based on manual quantification of Sashimi blots.

B, Temperature-induced skipping of *MDM4* exon 6 after 2 (grey) and 12 hours (red).

C, *MDM4* exon 6 skipping is strongly temperature- and OA-dependent, but less affected by TG003. PSI values are derived from Whippet.

Figure S7. Body temperature-regulated AS of cancer-associated genes is controlled by PP1/2A

A, Linear regression fit comparing splicing changes in DMSO 33°C vs 39°C to DMSO 35°C vs 39°C (top), TG003 35°C vs 39°C (middle), or OA 33°C vs 39°C (top). Plotted are all temperature-dependent splicing events either in DMSO 33°C vs 39°C or in DMSO 35°C vs 39°C (ΔPSI > 0.2; Probability > 0.99; n=1194). Highlighted in red are splicing events in cancer-associated genes (n=66; based on [25].) For cancer-associated genes the goodness of fit is indicated by R^2 and p-values. Additionally, 5 cancer-associated genes *BCL9L*, *DNAJB1*, *EIF4A2*, *MAPK1* and *FUS* are highlighted.

B, Examples of temperature – OA but not TG003 – dependent splicing events in cancer-associated genes. AA – alternative acceptor site, AD – alternative donor site, AL – alternative last exon, CE – cassette exon, IR – intron retention.

Figure S8. Body temperature-regulated AS of cancer-associated genes is controlled by PP1/2A

A, Sashimi plots showing temperature-dependent AS of *MKNK2* Exon 14 (E14). Warm temperatures favor the usage of an alternative 3' splice site in E14 leading to the production of the oncogenic Mnk2b isoform.

B, Top: Radioactive RT-PCR confirming heat-induced (8h at the respective temperatures) AS of *MKNK2* resulting in oncogenic Mnk2b, Bottom: Quantification (n=3, mean ± SD).

C, Temperature-dependent *MKNK2* splicing is OA- but not TG003-sensitive. PSI values were determined using Whippet. Statistical significance was determined by unpaired t-tests.

D, top: Schematic of mutated minigenes to identify the *cis*-regulatory element responsible for temperature-controlled *MKNK2* AS. Regions marked in red were deleted by PCR. Resulted minigenes were transfected in HEK293 cells, cells were incubated for 40h at 37°C before shifting the cells for 8h to the indicated temperatures. Dark red box indicates a region of 148 nt (harboring binding sites for hnRNPK, SRSF1 and SRSF2) which is crucial for temperature-mediated *MKNK2* AS. Bottom: qPCR analysis of Mnk2b AS (relative to total Mnk2, normalized to 33°C)(n=3, mean ± SD).

E, Venn diagram showing the numbers of overlapping of RBPs, which bind to the 148 nucleotides sequence in *MKNK2* E14a, predicted by the four RBP binding site prediction tools RBPdb[52], RBPmap[53], ATtRACT[54], and oRNAment[55].

F, siRNA screen to identify the *trans*-acting factor responsible for *MKNK2* AS. HEK293 cells were transfected with a pool of siRNAs against the respective target genes. The siRNA pool consisted of four individual siRNAs targeting the same gene. After 48h, the cells were harvested, total RNA was extracted and analyzed via radioactive RT-PCR for *MKNK2* AS (n = 2, mean ± SEM).

1 Pippa, R. & Odero, M. D. The Role of MYC and PP2A in the Initiation and Progression of Myeloid Leukemias. *Cells* **9**, doi:10.3390/cells9030544 (2020).

2 Graves, J. D. & Krebs, E. G. Protein phosphorylation and signal transduction. *Pharmacol Ther* **82**, 111-121, doi:10.1016/s0163-7258(98)00056-4 (1999).

3 Ruvolo, P. P. The broken "Off" switch in cancer signaling: PP2A as a regulator of tumorigenesis, drug resistance, and immune surveillance. *BBA Clin* **6**, 87-99, doi:10.1016/j.bbacli.2016.08.002 (2016).

4 Slupe, A. M., Merrill, R. A. & Strack, S. Determinants for Substrate Specificity of Protein Phosphatase 2A. *Enzyme Res* **2011**, 398751, doi:10.4061/2011/398751 (2011).

5 Shouse, G. P., Cai, X. & Liu, X. Serine 15 phosphorylation of p53 directs its interaction with B56gamma and the tumor suppressor activity of B56gamma-specific protein phosphatase 2A. *Molecular and cellular biology* **28**, 448-456, doi:10.1128/MCB.00983-07 (2008).

6 Soofiyani, S. R., Hejazi, M. S. & Baradaran, B. The role of CIP2A in cancer: A review and update. *Biomed Pharmacother* **96**, 626-633, doi:10.1016/j.biopha.2017.08.146 (2017).

7 Morita, K. *et al.* Allosteric Activators of Protein Phosphatase 2A Display Broad Antitumor Activity Mediated by Dephosphorylation of MYBL2. *Cell*, doi:10.1016/j.cell.2020.03.051 (2020).

8 Leonard, D. *et al.* Selective PP2A Enhancement through Biased Heterotrimer Stabilization. *Cell*, doi:10.1016/j.cell.2020.03.038 (2020).

9 Wust, P. *et al.* Hyperthermia in combined treatment of cancer. *Lancet Oncol* **3**, 487-497, doi:10.1016/s1470-2045(02)00818-5 (2002).

10 Skitzki, J. J., Repasky, E. A. & Evans, S. S. Hyperthermia as an immunotherapy strategy for cancer. *Curr Opin Investig Drugs* **10**, 550-558 (2009).

11 Refinetti, R. & Menaker, M. The circadian rhythm of body temperature. *Physiol Behav* **51**, 613-637, doi:10.1016/0031-9384(92)90188-8 (1992).

12 Preussner, M. *et al.* Body Temperature Cycles Control Rhythmic Alternative Splicing in Mammals. *Mol Cell* **67**, 433-446.e434, doi:10.1016/j.molcel.2017.06.006 (2017).

13 Haltenhof, T. *et al.* A conserved kinase-based body temperature sensor globally controls alternative splicing and gene expression. *Mol Cell* (2020).

14 Mermoud, J. E., Cohen, P. & Lamond, A. I. Ser/Thr-specific protein phosphatases are required for both catalytic steps of pre-mRNA splicing. *Nucleic Acids Res* **20**, 5263-5269, doi:10.1093/nar/20.20.5263 (1992).
15 Shi, Y. & Manley, J. L. A complex signaling pathway regulates SRp38 phosphorylation and pre-mRNA splicing in response to heat shock. *Mol Cell* **28**, 79-90, doi:10.1016/j.molcel.2007.08.028 (2007).
16 Cohen, P. Classification of protein-serine/threonine phosphatases: identification and quantitation in cell extracts. *Methods in enzymology* **201**, 389-398, doi:10.1016/0076-6879(91)01035-z (1991).
17 Goldammer, G. *et al.* Characterization of cis-acting elements that control oscillating alternative splicing. *RNA Biol* **15**, 1081-1092, doi:10.1080/15476286.2018.1502587 (2018).
18 Wera, S. & Hemmings, B. A. Serine/threonine protein phosphatases. *Biochem. J.* **311 (Pt 1)**, 17-29, doi:10.1042/bj3110017 (1995).
19 Wang, M., Herrmann, C. J., Simonovic, M., Szklarczyk, D. & von Mering, C. Version 4.0 of PaxDb: Protein abundance data, integrated across model organisms, tissues, and cell-lines. *Proteomics* **15**, 3163-3168, doi:10.1002/pmic.201400441 (2015).
20 Sterne-Weiler, T., Weatheritt, R. J., Best, A. J., Ha, K. C. H. & Blencowe, B. J. Efficient and Accurate Quantitative Profiling of Alternative Splicing Patterns of Any Complexity on a Laptop. *Mol Cell* **72**, 187-200.e186, doi:10.1016/j.molcel.2018.08.018 (2018).
21 Kuleshov, M. V. *et al.* Enrichr: a comprehensive gene set enrichment analysis web server 2016 update. *Nucleic acids research* **44**, W90-W97, doi:10.1093/nar/gkw377 %J Nucleic Acids Research (2016).
22 Miyaki, M. *et al.* Higher frequency of Smad4 gene mutation in human colorectal cancer with distant metastasis. *Oncogene* **18**, 3098-3103, doi:10.1038/sj.onc.1202642 (1999).
23 Wang, L. H., Wu, C. F., Rajasekaran, N. & Shin, Y. K. Loss of Tumor Suppressor Gene Function in Human Cancer: An Overview. *Cell Physiol Biochem* **51**, 2647-2693, doi:10.1159/000495956 (2018).
24 Cascon, A. & Robledo, M. MAX and MYC: a heritable breakup. *Cancer Res* **72**, 3119-3124, doi:10.1158/0008-5472.CAN-11-3891 (2012).
25 Futreal, P. A. *et al.* A census of human cancer genes. *Nat Rev Cancer* **4**, 177-183, doi:10.1038/nrc1299 (2004).
26 Junttila, M. R. *et al.* CIP2A inhibits PP2A in human malignancies. *Cell* **130**, 51-62, doi:10.1016/j.cell.2007.04.044 (2007).
27 Ohnishi, T. The role of the p53 molecule in cancer therapies with radiation and/or hyperthermia. *Journal of cancer research and therapeutics* **1**, 147-150, doi:10.4103/0973-1482.19594 (2005).
28 Gerhart, S. V. *et al.* Activation of the p53-MDM4 regulatory axis defines the anti-tumour response to PRMT5 inhibition through its role in regulating cellular splicing. *Scientific Reports* **8**, 9711, doi:10.1038/s41598-018-28002-y (2018).
29 Dewaele, M. *et al.* Antisense oligonucleotide-mediated MDM4 exon 6 skipping impairs tumor growth. *J Clin Invest* **126**, 68-84, doi:10.1172/JCI82534 (2016).
30 Karni, R. *et al.* The gene encoding the splicing factor SF2/ASF is a proto-oncogene. *Nat Struct Mol Biol* **14**, 185-193, doi:10.1038/nsmb1209 (2007).
31 Maimon, A. *et al.* Mnk2 alternative splicing modulates the p38-MAPK pathway and impacts Ras-induced transformation. *Cell Rep* **7**, 501-513, doi:10.1016/j.celrep.2014.03.041 (2014).
32 McCright, B., Rivers, A. M., Audlin, S. & Virshup, D. M. The B56 family of protein phosphatase 2A (PP2A) regulatory subunits encodes differentiation-induced phosphoproteins that target PP2A to both nucleus and cytoplasm. *J Biol Chem* **271**, 22081-22089, doi:10.1074/jbc.271.36.22081 (1996).
33 Strack, S., Zaucha, J. A., Ebner, F. F., Colbran, R. J. & Wadzinski, B. E. Brain protein phosphatase 2A: developmental regulation and distinct cellular and subcellular localization by B subunits. *J Comp Neurol* **392**, 515-527 (1998).

34 Shi, Y. Serine/threonine phosphatases: mechanism through structure. *Cell* **139**, 468-484, doi:10.1016/j.cell.2009.10.006 (2009).

35 Longin, S. *et al.* Selection of protein phosphatase 2A regulatory subunits is mediated by the C terminus of the catalytic Subunit. *J Biol Chem* **282**, 26971-26980, doi:10.1074/jbc.M704059200 (2007).

36 Stanevich, V. *et al.* The structural basis for tight control of PP2A methylation and function by LCMT-1. *Mol Cell* **41**, 331-342, doi:10.1016/j.molcel.2010.12.030 (2011).

37 Janssens, V., Goris, J. & Van Hoof, C. PP2A: the expected tumor suppressor. *Curr Opin Genet Dev* **15**, 34-41, doi:10.1016/j.gde.2004.12.004 (2005).

38 Lambrecht, C. *et al.* Loss of protein phosphatase 2A regulatory subunit B56delta promotes spontaneous tumorigenesis in vivo. *Oncogene* **37**, 544-552, doi:10.1038/onc.2017.350 (2018).

39 Arnold, H. K. & Sears, R. C. Protein phosphatase 2A regulatory subunit B56alpha associates with c-myc and negatively regulates c-myc accumulation. *Molecular and cellular biology* **26**, 2832-2844, doi:10.1128/MCB.26.7.2832-2844.2006 (2006).

40 Margolis, S. S. *et al.* Role for the PP2A/B56delta phosphatase in regulating 14-3-3 release from Cdc25 to control mitosis. *Cell* **127**, 759-773, doi:10.1016/j.cell.2006.10.035 (2006).

41 Perri, F., Pisconti, S. & Della Vittoria Scarpati, G. P53 mutations and cancer: a tight linkage. *Ann Transl Med* **4**, 522, doi:10.21037/atm.2016.12.40 (2016).

42 Sontag, E., Nunbhakdi-Craig, V., Lee, G., Bloom, G. S. & Mumby, M. C. Regulation of the phosphorylation state and microtubule-binding activity of Tau by protein phosphatase 2A. *Neuron* **17**, 1201-1207, doi:10.1016/s0896-6273(00)80250-0 (1996).

43 Liu, F., Grundke-Iqbal, I., Iqbal, K. & Gong, C. X. Contributions of protein phosphatases PP1, PP2A, PP2B and PP5 to the regulation of tau phosphorylation. *Eur J Neurosci* **22**, 1942-1950, doi:10.1111/j.1460-9568.2005.04391.x (2005).

44 Gong, C. X. *et al.* Phosphatase activity toward abnormally phosphorylated tau: decrease in Alzheimer disease brain. *J Neurochem* **65**, 732-738, doi:10.1046/j.1471-4159.1995.65020732.x (1995).

45 Sangodkar, J. *et al.* All roads lead to PP2A: exploiting the therapeutic potential of this phosphatase. *FEBS J* **283**, 1004-1024, doi:10.1111/febs.13573 (2016).

46 Sontag, E. *et al.* Altered expression levels of the protein phosphatase 2A ABalphaC enzyme are associated with Alzheimer disease pathology. *J Neuropathol Exp Neurol* **63**, 287-301, doi:10.1093/jnen/63.4.287 (2004).

47 Ganguli, M. & Rodriguez, E. Age, Alzheimer's disease, and the big picture. *Int Psychogeriatr* **23**, 1531-1534, doi:10.1017/S1041610211001906 (2011).

48 Wongsurawat, N., Davis, B. B. & Morley, J. E. Thermoregulatory failure in the elderly. St. Louis University Geriatric Grand Rounds. *J Am Geriatr Soc* **38**, 899-906, doi:10.1111/j.1532-5415.1990.tb05708.x (1990).

49 Walt, S. v. d., Colbert, S. C. & Varoquaux, G. The NumPy Array: A Structure for Efficient Numerical Computation. *Computing in Science & Engineering* **13**, 22-30, doi:10.1109/MCSE.2011.37 (2011).

50 Hunter, J. D. Matplotlib: A 2D Graphics Environment. *Computing in Science & Engineering* **9**, 90-95, doi:10.1109/MCSE.2007.55 (2007).

51 Clarke, D. J. B. *et al.* eXpression2Kinases (X2K) Web: linking expression signatures to upstream cell signaling networks. *Nucleic Acids Res.* **46**, W171-w179, doi:10.1093/nar/gky458 (2018).

52 Cook, K. B., Kazan, H., Zuberi, K., Morris, Q. & Hughes, T. R. RBPDB: a database of RNA-binding specificities. *Nucleic acids research* **39**, D301-308, doi:10.1093/nar/gkq1069 (2011).

53 Paz, I., Kosti, I., Ares, M., Jr., Cline, M. & Mandel-Gutfreund, Y. RBPmap: a web server for mapping binding sites of RNA-binding proteins. *Nucleic acids research* **42**, W361-367, doi:10.1093/nar/gku406 (2014).

54 Giudice, G., Sanchez-Cabo, F., Torroja, C. & Lara-Pezzi, E. ATtRACT-a database of RNA-binding proteins and associated motifs. *Database (Oxford)* **2016**, doi:10.1093/database/baw035 (2016).

55 Benoit Bouvrette, L. P., Bovaird, S., Blanchette, M. & Lecuyer, E. oRNAment: a database of putative RNA binding protein target sites in the transcriptomes of model species. *Nucleic acids research* **48**, D166-D173, doi:10.1093/nar/gkz986 (2020).

5.3 Publication 3

*Neumann, A., **Meinke, S.**, Goldammer, G., Strauch, M., Schubert, D., Timmermann, B., Heyd, F., Preußner, M. (2020) Alternative splicing coupled nonsense-mediated decay shapes the temperature-dependent transcriptome. bioRxiv, doi: 10.1101/2020.02.19.956037*

https://doi.org/10.1101/2020.02.19.956037

Alternative splicing coupled nonsense-mediated decay shapes the temperature-dependent transcriptome

Running title: AS-NMD generates cycling gene expression

Alexander Neumann[1], Stefan Meinke[1], Gesine Goldammer[1], Miriam Strauch[1], Daniel Schubert[2], Bernd Timmermann[3], Florian Heyd [1*], Marco Preußner [1*]

[1]Freie Universität Berlin, Institute of Chemistry and Biochemistry, Laboratory of RNA Biochemistry, Takustrasse 6, 14195 Berlin, Germany.

[2] Freie Universität Berlin, Epigenetics of Plants, Königin-Luise-Str. 12-16, 14195 Berlin, Germany

[3]Sequencing Core Facility, Max-Planck-Institute for Molecular Genetics, Ihnestraße 63-73, Berlin 14195, Germany

*Co-corresponding Authors: florian.heyd@fu-berlin.de, mpreussner@zedat.fu-berlin.de
Phone: +49 30 83870703
FAX: +49 30 838-4-62938

Abstract

Mammalian body temperature oscillates with the time of the day and is altered in diverse pathological conditions. We recently identified a body temperature-sensitive thermometer-like kinase, which alters SR protein phosphorylation and thereby globally controls alternative splicing (AS). AS can generate mRNA variants containing premature termination codons, which are degraded by nonsense-mediated decay (NMD). Here we show extensive coupling of body temperature-controlled AS to NMD, leading to global control of temperature-dependent gene expression (GE). Temperature-controlled NMD-inducing splicing events are evolutionarily conserved and pervasively found within RNA-binding proteins, including most SR proteins. NMD-inducing exons are essential for rhythmic GE of SR proteins and have a global role in establishing temperature-dependent rhythmic GE profiles, both, in mammals under circadian body temperature cycles and in plants in response to ambient temperature changes. Together, these data identify body temperature-driven AS-NMD as an evolutionary ancient, core clock-independent mechanism to generate rhythmic GE.

Keywords

Alternative splicing / circadian clock / NMD / SR proteins / temperature

Introduction

Circadian clocks act as cell autonomous time-measuring devices, which anticipate active and resting phases and coordinate behavior and physiology accordingly. The mammalian circadian timing system is organized in a hierarchical manner: The central pacemaker in the brain's suprachiasmatic nucleus (SCN) serves as a master regulator to coordinate circadian clocks throughout the body (Dibner, Schibler et al., 2010). Therefore, information on the geophysical time (light-dark) is transferred from the retina to the SCN, which then uses diverse neuronal and humoral cues to synchronize circadian clocks in other 'light-blind' parts of the brain and in other organs of the body (Gerber, Saini et al., 2015). Although the mechanisms of synchronization are different in the various organs, the conventional perception is that the majority of 24-hour rhythms depends on an identical transcription-translation feedback loop in each cell of the body (Ko & Takahashi, 2006). However, only ~50% of circadian mRNA rhythms depend on *de novo* transcription (Koike, Yoo et al., 2012, Menet, Rodriguez et al., 2012), strongly arguing for an involvement of other posttranscriptional mechanisms in generating rhythms (Preussner & Heyd, 2016, Shakhmantsir & Sehgal, 2019). Additionally, there is evidence for 24-hour rhythms which cycle independent of the central oscillator (Kornmann, Schaad et al., 2007). Core clock-independent 24-hour rhythms in GE may be difficult to discriminate from real circadian oscillations *in vivo* (reviewed in (Preussner & Heyd, 2018)) and our mechanistic understanding of these rhythms is limited.

Systemic body temperature cycles (Refinetti & Menaker, 1992) can synchronize the central oscillator in peripheral clocks (Brown, Zumbrunn et al., 2002, Buhr, Yoo et al., 2010, Saini, Morf et al., 2012), but can also directly result in rhythmic changes in GE. Examples include rhythmic expression of heat shock factors (Liu, Qian et al., 2019), of cold-induced RNA-binding proteins (RBPs), such as *Cirbp* (Liu, Hu et al., 2013, Morf, Rey et al., 2012), or rhythmic changes in the ratio of AS isoforms of *U2af26* and many other related genes (Goldammer, Neumann et al., 2018, Preussner, Goldammer et al., 2017, Preussner, Wilhelmi et al., 2014). All of these examples must be driven by highly sensitive mechanisms that are able to respond to 1-2°C changes in temperature (Gotic, Omidi et al., 2016, Preussner et al., 2017), but the global impact of these mechanisms (and more generally of body temperature) on GE patterns remains enigmatic so far. In our previous work, we revealed key components regulating temperature-dependent AS. Essential regulators are members of the family of SR proteins (13 canonical members in human), which share a domain rich in serine and arginine residues, known as the RS domain (Manley & Krainer, 2010). The phosphorylation level of SR proteins controls their activity and serves as a fast and extremely sensitive molecular thermometer transferring the signal 'body temperature' into

global changes in AS (Haltenhof, Kotte et al., 2020). SR proteins contain ultraconserved elements, allowing autoregulation of their own expression level (Lareau, Inada et al., 2007). Autoregulatory mechanisms can involve regulated inclusion of an exon containing a premature translation termination codon (PTC; (Sureau, Gattoni et al., 2001)), or AS such that the normal stop codon becomes a PTC (Goncalves & Jordan, 2015, Lareau et al., 2007). PTC-containing mRNAs are recognized and degraded by the NMD surveillance pathway and for SR proteins this is understood as a mechanism associated with homeostatic control (Ni, Grate et al., 2007). However, the extreme evolutionary conservation is a strong indicator for further biological functions. AS-inducing NMD (AS-NMD) is not restricted to SR proteins and can thus dynamically control global GE (Braunschweig, Gueroussov et al., 2013, Lykke-Andersen & Jensen, 2015). While several thousand genes are affected by inhibition of the NMD pathway (Hurt, Robertson et al., 2013), the role of NMD in dynamically and actively controlling GE in response to changing cellular conditions has been described only in isolated cases (Tabrez, Sharma et al., 2017, Wong, Ritchie et al., 2013).

Here, we investigated to which extend AS-NMD is regulated by temperature and how this mechanism globally regulates body temperature-dependent GE. We find that NMD isoforms of different RBPs, especially SR proteins, are highly responsive to changes in the physiological temperature range, and that temperature-controlled AS-NMD of SR proteins is sufficient to *de novo* generate 24-hour rhythms in GE. Temperature-dependent AS-NMD is conserved from plants to human, controls thousands of mRNAs and represents a global mechanism for the generation of rhythmic 24-hour GE *in viv*o. The temperature-sensing feedback loop inducing AS-NMD bears striking similarity to the classical circadian transcription-translation feedback loop, both relying on rhythmic expression of a core machinery that controls itself and many output genes, but represents an independent and widespread mechanism to generate rhythmic GE. Furthermore, this mechanism shows wider evolutionary conservation than the classical core clock, pointing to an essential role in integrating temperature signals beyond the classical day-night cycle into cellular GE programs.

Results

Temperature-dependent AS-NMD occurs frequently in primary mouse hepatocytes

The detection of temperature-dependent, PTC-containing isoforms requires depletion or pharmacological inhibition of the NMD pathway (Rehwinkel, Raes et al., 2006). NMD occurs co-translational, and therefore blocking translation (e.g. via cycloheximide (CHX)) represents a fast and reliable way of blocking the NMD pathway (Hurt et al., 2013). To identify temperature-

controlled splicing isoforms inducing NMD, we performed RNA-Seq on freshly-isolated primary mouse hepatocytes, incubated either at 34 or 38°C and treated either with DMSO or CHX (Figure 1A). A principal component analysis revealed clear clustering of the biological triplicates and comparable effects of both temperature and CHX on AS (Figure S1A). Using Whippet (Sterne-Weiler, Weatheritt et al., 2018), we initially identified over 3800 genes with CHX-sensitive splicing events at either 34°C or 38°C. A quarter of these events lie within genes previously associated with NMD (Figure S1B), validating our approach for identification of NMD-inducing isoforms. Next, we identified 4740 temperature-controlled (comparing 34°C and 38°C) splicing events in the CHX-treated cells (Figure S1C and Table S1). Only 1/3 of the strongest 1000 events and about 60% of all events respond in a similar manner in the DMSO control, indicating non-NMD events (Figures 1B and S1D, heat-skipped or cold-skipped). All other isoforms, almost 2000 in total (Table S1), lose their temperature-dependence in the DMSO control, indicating NMD-mediated degradation of one isoform, as it only accumulates in CHX-treated cells. These cases can be categorized into four groups: (I) cold-induced NMD via inclusion; (II) heat-induced NMD via inclusion; (III) cold-induced NMD via exclusion; and (IV) heat-induced NMD via exclusion. Examples for each of these categories were confirmed by radioactive RT-PCRs with RNAs from independently generated hepatocytes (Figures 1C and S1E) as follows: In *Mettl16,* exon 6 encodes a PTC, and the full length (fl) isoform – containing exon 6 – is therefore stabilized via CHX. Exon 6 inclusion is strongly promoted at 34°C, representing a cold-induced NMD event. In *Hnrnpdl,* exon 8 inclusion generates a second exon junction complex after the canonical stop in exon 7, turning this stop into a PTC (Lindeboom, Supek et al., 2016). The fl isoform is stabilized by CHX and, as it predominates at 38°C, represents a heat-induced NMD event. In *Hnrnph1* and *Slc9a8,* skipping of an exon (length not divisible by 3) generates a frameshift and a PTC in a downstream exon.

Globally, the NMD-inducing isoforms are dramatically stabilized by CHX, often with changes in NMD exon abundance of 60% or more, at either cold or heat conditions. In addition to skipped exon events, we also find temperature-dependent AS-NMD in the form of alternative 3' or 5' splice sites, intron retention, mutually exclusive exons, transcription starts and transcription ends (Table S1 and below), and the quantity and diversity of temperature- and CHX-controlled isoforms is indicative for a global impact on temperature-dependent GE levels. Additionally, certain NMD isoforms are almost exclusively found at one temperature (examples in *Rsrp1* and *Fus*; Figure S1E) and our approach of screening for AS-NMD at different temperatures thus expands the collection of known NMD-inducing isoforms.

Overall, inclusion levels (percent spliced in, PSI) predicted by Whippet and validated by RT-PCR from independent biological samples show strong correlation, allowing us to draw reliable conclusions from our bioinformatics analysis (Figure S1F). In all presented examples, as well as

globally, the direction of PSI changes in DMSO correlate with PSI changes in CHX, confirming that these variants are present also in DMSO but are stabilized after CHX treatment (Figure S1G). When analyzing all genes with potential NMD events (all isoforms stabilized by CHX at 34 or 38°C) we find that almost 40% of these genes contain temperature-regulated NMD isoforms (Figures 1D and S1H), showing that NMD isoforms are pervasively responsive to temperature changes, which is consistent with a global role in shaping temperature-controlled GE. Interestingly, we find temperature-controlled NMD events enriched in RBPs (Figure 1E and below), which could represent the temperature-controlled core machinery that is able to amplify the temperature signal to control further downstream output events. In summary, temperature-controlled AS-NMD represents a frequent mode of posttranscriptional regulation, with wide implications for temperature-controlled GE levels.

RBP expression is controlled through temperature-dependent AS-NMD

Our bioinformatics analysis identified over 60 RBPs with temperature-regulated NMD exons of different types (Figure 2A, see also Table S1). Most of these AS-NMD events are alternative cassette exons (e.g. *Hnrnpdl, Hnrnph3*), but there are also different types such as alternative last exons (e.g. *Cirbp*). In the presented examples, a temperature change of 4°C is sufficient to change AS by 20-30%, e.g. *Hnrnpdl* 60% to 95%, indicating a strong regulatory impact on the expression of the respective RBPs (Figure 2A). We have recently shown this particular temperature-dependent AS event in *Cirbp* to be regulated by CLK activity and found that E7b inclusion reduces *Cirbp* GE (Haltenhof et al., 2020). In line with these findings, we find the E7b isoform to be strongly stabilized by CHX and observe a correlation of higher abundance of the NMD isoforms (particularly in the CHX condition) with decreased overall GE in the DMSO control in *Cirbp* and all other cases analyzed (Figure 2B). For example, in *Hnrnpdl* the NMD isoform makes more than 90% at 38°C, correlating with a 4-fold reduction in GE. Note, that although the change in *Cirbp* exon 7b inclusion between the two CHX conditions is visible as a drastic change in the Sashimi plot (Figure 2A, only 10% of reads from exon 6 span to exon 7b at 34°C, while this is the case for almost 70% of reads at 38°C), Whippet quantifies this as a still severe but lower difference of about 15% (Figure 2B). For global correlations, we therefore include only skipped exon events, which are more robust to quantification. When considering all candidate RBPs with temperature-dependent AS-NMD skipped exon events, we observe a highly significant global correlation of temperature-dependent NMD-isoform generation and reduced GE levels in DMSO control (Figure 2C, left). Consistent with CHX preventing degradation of NMD-inducing isoforms, this correlation is completely abolished in the CHX samples (Figure 2C, right), strongly arguing for AS-NMD being the primary cause of temperature-dependent changes in GE levels. Looking at all genes with temperature-controlled

cassette exon NMD events, the global trend is still present, although to a lesser extent (Figure S2), indicating that temperature-dependent GE requires AS-NMD but is additionally controlled by other mechanisms. In summary, these data reveal a mechanism that globally controls GE in a temperature-regulated manner via AS coupled to the NMD pathway.

Temperature-controlled AS-NMD is evolutionarily conserved across endotherms

We next elucidated the evolutionary conservation of temperature-regulated AS-NMD. For SR proteins, it was previously described that these have NMD-inducing exons with ultraconserved regions (Lareau et al., 2007) but their function was only linked to producing homeostatic GE levels. We hypothesized that these ultraconserved regions likely have additional functionalities and could be involved in controlling temperature-dependent GE of SR proteins via AS-NMD. We indeed detect AS-NMD variants for most SR proteins, ranging from temperature-insensitive to strongly temperature-dependent (Figure S3A). Two extreme examples for heat-induced and cold-induced non-productive splicing events are ultraconserved exons in *Srsf2* and *Srsf10*. For *Srsf2* we observed and validated strong heat-induced inclusion of the PTC-encoding exon 3 (ΔPSI in CHX =46%, Figures 3A, left and S3B). In contrast, we observed almost cold-restricted generation of a non-productive isoform for *Srsf10*, namely exon 3 inclusion coupled to the use of an alternative splice site in exon 2 (ΔPSI in CHX =19%, Figures 3A, right and S3C), indicating antagonistic effects of temperature on different SR proteins. Again, the heat-induced NMD exon inclusion of *Srsf2* correlates with decreased GE in heat and vice versa for *Srsf10* (Figures 3A, center). To investigate whether temperature cycles could lead to rhythmic splicing of NMD inducing exons, we applied a modified simulated body temperature regime (Brown et al., 2002, Preussner et al., 2017) to human Hek293 cells. Consistent with our data from mouse hepatocytes, the corresponding AS events in *Srsf2* and *Srsf10* respond to 24-hour square-wave 34/38°C temperature rhythms in human Hek293 (Figure 3B), showing a cell-type-independent and evolutionarily-conserved regulation of SR proteins through (circadian) temperature changes. We also note that splicing-regulation is reverted already within 4-8 hours at one temperature, which is indicative for an autoregulatory feedback loop. Furthermore, we have validated additional temperature-dependent NMD isoforms for *Hnrnpdl*, *Hnrnph3*, and *Cirbp* in Hek293 cells (Figure 3C), consistent with high evolutionary conservation (see conservation track in Figure 2A). Importantly, we find that all temperature-controlled AS-NMD exons as well as several 100 nucleotides in the surrounding introns are extremely conserved across placental organisms (Figure 3D and conservation tracks in Sashimi plots in Figures 2A and 3A), arguing for an evolutionarily vital function. Consistent with (Thomas, Polaski et al., 2020), this conservation is

present in all AS-NMD exons. Finally, we exemplarily investigated temperature-controlled *Srsf2* AS in hamster, rabbit and chicken cell lines (chicken as a non-placental endothermic organism), and strikingly find exon 3 inclusion promoted by heat and CHX in all cases (Figure 3E), thus demonstrating conserved regulation in all investigated endothermic organisms. The percentage of heat-induced NMD exon inclusion varies between 8% in rabbit cell or human Hek293 and up to 80% in primary mouse hepatocytes indicating species- or tissue-specific differences in SRSF10 expression or activity. In summary, we find that temperature-dependent NMD exon inclusion in SR proteins anticorrelates with SR protein expression and is highly evolutionarily conserved, indicating an essential function in regulating temperature-dependent GE.

Temperature rhythms are sufficient to generate GE rhythms depending on AS-NMD

To investigate whether external 24-hour rhythms in temperature are sufficient to generate rhythmic GE, we analyzed *Srsf2* and *Srsf10* GE in response to square-wave temperature rhythms (Figure 4A). Both genes clearly show 24-hour rhythms in gene expression, with *Srsf2* showing higher expression during the cold-phase (heat-induced NMD) and *Srsf10* showing higher expression during the warm phase (cold-induced NMD; WT in Figures 4B and 4C). Next, we generated CRISPR/Cas9-edited cell lines lacking either *Srsf2* exon 3 or *Srsf10* exon 3 and confirmed removal of the respective exons on RNA level (Figures S4A and S4B). Applying square-wave temperature rhythms to these cell lines, we find that removing the temperature-dependent exon is sufficient to abolish rhythms driven by external temperature cycles in both cases (∆E3 in Figures 4B and 4C), showing that conserved NMD-inducing alternative exons in SR proteins indeed are necessary for their temperature-dependent GE.

Temperature-dependent AS-NMD regulates expression levels of SR proteins in *A. thaliana*

The pervasive identification of temperature-controlled AS-NMD in distinct SR proteins (and other RBPs) indicates an evolutionary advantage in homeotherms. To span a broader evolutionary spectrum, we next asked whether a similar mechanism is also in place for poikilotherms, which experience much greater differences in (body) temperature (10°C during a day-night cycle and often 50°C in seasonal changes compared to 1-2°C change in body temperature in mice). We therefore examined temperature-dependent SR protein splicing and expression in *A. thaliana*, encoding 18 SR proteins (based on (Barta, Kalyna et al., 2010)) with evolutionary conserved regions triggering AS-NMD (Palusa & Reddy, 2010, Rauch, Patrick et al., 2014, Richardson, Rogers et al., 2011). We analyzed a publicly-available RNA-Seq time course dataset from plants kept at 20°C for 24 hours and then shifted to 4°C for the next 24 hours, while being under a 12-

hour dark-light regime (Calixto, Guo et al., 2018), allowing us to distinguish between light- and temperature-dependent effects. When assessing changes in GE, we strikingly find that all 18 SR proteins show a clear temperature-dependent regulation (Figure 5A). Some genes additionally show a light-dependent expression pattern, but temperature is in general the dominant signal. About half of the regulated SR proteins show higher GE at 20°C, while the other half is cold-induced. Interestingly, we find at least one example for both warm- and cold-expressed SR genes in all but one SR protein subfamilies (Figure 5B), which may suggest partially complementing functions. Within the RNA-Seq data we find clear evidence for NMD-inducing AS that is antagonistically regulated to GE in 50% of temperature regulated SR proteins (Figures S5A and S5B), for example in At-SR34 and At-SCL33 (Figure 5C), consistent with previous notions (Calixto et al., 2018, Staiger & Brown, 2013). In all tested examples, temperature-dependent splicing and GE changes could be confirmed by RT-PCR from independently-generated plant samples (Figures 5D and S5C). To systematically characterize temperature-dependent AS-NMD events in plants, we first used RNA-Seq data of CHX-treated plants to identify NMD events (Drechsel, Kahles et al., 2013) and then quantified temperature regulation of these targets in samples without NMD inhibition (data from (Calixto et al., 2018)). Although detection of NMD isoforms is challenging without stabilization of the respective isoforms, we were able to identify 80 NMD isoforms clearly affected by temperature (Table S1). Consistent with our findings in mouse, there is a highly significant anti-correlation between NMD isoform inclusion and GE (Figure 5E). This includes a temperature-controlled AS-NMD event in the snRNP assembly factor At-GEMIN2 (Figure S5D), which was previously identified as a key regulator of downstream temperature-dependent clock-related splicing events (Schlaen, Mancini et al., 2015). In conclusion, these data expand our findings from the mammalian to the plant system, identifying temperature-dependent AS-NMD as an evolutionary pervasive mechanism that adapts SR protein expression to changing temperatures. During mammalian evolution, AS-NMD in SR genes arose independently, evolutionary rapid and in an SR protein specific manner (Lareau & Brenner, 2015), thus showing that *cis*-regulatory elements regulating temperature-dependent AS-NMD independently arose in homeotherms and poikilotherms. This suggests a broad evolutionary advantage of temperature-dependent SR protein expression and is indicative for an evolutionary-conserved and -adapted temperature sensor controlling SR protein activity.

Body temperature-regulated AS-NMD generates 24-hour rhythms in GE

Finally, we address the question to which extent rhythmic GE *in vivo* is depending on naturally-occurring body temperature cycles. We therefore compared the acrophase (time of maximal GE) of heat and cold-induced genes across a circadian cycle in mouse liver (Atger, Gobet et al., 2015).

Strikingly, we find that genes with higher expression at 38°C in hepatocytes predominantly peak during the night when mice are active and have a higher body temperature. In contrast, cold-induced genes from hepatocytes rather peak during the colder day (Figure 6A, top), providing evidence for a direct function of body temperature cycles in generating 24-hour rhythmic GE. Consistent with a function of temperature-dependent AS-NMD in this mechanism, we additionally find that genes with a cold-induced NMD skipped exon event peak during the night, while genes with a heat-induced NMD skipped exon event tend to peak during the day (Figure 6A, bottom). Of note, of the 254 genes with temperature-induced AS-NMD skipped exon events, 102 were found to exhibit cyclic expression.

As one particular example, we analyzed *Srsf10* expression *in vivo* in detail and find a clear time of the day-dependent formation of the non-productive *Srsf10* isoform (Figure 6B, right y-axis). Consistent with our data from cultured hepatocytes, we observe antagonistic 24-hour rhythms in GE across a circadian day *in vivo* in liver (Figure 6B, left y-axis). This is not a tissue-specific but a general effect, as shown by validations in samples from mouse cerebellum confirming increased non-productive splicing in combination with lower GE during the day (Figure S6A). Similar to other temperature-driven AS events (Preussner et al., 2014), we find that *Srsf10* AS persists in constant darkness and is entrainable to a new light-dark regime (Figures S6B and S6C), highlighting common, e.g. body temperature-dependent, regulatory principles. Finally, we found that AS-NMD driven rhythms in GE are also reflected at the protein level by confirming daytime-dependent SRSF10 protein expression in mouse liver (Figures 6C and 6D). In summary, these data point to a fundamental role of mammalian body temperature in generating rhythmic GE *in vivo*, which is independent from the classical, circadian clock-mediated generation of 24-hour rhythms (Figure 7).

Discussion

Here we report that temperature-regulated AS coupled to NMD occurs frequently in diverse genes from evolutionary distant species. We furthermore show that these splicing events are sufficient to generate temperature-dependent GE changes and to induce 24-hour rhythms in GE. Together, these data are consistent with a model where body temperature-controlled AS-NMD represents a second, core clock-independent generator of 24-hour rhythmic GE. Classical circadian cycles in GE are driven by a transcription-translation feedback loop (Figure 7, inner ring). Here, transcriptional activation trough CLOCK/BMAL1 results in accumulation of PERIOD (PER) and CRYPTOCHROME (CRY). When a critical protein level is reached, these factors dimerize, enter the nucleus and repress their own GE. This results in low mRNA and protein expression, again allowing activation through CLOCK and BMAL1. Together with *Per* and *Cry*, many other Clock-

controlled genes oscillate through this feedback loop. Circadian oscillations are robust to environmental changes and continue to oscillate with only mildly-affected amplitude in the absence of rhythmic stimuli (Figure 7, center). In a second and largely independent cycle, body temperature induces rhythmic GE through AS-NMD (Figure 7, outer ring). Here, body temperature cycles control the activity and AS-NMD-mediated autoregulation of SR proteins. An SR protein that is inactive due to its phosphorylation level results in the accumulation of its mRNA and (inactive) protein. Upon a switch to the activating body temperature, phosphorylation of the SR protein changes through altered CLK activity (Haltenhof et al. 2020) and the activated SR proteins promotes NMD exon inclusion (within their own pre-mRNA). Degradation of the unproductive mRNA isoform then leads to low but active protein levels. Only upon a second switch to the inactivating temperature, predominant formation of the productive isoforms becomes possible, again resulting in accumulation of the respective SR protein. As for the classic circadian feedback loop, autoregulation of SR proteins represents the core machinery, which then controls other genes containing NMD exons to also cycle in response to rhythmic body temperature changes. As long as the body temperature oscillates, AS-NMD-driven GE also cycles in a circadian-like manner (Figure 7, center). This however requires continuous input and the rhythmicity is lost under constant conditions, which sets it apart from classic circadian GE.

In addition to SR proteins, we identified temperature-controlled NMD-inducing splicing isoforms in many other RBPs. Mechanistically, it will be interesting to investigate, whether these splicing events are directly controlled by SR proteins or whether temperature also controls the activity of other RBPs (e.g. by phosphorylation or other post-translational modifications). The presence of temperature-regulated AS-NMD isoforms in many RBPs is indicative for an interlocked network of RBPs to post-transcriptionally adapt GE to temperature, representing a potential layer of signal amplification. In mammals, this network requires sensors and modulators that are sensitive enough to respond to temperature differentials of around 1°C, to be able to respond to daily changes in body temperature. In recent work we have characterized CLK kinases as the direct molecular sensor of such temperature changes (Haltenhof et al., 2020). Interestingly we find in evolutionary distant species, that groups of SR proteins are antagonistically-affected by temperature, such that one group is activated by hyperphosphorylation, whereas this leads to inactivation of another group of SR proteins. While we observe this regulatory pattern in evolutionary distant species such as plants and humans, pointing to an important functionality, it remains unknown, how phosphorylation of SR proteins can have opposing effect on their activity. Autoregulatory feedback loops were initially characterized as a mechanism allowing homeostatic regulation of SR proteins (Lareau et al., 2007, Ni et al., 2007). Here, we report that the same autoregulatory feedback loop is capable of producing rhythms in GE. An input signal controlling

SR protein activity is sufficient to change SR protein expression. This has also intriguing consequences for SR protein target genes, as activation of a protein reduces total levels of the same protein. Target genes with high-affinity binding sites might therefore be bound and activated (including the own pre-mRNA) while target genes with low affinity binding sites are not bound, due to the reduced total protein levels, and therefore rather repressed.

At first sight the existence of two independent 24-hour rhythms appears puzzling, but these two rhythms are fundamentally different: While classical circadian rhythms depend on transcription-translation feedback loops and are robust to minor ambient changes (Gonze, Halloy et al., 2002), temperature-induced rhythms are generated post-transcriptionally and can quickly adapt GE in response to changing temperatures. Therefore, temperature-induced rhythms can stabilize circadian rhythms under circadian temperature cycles (Morf et al., 2012) but can additionally adapt GE in response to sudden temperature changes, i.e. under disease-associated stress conditions, and are therefore able to integrate all temperature-changing signals into complex GE programs. In mammals, this could example involve body temperature changes associated with the female hormone cycle (Nagashima, 2015) or with aging (Keil, Cummings et al., 2015). Furthermore, the interplay of these two mechanisms could be involved in seasonal control of GE by integrating light and temperature signals. For example, At-RS40 exhibits an intriguing upregulation of GE in cold light conditions (Figure 5A) and could therefore realize specific effects during winter days.

Homeothermic and poikilothermic organisms experience quite different differentials in body temperature, and it is therefore a striking finding that in mouse/human (1-2°C) and plants (>20°C) an almost identical mechanism controls SR protein levels. The evolution of AS-NMD in SR proteins (Lareau & Brenner, 2015) indicates an evolutionary independent origin of the temperature-controlled exons/introns. Mechanistically it will therefore be interesting to investigate how cis-regulatory elements, SR proteins and kinases are evolutionary adapted to allow control of SR protein expression in the body temperature range of diverse organisms. The evolutionary-pervasive identification of temperature-controlled AS-NMD in SR proteins is indicative for an important function in temperature adaptation. Additionally, the fact that ultraconserved elements within SR proteins have evolved rapidly and are effectively ‘frozen’ in mammals and birds (Bejerano, Pheasant et al., 2004), which are all endothermic homeotherms, represents a strong connection to endothermy. Because of the high sensitivity of temperature-controlled AS-NMD, this mechanism could be involved in setting or maintaining a constant body temperature. The clinical importance of ultraconserved exons triggering NMD is furthermore highlighted by their potential tumor suppressive function (Thomas et al., 2020) and the association of NMD isoforms with neuronal diseases (Jaffrey & Wilkinson, 2018). Therefore, the *de novo* identification of temperature-restricted NMD isoforms might reveal novel candidates for antisense

oligonucleotide-based therapies in human (Bennett, Krainer et al., 2019). Overall, we describe a surprisingly widespread mechanism that integrates diverse environmental signals to induce AS-NMD cycles and generate GE rhythms from plants to human, constituting a plethora of future implications.

Materials & Methods

Mouse maintenance

All animal experiments were performed with C57BL/6 mice in accordance with institutional and governmental recommendations and laws. Mice were kept under constant 12-hour light-dark conditions. RNA samples across a circadian day, from constant darkness or after jet-lag were previously generated (Preussner et al., 2014). Mice of both genders were used. For preparation of RNA, tissues were quickly removed, frozen in liquid nitrogen and homogenized in RNATri (Bio&Sell). For preparation of nuclear extracts, we first prepared single cell suspensions of freshly isolated liver samples.

Tissue culture cells

The HEK293T cell line has been present in the lab for over 5 years and is maintained in liquid nitrogen. Early passage aliquots are thawed periodically. Rabbit RK-13, Chinese hamster CHO and chicken enterocyte 8E11 cell lines were a kind gift from Dusan Kunec (FU Berlin). For all cell lines, cell morphology and growth is routinely assessed and corresponds to the expected phenotype. Cell cultures are tested for mycoplasma contamination monthly using a PCR-based assay. HEK293T and 8E11 cell lines were maintained in DMEM medium containing 10% FBS and Pen/Strep (Invitrogen). RK13 cells were maintained in EMEM medium containing 10% FBS and Pen/Strep (Invitrogen). CHO cells in Ham's F12 medium containing 10% FBS and Pen/Strep. All cell lines were usually maintained at 37°C and 5% CO^2, except for 8E11 cells (39°C). For square-wave temperature cycles we used two incubators set to 34°C and 38°C and shifted the cells every 12 hours. See (Preussner et al., 2017) for an image of the square-wave temperature cycles with temperatures and time points. For chicken cells we used 34°C and 40°C (as 37°C degrees would already be a reduced temperature). Transfections of Hek293T using Rotifect (Roth) were performed according to the manufacturer's instructions. Cycloheximide (Sigma) was used at 40µg/ml final concentration or DMSO as solvent control.

To isolate primary mouse hepatocytes, liver was perfused with PBS and digested using Collagen digestion solution. Liver was transferred into a Petri dish and cells were liberated by mechanical force. Cells were washed three time with Williams Medium E and 10% FCS and plated.

A. thaliana

To confirm temperature-dependent alternative splicing and gene expression in *A. thaliana* we isolated RNA from 28-day old Col-0 plants kept only at 20°C or 31-day old Col-0 plants kept at 4°C for the last 3 days. For RNA isolation using Trizol (see below) we used ~100mg material from leaves.

RT-PCR and RT-qPCR

RT-PCRs were done as previously described (Preussner et al., 2014). Briefly, RNA was extracted using RNATri (Bio&Sell) and 1µg RNA was used in a gene specific RT-reaction. For analysis of minigene splicing the RNA was additionally digested with DNase I and re-purified. Low-cycle PCR with a ^{32}P-labeled forward primer was performed, products were separated by denaturing PAGE and quantified using a Phosphoimager and ImageQuantTL software. For qRT-PCR up to 4 gene-specific primers were combined in one RT reaction. qPCR was then performed in a 96 well format using the ABsolute QPCR SYBR Green Mix (Thermo Fisher) on Stratagene Mx3000P instruments. qPCRs were performed in duplicates, mean values were used to normalize expression to a housekeeping gene (mouse: *Hprt*, human: *Gapdh*, plants: *Ipp2*; ΔCT) and $\Delta(\Delta CT)$s were calculated for different conditions. See Table S2 for primer sequences.

RNA-Seq analysis and bioinformatics

Mapping of reads to reference genomes was performed using STAR version 2.5.3a (Dobin, Davis et al., 2012). Reference genomes mm10 (mouse) and TAIR10 (*A.* thaliana) were applied. Gene expression analysis was performed using Salmon version 0.11.3 transcript quantification (Patro, Duggal et al., 2017) followed by DESeq2 version 1.22.2 quantification (Love, Huber et al., 2014) both used according to their documentation.

Whippet version 0.11 (Sterne-Weiler et al., 2018) was used to obtain splicing ratios and transcript per million GE quantifications. To obtain splicing quantifications of AS-NMD events, index creation was supplemented with mapped reads of NMD-inhibited sequencing samples (see Table S1 for plant accession numbers) and the low TSL flag was not set. A splice event was considered significantly different between two conditions with a $|\Delta PSI| > 15\%$, probability > 85% and on average more than 10 junction reads. For AS-NMD events of SR proteins that could not be properly quantified by Whippet, PSI values were calculated based on junction read counts (e.g. Srsf7). Downstream analyses were performed using Python3, bash and R scripts. Most relevant

Python packages used were pandas (general secondary data analysis, (McKinney, 2010)), numpy (numerical operations, (Walt, Colbert et al., 2011)), Matplotlib (data visualization, (Hunter, 2007)) and scikit-learn (principle component analysis, (Pedregosa, Varoquaux et al., 2011)). Molecular function analysis was performed using PANTHER version 14.1 (Mi, Muruganujan et al., 2013) with all genes expressed above 1 TpM as background. Sashimi plots were generated using a customized version of ggsashimi (Garrido-Martin, Palumbo et al., 2018), which additionally displays conservation scores. Junction reads with low count numbers were removed for clarity. Phylogenetic p-value conservation score data of placental organisms was downloaded from UCSC (mm10 phyloP60way placental, (Pollard, Hubisz et al., 2010, Siepel, Bejerano et al., 2005)) and manipulated with BEDOPS version 2.4.26 and bedtools version 2.26.0 (Neph, Kuehn et al., 2012, Quinlan & Hall, 2010).

For mouse data, splicing events were classified into the following groups:

1) events that show differential splicing upon temperature (34°C vs 38°C between DMSO or CHX conditions)
2) events that show differential splicing upon CHX treatment (DMSO vs CHX in 34°C or 38°C conditions) and no temperature-dependent differential splicing (34°C vs 38°C in CHX)
3) events that show differential splicing upon CHX treatment (DMSO vs CHX in 34°C or 38°C conditions) and additional temperature-dependent differential splicing (34°C vs 38°C in CHX)
4) events that do not fall into any of the above categories

Splicing events in groups 2) and 3) were identified as AS-NMD events. The temperature-regulated events were further divided into cold-induced and heat-induced AS-NMD events (considering directionality of the CHX-induction). AS-NMD events that showed different directionality upon CHX treatment at the two temperatures were omitted from the analysis (these made up <2% of CHX-induced events).

For *A. thaliana*, AS-NMD events were identified by using independent RNA-seq data from CHX-treated plants. These data did not include a temperature shift and therefore the classification between temperature-dependent and -independent AS-NMD events has been done using temperature shifted but not CHX treated data. Otherwise the classification was performed as for mouse.

For preparation of rose plots, gene acrophases (time of highest expression) from (Atger et al., 2015) were used and combined with information about temperature-regulation on expression (based on DESeq2 analysis, padj < 0.05) and AS-NMD level (based on Whippet and post-analysis, see above). Genes were sorted into 24 bins that represent 1h each. As the data are highly skewed, normalization was needed. Therefore, the percentage of genes falling into each

bin was calculated for all genes obtained from (Atger et al., 2015), and the subsets of heat-expressed and cold-expressed genes as well as those of genes with cold-induced and heat-induced NMD events. The percentages for each bin in the subsets was then divided by this bin's percentage of overall genes. The black circles shown in Figure 6A represent the normalization line (expected proportion of genes if no effect was present).

Generation of CRISPR/Cas9 modified cell lines.

For genome-engineering in Hek293T cells, sequences flanking the conserved exons of Srsf2 or Srsf10 (human) sgRNA candidates *in silico* using the Benchling tool. Upstream and downstream of each exon at least one pair of oligos for the highest ranked candidate sgRNA (Ran, Hsu et al., 2013) was synthesized and subcloned into the PX459 vector (kindly provided by Stefan Mundlos). sgRNA sequences are available on request. Cells were transfected in 6-well plates using Rotifect following the manufacturer's protocol. 48 hours after transfection, the transfected cells were selected with 1 µg/ml puromycin and clonal cell lines were isolated by dilution (Ran et al., 2013). Genomic DNA was extracted using DNA extraction buffer (200 mM Tris pH 8.3, 500 mM KCl, 5 mM $MgCl_2$, 0.1% gelatin in H_2O) and a PCR was performed using gene-specific primers to confirm the exon knockout on DNA level. In promising clones the exon knockout was additionally confirmed after RNA isolation by splicing sensitive PCR.

Western Blot

Nuclear fractionations (NX) were performed as previously described (Heyd & Lynch, 2010). SDS-PAGE and Western blotting followed standard procedures. Western blots were quantified using the ImageQuant TL software. The following antibodies were used for Western blotting: hnRNP L (4D11, Santa Cruz), SRSF10 (T-18, Santa Cruz).

Quantification and statistical analysis

Figure legends contain information on repetitions and statistical tests used.

Data and Software Availability

Full gel images and raw data files will be deposited as Mendeley Data. RNA sequencing data are available under GEO XXX.

Contact for Reagent and Resource Sharing

Please contact M.P. (mpreussner@zedat.fu-berlin.de) for reagents and resources generated in this study. Accession numbers to all RNA-seq datasets used in this study are noted in Table S1.

Acknowledgments

The authors would like to thank Jessica Stock, Alena Lohnert, Kevin Huolt and Hoonsung Cho for their contribution to this work as rotation students. Furthermore, we would like to thank Dirk Hincha for discussing AS-NMD in plants, Tom Haltenhof for the isolation of primary hepatocytes, the SeqCore facility for generation of RNA Sequencing data and the HPC Service of ZEDAT, Freie Universität Berlin, for computing time. This work was funded through DFG grants HE5398/4-2 and 278001972 - TRR 186 to FH. MP is funded by a stipend from the Peter Traudl Engelhorn Foundation.

Author Contributions

SM, GG, MS and MP performed experiments. AN performed the bioinformatics analysis. DS provided plant material. BT performed RNA-sequencing. AN, MP and FH designed the study, planned experiments, analyzed data and wrote the manuscript with help from SM. MP and FH conceived and supervised the work.

Conflict of interest

The authors declare no conflict of interest.

References

Atger F, Gobet C, Marquis J, Martin E, Wang J, Weger B, Lefebvre G, Descombes P, Naef F, Gachon F (2015) Circadian and feeding rhythms differentially affect rhythmic mRNA transcription and translation in mouse liver. *Proceedings of the National Academy of Sciences of the United States of America* 112: E6579-88

Barta A, Kalyna M, Reddy AS (2010) Implementing a rational and consistent nomenclature for serine/arginine-rich protein splicing factors (SR proteins) in plants. *Plant Cell* 22: 2926-9

Bejerano G, Pheasant M, Makunin I, Stephen S, Kent WJ, Mattick JS, Haussler D (2004) Ultraconserved elements in the human genome. *Science* 304: 1321-5

Bennett CF, Krainer AR, Cleveland DW (2019) Antisense Oligonucleotide Therapies for Neurodegenerative Diseases. *Annu Rev Neurosci* 42: 385-406

Braunschweig U, Gueroussov S, Plocik AM, Graveley Brenton R, Blencowe Benjamin J (2013) Dynamic Integration of Splicing within Gene Regulatory Pathways. *Cell* 152: 1252-1269

Brown SA, Zumbrunn G, Fleury-Olela F, Preitner N, Schibler U (2002) Rhythms of mammalian body temperature can sustain peripheral circadian clocks. *Curr Biol* 12: 1574-83

Buhr ED, Yoo SH, Takahashi JS (2010) Temperature as a universal resetting cue for mammalian circadian oscillators. *Science* 330: 379-85

Calixto CPG, Guo W, James AB, Tzioutziou NA, Entizne JC, Panter PE, Knight H, Nimmo HG, Zhang R, Brown JWS (2018) Rapid and Dynamic Alternative Splicing Impacts the Arabidopsis Cold Response Transcriptome. *Plant Cell* 30: 1424-1444

Dibner C, Schibler U, Albrecht U (2010) The mammalian circadian timing system: organization and coordination of central and peripheral clocks. *Annu Rev Physiol* 72: 517-49

Dobin A, Davis CA, Schlesinger F, Drenkow J, Zaleski C, Jha S, Batut P, Chaisson M, Gingeras TR (2012) STAR: ultrafast universal RNA-seq aligner. *Bioinformatics* 29: 15-21

Drechsel G, Kahles A, Kesarwani AK, Stauffer E, Behr J, Drewe P, Ratsch G, Wachter A (2013) Nonsense-mediated decay of alternative precursor mRNA splicing variants is a major determinant of the Arabidopsis steady state transcriptome. *Plant Cell* 25: 3726-42

Garrido-Martin D, Palumbo E, Guigo R, Breschi A (2018) ggsashimi: Sashimi plot revised for browser- and annotation-independent splicing visualization. *PLoS Comput Biol* 14: e1006360

Gerber A, Saini C, Curie T, Emmenegger Y, Rando G, Gosselin P, Gotic I, Gos P, Franken P, Schibler U (2015) The systemic control of circadian gene expression. *Diabetes Obes Metab* 17 Suppl 1: 23-32

Goldammer G, Neumann A, Strauch M, Muller-McNicoll M, Heyd F, Preussner M (2018) Characterization of cis-acting elements that control oscillating alternative splicing. *RNA Biol* 15: 1081-1092

Goncalves V, Jordan P (2015) Posttranscriptional Regulation of Splicing Factor SRSF1 and Its Role in Cancer Cell Biology. *Biomed Res Int* 2015: 287048

Gonze D, Halloy J, Goldbeter A (2002) Robustness of circadian rhythms with respect to molecular noise. *Proceedings of the National Academy of Sciences of the United States of America* 99: 673-678

Gotic I, Omidi S, Fleury-Olela F, Molina N, Naef F, Schibler U (2016) Temperature regulates splicing efficiency of the cold-inducible RNA-binding protein gene Cirbp. *Genes Dev* 30: 2005-17

Haltenhof T, Kotte A, De Bortoli F, Schiefer S, Meinke S, Emmerichs AK, Petermann KK, Timmermann B, Imhof P, Franz A, Loll B, Wahl MC, Preussner M, Heyd F (2020) A conserved kinase-based body temperature sensor globally controls alternative splicing and gene expression. *Mol Cell*

Heyd F, Lynch KW (2010) Phosphorylation-dependent regulation of PSF by GSK3 controls CD45 alternative splicing. *Mol Cell* 40: 126-37

Hunter JD (2007) Matplotlib: A 2D Graphics Environment. *Computing in Science & Engineering* 9: 90-95

Hurt JA, Robertson AD, Burge CB (2013) Global analyses of UPF1 binding and function reveal expanded scope of nonsense-mediated mRNA decay. *Genome Res* 23: 1636-50

Jaffrey SR, Wilkinson MF (2018) Nonsense-mediated RNA decay in the brain: emerging modulator of neural development and disease. *Nat Rev Neurosci* 19: 715-728

Keil G, Cummings E, de Magalhães JP (2015) Being cool: how body temperature influences ageing and longevity. *Biogerontology* 16: 383-397

Ko CH, Takahashi JS (2006) Molecular components of the mammalian circadian clock. *Hum Mol Genet* 15 Spec No 2: R271-7

Koike N, Yoo SH, Huang HC, Kumar V, Lee C, Kim TK, Takahashi JS (2012) Transcriptional architecture and chromatin landscape of the core circadian clock in mammals. *Science* 338: 349-54

Kornmann B, Schaad O, Bujard H, Takahashi JS, Schibler U (2007) System-Driven and Oscillator-Dependent Circadian Transcription in Mice with a Conditionally Active Liver Clock. *PLoS Biol* 5: e34

Lareau LF, Brenner SE (2015) Regulation of splicing factors by alternative splicing and NMD is conserved between kingdoms yet evolutionarily flexible. *Mol Biol Evol* 32: 1072-1079

Lareau LF, Inada M, Green RE, Wengrod JC, Brenner SE (2007) Unproductive splicing of SR genes associated with highly conserved and ultraconserved DNA elements. *Nature* 446: 926-9

Lindeboom RGH, Supek F, Lehner B (2016) The rules and impact of nonsense-mediated mRNA decay in human cancers. *Nat Genet* 48: 1112-1118

Liu Y, Hu W, Murakawa Y, Yin J, Wang G, Landthaler M, Yan J (2013) Cold-induced RNA-binding proteins regulate circadian gene expression by controlling alternative polyadenylation. *Sci Rep* 3: 2054

Liu Z, Qian M, Tang X, Hu W, Sun S, Li G, Zhang S, Meng F, Cao X, Sun J, Xu C, Tan B, Pang Q, Zhao B, Wang Z, Guan Y, Ruan X, Liu B (2019) SIRT7 couples light-driven body temperature cues to hepatic circadian phase coherence and gluconeogenesis. *Nature Metabolism* 1: 1141-1156

Love MI, Huber W, Anders S (2014) Moderated estimation of fold change and dispersion for RNA-seq data with DESeq2. *Genome biology* 15: 550

Lykke-Andersen S, Jensen TH (2015) Nonsense-mediated mRNA decay: an intricate machinery that shapes transcriptomes. *Nature Reviews Molecular Cell Biology* 16: 665

Manley JL, Krainer AR (2010) A rational nomenclature for serine/arginine-rich protein splicing factors (SR proteins). *Genes Dev* 24: 1073-1074

McKinney WT (2010) Data Structures for Statistical Computing in Python. *Proceedings of the 9th Python in Science Conference* 51-56

Menet JS, Rodriguez J, Abruzzi KC, Rosbash M (2012) Nascent-Seq reveals novel features of mouse circadian transcriptional regulation. *Elife* 1: e00011

Mi H, Muruganujan A, Thomas PD (2013) PANTHER in 2013: modeling the evolution of gene function, and other gene attributes, in the context of phylogenetic trees. *Nucleic Acids Res* 41: D377-86

Morf J, Rey G, Schneider K, Stratmann M, Fujita J, Naef F, Schibler U (2012) Cold-inducible RNA-binding protein modulates circadian gene expression posttranscriptionally. *Science* 338: 379-83

Nagashima K (2015) Thermoregulation and menstrual cycle. *Temperature (Austin)* 2: 320-321

Neph S, Kuehn MS, Reynolds AP, Haugen E, Thurman RE, Johnson AK, Rynes E, Maurano MT, Vierstra J, Thomas S, Sandstrom R, Humbert R, Stamatoyannopoulos JA (2012) BEDOPS: high-performance genomic feature operations. *Bioinformatics* 28: 1919-20

Ni JZ, Grate L, Donohue JP, Preston C, Nobida N, O'Brien G, Shiue L, Clark TA, Blume JE, Ares M, Jr. (2007) Ultraconserved elements are associated with homeostatic control of splicing regulators by alternative splicing and nonsense-mediated decay. *Genes Dev* 21: 708-18

Palusa SG, Reddy AS (2010) Extensive coupling of alternative splicing of pre-mRNAs of serine/arginine (SR) genes with nonsense-mediated decay. *New Phytol* 185: 83-9

Patro R, Duggal G, Love MI, Irizarry RA, Kingsford C (2017) Salmon provides fast and bias-aware quantification of transcript expression. *Nat Methods* 14: 417-419

Pedregosa F, Varoquaux G, Gramfort A, Michel V, Thirion B, Grisel O, Blondel M, Prettenhofer P, Weiss R, Dubourg V, Vanderplas J, Passos A, Cournapeau D, Brucher M, Perrot M, Duchesnay E (2011) Scikit-learn: Machine Learning in Python. *Journal of Machine Learning Research* 12: 2825-2830

Pollard KS, Hubisz MJ, Rosenbloom KR, Siepel A (2010) Detection of nonneutral substitution rates on mammalian phylogenies. *Genome Res* 20: 110-21

Preussner M, Goldammer G, Neumann A, Haltenhof T, Rautenstrauch P, Muller-McNicoll M, Heyd F (2017) Body Temperature Cycles Control Rhythmic Alternative Splicing in Mammals. *Mol Cell* 67: 433-446.e4

Preussner M, Heyd F (2016) Post-transcriptional control of the mammalian circadian clock: implications for health and disease. *Pflugers Arch* 468: 983-91

Preussner M, Heyd F (2018) Temperature-controlled Rhythmic Gene Expression in Endothermic Mammals: All Diurnal Rhythms are Equal, but Some are Circadian. *Bioessays* 40: e1700216

Preussner M, Wilhelmi I, Schultz AS, Finkernagel F, Michel M, Moroy T, Heyd F (2014) Rhythmic U2af26 alternative splicing controls PERIOD1 stability and the circadian clock in mice. *Mol Cell* 54: 651-62

Quinlan AR, Hall IM (2010) BEDTools: a flexible suite of utilities for comparing genomic features. *Bioinformatics* 26: 841-2

Ran FA, Hsu PD, Wright J, Agarwala V, Scott DA, Zhang F (2013) Genome engineering using the CRISPR-Cas9 system. *Nat Protoc* 8: 2281-308

Rauch HB, Patrick TL, Klusman KM, Battistuzzi FU, Mei W, Brendel VP, Lal SK (2014) Discovery and expression analysis of alternative splicing events conserved among plant SR proteins. *Mol Biol Evol* 31: 605-13

Refinetti R, Menaker M (1992) The circadian rhythm of body temperature. *Physiol Behav* 51: 613-37

Rehwinkel J, Raes J, Izaurralde E (2006) Nonsense-mediated mRNA decay: Target genes and functional diversification of effectors. *Trends Biochem Sci* 31: 639-46

Richardson DN, Rogers MF, Labadorf A, Ben-Hur A, Guo H, Paterson AH, Reddy AS (2011) Comparative analysis of serine/arginine-rich proteins across 27 eukaryotes: insights into sub-family classification and extent of alternative splicing. *PLoS One* 6: e24542

Saini C, Morf J, Stratmann M, Gos P, Schibler U (2012) Simulated body temperature rhythms reveal the phase-shifting behavior and plasticity of mammalian circadian oscillators. *Genes Dev* 26: 567-80

Schlaen RG, Mancini E, Sanchez SE, Perez-Santangelo S, Rugnone ML, Simpson CG, Brown JW, Zhang X, Chernomoretz A, Yanovsky MJ (2015) The spliceosome assembly factor GEMIN2 attenuates the effects of temperature on alternative splicing and circadian rhythms. *Proceedings of the National Academy of Sciences of the United States of America* 112: 9382-7

Shakhmantsir I, Sehgal A (2019) Splicing the Clock to Maintain and Entrain Circadian Rhythms. *J Biol Rhythms* 34: 584-595

Siepel A, Bejerano G, Pedersen JS, Hinrichs AS, Hou M, Rosenbloom K, Clawson H, Spieth J, Hillier LW, Richards S, Weinstock GM, Wilson RK, Gibbs RA, Kent WJ, Miller W, Haussler D (2005) Evolutionarily conserved elements in vertebrate, insect, worm, and yeast genomes. *Genome Res* 15: 1034-50

Staiger D, Brown JW (2013) Alternative splicing at the intersection of biological timing, development, and stress responses. *Plant Cell* 25: 3640-56

Sterne-Weiler T, Weatheritt RJ, Best AJ, Ha KCH, Blencowe BJ (2018) Efficient and Accurate Quantitative Profiling of Alternative Splicing Patterns of Any Complexity on a Laptop. *Mol Cell* 72: 187-200.e6

Sureau A, Gattoni R, Dooghe Y, Stévenin J, Soret J (2001) SC35 autoregulates its expression by promoting splicing events that destabilize its mRNAs. *The EMBO Journal* 20: 1785-1796

Tabrez SS, Sharma RD, Jain V, Siddiqui AA, Mukhopadhyay A (2017) Differential alternative splicing coupled to nonsense-mediated decay of mRNA ensures dietary restriction-induced longevity. *Nature communications* 8: 306

Thomas JD, Polaski JT, Feng Q, De Neef EJ, Hoppe ER, McSharry MV, Pangallo J, Gabel AM, Belleville AE, Watson J, Nkinsi NT, Berger AH, Bradley RK (2020) RNA isoform screens uncover the essentiality and tumor-suppressor activity of ultraconserved poison exons. *Nat Genet* 52: 84-94

Walt Svd, Colbert SC, Varoquaux G (2011) The NumPy Array: A Structure for Efficient Numerical Computation. *Computing in Science & Engineering* 13: 22-30

Wong JJ, Ritchie W, Ebner OA, Selbach M, Wong JW, Huang Y, Gao D, Pinello N, Gonzalez M, Baidya K, Thoeng A, Khoo TL, Bailey CG, Holst J, Rasko JE (2013) Orchestrated intron retention regulates normal granulocyte differentiation. *Cell* 154: 583-95

Figures

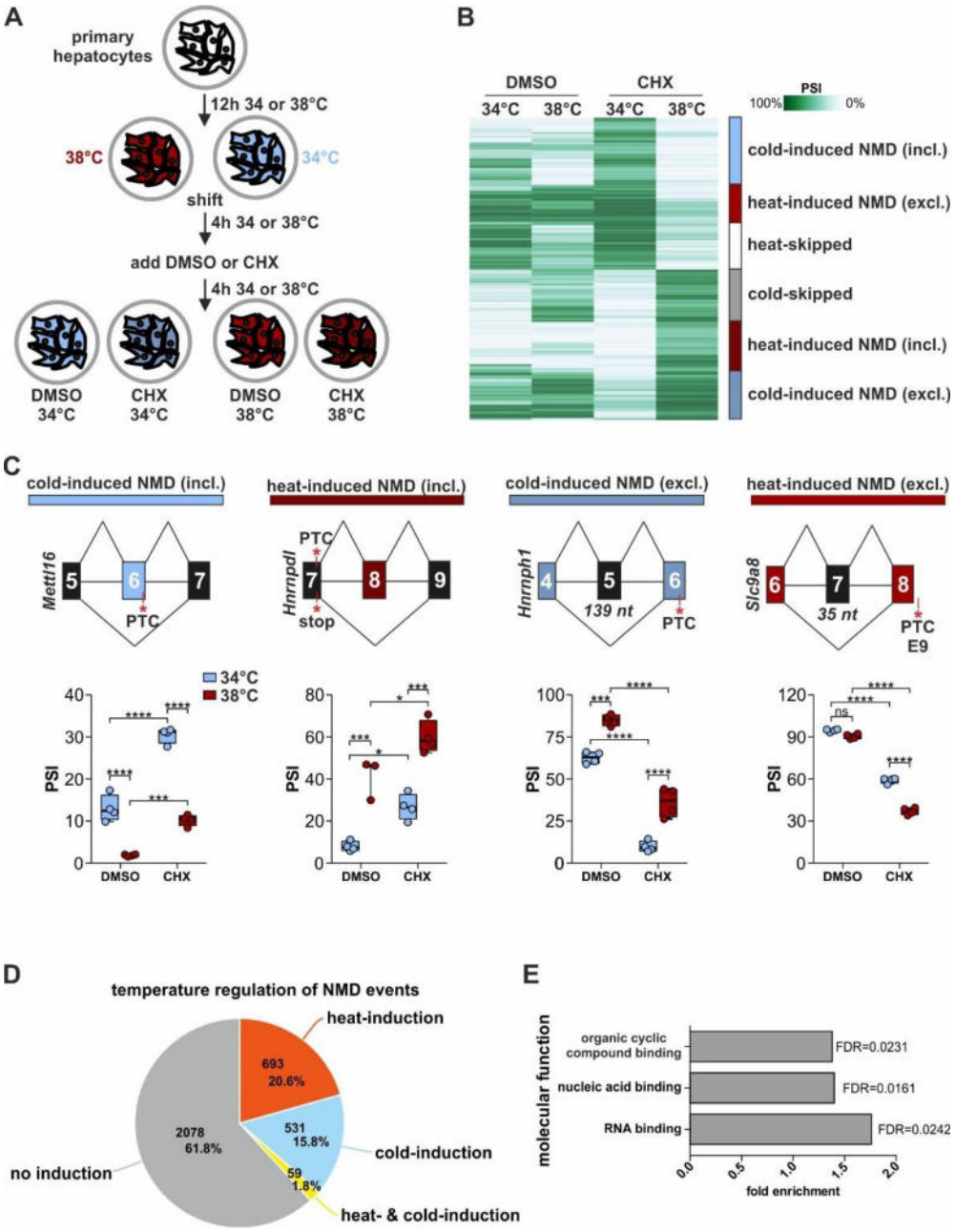

Figure 1. Characterization of temperature-controlled AS-NMD in mammalian cells

(A) Generation of RNA samples from mouse primary hepatocytes for analysis of temperature-dependent AS-NMD.

(B) Automatic cluster-mapping of the temperature-dependent splicing changes in CHX, based on changes in PSI (percent spliced in). Categories (right) were manually assigned. Here the top 1000 events are shown, see also Figure S1B for all events.

(C) Examples for cold-induced (blue) or heat-induced (red) AS-NMD via exon inclusion or exon skipping. In each example, on top a simplified exon-intron structure is given, PTCs and the length of frameshift inducing exons are highlighted. Predicted splicing changes were validated by radioactive RT-PCR with primers binding to the surrounding constitutive exons. Box plots show median PSI of validation PCRs of four different

samples from at least two different mice, whiskers show min to max. Individual data points are shown as circles. Statistical significance was determined by 2-way ANOVA and is indicated by asterisks: adjusted p values: not significant (ns), *p<0.05, ***p<0.001, ****p<0.0001. See Figures S1C and S1E for further examples.
(D) Classification of temperature-dependence in genes with NMD events. Number of genes and percentages are indicated.
(E) GO-term analysis of temperature-controlled AS-NMD genes. All expressed genes (mean tpm > 0) served as background.
See also Figure S1.

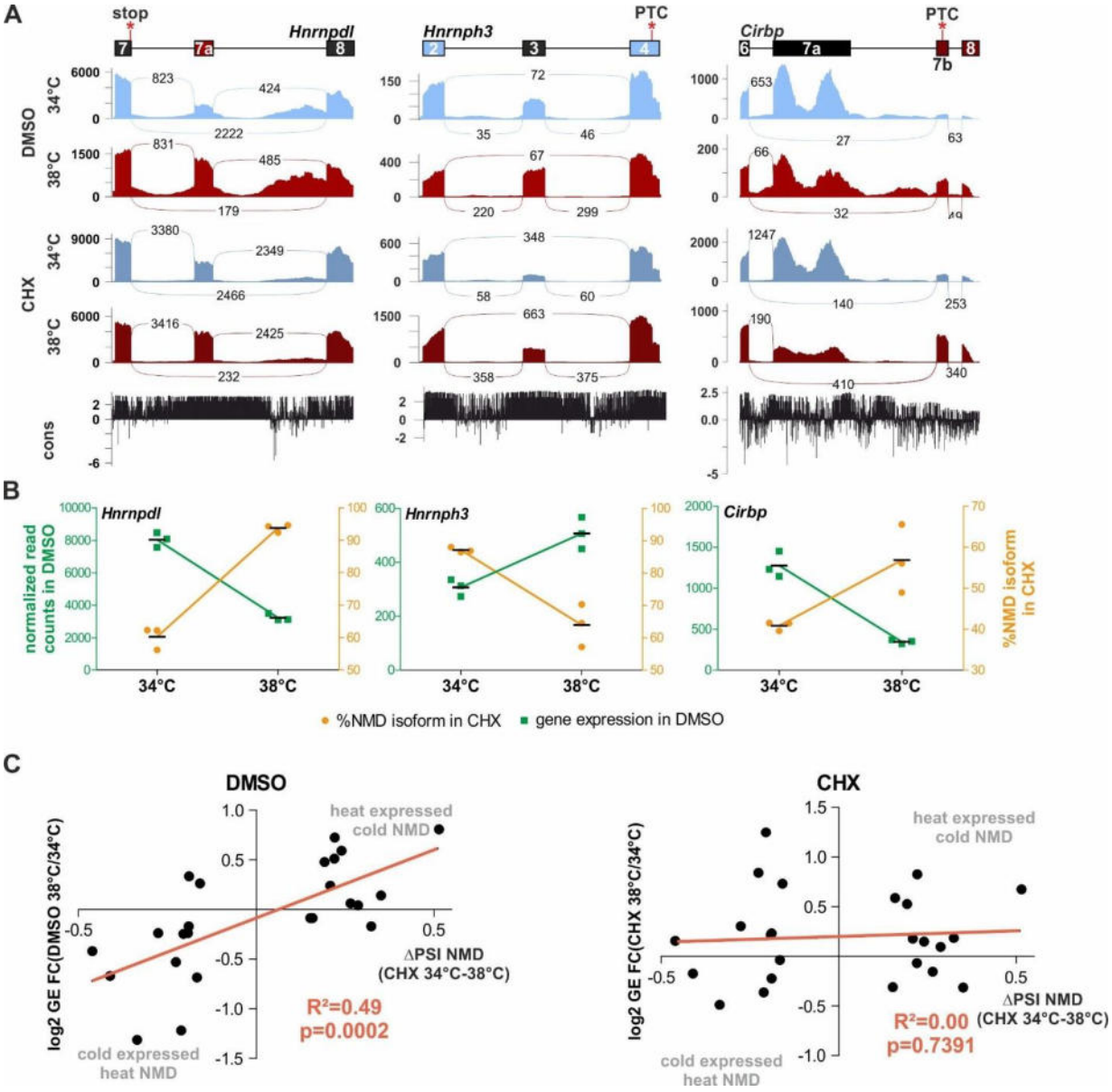

Figure 2. Temperature-dependent AS-NMD events globally regulate GE

(A) Temperature-dependent AS-NMD events in *Hnrnpdl* (left, see also Figure 1C), *Hnrnph3* (middle) and *Cirbp* (right). For each target, on top a simplified exon-intron structure is given and below Sashimi plots show the distribution of raw sequencing reads. Exon-Exon junction reads are indicated by the numbers connecting the exons. Below, sequence conservation across placental species is indicated. *Hnrnpdl* exhibits a heat-included exon that leads to a PTC, *Hnrnph3* a cold-skipped exon that leads to a frameshift, and in *Cirbp*, heat leads to inclusion of an alternative transcript end, which leads to formation of a PTC.

(B) For each gene from A, the triplicate normalized read counts in DMSO (left y-axis, green) and the percentage of the NMD isoform in CHX (right y-axis, orange) are plotted at the two temperatures.

(C) Correlation of NMD isoform inclusion and GE levels for all RBPs with temperature-dependent AS-NMD skipped exon events. Shown are the log2 fold change (FC) in GE versus the ΔPSI of the NMD isoform between the CHX samples. Left shows the GE change between the DMSO samples and right between the CHX samples. R^2 and P (deviation from zero slope) are indicated. N=24.

See also Figure S2.

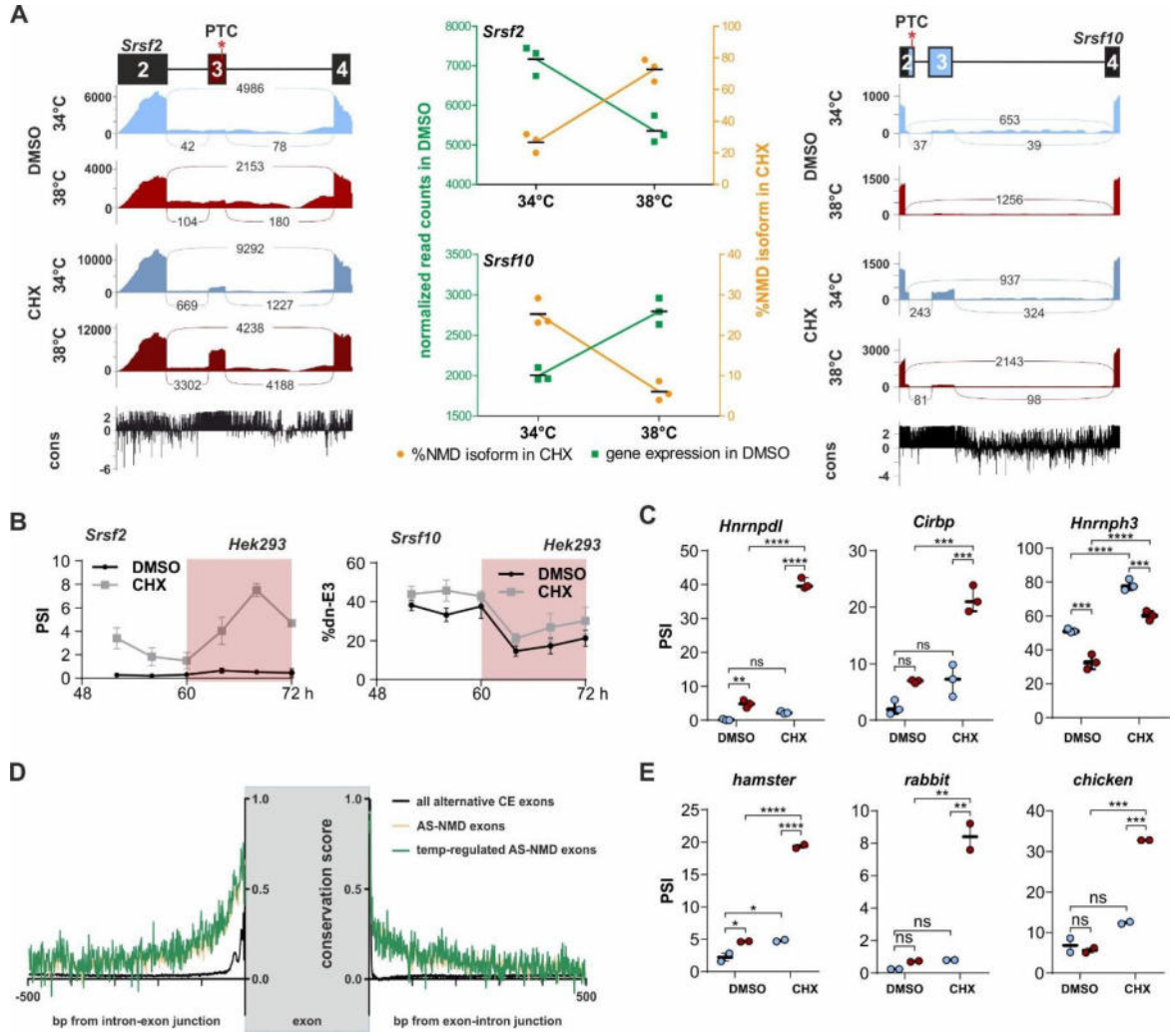

Figure 3. Temperature-dependent AS-NMD is evolutionarily conserved

(A) SR protein specific temperature-dependent AS-NMD. Sashimi plots are shown for heat-induced NMD exon inclusion for *Srsf2* (left) and cold-induced NMD isoform formation for *Srsf10* (right). In the center, quantification of GE and AS (as in Figure 2B).

(B) NMD exon inclusion for *Srsf2* (left) and *Srsf10* (right) in a 24h temperature-rhythm in human cells. Hek293 cells were pre-entrained with square-wave temperature cycles (12h 34°C/ 12h 38°C) for 48h. For the last 24h cells were treated with DMSO or CHX every 4h and harvested after 4h and analyzed by splicing sensitive RT-PCR (n=3, mean ± SD). White area: 34°C; Red area: 38°C. In Hek293 cells, inclusion of *Srsf10* exon 3 is coupled to polyadenylation making it a weak NMD target.

(C) AS-NMD of human targets at 34°C (blue) and 38°C (red) was investigated after a square-wave temperature regime (see B). RNAs were harvested after 56 and 68 hours, respectively. Statistical significance was determined by 2-way ANOVA and is indicated by asterisks: adjusted p values: not significant (ns), **p<0.01, ***p<0.001, ****p<0.0001.

(D) Intron conservation of alternative cassette exons. Shown are average placental conservation scores introns surrounding all alternative exons (black, N=46,901), AS-NMD exons (yellow, N=453) and temperature-regulated AS-NMD exons (green, N=139).

(E) Quantification of *Srsf2* AS-NMD in hamster, rabbit and chicken cells (n=2, mean ± SD). Statistical significance was determined by 2-way ANOVA, asterisks as in D, *p<0.05.

See also Figure S3.

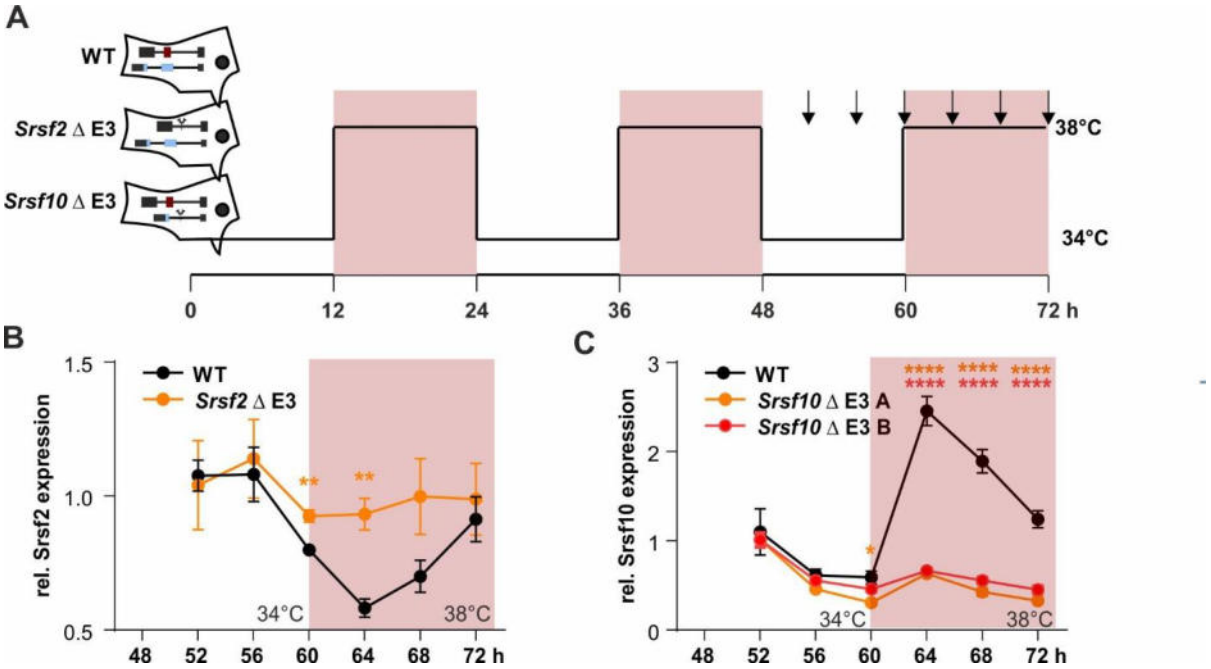

Figure 4. Temperature-dependent AS-NMD is necessary for rhythmic GE

(A) WT Hek293 and cell lines lacking either *Srsf2* or *Srsf10* exon 3 (ΔNMD Exon) through CRISPR/Cas9-mediated genome editing (see also Figure S4) where temperature entrained through 3 consecutive days of square-wave temperature rhythm (12 hours at 34°C and 38°C, respectively). Time points for harvest are indicated by arrows.

(B, C) Rhythmic *Srsf2* (B) and *Srsf10* (C) productive mRNA levels (relative to *Gapdh*) were analyzed by RT-qPCR. For each clone, expression is normalized to time point 52h, (B) n = 3, (C) n =4, mean ± SEM. For *Srsf10* two independently generated clones were investigated (ΔE3 A and B). Statistical significance was determined by unpaired t-test and is indicated by asterisks: p values: *p<0.05, **p<0.01, ****p<0.0001. See also Figure S4.

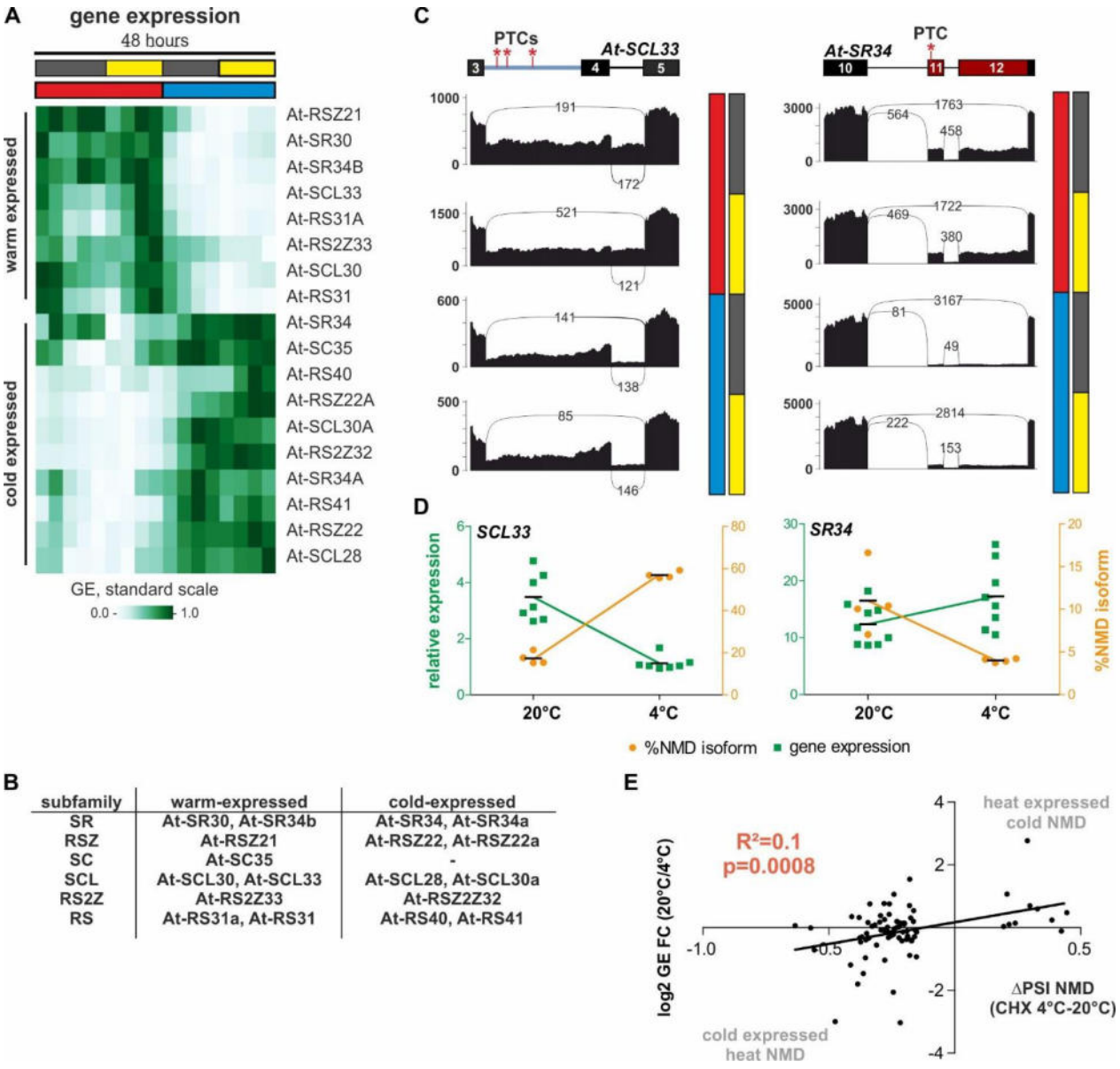

subfamily	warm-expressed	cold-expressed
SR	At-SR30, At-SR34b	At-SR34, At-SR34a
RSZ	At-RSZ21	At-RSZ22, At-RSZ22a
SC	At-SC35	-
SCL	At-SCL30, At-SCL33	At-SCL28, At-SCL30a
RS2Z	At-RS2Z33	At-RSZ2Z32
RS	At-RS31a, At-RS31	At-RS40, At-RS41

Figure 5. Temperature-dependent AS-NMD of SR proteins is conserved in plants

(A) Normalized GE values of plant SR proteins in a 48-hour time course. In the first day, plants were kept at 20°C (red) and shifted to 4°C (blue) for the second day. Plants were under a 12-hour dark/light regimen (gray/yellow bars). Warm- and cold-expressed genes are indicated.

(B) *A. thaliana* SR proteins divided in their subfamilies and classified as warm- or cold-expressed.

(C) Sashimi plots as shown in Figure 2A (without conservation score) for NMD-inducing AS events upon cold (At-SCL33, left) or warm temperature (At-SR34, right). Data shown represent, from top to bottom, warm-dark, warm-light, cold-dark and cold-light conditions as indicated on the right of the plots.

(D) For validation *A. thaliana* were incubated for 3 days either at 20°C or 4°C and RNA was investigated for gene expression (green, left y-axis) and NMD isoform formation (orange, right y-axis). Gene expression of At-SCL33 (left) or At-SR34 (right) is shown relative to Ipp2.

(E) Correlation of NMD isoform inclusion and GE levels for temperature-dependent AS-NMD skipped exon events. Shown are the log2 fold change (FC) in GE versus the ΔPSI of the NMD isoform between the CHX samples. R^2 and P(deviation from zero slope) are indicated. N=80 (see main text for details).

See also Figure S5.

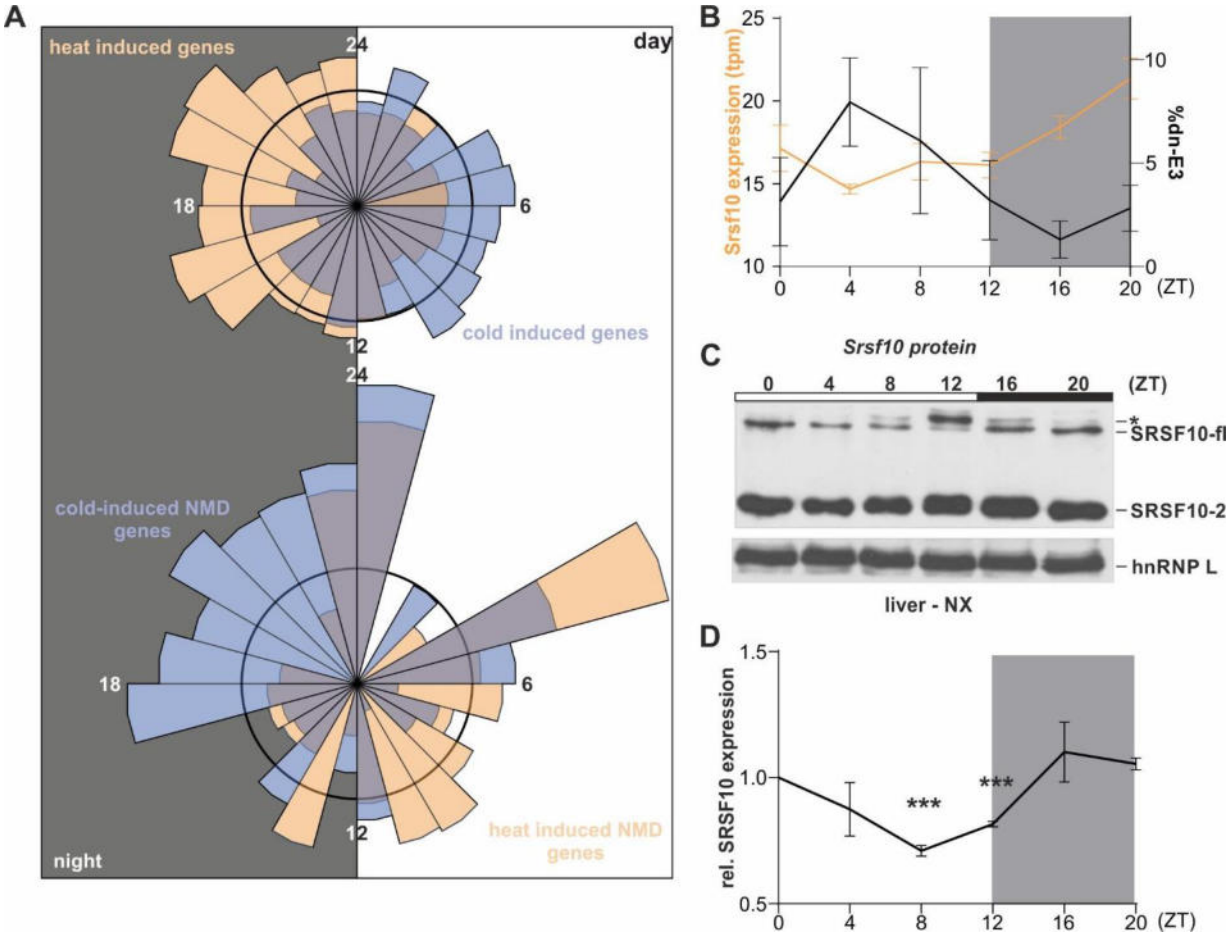

Figure 6. AS-NMD generates GE rhythms *in vivo*

(A) Top: Rose plot visualizing the acrophases (based on rhythmic genes in the liver transcriptome from (Atger et al., 2015)) of genes exhibiting heat-induced (orange, n=797) and cold-induced (blue, n=828) upregulation of GE in mouse hepatocytes, respectively. Bottom: Acrophases of genes with cold-induced (blue, n=55) and heat-induced (orange, n=47) skipped exon NMD events, respectively. Numbers indicate respective ZT, with the left half representing night (at which mice are active and have an elevated body temperature) and the right half representing day (at which mice are asleep with lower body temperature). The black circles represent expected normal distribution if data would be randomly sampled.

(B) Correlation of rhythmic *Srsf10* expression (orange, left y-axis) and exon 3 inclusion (black, right y-axis) in mouse liver samples from the indicated ZTs (n=4, mean +/- SEM). Quantifications were obtained by RNA-seq analysis of datasets from (Atger et al., 2015).

(C) Representative Western blot of SRSF10 protein levels from mouse liver nuclear extracts (NX) from different ZTs. The different SRSF10 variants are highlighted on the right. hnRNP L was used as a loading control. The asterisks could represent hyperphosphorylated SRSF10-fl through higher CLK activity during the day.

(D) Quantification of SRSF10-fl + SRSF10-2 relative to ZT0 and hnRNP L (mean of at least 3 mice ± SEM). Student's unpaired t test-derived p values ***p<0.001.

See also Figure S6.

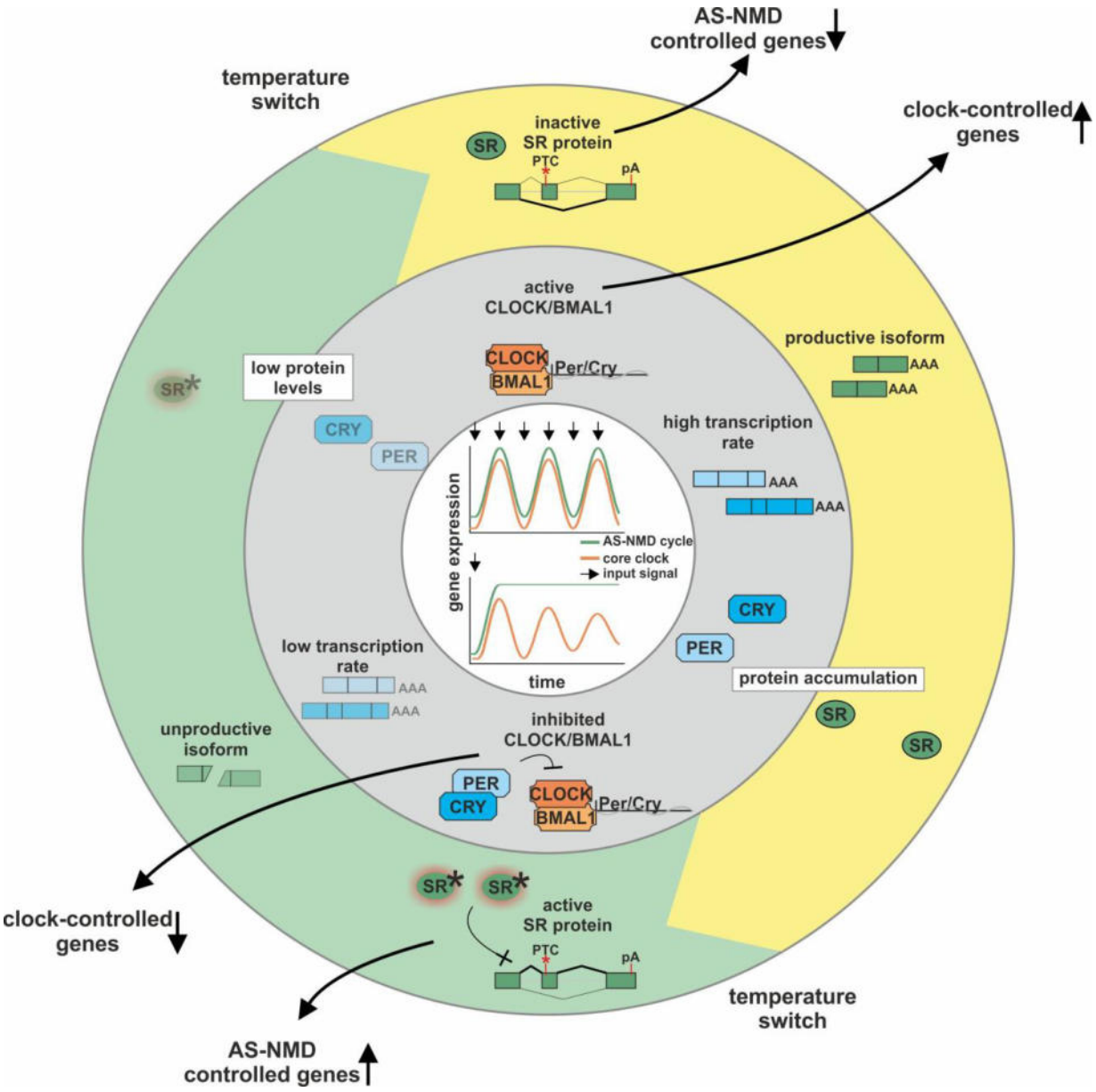

Figure 7. A model of two independent cycles generating rhythmic GE

Inner ring (grey): Classical transcription-translation feedback loop or the central circadian clock, involving the transcription activator CLOCK and BMAL1 and the transcription targets/repressors *Period* (Per) and *Cryptochrome* (Cry). Outer ring (green/yellow): Model of rhythmic GE driven via AS-NMD. AS regulates the formation of productive stable or unproductive instable isoforms, thereby regulating the abundance of SR protein mRNA and protein. An additional regulatory layer is achieved through temperature-mediated control of SR protein activity (active SR proteins are indicated by an asterisks), resulting in rhythmic GE of SR proteins themselves and output target genes. GE in response to continuous (top) or single (bottom) input signal (indicated by arrows) is shown in the center.

Supplemental information

Figures S1-S6

Table S1. RNA Sequencing

Table S2. Primer sequences, Related to STAR methods

Neumann et al., Supplemental figures

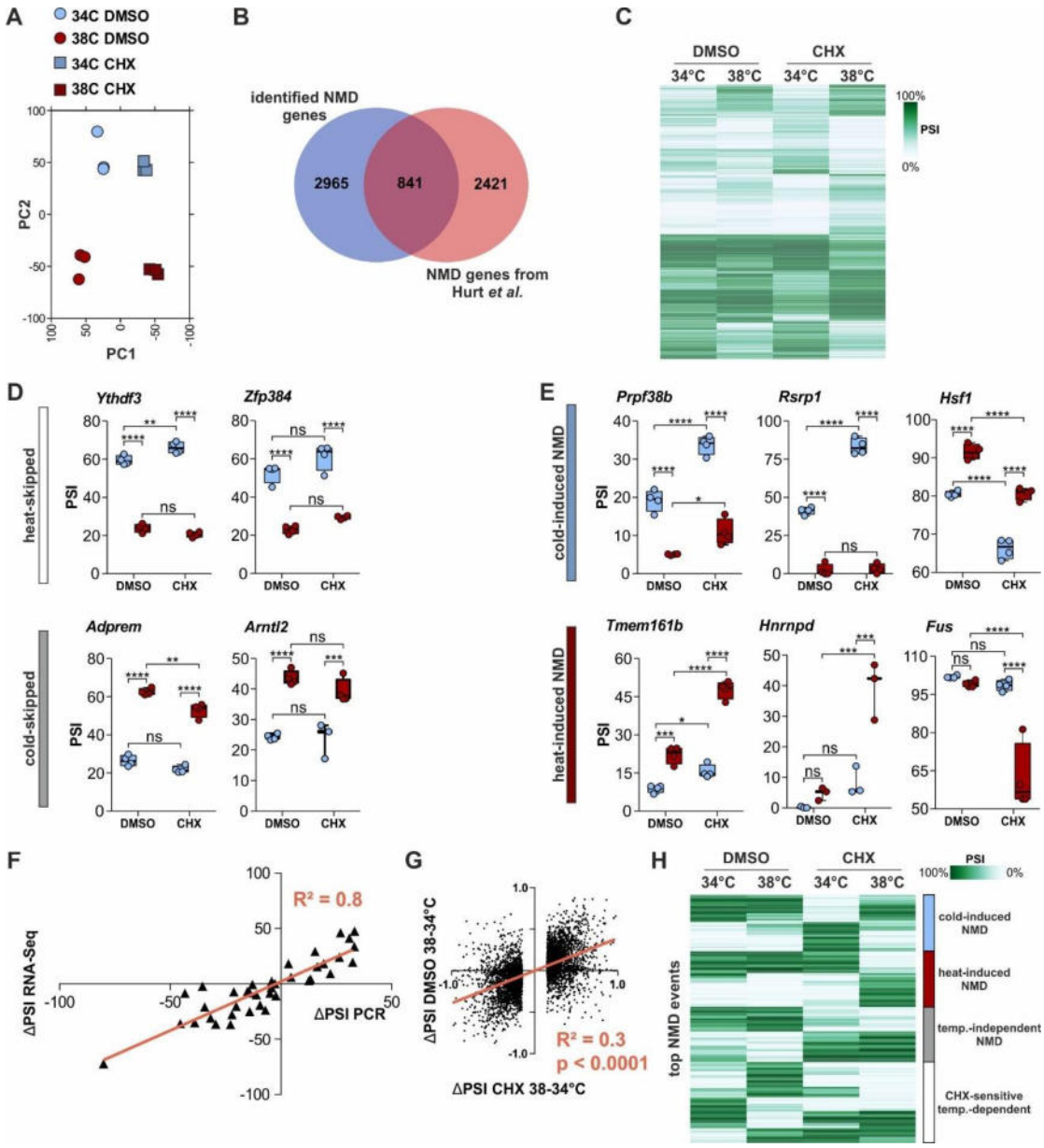

Figure S1. Validation of temperature-dependent AS in mammalian cells

(A) Principle component analysis of the investigated triplicate samples by RNA sequencing.

(B) Overlap of genes with NMD events identified in our study in primary mouse hepatocytes (34 and 38°C) and by Hurt et al., 2013 in embryonic stem cells (37°C).

(C) Automatic cluster-mapping of temperature-dependent splicing changes in CHX, based on PSI (percent spliced in). All events with |ΔPSI|>0.15 and p>0.85 between CHX 34 and 38°C are shown. N=4740.

(D) Examples for heat-skipped (white) or cold-skipped (grey) splicing events. Analysis as in Figure 1C. Note that these splicing events are barely affected by CHX.

(E) Further examples for cold-induced (blue) or heat-induced (red) AS-NMD events. Analysis as in Figure 1C.

(F) Comparison of temperature-regulated AS events predicted by Whippet RNA-Seq analysis and validated by RT-PCR from independent samples. The line depicts linear regression, goodness of fit is represented by R^2.
(G) Comparison of splicing changes in CHX (x-axis) and DMSO (y-axis) for all events presented in S1B. The line depicts linear regression, goodness of fit is represented by R^2, N=4740. The p value represents statistical probability of the slope being different from 0. Splicing changes in DMSO and CHX have the same directionality but ΔPSI values are generally larger in CHX.
(H) Temperature dependence of the strongest NMD events (top 500, largest ΔPSI in either 34 or 38°C comparison of DMSO vs CHX). Categories (right) were manually assigned. We assign four categories: (I) cold-induced NMD, (II) heat-induced NMD, (III) temperature independent NMD, and (IV) CHX-sensitive temperature-dependent splicing events. The generation of these isoforms could depend on *de novo* protein synthesis.

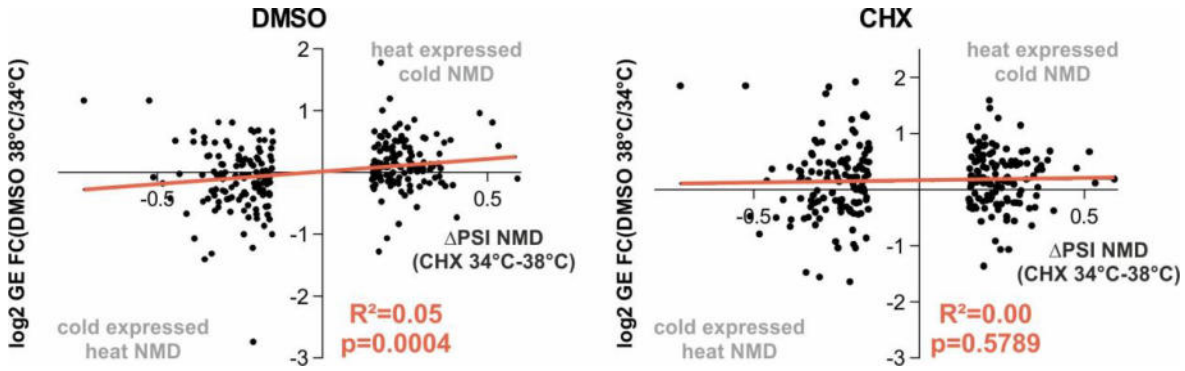

Figure S2. Temperature-dependent AS-NMD events globally regulate GE

Global correlation of NMD isoform inclusion and GE levels for all genes with temperature-dependent AS-NMD skipped exon events. Shown are the log2 fold change (FC) in GE versus the ΔPSI of the NMD isoform between the CHX samples. Left shows the GE change between the DMSO samples and right the between the CHX samples at the two temperatures. R^2 and P (deviation from zero slope) are indicated, N=254.

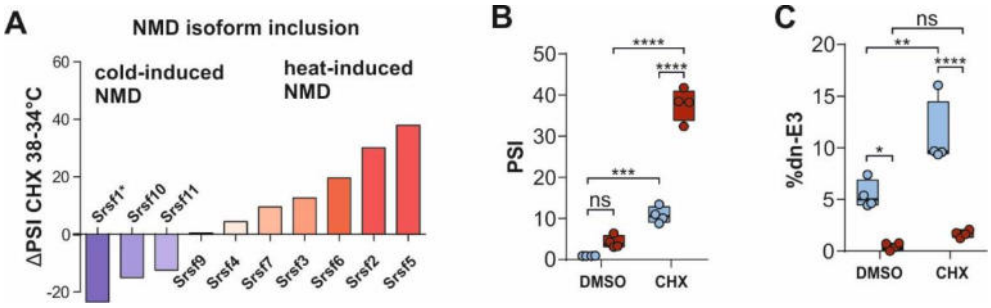

Figure S3. Temperature-dependent AS-NMD is evolutionary conserved

(A) Comparing temperature-dependent AS-NMD (ΔPSI of 38°C-34°C in CHX) of SR proteins in primary mouse hepatocytes. The NMD event in *Srsf1* (*) escaped the computational analysis; data are derived from radioactive RT-PCR.

(B) Validation of *Srsf2* temperature-dependent AS-NMD by radioactive RT-PCR as described in Figure 1C. Statistical significance was determined by 2-way ANOVA and is indicated by asterisks: adjusted p values: not significant (ns), ***p<0.001, ****p<0.0001.

(C) Validation of *Srsf10* temperature-dependent AS-NMD by radioactive RT-PCR as described in A. Asterisks as in B, *p<0.05.

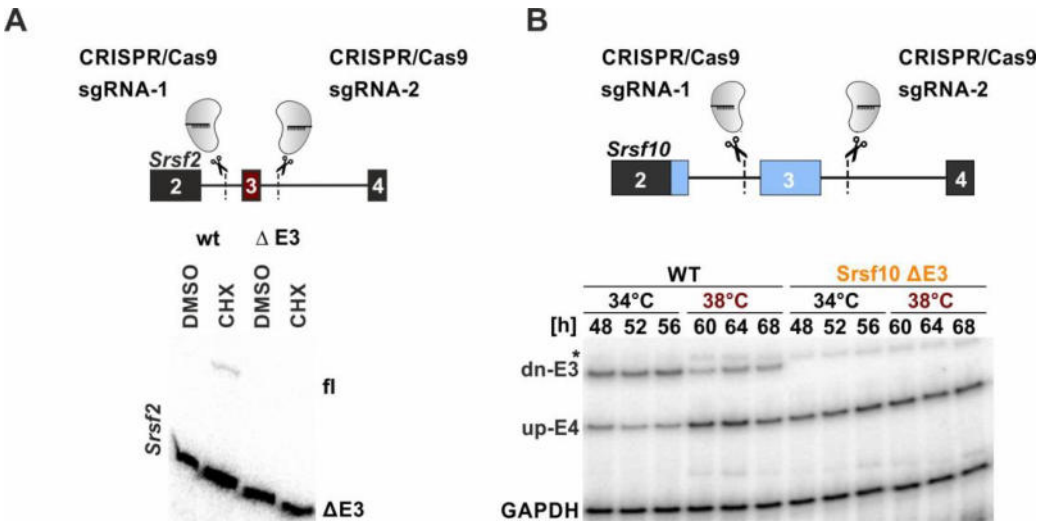

Figure S4. Temperature-dependent AS-NMD is necessary for rhythmic GE

(A, B) CRISPR/Cas9 strategy for cell lines lacking NMD exons for *Srsf2* (A) and *Srsf10* (B). Lack of NMD exons in clonal *Srsf2* CRISPR/Cas9-edited cell lines was confirmed by splicing sensitive RT-PCR (bottom). WT and mutant cell lines were treated with DMSO or CHX at 38°C and inclusion of the NMD isoform was investigated by splicing sensitive RT-PCR (A). Investigation of *Srsf10* dn-E3 splicing in samples from Figure 4C. AS was analyzed by RT-PCR. A *Gapdh* PCR was performed simultaneously and served as a loading control. A representative gel image is shown. The asterisk indicates an unspecific product.

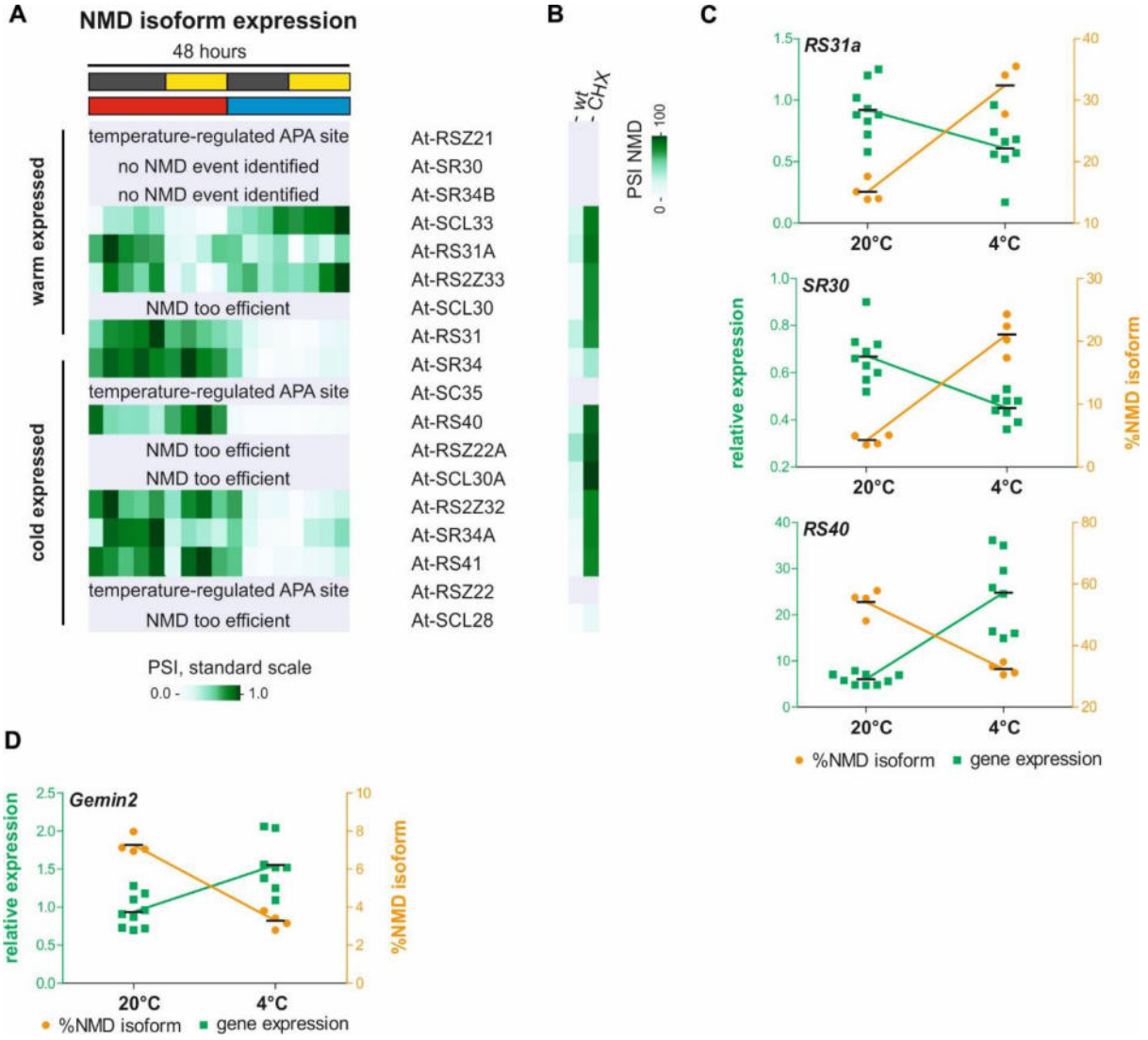

Figure S5. Temperature-dependent AS-NMD of SR proteins is conserved in plants

(A) Normalized NMD isoform expression of plant SR proteins as in Figure 5A. In this dataset, without inhibition of the NMD pathway, the identification of NMD isoforms is likely incomplete (compare to B). In three cases, a clear temperature-regulated alternative poly-adenylation (APA) event occurred but was not quantified (also indicating a post-transcriptional origin of temperature-dependent GE). In two cases, no NMD event could be identified. Four times NMD seemed to be too efficient, as no events could be identified without CHX treatment

(B) AS-NMD isoform inclusion in wt or CHX-treated plants for the same genes as in A. Here the amount of the respective isoforms was compared in control and CHX treated samples (based on another RNA-Seq dataset (Drechsel et al., 2013), see Table S1). Note that most temperature depend isoforms from A are indeed stabilized upon CHX treatment.

(C) Validation RT-PCRs and qPCRs of NMD events in further plant SR proteins as shown in Figure 5D. For each case, NMD isoform inclusion correlates with lower GE.

(D) Validation of an AS-NMD event in Gemin2, in which cold-induced inclusion of the NMD isoform correlates with lower GE.

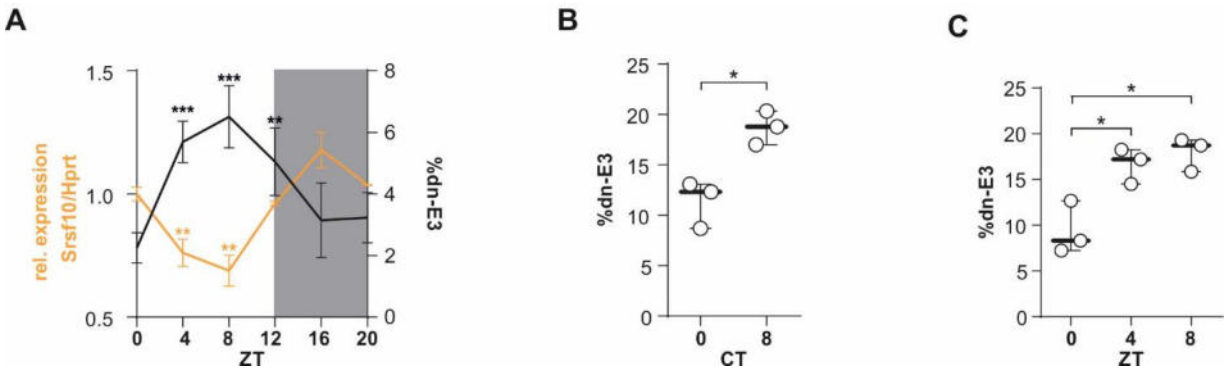

Figure S6. AS-NMD generates GE rhythms *in vivo*

(A) Correlation of rhythmic productive *Srsf10* mRNA expression (orange, left y-axis) and exon 3 inclusion (black, right y-axis) in mouse cerebellum samples from the indicated ZTs. Splicing was analyzed using radioactive RT-PCR of at least 3 mice per time point. Expression was determined by RT-qPCR and is shown relative to *Hprt* and ZT0 (mean of at least 3 mice ± SEM). Student's unpaired t test-derived p values **p<0.01 indicate difference from ZT0.

(B) Rhythmic *Srsf10* AS persists in constant darkness. Mice were kept in constant darkness for 24h and sacrificed at the indicated circadian times (CTs) of the following subjective day. RT-PCR analysis as in A (n=3, mean ± SD). Student's unpaired t test-derived p values *p<0.05.

(C) Entrained *Srsf10* AS. Mice were 8-hour phase delayed and on the 4th day sacrificed at the indicated ZTs. RT-PCR analysis as in A (n=3, mean ± SD). Student's unpaired t test-derived p values *p<0.05.

5.4 Publication 4

***Meinke, S.**, Goldammer, G., Weber, A.I., Tarabykin, V., Neumann, A., Preußner, M., Heyd, F. (2020). Srsf10 and the minor spliceosome control tissue-specific and dynamic SR protein expression. Elife. 2020 Apr 27;9. Doi: 10.7554/eLife.56075*

https://doi.org/10.7554/eLife.56075

SHORT REPORT

Srsf10 and the minor spliceosome control tissue-specific and dynamic SR protein expression

Stefan Meinke[1], Gesine Goldammer[1], A Ioana Weber[1,2], Victor Tarabykin[2], Alexander Neumann[1†], Marco Preussner[1]*, Florian Heyd[1]*

[1]Freie Universität Berlin, Institute of Chemistry and Biochemistry, Laboratory of RNA Biochemistry, Berlin, Germany; [2]Institute of Cell Biology and Neurobiology, Charité-Universitätsmedizin Berlin, corporate member of Freie Universität Berlin, Humboldt-Universität zu Berlin, and Berlin Institute of Health, Berlin, Germany

Abstract Minor and major spliceosomes control splicing of distinct intron types and are thought to act largely independent of one another. SR proteins are essential splicing regulators mostly connected to the major spliceosome. Here, we show that *Srsf10* expression is controlled through an autoregulated minor intron, tightly correlating Srsf10 with minor spliceosome abundance across different tissues and differentiation stages in mammals. Surprisingly, all other SR proteins also correlate with the minor spliceosome and *Srsf10*, and abolishing *Srsf10* autoregulation by Crispr/Cas9-mediated deletion of the autoregulatory exon induces expression of all SR proteins in a human cell line. Our data thus reveal extensive crosstalk and a global impact of the minor spliceosome on major intron splicing.

***For correspondence:**
mpreussner@zedat.fu-berlin.de (MP);
florian.heyd@fu-berlin.de (FH)

Present address: †Omiqa Corporation, c/o Freie Universität Berlin, Altensteinstraße, Germany

Competing interests: The authors declare that no competing interests exist.

Funding: See page 13

Received: 16 February 2020
Accepted: 24 April 2020
Published: 27 April 2020

Reviewing editor: Timothy W Nilsen, Case Western Reserve University, United States

Introduction

Alternative splicing (AS) is a major mechanism that controls gene expression (GE) and expands the proteome diversity generated from a limited number of primary transcripts (***Nilsen and Graveley, 2010***). Splicing is carried out by a multi-megadalton molecular machinery called the spliceosome of which two distinct complexes exist. The more abundant major spliceosome that consists of the U1, U2, U4, U5, U6 small nuclear ribonucleoprotein particles (snRNPs) and multiple non-snRNP splicing factors. Additionally, the cells of most eukaryotes contain the minor spliceosome, which is composed of the minor-specific snRNPs U11, U12, U4atac, U6atac, and the shared U5 snRNP. While the major spliceosome catalyzes splicing of around 99.5% of all introns, mainly so-called U2-type introns with the characteristic GT-AG splice sites, the minor spliceosome recognizes introns of the U12-type containing non-consensus AT-AC splice sites and distinct branch point and polypyrimidine sequences (***Jackson, 1991***; ***Turunen et al., 2013***). However, despite its low abundance, the minor spliceosome plays a fundamental role in ontogenesis, as deficiencies in minor spliceosome activity or minor intron splicing are lethal or result in developmental defects and disorders (***Doggett et al., 2018***; ***Verma et al., 2018***).

AS is highly regulated by *cis*-acting splicing enhancer and silencer elements, which are recognized by various RNA binding proteins, such as SR proteins and heterogeneous nuclear ribonucleoproteins (***Hastings et al., 2001***). The protein family of SR proteins, with 13 canonical members in humans, is characterized by an arginine and serine rich domain (RS domain) (***Manley and Krainer, 2010***). Aside from their role in mRNA nuclear export and GE they are essential regulators of AS (***Long and Caceres, 2009***). Every SR protein contains ultraconserved elements in alternative exons that control the presence of premature translation termination codons (PTC). This allows them to regulate their own abundance through nonsense-mediated decay (NMD) (***Lareau et al., 2007***). While many SR

proteins and RBPs use autoregulation to maintain a stable expression level (**Müller-McNicoll et al., 2019**), their expression level changes in a tissue-specific manner (**Wang et al., 2008**; **Olthof et al., 2019**). Therefore, mechanisms aside from autoregulation are most likely employed to control SR protein levels under different conditions, for instance in different tissues or during differentiation. However, the mechanisms that coordinately regulate SR protein expression levels remain elusive.

SRSF10 is a unique SR protein, as it activates splicing in its phosphorylated state but becomes a general splicing inhibitor upon dephosphorylation (**Feng et al., 2008**; **Zhou et al., 2014**). We used SRSF10 as a case study of how tissue-specific differences in SR protein levels can be achieved by employing an autoregulatory feedback loop. We show that Srsf10 recognizes a highly conserved splicing enhancer element within its own pre-mRNA, which results in the production of a non-protein coding mRNA isoform and thereby the regulation of its own expression level. An additional layer of *Srsf10* regulation is added by the presence of competing major and minor splice sites which control this autoregulatory AS event. The minor splice site leads to the formation of the protein-coding mRNA, whereas splicing mediated by the major spliceosome leads to the non-protein-coding mRNA. Consequently, *Srsf10* levels correlate with the level of the minor spliceosome in a tissue- and developmental stage-specific manner. Surprisingly, we also found that the expression levels of most other SR proteins correlate with *Srsf10* expression. This is directly mediated through the levels of *Srsf10* and the competition between major and minor splice sites, as CRISPR/Cas9-mediated removal of the autoregulatory exon 3 of *Srsf10* increases not only the expression of *Srsf10*, but also the expression of the other SR proteins. These data connect the minor spliceosome with *Srsf10* and SR protein expression in a tissue- and differentiation state-specific manner. We thus reveal a mechanism that coordinately controls SR protein expression in different cellular conditions and that connects the minor spliceosome with global (alternative) splicing of major introns.

Results and discussion

Srsf10 autoregulates its own splicing and expression

Autoregulation has been described for many RBPs including most SR proteins (**Lejeune et al., 2001**; **Sureau, 2001**), but not for Srsf10. *Srsf10* represents a particularly interesting example as its conserved region contains two competing 5' splice sites in exon 2 (E2), which are recognized by either the minor or the major spliceosome. The upstream (up) minor splice site is coupled to E4 inclusion and production of a protein coding mRNA, while use of the downstream (dn) major splice site is coupled to E3 inclusion, the presence of a PTC and the use of an alternative polyadenylation site in E3 (**Figure 1A**). The dn-E3 variant is not a canonical NMD target, as the stop codon in E2 is less than 50 nucleotides upstream of the E2/3 junction (**Nagy and Maquat, 1998**) and could thus encode for a hypothetical short protein (Srsf10-s, see below). To investigate whether AS of the competing minor and major splice site in exon 2 of *Srsf10* depends on an autoregulatory feedback loop, we generated an *Srsf10* minigene containing mouse exons 2 to 4 (**Figure 1B**, top). We transfected this minigene into human HeLa cells and investigated AS after knocking down the endogenous *SRSF10*. These experiments revealed strong autoregulation, as *SRSF10* knockdown decreased the dn-E3 isoform and increased the up-E4 product and retention of intron 2 (IR, **Figure 1B**, bottom). We confirmed the knockdown of *SRSF10* (**Figure 1—figure supplement 1A and B**) and observed a reduced E3/E4 ratio for endogenous *SRSF10* mRNA (**Figure 1—figure supplement 1B**), consistent with SRSF10 activating E3 inclusion.

AS of *Srsf10* results in three possible protein isoforms: SRSF10-fl (inclusion of exon 7a), SRSF10-2 (inclusion of exon 7b, see **Figure 1A**), and a hypothetical protein resulting from exon 3 inclusion (stop codon within the dn-E2 sequence, see **Figure 1A**). To investigate the activity of these protein isoforms in regulating AS, we performed rescue experiments with GFP-tagged Srsf10 mouse variants (not targeted by the human-specific siRNA). A Western blot against Srsf10 shows expression of GFP-Srsf10-fl and GFP-Srsf10-2 close to endogenous levels, while GFP-Srsf10-s was not detectable (**Figure 1—figure supplement 1C**, top). Consistently, Srsf10-fl and Srsf10-2 clearly rescue exon 3 mis-splicing caused by the knockdown of endogenous *SRSF10*, while transfecting Srsf10-s has no effect on *Srsf10* AS (**Figure 1C**). We obtained the same result when overexpressing the different Srsf10 variants with no knockdown of the endogenous protein, confirming Srsf10-fl and Srsf10-2 as activators of exon 3 inclusion and Srsf10-s as a barely expressed protein (**Figure 1—figure supplement 1C**).

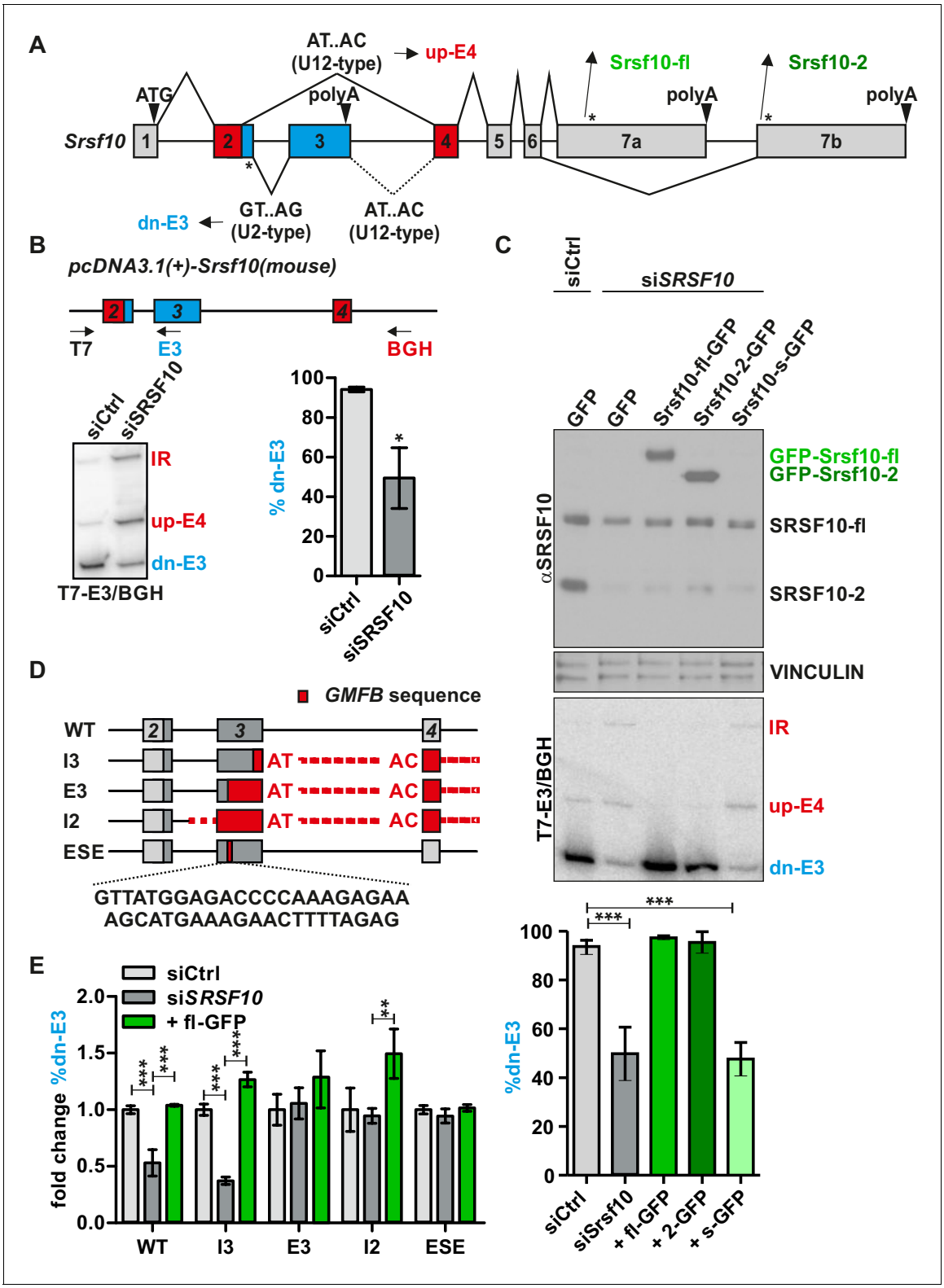

Figure 1. Srsf10 autoregulates its own splicing through a conserved enhancer in exon 3. (**A**) Schematic of the exon/intron structure of Srsf10. Usage of the downstream (dn) major splice site in Srsf10 exon 2 (GT.AG, U2-type) leads to exon 3 inclusion and a non-protein coding isoform, while usage of the upstream minor splice site (AT.AC, U12-type) results in exon 4 inclusion. A minor 5' splice site in exon 3 is present but not used in the endogenous context (dotted lines). * indicate stop codons. (**B**) Srsf10 minigene splicing upon siRNA-mediated knockdown of endogenous Srsf10. Top: exon/intron

Figure 1 continued on next page

Figure 1 continued

structure of the Srsf10 minigene reporter containing mouse exons 2 to 4 (and complete intervening introns) with indicated primer binding sites (arrows). HeLa cells were transfected with control siRNA (siCtrl) or against human Srsf10 (siSrsf10), incubated for 24 hr followed by minigene transfection. After 48 hr splicing was analyzed with the indicated primers. Bottom: exemplary gel and quantification of the dn-E3 isoform (n = 5, mean ± SD). (**C**) Knockdown and rescue of SRSF10. Top: Western Blot of SRSF10 after siRNA-mediated knockdown and transfection with overexpression vectors for the different GFP-tagged Srsf10 isoforms. VINCULIN was used as loading control. Middle: Exemplary gel of Srsf10 minigene splicing upon knockdown and rescue. Bottom: Quantification of the dn-E3 isoform (n ≥ 3, mean ± SD). (**D**) Exon/intron structure of the Srsf10 minigenes used for mutational analysis. Exon and intron sequences were replaced by sequences containing a minor intron from glia maturation factor beta (Gmfb exons 4 to 5 including the minor intron 4, marked in red). Below the sequence of the identified ESE is shown. (**E**) Quantification of Srsf10 minigene splicing upon knockdown and rescue. HeLa cells were transfected with the mutated minigenes (**D**) and analyzed as in (**B**). Splicing of mutants is shown relative to the wt from (**B**) and for each mutant relative to the Ctrl siRNA (n = 5, mean ± SD). Student's t test-derived p values *p<0.05, **p<0.01, ***p<0.001.
The online version of this article includes the following figure supplement(s) for figure 1:

Figure supplement 1. Srsf10 autoregulates its own splicing.
Figure supplement 2. Srsf10 autoregulates its own splicing through a conserved enhancer in exon 3.
Figure supplement 3. Alignment of the 5' sequence of Srsf10 exon 3, which includes the identified ESE region (marked in red), showing high conservation across 7 mammals.

Since the presence of Srsf10-s is hardly detectable, even with a stabilizing GFP tag, we assume that this protein variant is highly instable and does not have a biological function. To compare the activities of Srsf10-fl and Srsf10-2, we performed titration experiments. This demonstrated highly sensitive *Srsf10* autoregulation, with Srsf10-fl, despite its lower expression levels, being a more potent activator of E3 inclusion than Srsf10-2 (***Figure 1—figure supplement 1D***). These data identify Srsf10 as an activator of the major intron between exons 2 and 3 and suggest that Srsf10 autoregulates its own expression level via a negative feedback loop, as higher Srsf10 levels result in the formation of the non-protein-coding dn-E3 isoform.

To identify the cis-regulatory element required for autoregulation, we used systematic mutational analysis of the *Srsf10* minigene (***Figure 1D***, ***Figure 1—figure supplement 2, A–D***). First, we replaced sequences downstream of exon 3 by human Gmfb sequences from exons 4 to 5, including a minor intron (mutant I3, see 'Material and Methods' for details). This reflects the endogenous situation, as *Srsf10* exon 3 contains a minor 5' splice site, which, however, is rarely used, since the polyadenylation site in exon 3 appears to be dominant (***Figure 1A***). The resulting minigene clearly remains responsive to *SRSF10* knockdown and overexpression (***Figure 1E***, I3). In contrast, replacing sequences starting from exon 3 (E3) or in intron 2 (I2) by *Gmfb* sequences results in splicing unresponsive to *SRSF10* knockdown and barely responsive to SRSF10 overexpression (***Figure 1E***; mutants E3 and I2). These data suggest that SRSF10 controls its own splicing via binding to exon 3, which, indeed, contains a GA-rich element representing the previously identified SRSF10 consensus binding site (***Shin and Manley, 2002***; ***Zhou et al., 2014***). Replacing nucleotides 17 to 60 of exon 3 by *GMFB* exon 4 sequence was sufficient to abolish SRSF10-mediated AS (***Figure 1D and E***, ESE; ***Figure 1—figure supplement 3***), thus identifying this GA-rich element as an SRSF10-dependent exonic splicing enhancer (ESE). Together, these data identify a highly conserved element in *Srsf10* exon 3 which is necessary for an autoregulatory feedback loop that controls Srsf10 expression levels.

The minor spliceosome controls Srsf10 expression

Exon 2 of *Srsf10* contains two competing 5' splice sites, which are specifically recognized by either the minor or the major spliceosome. To investigate the relevance of these splice sites for *Srsf10* autoregulation, we generated mutated minigenes containing either only major or only minor splice site (***Figure 2A***) and analyzed AS of the resulting minigenes. Mutated minigenes remained clearly responsive to SRSF10 knockdown and rescue, demonstrating that SRSF10 can regulate AS through both major and minor spliceosomes. However, in the control conditions (siCtrl), we observed that both minor-only or major-only minigenes show a strong increase in the use of exon 4 (***Figure 2B***). Exon 3 is hardly included at all in any of the two minigenes. Additionally, in the presence of a directly competing upstream splice site in exon 2, the downstream splice site is no longer used (***Figure 2B***, ***Figure 2—figure supplement 1***). These data indicate that, in vivo, the use of the minor splice site that leads to productive *Srsf10* splicing, is reduced through the presence of a competing major splice site. This arrangement could render *Srsf10* expression susceptible to dynamic control through

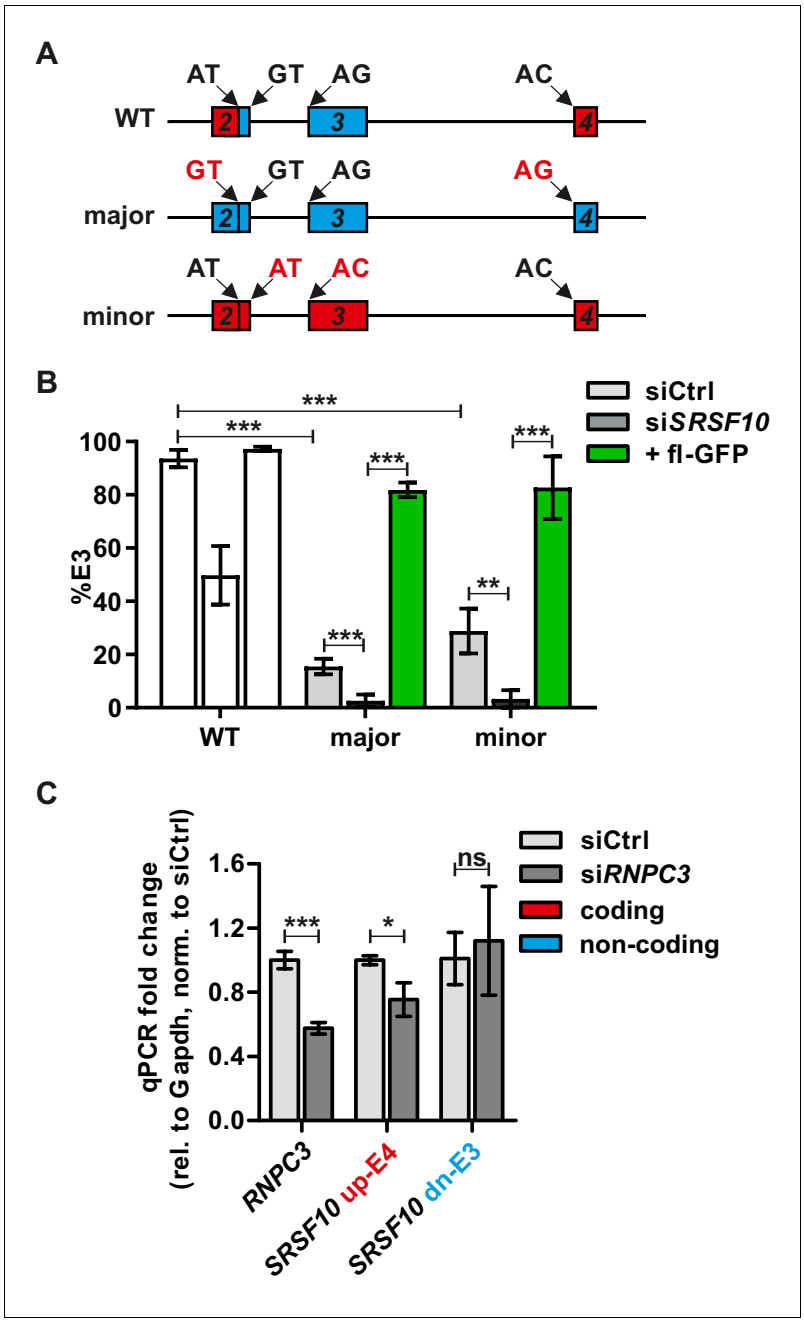

Figure 2. The minor spliceosome controls Srsf10 expression. (**A**) Schematic of the exon/intron structure of the Srsf10 WT and mutated minigenes harboring only major (GT.AG, blue) or minor (AT.AC, red) splice sites. Mutated splice sites are marked in red. (**B**) Minigenes from (**A**) were analyzed as in ***Figure 1***. Quantification of splicing-sensitive RT-PCRs is shown relative to the WT from ***Figure 1B*** (n = 4, mean +/- SD). A representative gel is shown in ***Figure 2—figure supplement 1***. (**C**) RT-qPCRs confirm siRNA-mediated knockdown of Rnpc3 (left) and changes in Srsf10 expression levels in HEK293. Expression relative to Gapdh and normalized to siCtrl (n = 3, mean +/- SD). Student's t test-derived p values *p<0.05, **p<0.01, ***p<0.001.

The online version of this article includes the following figure supplement(s) for figure 2:

Figure supplement 1. Competition of minor and major splice sites favors the downstream 5' splice site A representative gel of only minor or major splice site containing minigenes.

alterations in the activity of the minor spliceosome. To directly investigate this hypothesis, we inhibited minor spliceosome activity by performing an siRNA-mediated knockdown of the essential U11/U12 snRNP component *RNPC3* (***Figure 2C***). Indeed, the expression of the coding *SRSF10* mRNA (up-E4) was significantly decreased, while the levels of the non-coding dn-E3 mRNA are unaffected or slightly increased (***Figure 2C***). This result indicates that the abundance of the minor spliceosome directly correlates with *Srsf10* GE through controlling productive vs. non-productive AS. Furthermore, regulation through the activity of the minor spliceosome appears to, at least partially, overrule the autoregulatory feedback loop. This suggests a model in which the activity of the minor spliceosome sets the expression level of *Srsf10*, which is then maintained through autoregulation.

Minor spliceosome and SR protein expression correlate in a tissue-specific manner

To investigate the relevance of this mechanism in vivo, we analyzed the correlation of *Srsf10* GE levels with expression of the minor spliceosome component *Rnpc3* across 25 different mouse tissues (***Figure 3A***). Calculated transcripts per million (tpm) values using Whippet Quant (***Sterne-Weiler et al., 2018***) revealed clear tissue-specific expression patterns for both *Srsf10* and *Rnpc3*. Both genes show the lowest GE in blood cells and the highest in thymus (***Figure 3A***). Notably, a linear regression fit revealed an almost perfect correlation of *Srsf10* and *Rnpc3* expression across the 25 investigated tissues (R^2=0.85, p<0.0001, ***Figure 3B***). Similarly, *SRSF10* and *RNPC3* GE levels correlate across 31 human tissues (R^2=0.33, p=0.0006, ***Figure 3—figure supplement 1A***). In contrast, the levels of the housekeeping gene *Gapdh*, which contains no minor intron, do not correlate with *Rnpc3* (R^2=0.01, p=0.4071, ***Figure 3C***). Similar correlation coefficients were obtained with gene expression values determined independently using Salmon (***Patro et al., 2017***; ***Figure 3—figure supplement 1B and C***). Globally, minor intron-containing genes correlate much more strongly with *Rnpc3* levels than a randomly chosen group of expression level-matched genes containing only major introns (***Figure 3D***), indicating that *Rnpc3* levels represent an adequate indicator for minor spliceosome activity. Consistently, *Rnpc3* levels, and therefore *Srsf10* levels, also correlate with the expression levels of two other minor spliceosome components, namely *Snrnp25* and *Snrp48* (***Figure 3—figure supplement 1D and E***). These in vivo GE data are consistent with our model that minor spliceosome activity controls *Srsf10* levels. As an additional model system, we compared *Rnpc3* and *Srsf10* levels during neuronal differentiation of mouse embryonic stem cells (ES cells). GE levels correlate significantly (R^2=0.34, p=0.0006, ***Figure 3—figure supplement 1F***), while *Gapdh* levels do not correlate with *Rnpc3* (R^2=0.02, p=0.4365, ***Figure 3—figure supplement 1G***). Again, globally, minor intron-containing genes show a stronger correlation with *Rnpc3* levels than genes containing only major introns (***Figure 3—figure supplement 1H***). The *Srsf10*/*Rnpc3* correlation in ES cell differentiation is less pronounced – also with Salmon derived tpm values (***Figure 3—figure supplement 1I***) – indicating other factors influencing gene expression. Normalization of gene expression using DESeq2 (***Love et al., 2014***) strongly increases this correlation (***Figure 3—figure supplement 1J***), which is consistent with a direct role of the minor spliceosome in regulating *Srsf10* levels across different tissues and development stages. In summary, together with our minigene and knockdown results, these data indicate that the activity of the minor spliceosome controls productive vs unproductive *Srsf10* splicing and expression levels during development and in a tissue-specific manner.

SRSF10 and the minor spliceosome control tissue-specific and dynamic SR protein expression

To investigate whether the minor spliceosome exclusively controls *Srsf10* expression, we next examined the expression levels of all other SR proteins in a tissue- and developmental stage-specific manner. Surprisingly, we found that the expression of all SR proteins correlates with the minor spliceosome, represented by *Rnpc3*, in the 25 investigated tissues (R^2>0.42, p<0.0001, ***Figure 4A*** and ***Figure 4—figure supplement 1A***). Additionally, we observed a highly similar expression pattern for all SR proteins during neuronal differentiation of mouse ES cells (***Figure 4B*** and ***Figure 4—figure supplement 1B***) and a significant correlation with *Rnpc3* (***Figure 4—figure supplement 1C***). To experimentally confirm these results in vivo, we isolated RNA from mouse cerebral cortices from embryonic days (E) 12.5 and 15.5. RT-qPCR *analysis* revealed a significant increase of *Rnpc3* GE from E 12.5 to E 15.5 and, in parallel, Srsf10 levels also increased (***Figure 4C and D***). This is

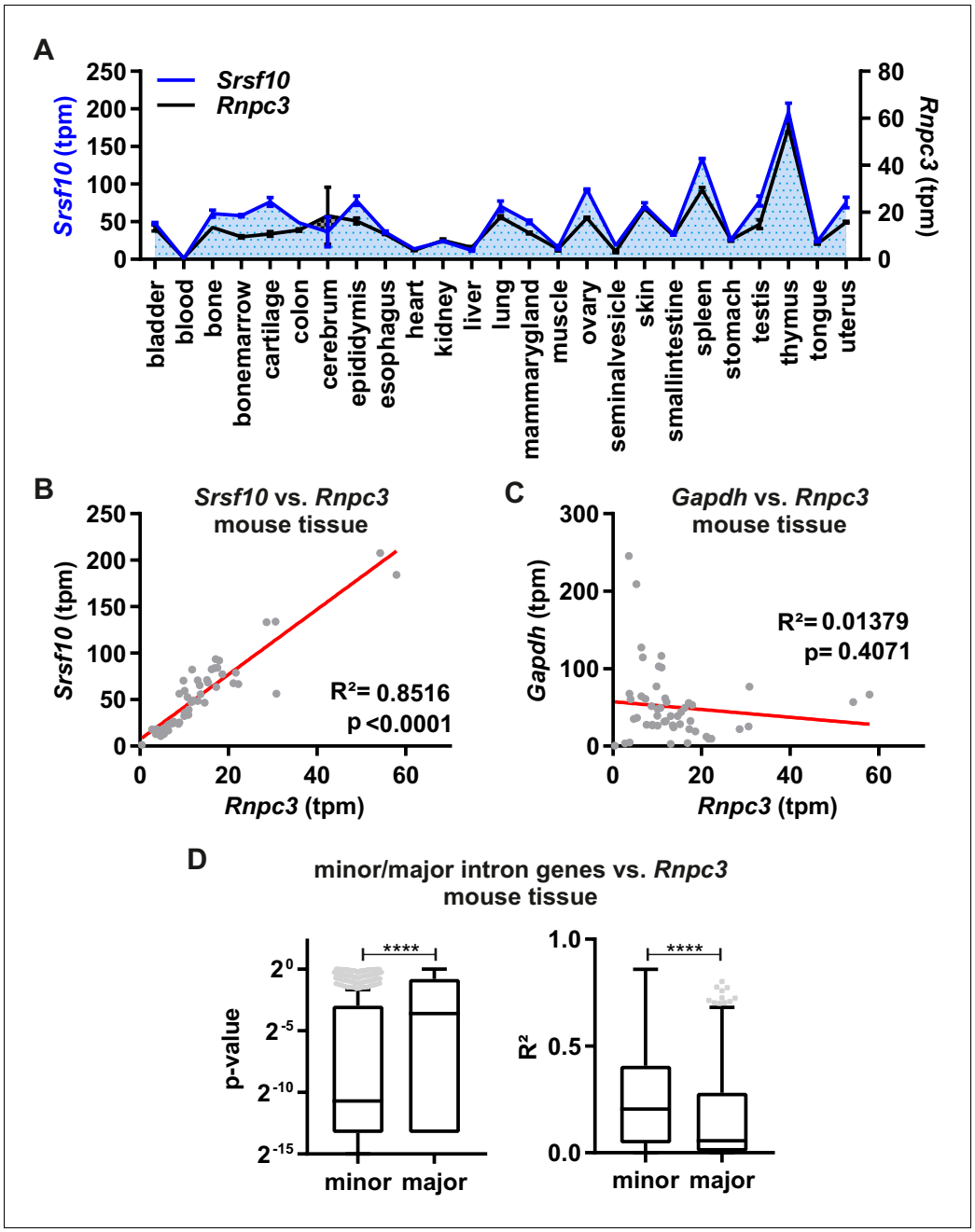

Figure 3. Minor spliceosome and Srsf10 expression correlate in a tissue-specific manner. (**A**) Relative GE levels of Srsf10 and Rnpc3 across 25 mouse tissues (x-axis). Transcripts per million (tpm) values were calculated using Whippet (***Sterne-Weiler et al., 2018***) (n ≥ 2, mean +/- SEM). (**B, C**) Linear regression fit for comparison of Srsf10 (**B**) and Gapdh (**C**) GE/tpm values with Rnpc3 across the 25 different mouse tissues. Goodness of fit is represented by R^2 and p-values. (**D**) Calculated p-values (left) and R^2 values (right) of a global correlation analysis of Rnpc3 with minor intron containing genes (n = 587) or randomly chosen expression matched genes, containing only major introns (n = 629). Statistical significance was determined by an unpaired t-test ****p<0.0001.
The online version of this article includes the following figure supplement(s) for figure 3:

Figure supplement 1. Minor spliceosome and Srsf10 expression correlate in a tissue-specific manner and during development.

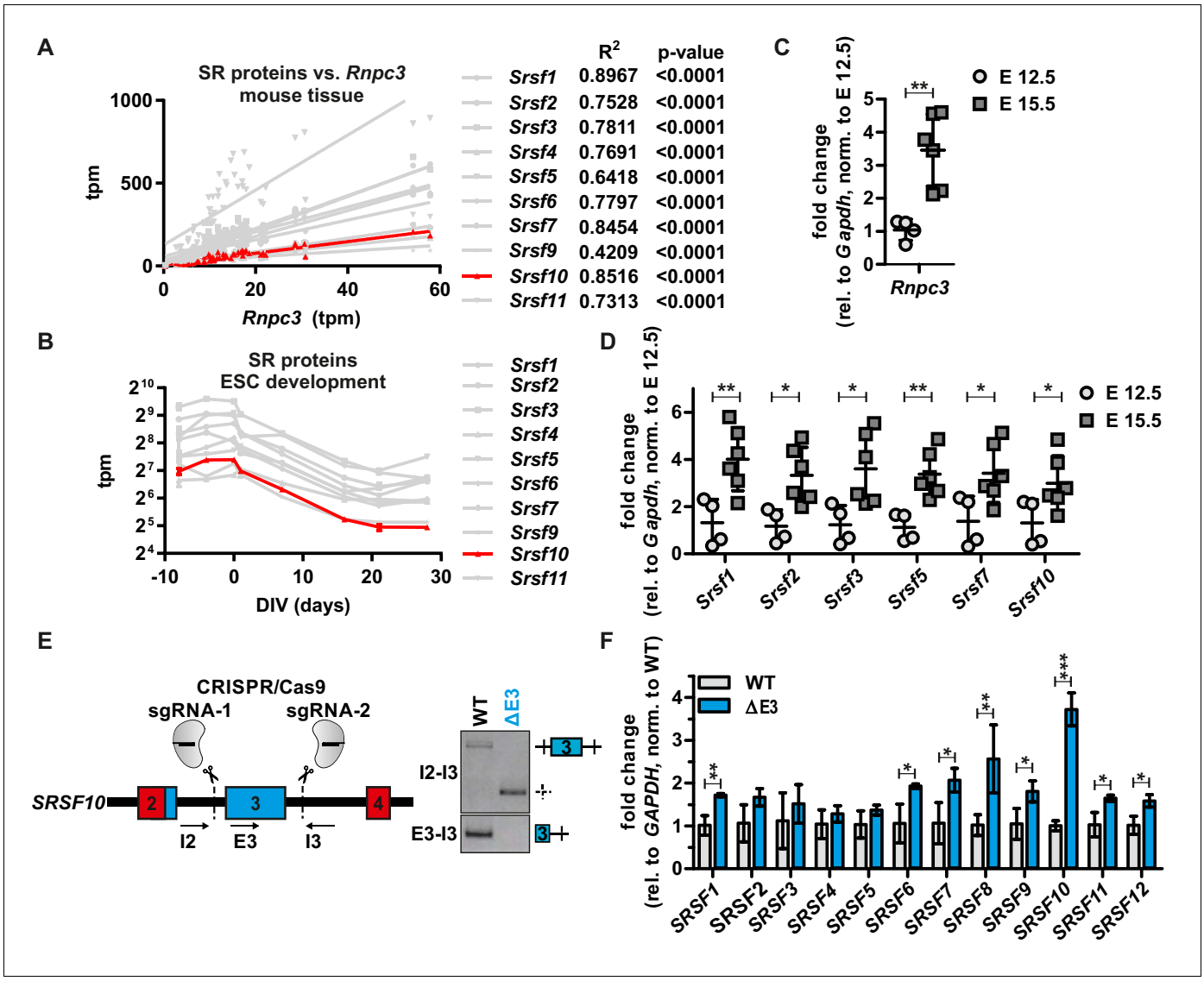

Figure 4. SRSF10 and the minor spliceosome control tissue-specific and dynamic SR protein expression. (**A**) Linear regression analysis of calculated tpm values for SR proteins against Rnpc3 in 25 different mouse tissues. R^2 and p-values are shown on the right. See also ***Figure 4—figure supplement 1A*** with all SR proteins colored. Due to generally low expression levels Srsf12 was omitted. (**B**) Comparison of tpm values of SR proteins during mouse ES cell differentiation (n ≥ 3, mean ± SD). See also ***Figure 4—figure supplement 1B and C***. (**C**) Rnpc3 GE levels in mouse cortex samples of the developmental stages E 12.5 and E 15.5 (relative to Gapdh, normalized to time point E 12.5) (n ≥ 4, mean ± SD). (**D**) SR protein expression in mouse cortex samples of the developmental stages E 12.5 and E 15.5. For Srsf10 only the functional up-E4 isoform was analyzed (relative to Gapdh, normalized to time point E 12.5) (n ≥ 4, mean ± SD). (**E**) Generation of clonal HEK293 cell lines lacking the regulatory Srsf10 exon 3. Left: Schematic of CRISPR/Cas9-mediated deletion of Srsf10 exon 3. Arrows indicate primer binding sites. Right: genotyping PCR on genomic DNA. (**F**) Relative SR protein expression in WT HEK293 cells or Srsf10ΔE3 cells. For Srsf10 only the functional up-E4 isoform was analyzed (relative to Gapdh, normalized to WT) (n = 3, mean +/- SD). Statistical significance was determined by an unpaired t-test *p<0.05, **p<0.01, ***p<0.001.
The online version of this article includes the following figure supplement(s) for figure 4:

Figure supplement 1. SRSF10 and the minor spliceosome control tissue specific and dynamic SR protein expression.
Figure supplement 2. Model for minor spliceosome-mediated control of SR proteins AS of SRSF10 mirrors minor spliceosome activity.

consistent with our model that higher minor spliceosome activity (indicated by higher *Rnpc3* abundance) results in preferential usage of the *Srsf10* up-E4 minor splice site, which leads to an increase in protein coding *Srsf10* mRNA. Consistent with SR protein expression patterns from different tissues or stem cell development in RNA-Seq data (***Figure 4A and B***), all other tested SR proteins are also

upregulated during the transition from E 12.5 to E 15.5 (**Figure 4D**), which, again, indicates a co-regulation of SR proteins, even though *Srsf10* is the only SR protein that contains a minor intron. As SR proteins are known to cross-regulate each other (**Bradley et al., 2015**), we hypothesized that a change in *Srsf10* levels could directly influence the levels of other SR proteins. To test this, we generated a CRISPR/Cas9-edited cell line lacking the non-productive *SRSF10* exon 3 (**Figure 4E**, left). Homozygous removal of exon 3 was confirmed by PCRs at the genomic level (**Figure 4E**, right) and, as expected, we observe increased *SRSF10* expression (**Figure 4F**, see **Figure 4—figure supplement 1D** for protein expression). Interestingly, we observe a stronger increase in the less active SRSF10-2 isoform (**Figure 4—figure supplement 1D**), indicating that AS of the last exon could be used to partially compensate for the loss of autoregulation via exon 3. Next, to examine whether manipulation of *SRSF10* autoregulation is sufficient to change the overall activity of SRSF10, we analyzed AS of SRSF10 target exons (**Zhou et al., 2014**; **Wei et al., 2015**). Consistent with increased *SRSF10* expression, the inclusion of alternative exons in *BCLAF1*, *PTBP2* and *ZFP207* is promoted in the CRISPR/Cas9-edited cells, and the opposite is observed by knockdown of *SRSF10* (**Figure 4—figure supplement 1E**). Notably, increased SRSF10 in our CRISPR/Cas9-edited cell line was sufficient for subtle upregulation of the mRNA levels of all other SR proteins (**Figure 4F**). In addition, reduced *SRSF10* expression upon *RNPC3* knockdown also correlates with slightly decreased expression of most other SR proteins (**Figure 4—figure supplement 1F**). In summary, these data suggest a model where minor spliceosome activity directly controls *SRSF10* levels, which is sufficient to change expression levels of the other SR proteins in a tissue- and differentiation state-specific manner (**Figure 4—figure supplement 2**). An exciting question that remains is how SRSF10 is able to coordinately regulate the abundance of the other SR proteins. Cross-regulatory mechanisms are known for many RBPs (**Kumar and Lopez, 2005**; **Rossbach et al., 2009**) and we therefore speculate that SRSF10 could regulate other SR proteins (and potentially other RBPs) by repressing the formation of NMD-targeted isoforms from their pre-mRNAs. This could be mediated either directly, by binding to the respective pre-mRNAs, or indirectly, through interactions with other SR proteins. Additionally, differences in SR protein abundance could be achieved by changing their activity. Higher mRNA abundance could be the consequence of reduced SR protein activity, resulting in reduced autoregulatory NMD exon inclusion and therefore higher mRNA expression levels (**Ni et al., 2007**). The activity of SR proteins is, amongst others, controlled by their phosphorylation level (**Goldammer et al., 2018**), and could be controlled by a direct or indirect effect of SRSF10 on the regulating kinases and phosphatases. While these mechanistic details remain to be investigated, the control of SR protein levels through the minor spliceosome and SRSF10 is of fundamental importance, as SR protein levels will have consequences for the splicing of most major introns. Our data thus reveal a mechanism through which the activity of the minor spliceosome controls major intron splicing in a tissue- and differentiation state-specific manner. This may also be relevant for diseases caused by minor spliceosome deficiencies (**Jutzi et al., 2018**; **Verma et al., 2018**), as misregulation of SR proteins and consequently, defects in major intron splicing (**Cologne et al., 2019**), may contribute to the observed phenotypes.

Materials and methods

Key resources table

Reagent type (species) or resource	Designation	Source or reference	Identifiers	Additional information
Gene (*Mus musculus*)	Srsf10	ncbi	GeneID:14105	Exons 2–4
Gene (*Homo sapiens*)	Gmfb	ncbi	GeneID:2764	Exon 4–5
Gene (*Homo sapiens*)	Srsf10	ncbi	GeneID:10772	
Cell line (*Homo sapiens*)	HeLa	ATCC	RRID:CVCL_0030	

Continued on next page

Continued

Reagent type (species) or resource	Designation	Source or reference	Identifiers	Additional information
Cell line (*Homo sapiens*)	HEK293	ATCC	RRID:CVCL_0045	
Cell line (*Homo sapiens*)	HEK293ΔE3	This paper		CRISPR/Cas9-mediated deletion of Srsf10 exon 3; see ***Figure 4*** and Materials and methods Part
Biological sample (*Mus musculus*, NMRI strain)	Cortices	This paper		developmental stages E 12.5 and E 15.5; see ***Figure 4*** and Materials and methods Part
Antibody	anti-FUSIP1 (T-18) (human, monoclonal)	Santa Cruz Biotechnology	RRID:AB_1123037	1:1000
Antibody	Anti-GFP (B-2) (monoclonal)	Santa Cruz Biotechnology	RRID:AB_627695	1:5000
Antibody	anti-Vinculin (H-300) (rabbit, polyclonal)	Santa Cruz Biotechnology	RRID:AB_2214507	1:1000
Antibody	anti-hnRNP L (4D11) (human, monoclonal)	Santa Cruz Biotechnology	RRID:AB_627736	1:10000
Recombinant DNA reagent	Mouse Srsf10 minigene	This paper		See ***Figure 1*** + with ***Figure 1—figure supplements 1*** and ***2***; and Materials and methods part
Recombinant DNA reagent	mouse Srsf10-fl-GFP	This paper		See ***Figure 1*** + with ***Figure 1—figure supplements 1*** and ***2***; and Materials and methods part
Recombinant DNA reagent	mouse Srsf10-2-GFP	This paper		See ***Figure 1*** + with ***Figure 1—figure supplements 1*** and ***2***; and Materials and methods part
Recombinant DNA reagent	mouse Srsf10-s-GFP	This paper		See ***Figure 1*** + with ***Figure 1—figure supplements 1*** and ***2***; and Materials and methods part
Recombinant DNA reagent	PX459 vector	Kindly provided by Stefan Mundlos	RRID:Addgene_62988	For sgRNA cloning and transfection
Recombinant DNA reagent	pEGFP-N3	Clontech		SRSF10 expression construct
Recombinant DNA reagent	pcDNA3.1(+)	Invitrogen	Catalog no: V79020	Minigene cloning
Sequence-based reagent	siRNA against human Srsf10 (siSrsf10)	This paper	GCGUGAAUUUGGUUAUdTdT	Knockdown of endogenous Srsf10
Sequence-based reagent	siRNA against human Rnpc3 (siRnpc3)	This paper	GAAAGAAGGUCGUAUGAAAdTdT	Knockdown of endogenous Rnpc3
Sequence-based reagent	Control siRNA (siCtrl)	This paper	UUUGUAAUCGUCGAUACCCdTdT	
Sequence-based reagent	sgRNA: SRSF10_E3_3fw	Benchling Tool	RRID:SCR_013955	Sequence: caccgctactttact cggtaagcca; CRISPR/ Cas9-mediated deletion of Srsf10 exon 3

Continued on next page

Continued

Reagent type (species) or resource	Designation	Source or reference	Identifiers	Additional information
Sequence-based reagent	sgRNA: SRSF10_E3_3rv	Benchling Tool	RRID:SCR_013955	Sequence: aaactggcttaccg agtaaagtagc; CRISPR/ Cas9-mediated deletion of Srsf10 exon 3
Sequence-based reagent	sgRNA: SRSF10_E3_5fw	Benchling Tool	RRID:SCR_013955	Sequence: caccgtgagtttc agaagcatgaat; CRISPR/ Cas9-mediated deletion of Srsf10 exon 3
Sequence-based reagent	sgRNA: SRSF10_E3_5rv	Benchling Tool	RRID:SCR_013955	sequence: aaacattcatgctt ctgaaactcac; CRISPR/ Cas9-mediated deletion of Srsf10 exon 3
Commercial assay or kit	PowerUp SYBR Green Mastermix	ThermoFisher Scientific	A25742	RT-qPCR
Chemical compound, drug	Roti-Fect	Carl Roth	Order no:P001.1	Plasmid vector transfection
Software, algorithm	GraphPad Prism 7.05	GraphPad	RRID:SCR_002798	Statistical analysis
Software, algorithm	ImageQuant TL	GE Life Sciences	RRID:SCR_014246	quantification
Software, algorithm	Whippet v0.11	***Sterne-Weiler et al., 2018***	RRID:SCR_018349	Tpm calculation
Software, algorithm	Salmon v1.2.0	***Patro et al., 2017***	RRID:SCR_017036	Tpm calculation
Software, algorithm	TxImport v1.14.0	***Soneson et al., 2015***	RRID:SCR_016752	Import of transcript counts to R for normalization wit DESeq
Software, algorithm	DESeq2 v1.26.0	***Love et al., 2014***	RRID:SCR_015687	Transcript counts normalization

Tissue cell culture

HEK293 and HeLa cells were cultured in standard conditions. Transfections were done with Rotifect according to the manufacturer's instructions. For siRNA sequences see ***Supplementary file 1***. Minigenes were transfected 24 hr after knockdown and RNAs were isolated 48 hr later. For overexpression and rescue experiments, cells were transfected using 0.4 µg of minigenes and 0.4 µg expression vectors for GFP-tagged Srsf10-fl, Srsf10-2 or Srsf10-s (or GFP alone). 48 hr after transfection cells were harvested for protein and/or RNA preparation. We perform monthly test for mycoplasms using PCR. Cell have been tested negative in all tests during the experiments performed for the present study. The cells morphologically appear as expected for Hek293 and HeLa cells respectively. We have used these Hek293 cells in several RNA-Seq experiments and compared gene expression with published Hek293 datasets and found very good correlation.

Preparation of embryonic mouse cortices for RNA extraction

Colonies of wild type mice of the NMRI strain were maintained in the animal facilities of Charité-Universitätsmedizin Berlin. Tissue collection was performed in compliance with German Animal Welfare Law and regulations imposed by the State Office for Health and Social Affairs Council in Berlin/Landesamt für Gesundheit und Soziales (LAGeSo).

Mice were bred for timed pregnancies, and the date of vaginal plug detection was considered embryonic day 0.5. Pregnancies were timed accordingly, and embryos prepared at the indicated embryonic days. Prior to the preparation of embryos, all tools were thoroughly cleaned with RNAse AWAY solution (Thermo Fisher, cat. no. 10328011). The uteri were dissected into DEPC-treated PBS,

and the embryonic brains quickly transferred to a solution of 2M NaCl in PBS for RNA stabilization. Cortices were dissected and then snap frozen in liquid nitrogen.

Molecular cloning

For cloning of the different Srsf10 overexpression constructs inserts were amplified from mouse cDNA and cloned into pEGFP-N3 (Clontech) using XhoI and BamHI restriction sites introduced through PCR primers. For minigene cloning, mouse genomic DNA was used as template to amplify *Srsf10* exons 2 to 4 and the product was cloned into pcDNA3.1(+). See ***Supplementary file 1*** for cloning primer sequences. For mutational analysis *Srsf10* exons/introns were replaced by sequences from the human *GMFB* gene: exons 4 to 5, intron 4 is a minor intron. New inserts were amplified by 1-step or 2-step PCR and cloned into pcDNA3.1(+) using BamHI and XhoI or into the WT minigene using internal restrictions sites (BsrGI for exon 3 and XbaI for intron 3). In the I3 mutant 356 nt of Srsf10 exon 3 were maintained, the downstream sequence was replaced by the 5' splice site of *GMFB* exon 4 (TCGatatcc...) and downstream sequence. For the E3 mutant sequences downstream of the BsrGI site (+16 in exon 3) were replaced by *GMFB* exon 4 to 5 sequence starting with (5'-CACCAGA...). For the ESE mutant nucleotids 17 to 60 of exon 3 were replaced by *GMFB* exon 4 sequence. For the minigene containing only minor splice sites we replaced the major splice sites of *Srsf10* intron 2 by minor splice sites of *GMFB* intron 4 (5' splice site: 5'-TCGatatcc; 3' splice site: 5'-ttctttaacttgagaaaaacCTT). In the minigene containing only major splice sites the upstream 5' splice site of exon 2 and the 3' splice site of exon 4 were replaced by major splice sites from *GMFB* intron 5 or 3, respectively (5' splice site: 5'-TTGgtaagt; 3' splice site: 5'-gcttttctctgtggtgccagGGC). All constructs were confirmed by sequencing.

RT-PCR and RT-qPCR

RT-PCRs and RT-qPCRs were performed as previously described (***Preußner et al., 2017***). See ***Supplementary file 1*** for primer sequences.

Western blot

Western Blot analyses were done as previously described (***Preußner et al., 2017***). The following antibodies were used: αSRSF10/FUSIP1 (T-18, Santa Cruz), αGFP (B-2, Santa Cruz), αVINCULIN (H-300, Santa Cruz) and αHNRNPL (4D11, Santa Cruz) antibodies. Western blots were quantified using the ImageQuant TL software.

RNA-Seq analysis

Transcripts per million (tpm) values were extracted from previously published RNA sequencing data using Whippet version 0.11 (***Sterne-Weiler et al., 2018***) and mouse reference genome mm10. Data for mouse tissues were obtained from WT control samples from SRA study DRP003641 (***Tanikawa et al., 2017***), data for neuronal differentiation of mouse ES cells from SRA study SRP017778 (***Hubbard et al., 2012***). Additionally, skin samples from SRP115206 were analyzed. For comparison, transcript abundances were additionally quantified using salmon version 1.2.0 (***Patro et al., 2017***). To obtain normalized expression counts, transcripts were imported to R using TxImport version 1.14.0 (***Soneson et al., 2015***) and count normalization was performed using DESeq2 version 1.26.0 (***Love et al., 2014***). DESeq2 based normalized expression counts dramatically increased the variance of replicate tissue samples (but not of ES cell differentiation), which is why we chose to analyze only the un-normalized values for the tissue comparisons. To investigate GE levels from different human tissues, fpkm values were directly used from ***Uhlén et al. (2015)***. Linear regression fits were performed in GraphPad Prism 7.05. A list of minor intron containing genes is based on ***Olthof et al. (2019)***. Genes with a comparable distribution of GE levels were randomly chosen from the remaining only major intron containing genes. The GE of each gene was compared to Rnpc3 levels across tissues or development stages. Unexpressed genes were excluded from the analysis. Downstream analyses were performed using standard Python 2 code and GraphPad Prism.

Generation of CRISPR/Cas9-edited cell lines

For CRISPR/Cas9-mediated deletion of *SRSF10* exon 3 sgRNAs were designed using the Benchling tool (for sequences see ***Supplementary file 1***) and cloned into the PX459 vector. Cells were

transfected using Rotifect following the manufacturer's protocol. 48 hr after transfection, transfected cells were selected with 1 µg/ml puromycin and clonal cell lines were isolated by dilution (***Ran et al., 2013***). Genomic DNA from clonally expanded lines was extracted and analyzed by PCR.

Acknowledgements

The authors wish to thank members of the Heyd lab for constructive comments and the HPC Service of ZEDAT, Freie Universität Berlin, for computing time. This work was funded by DFG grant 278001972 - TRR 186 to FH and DFG grant TA303/8-1 to VT. IW was supported by a PhD fellowship of the Boehringer Ingelheim Fonds and the Charité Promotionsstipendium. MP is funded by a post-doc stipend of the Peter and Traudl Engelhorn Foundation.

Additional information

Funding

Funder	Grant reference number	Author
Deutsche Forschungsgemeinschaft	278001972 - TRR 186	Florian Heyd
Deutsche Forschungsgemeinschaft	TA303/8-1	Victor Tarabykin
Boehringer Ingelheim Fonds	PhD fellowship	A Ioana Weber
Charité Promotionsstipendium		A Ioana Weber
Peter and Traudl Engelhorn Foundation	Postdoc stipend	Marco Preussner

The funders had no role in study design, data collection and interpretation, or the decision to submit the work for publication.

Author contributions

Stefan Meinke, Data curation, Formal analysis, Investigation, Methodology, Writing - original draft, Writing - review and editing; Gesine Goldammer, Investigation, Methodology; A Ioana Weber, Formal analysis, Investigation, Writing - review and editing; Victor Tarabykin, Resources; Alexander Neumann, Formal analysis; Marco Preussner, Conceptualization, Data curation, Formal analysis, Supervision, Investigation, Methodology, Writing - original draft, Writing - review and editing; Florian Heyd, Conceptualization, Formal analysis, Supervision, Funding acquisition, Methodology, Writing - original draft, Writing - review and editing

Author ORCIDs

Stefan Meinke https://orcid.org/0000-0001-5083-3383
Marco Preussner https://orcid.org/0000-0001-5155-0844
Florian Heyd https://orcid.org/0000-0001-9377-9882

Ethics

Animal experimentation: Colonies of wild type mice of the NMRI strain were maintained in the animal facilities of Charité-Universitätsmedizin Berlin. Tissue collection was performed in compliance with German Animal Welfare Law and regulations imposed by the State Office for Health and Social Affairs Council in Berlin / Landesamt für Gesundheit und Soziales (LAGeSo) under licence T102/11.

Decision letter and Author response

Decision letter https://doi.org/10.7554/eLife.56075.sa1
Author response https://doi.org/10.7554/eLife.56075.sa2

Additional files

Supplementary files

- Supplementary file 1. Oligonucleotide sequences of primers, siRNAs, and guide RNAs.

- Transparent reporting form

Data availability

All data are previously published and publicly available.

The following previously published datasets were used:

Author(s)	Year	Dataset title	Dataset URL	Database and Identifier
Human Genome Center, The University of Tokyo	2017	p53 mouse multi-tissue transcriptome analysis	https://www.ncbi.nlm.nih.gov/sra/?term=DRP003641	NCBI Sequence Read Archive, DRP003641
USAMRICD	2012	Deep transcriptional profiling of longitudinal changes during neurogenesis and network maturation in vivo	https://www.ncbi.nlm.nih.gov/sra/?term=SRP017778	NCBI Sequence Read Archive, SRP017778

References

Bradley T, Cook ME, Blanchette M. 2015. SR proteins control a complex network of RNA-processing events. *RNA* **21**:75–92. DOI: https://doi.org/10.1261/rna.043893.113, PMID: 25414008

Cologne A, Benoit-Pilven C, Besson A, Putoux A, Campan-Fournier A, Bober MB, De Die-Smulders CEM, Paulussen ADC, Pinson L, Toutain A, Roifman CM, Leutenegger AL, Mazoyer S, Edery P, Lacroix V. 2019. New insights into minor splicing-a transcriptomic analysis of cells derived from TALS patients. *RNA* **25**:1130–1149. DOI: https://doi.org/10.1261/rna.071423.119, PMID: 31175170

Doggett K, Williams BB, Markmiller S, Geng FS, Coates J, Mieruszynski S, Ernst M, Thomas T, Heath JK. 2018. Early developmental arrest and impaired gastrointestinal homeostasis in U12-dependent splicing-defective *Rnpc3*-deficient mice. *RNA* **24**:1856–1870. DOI: https://doi.org/10.1261/rna.068221.118, PMID: 30254136

Feng Y, Chen M, Manley JL. 2008. Phosphorylation switches the general splicing repressor SRp38 to a sequence-specific activator *nature structural &amp. Molecular Biology* **15**:1040–1048. DOI: https://doi.org/10.1038/nsmb.1485

Goldammer G, Neumann A, Strauch M, Müller-McNicoll M, Heyd F, Preußner M. 2018. Characterization of cis-acting elements that control oscillating alternative splicing. *RNA Biology* **15**:1–12. DOI: https://doi.org/10.1080/15476286.2018.1502587, PMID: 30200840

Hastings ML, Wilson CM, Munroe SH. 2001. A purine-rich intronic element enhances alternative splicing of thyroid hormone receptor mRNA. *RNA* **7**:859–874. DOI: https://doi.org/10.1017/S1355838201002084, PMID: 11421362

Hubbard KS, Gut IM, Lyman ME, Tuznik KM, Mesngon MT, McNutt PM. 2012. High yield derivation of enriched glutamatergic neurons from suspension-cultured mouse ESCs for neurotoxicology research. *BMC Neuroscience* **13**:127. DOI: https://doi.org/10.1186/1471-2202-13-127, PMID: 23095170

Jackson IJ. 1991. A reappraisal of non-consensus mRNA splice sites. *Nucleic Acids Research* **19**:3795–3798. DOI: https://doi.org/10.1093/nar/19.14.3795, PMID: 1713664

Jutzi D, Akinyi MV, Mechtersheimer J, Frilander MJ, Ruepp MD. 2018. The emerging role of minor intron splicing in neurological disorders. *Cell Stress* **2**:40–54. DOI: https://doi.org/10.15698/cst2018.03.126, PMID: 31225466

Kumar S, Lopez AJ. 2005. Negative feedback regulation among SR splicing factors encoded by Rbp1 and Rbp1-like in *Drosophila*. *The EMBO Journal* **24**:2646–2655. DOI: https://doi.org/10.1038/sj.emboj.7600723, PMID: 15961996

Lareau LF, Inada M, Green RE, Wengrod JC, Brenner SE. 2007. Unproductive splicing of SR genes associated with highly conserved and ultraconserved DNA elements. *Nature* **446**:926–929. DOI: https://doi.org/10.1038/nature05676, PMID: 17361132

Lejeune F, Cavaloc Y, Stevenin J. 2001. Alternative splicing of intron 3 of the serine/arginine-rich protein 9g8 gene identification of flanking exonic splicing enhancers and involvement of 9g8 as a trans-acting factor. *The Journal of Biological Chemistry* **276**:7850–7858. DOI: https://doi.org/10.1074/jbc.M009510200, PMID: 11096110

Long JC, Caceres JF. 2009. The SR protein family of splicing factors: master regulators of gene expression. *Biochemical Journal* **417**:15–27. DOI: https://doi.org/10.1042/BJ20081501, PMID: 19061484

Love MI, Huber W, Anders S. 2014. Moderated estimation of fold change and dispersion for RNA-seq data with DESeq2. *Genome Biology* **15**:550. DOI: https://doi.org/10.1186/s13059-014-0550-8, PMID: 25516281

Manley JL, Krainer AR. 2010. A rational nomenclature for serine/arginine-rich protein splicing factors (SR proteins). *Genes & Development* **24**:1073–1074. DOI: https://doi.org/10.1101/gad.1934910, PMID: 20516191

Müller-McNicoll M, Rossbach O, Hui J, Medenbach J. 2019. Auto-regulatory feedback by RNA-binding proteins. *Journal of Molecular Cell Biology* **11**:930–939. DOI: https://doi.org/10.1093/jmcb/mjz043, PMID: 31152582

Nagy E, Maquat LE. 1998. A rule for termination-codon position within intron-containing genes: when nonsense affects RNA abundance. *Trends in Biochemical Sciences* **23**:198–199. DOI: https://doi.org/10.1016/S0968-0004(98)01208-0, PMID: 9644970

Ni JZ, Grate L, Donohue JP, Preston C, Nobida N, O'Brien G, Shiue L, Clark TA, Blume JE, Ares M. 2007. Ultraconserved elements are associated with homeostatic control of splicing regulators by alternative splicing and nonsense-mediated decay. *Genes & Development* **21**:708–718. DOI: https://doi.org/10.1101/gad.1525507, PMID: 17369403

Nilsen TW, Graveley BR. 2010. Expansion of the eukaryotic proteome by alternative splicing. *Nature* **463**:457–463. DOI: https://doi.org/10.1038/nature08909, PMID: 20110989

Olthof AM, Hyatt KC, Kanadia RN. 2019. Minor intron splicing revisited: identification of new minor intron-containing genes and tissue-dependent retention and alternative splicing of minor introns. *BMC Genomics* **20**:686. DOI: https://doi.org/10.1186/s12864-019-6046-x, PMID: 31470809

Patro R, Duggal G, Love MI, Irizarry RA, Kingsford C. 2017. Salmon provides fast and bias-aware quantification of transcript expression. *Nature Methods* **14**:417–419. DOI: https://doi.org/10.1038/nmeth.4197, PMID: 28263959

Preußner M, Goldammer G, Neumann A, Haltenhof T, Rautenstrauch P, Müller-McNicoll M, Heyd F. 2017. Body temperature cycles control rhythmic alternative splicing in mammals. *Molecular Cell* **67**:433–446. DOI: https://doi.org/10.1016/j.molcel.2017.06.006, PMID: 28689656

Ran FA, Hsu PD, Wright J, Agarwala V, Scott DA, Zhang F. 2013. Genome engineering using the CRISPR-Cas9 system. *Nature Protocols* **8**:2281–2308. DOI: https://doi.org/10.1038/nprot.2013.143

Rossbach O, Hung L-H, Schreiner S, Grishina I, Heiner M, Hui J, Bindereif A. 2009. Auto- and Cross-Regulation of the hnRNP L proteins by alternative splicing. *Molecular and Cellular Biology* **29**:1442–1451. DOI: https://doi.org/10.1128/MCB.01689-08

Shin C, Manley JL. 2002. The SR protein SRp38 represses splicing in M phase cells. *Cell* **111**:407–417. DOI: https://doi.org/10.1016/S0092-8674(02)01038-3, PMID: 12419250

Soneson C, Love MI, Robinson MD. 2015. Differential analyses for RNA-seq: transcript-level estimates improve gene-level inferences. *F1000Research* **4**:1521. DOI: https://doi.org/10.12688/f1000research.7563.1

Sterne-Weiler T, Weatheritt RJ, Best AJ, Ha KCH, Blencowe BJ. 2018. Efficient and accurate quantitative profiling of alternative splicing patterns of any complexity on a laptop. *Molecular Cell* **72**:187–200. DOI: https://doi.org/10.1016/j.molcel.2018.08.018

Sureau A. 2001. SC35 autoregulates its expression by promoting splicing events that destabilize its mRNAs. *The EMBO Journal* **20**:1785–1796. DOI: https://doi.org/10.1093/emboj/20.7.1785

Tanikawa C, Zhang YZ, Yamamoto R, Tsuda Y, Tanaka M, Funauchi Y, Mori J, Imoto S, Yamaguchi R, Nakamura Y, Miyano S, Nakagawa H, Matsuda K. 2017. The transcriptional landscape of p53 signalling pathway. *EBioMedicine* **20**:109–119. DOI: https://doi.org/10.1016/j.ebiom.2017.05.017, PMID: 28558959

Turunen JJ, Niemelä EH, Verma B, Frilander MJ. 2013. The significant other: splicing by the minor spliceosome. *Wiley Interdisciplinary Reviews: RNA* **4**:61–76. DOI: https://doi.org/10.1002/wrna.1141, PMID: 23074130

Uhlén M, Fagerberg L, Hallström BM, Lindskog C, Oksvold P, Mardinoglu A, Sivertsson Å, Kampf C, Sjöstedt E, Asplund A, Olsson I, Edlund K, Lundberg E, Navani S, Szigyarto CA, Odeberg J, Djureinovic D, Takanen JO, Hober S, Alm T, et al. 2015. Proteomics Tissue-based map of the human proteome. *Science* **347**:1260419. DOI: https://doi.org/10.1126/science.1260419, PMID: 25613900

Verma B, Akinyi MV, Norppa AJ, Frilander MJ. 2018. Minor spliceosome and disease. *Seminars in Cell & Developmental Biology* **79**:103–112. DOI: https://doi.org/10.1016/j.semcdb.2017.09.036, PMID: 28965864

Wang ET, Sandberg R, Luo S, Khrebtukova I, Zhang L, Mayr C, Kingsmore SF, Schroth GP, Burge CB. 2008. Alternative isoform regulation in human tissue transcriptomes. *Nature* **456**:470–476. DOI: https://doi.org/10.1038/nature07509, PMID: 18978772

Wei N, Cheng Y, Wang Z, Liu Y, Luo C, Liu L, Chen L, Xie Z, Lu Y, Feng Y. 2015. SRSF10 plays a role in myoblast differentiation and glucose production via regulation of alternative splicing. *Cell Reports* **13**:1647–1657. DOI: https://doi.org/10.1016/j.celrep.2015.10.038

Zhou X, Wu W, Li H, Cheng Y, Wei N, Zong J, Feng X, Xie Z, Chen D, Manley JL, Wang H, Feng Y. 2014. Transcriptome analysis of alternative splicing events regulated by SRSF10 reveals position-dependent splicing modulation. *Nucleic Acids Research* **42**:4019–4030. DOI: https://doi.org/10.1093/nar/gkt1387, PMID: 24442672

6 List of abbreviations

AS	alternative splicing
AS-NMD	AS coupled to NMD
ASO	antisense oligonucleotide
BCL-2	B cell lymphoma 2
BCLAF1	BCL-2-associated transcription factor 1
BP	branch point
CamKIIb	calcium/calmodulin-dependent protein kinase type IIβ
CDC25	cell division cycle 25
CE	cassette exon
CIP2A	cancerous inhibitor of PP2A
CIRBP	cold-inducible RNA binding protein
CLK	Cdc2-like kinase
COPII	coat protein complex II
DMSO	dimethyl sulfoxide
DNA	deoxyribonucleic acid
DSCAM	human Down syndrome cell adhesion molecule
EGFR	epidermal growth factor receptor
ESC	embryonic stem cell
ESE	exonic splicing enhancer
ESS	exonic splicing silencer
fpkm	fragments per kilobase of exon model per million reads mapped
GE	gene expression
h	hours
hnRNP	heterogeneous nuclear ribonucleoprotein
ISE	intronic splicing enhancer
ISS	intronic splicing silencer
LCMT-1	leucine carboxyl methyltransferase 1
MAPK	mitogen-activated protein kinase
Mnk2	MAPK-interacting kinase 2
mRNA	messenger RNA
NMD	nonsense-mediated mRNA decay

NOVA	neuro-oncological ventral antigen
OA	okadaic acid
PME-1	phosphatase methylesterase 1
PP1/2A	protein phosphatases 1 and 2A
PP2A	protein phosphatase 2A
PP2AC	PP2A catalytic subunit
pre-mRNA	precursor messenger RNA
PTC	premature translation termination codon
RBP	RNA binding protein
RNA	ribonucleic acid
RNA-Seq	RNA sequencing
RNPC3	RNA binding region (RNP1, RRM) containing 3
RRM	RNA recognition motif
RS	arginine (R) and serine (S)-rich
RT	room temperature
SF1	splicing factor 1
snRNP	small nuclear ribonucleoprotein particles
SR	serine/arginine-rich
SRPK	serine/arginine protein kinase
tpm	transcripts per million
U2AF	U2 auxiliary factor
vs.	versus
WT	wild type

7 List of Figures

8 Curriculum vitae

For reasons of data protection, the curriculum vitae is not published in the electronic version.

Selbstständigkeitserklärung

Gem. § 7 Abs. 4 der Promotionsordnung basierend auf den Mitteilungen im Amtsblatt der Freien Universität Berlin Nr. 52/2007 vom 04.09.2007 und Nr. 04/2008 vom 07.02.2008 und Nr. 02/2012 vom 18.02.2012.

Hierdurch versichere ich, dass ich die vorliegende Dissertation selbstständig und ohne unerlaubte Hilfe angefertigt habe.

Hierdurch versichere ich, dass meine Dissertation nicht auf meiner Masterarbeit aufbaut bzw. nicht daraus erwachsen ist.

Hierdurch versichere ich, dass ich meine Dissertation im Einvernehmen mit meinem Betreuer Prof. Dr. Florian Heyd in Teilen veröffentlicht habe. Die Publikationen sind Bestandteil der kumulativen Dissertation.